A University of Sussex PhD thesis

Available online via Sussex Research Online:

http://sro.sussex.ac.uk/

This thesis is protected by copyright which belongs to the author.

This thesis cannot be reproduced or quoted extensively from without first obtaining permission in writing from the Author

The content must not be changed in any way or sold commercially in any format or medium without the formal permission of the Author

When referring to this work, full bibliographic details including the author, title, awarding institution and date of the thesis must be given

Please visit Sussex Research Online for more information and further details

The role of microRNAs in *Drosophila* larval locomotion

Edward O'Garro-Priddie

Submitted in partial fulfilment of the requirements for the degree of Doctor of Philosophy at the University of Sussex

March 2021

I hereby declare that this thesis has not been and will not be, submitted in whole or in part to another University for the award of any other degree.

Signed:.....

Edward O’Garro-Priddie

University of Sussex
Edward O'Garro-Priddie

Summary

microRNAs (miRNAs) are small, non-coding RNAs that negatively regulate genetic expression and have been shown to regulate motor control in several animals, including *Drosophila melanogaster*. Previous work in our laboratory showed that miRNA-based regulation of self-righting behaviour in *Drosophila* larvae is pervasive and we therefore endeavour to establish the behaviour's neural substrates. Here, we use neuronal reconstruction to identify neurons connected to the LT-1/2 motor neurons, themselves essential for self-righting. Combining this with connectomics work, we produce a neural wiring diagram for self-righting which we functionally test by thermogenetically inhibiting individual cellular components - finding that the normal activity of most neurons in our wiring diagram is essential for normal self-righting. Building on this, we examine miRNA regulation in general larval locomotion by screening a mutant collection affecting most miRNAs expressed in early-stage *Drosophila* larvae. Using high-throughput larval tracking, we observe that the vast majority of miRNA mutants show reduced crawling speed and impacted bending and pausing behaviours. Examining how consistent miRNA-dependent effects are through development, we also test a subset of miRNA mutants at the third-instar larval stage. We demonstrate that effects of specific mutations vary over development, suggesting a complex relationship between miRNA function and larval development. Finally, we select *miR-133* for detailed mechanistic study, find that its mutation produces significant increases in rearing and identify tryptophan hydroxylase (Trh) as a potential regulatory target. Target expression analysis confirms an increase in Trh expression and serotonin production in *miR-133* mutants. Moreover, gene expression analysis shows *miR-133* expression within serotonergic neurons and we successfully phenocopy the increased rearing observed in *miR-133* mutant larvae by overexpressing Trh. Altogether, our studies demonstrate the general role of miRNA regulation in *Drosophila* larval locomotion. Constructing a neuronal wiring diagram for self-righting also identifies the behaviour's neural basis and opens possibilities for future mechanistic study.

Acknowledgements

Firstly, I would like to thank Professor Claudio Alonso for supervising the project and Professor Paul Graham for being an extremely supportive and helpful co-supervisor. I would also like to thank Dr. Albert Cardona for hosting me in Janelia and send a special thank you to Dr. Joao Picao-Osorio for all of your help with Chapters 3 and 4, as well as to Clare Hancock for your contribution to Chapter 4.

To all my past and present Alonso labmates: I thank you all for the laughs, the support, the lab meetings, the hugs, the snack runs, the football debates and the therapy sessions.

I thank my family (near or far, here and not here), Leaford and Eric (for being constant sources of advice, motivation, and inspiration), Chad, Tess and Claire (for making Summer 2017 the best Summer ever!) and, of course - Minh, TJ, Adnan, Lish, Ibrahim, Anas and every single one of the Central boys for being the best friends anyone could ask for.
Finally, I thank the two people who kept me going every single day.

Mum. For encouraging me to dream big, for always being my biggest supporter and for every sacrifice you've ever made for me. This is yours too.

Abby. For the endless amounts of support, love and patience you've showed these past few years. I couldn't have done it without you and I'm eternally grateful.

Table of Contents

List of Figures

List of Tables

Abbreviations

AP axis Anteroposterior axis

AEL After egg laying

Ago Argonaute

Avi Audio video interleave

CATMAID Collaborative Annotation Toolkit for Massive Amounts of Image Data

cDNA Complementary DNA

CNS Central nervous system

CPG Central pattern generators

DAPI 4',6-diamidino-2-phenylindole

DEPC Diethyl pyrocarbonate

DNA Deoxyribonucleic acid

DNase Deoxyribonuclease

DNTP Deoxynucleoside triphosphate

EDTA Ethylenediaminetetraacetic acid

EM Electron microscopy

Elav Embryonic lethal abnormal vision

FIJI Fiji is just ImageJ

FIM FTIR-based imaging method

FTIR Frustrated total internal reflection

GCaMP Green fluorescent–calmodulin–M13 fusion protein

GFP Green fluorescent protein

h Hours

ISN Intersegmental nerve

lncRNA long non-coding RNA

L1 First instar larva

L2 Second instar larva

L3 Third instar larva

LT 1/2 MN Lateral-transversal motor neurons 1 and 2

miR microRNA

miRNA microRNA

Min(s) Minute(s)

mm Millimetre

MMLV-RT Moloney Murine Leukaemia Virus Reverse Transcriptase

mRNA messenger RNA

nt Nucleotide(s)

PBS Phosphate buffered saline

PBTx Phosphate buffered saline with Triton-X 100 detergent

PCR Polymerase chain reaction

pri-miRNA Primary miRNA

qPCR Quantitative real-time PCR

RISC RNA induced silencing complex

RNA Ribonucleic acid

RNAi RNA interference

RNase Ribonuclease

Rpm Rotations per minute

RT Reverse transcriptase

RT-PCR Reverse transcription polymerase chain reaction

sec Second(s)

SEM Standard error of the mean

SN Segmental nerve

SR Self-righting

SRC Self-righting circuit

ssTEM Serial section transmission electron microscopy

Tif Tagged image format

Trh Tryptophan hydroxylase

UAS Upstream activation sequence

Ubx Ultrabithorax

UTR Untranslated region

VNC Ventral nerve cord

xG times gravity

ΔmiR miRNA null mutant strain

µm Micrometres

Chapter 1

General Introduction

1.1 Preface

The control of behaviour is facilitated by the co-ordinated activity of the central nervous system. Information flow between neurons occurs through interactions between neurons across synapses and these synaptically-connected neurons form sensorimotor circuits; enabling organisms to perceive information about the outside world and respond to stimuli appropriately. Serial reconstruction has been used for centuries to provide insights about the structure of the circuits that facilitate behaviour through direct observation of the synapses connecting neurons (Ware and Lopresti, 1975). With the advent of *in silico* serial reconstruction and the development of ever more complex connectomics analyses, researchers are able to characterise and analyse neuronal circuit structures in more detail than ever before. These approaches have provided the ability to identify several of the circuits underlying motor behaviour in the *Drosophila melanogaster* larva (Ohyama *et al.,* 2015; Fushiki *et al.,* 2016; Burgos *et al.,* 2018) as well as circuits in other organisms such as the zebrafish (Wanner *et al.,* 2016) and the nematode worm *Caenorhabditis elegans* (Hall and Russell, 1991).

The cellular substrates underlying behaviour also rely upon tightly co-ordinated gene expression at the individual level to function properly and changes to gene expression can affect behavioural output in a variety of unicellular and multicellular organisms (Kung, 1971; Hotta and Benzer, 1972; Brenner, 1974). In this manner, normal behavioural output can therefore be considered to be dependent on the regulation of gene expression in organisms and this can occur at different stages during the journey from gene to protein.

In particular, post-transcriptional regulation of gene expression by the microRNA (or ‘miRNA’) has emerged as a key mechanism for the development and functionality of a central nervous system able to facilitate the full repertoire of behaviours in organisms. miRNAs are small non-coding RNAs approximately 22 nucleotides in length that are negative regulators of gene expression. miRNAs bind to short, complementary sequences usually found in the 3’ UTRs of target mRNA transcripts and promote their degradation, silencing the expression of targeted genes (Bartel, 2004). In a variety of organisms, the activity of miRNAs in the nervous system has been shown to facilitate normal behavioural output (Dulcis *et al.,* 2017; Watts *et al.,* 2020) however, overall, few fully-characterised mechanisms for this have been described.

Here, we use the genetically amenable *D. melanogaster* larva as a model system to investigate the role of miRNAs in the control of larval locomotor behaviour. Building on the previous identification of the complex larval self-righting response as a behaviour facilitated by repression of the Hox gene *Ultrabithorax* by the miRNA, *miR-iab-4* in two metameric motor neurons (Picao-Osorio *et al.,* 2015; Issa *et al.,* 2019), we aim to identify other potential cellular substrates of self-righting behaviour through a combination of *in silico* neuronal reconstruction, connectomics analysis and functional testing. Regulation of self-righting behaviour by miRNAs is extremely pervasive (Picao-Osorio *et al.,* 2017) and in this study, we question whether general larval locomotor behaviour also relies on normal miRNA expression (and if so, we question through what mechanisms this regulation occurs).

1.2 Investigating the neural control of behaviour

1.2.1 The CNS as a network of connected neurons

The biological systems underlying the control of behaviour have been a topic of scientific investigation for thousands of years. As far back as the 5th century BC, the natural philosopher Alcmaeon of Croton proposed that the mind (and specifically, sensory cognition) was housed within the brain (Celesia, 2012) and in the 4th Century BC Herophilus of Chalcedon built on this, laying the foundations for our modern understanding of the central nervous system (or 'CNS') as a network extending throughout the body. Herophilus proposed that the brain and body were connected by "channels" and experimentally demonstrated that "channels" connected to muscles (now recognised as motor nerves) were able to instigate motion through stimulation of muscle contraction (Longrigg, 1993).

It was not until the 19th Century, however, that the dedicated illustrative efforts of the celebrated Spanish neuroscientist Santiago Ramón y Cajal led to the postulation of the neuron doctrine. In this conceptual framework, the CNS is comprised of discrete individual cells that communicate with each other as functional units (rather than a single, continuous network of branching fibres). For years following this, the question of exactly how the neurons of this network communicated with each other to enable information flow across the CNS remained until, in the mid-20th Century, the work of Hodgkin and Huxley produced the eponymous Hodgkin-Huxley model (Hodgkin and Huxley, 1952).

Building on insights gained from the analysis of signal propagation in the easily-accessible squid giant axon, Hodgkin and Huxley's model described the

initiation and propagation of action potentials along axons and modelled the mechanisms responsible for the sequential excitation and relaxation of synaptically-connected neurons. The development of this model, however, opened more questions about the relationship between behavioural output and the structure of neuronal networks, and led to the development of approaches to the study of the workings of the CNS from a cellular perspective.

1.2.2 Methods for investigating neural circuit structure

Early attempts to isolate the structure of the cellular networks underlying behaviour mainly relied on ablation studies, in which the brains of animals would be purposely damaged in specific areas to understand their relationship to behavioural control (Flourens, 1824; 1825). It was Santiago Ramón y Cajal who identified, what we now call synapses, as “articulations” between neurons (DeFelipe, 2015) but for decades, precisely which neurons connected to each other to form the networks that facilitate behaviours remained unclear.

One approach developed in the early 20th Century to address this question was ‘tract-tracing’. In the earliest days of this technique, solutions of silver nitrate or phosphotungstic acid would be used to stain fixed central nervous systems, allowing researchers to not only visualise the projections of neurons of interest but also identify their synaptic partners (Hoff, 1932; Nauta 1952, Gray, 1963, Fink and Heimer, 1967). Over time, this technique has evolved to the point where tract-tracing can be performed in live animals by injecting fluorescent dyes that can are transported around a cell to reveal its morphology (reviewed

in Köbbert *et al.,* 2000) or applying viruses to label synaptically-connected neurons (Ugolini, 1995).

An alternative approach to the determination of circuit structure is the use of ‘serial reconstruction’. Serial reconstruction has been used since at least the late 19th Century (His, 1880) and consists of the sectioning of an animal’s CNS using a microtome and the subsequent imaging of these sections. The three-dimensional morphology of neurons is then “reconstructed” by tracking the position of a neuron of interest throughout the collection of images (or ‘image volume’) and graphically representing this separately. The positions of CNS features such as synapses, glia and cell bodies can be identified within the image volume providing researchers with insights about which neurons are synaptically connected, the directionality of connections (i.e., which neuron is pre- and post- synaptic) and the locations of these connections throughout the neuron.

In the very earliest days of serial reconstruction, microtome sections were embedded in wax and scientists often had to collaborate with artists to produce faithful graphical representations of the biological structures being reconstructed. The resolution of microscopy techniques at the time also presented a limit on the size of the biological structures that could be resolved in detail and difficulties in the alignment of sections from which reconstructions were produced could lead to inaccuracies in final graphical representations (Ware and Lopresti, 1975). The advent of the electron microscope in the early 20th Century (described in Mulvey, 1962) and its subsequent refinement over the following years, however, presented researchers with the opportunity to incorporate high-resolution microscopy into serial reconstruction approaches

and this was particularly relevant for reconstruction of nervous systems (Sjöstrand, 1958).

1.2.3 Connectomics and *in silico* serial reconstruction

The ability to identify synaptic interactions between particular neurons has supported the development of 'connectomic' investigations, in which maps of the connections between the neurons of a CNS are developed. The nematode worm, *Caenorhabditis elegans*, has a small nervous system of 302 neurons (Chiu *et al.,* 2011) and the use of serial reconstruction has been instrumental in the development of full connectomes for the animal's CNS (White *et al.,* 1986; Hall and Russell, 1991). As time has progressed, development of *in silico* methods for connectomic analyses of data from serial reconstructions has enabled the full and partial determinations of connectomes for a variety of animals including the marine ragworm *Platynereis dumerilii* (Randel *et al.,* 2015; Veraszto *et al.,* 2020), the zebrafish (Wanner *et al.,* 2016, Hildebrand *et al.,* 2017) and the mouse (Helmstaedter *et al.,* 2013; Motta *et al.,* 2019).

A number of these studies have utilised a platform originally developed to aid in the determination of the connectome of the fruit fly *Drosophila melanogaster.* The *in silico* Collaborative Annotation Toolkit for Massive Amounts of Image Data (or CATMAID) was developed by Saalfeld and colleagues in 2009 (Saalfeld *et al.,* 2009).

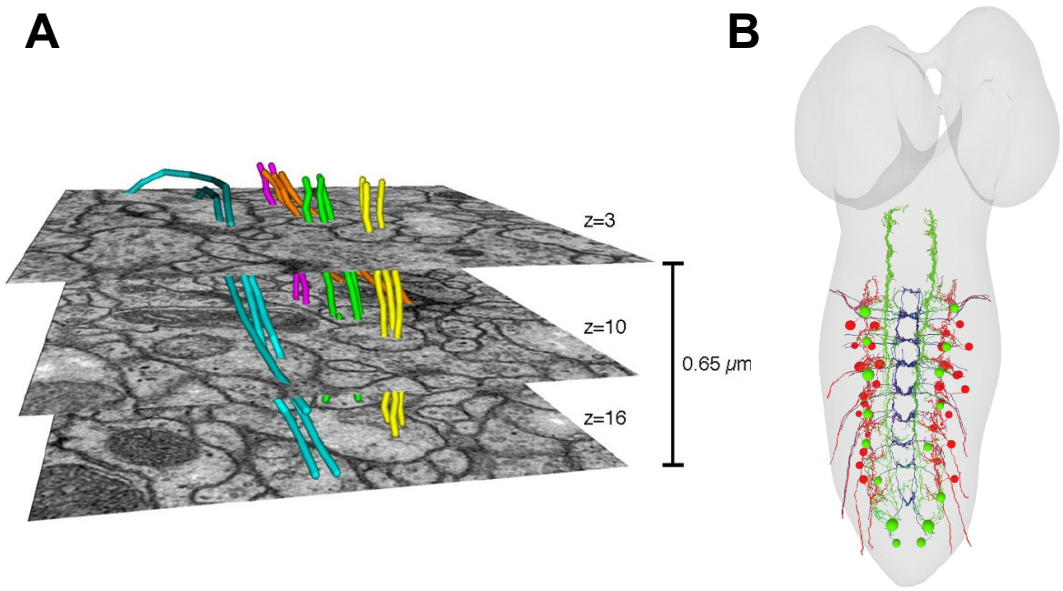

Figure 1.1 *In silico* serial reconstruction of the *Drosophila* CNS

(A) *Adapted from Schneider-Mizell et al., 2016*. By loading large volumes of EM images of central nervous systems onto computer-based systems, researchers can scroll through them at will and serially reconstruct the morphologies of neurons or other organelles in a virtual environment. Here, the microtubules of selected *Drosophila melanogaster* larval neurons are reconstructed from an EM image volume using the TrakEM2 program. Each group of independently-coloured strands represents the three-dimensional morphology of microtubules from a single neuron. **(B)** Using CATMAID, virtual skeletonised neuronal morphologies are produced via serial reconstruction, and data on synaptic connectivity is stored automatically. Here, the multidendritic class IV sensory neurons (blue), A19f interneurons (green) and LT-1/2 motor neurons (red) have been reconstructed in the abdominal hemisegments of the *Drosophila* ventral nerve cord, analogous to the human spine.

Image volumes of invertebrate nervous systems often comprised thousands of images from section and a large number of work-hours was therefore necessary to produce serial reconstructions (Ware and Lopresti, 1975). To address these issues, the CATMAID tool was designed to be an online platform, enabling researchers to access large volumes of electron microscopy (or 'EM') images and serially reconstruct neuronal morphologies in a collaborative manner (Figure 1.1).

In terms of connectomics, CATMAID also provides the ability to annotate synaptic connections between neurons and the tool automatically stores this connectomic information, using it to calculate connectivity-related metrics. For *D. melanogaster*, this approach has provided an efficient way for researchers to gain insights about the architectures of neuronal networks potentially underlying behaviour in both the adult and larval fly (Schneider-Mizell *et al.,* 2016; Eichler *et al.,* 2017; Zheng *et al.,* 2018).

1.2.4 Functional validation of neural wiring diagrams

Once the wiring diagrams of neuronal networks produced via connectomic analyses are finalised, they can then be functionally tested *in vivo* to establish the existence of neuronal circuits driving behaviour. One approach for this is the targeted expression of genetically encoded calcium reporters (or GECIs) in particular neuronal subsets. In both mammalian and non-mammalian organisms, GECIs allow researchers to examine the level of neuronal activity occurring during both fictive and actual exhibitions of behaviours of interest (Tian *et al.,* 2009).

In *D. melanogaster* larvae, this approach has been used to demonstrate the activity of the cellular substrates involved in locomotion (Heckscher *et al.,* 2015; Pulver *et al.,* 2015; Karagyozov *et al.,* 2018) and (combined with targeted expression of channelrhodopsins) to demonstrate functional connections between two neurons (Yoshino *et al.,* 2017; Tastekin *et al.,* 2018). This approach for functionally demonstrating synaptic connection has also been applied in the nervous system of other model organisms such as the mouse (Bovetti *et al.,* 2017), *C. elegans* (Li *et al.,* 2014) and the zebrafish (Matsui *et al.,* 2014) demonstrating its versatility as a strategy for the validation of neural circuits.

Another strategy used for neural circuit validation is the dynamic activation and inhibition of individual neurons in a wiring diagram and the analysis resulting changes to behaviour. Binary expression systems (discussed further in Section 1.5.4) can be used to target expression of light-sensitive or heat-sensitive manipulators of neural activity to neurons of interest. For example, the channelrhodopsins ChR2 and Chrimson can be targeted to neurons to enable their activation in the presence of light of a specific wavelength (Simpson and Looger, 2018) while the anion channelrhodopsins (e.g., GtACR) can be used to inhibit neural activity in the same way (Mohammad *et al.,* 2017). Alternatively, selective expression of the thermosensitive ion channel dTRPA1 (Hamada *et al.,* 2008) can be used to stimulate neural activity in the presence of increased temperatures while the temperature sensitive allele of the *shibire* gene can be used to inhibit neural activity at restrictive temperatures (Kitamoto, 2001).

These techniques facilitate the ability to dissect the contribution of neurons within wiring diagrams to behaviour and perception (Green *et al.,* 2017; Stensmyr *et al.,* 2012) and are relatively efficient approaches compared to simultaneous expression of functional effectors with GECIs.

1.3 Central pattern generators

In particular, the functional validation of neural circuits serves to address our questions on the nature of the CPGs underlying rhythmic behaviours in animals.

Central pattern generators (or 'CPGs') are groups of neurons able to produce rhythmic output even in the absence of rhythmic input. CPGs typically facilitate repetitive, stereotyped locomotor behaviours such as walking, running, and swimming and are responsible for the generation of flight behaviour in insects.

The concept of groups of neurons able to produce rhythmic output without rhythmic input was first proposed in the early 20th Century as a way to facilitate alternate flexion and extension of limbs during locomotion. Seminal work by Brown in the cat (Brown, 1911) showed that even after decerebration, locomotor output was still possible and he hypothesised that this phenomenon was the result of neurons in the cat's legs functioning as "half-centers". Each "half-center" would be composed of reciprocally inhibitory neurons such that the flexion of one leg would automatically lead to the extension of the other, producing repetitive and stereotyped movement without the need for external input.

Behavioural output without the need for external input was subsequently observed in a number of species over the next few decades. Mating behaviour in the mantis and cockroach (Roeder *et al.,* 1960) and flight behaviour in the locust (Wilson, 1961) were both shown to be facilitated by the activity of neuronal centers able to produce their own intrinsic rhythm and, in the human, evidence of spontaneous alternating extension and flexion of the lower limbs in a patient with a cervical spinal cord injury has also been demonstrated (Calancie *et al.,* 1994).

This spontaneous movement pattern could be instigated by the extension of the patient's hips and knees while lying supine and although its neuronal basis was not elucidated, the authors concluded that its rhythmic and spontaneous nature provided evidence for a locomotor network able to function without rhythmic input.

1.4 Neuromodulation

In the wild, although stereotyped and repetitive, animal locomotor behaviour must be adaptable in the face of external appetitive and aversive stimuli. At the level of the neural substrates underlying locomotor behaviours, therefore, mechanisms must be in place to adjust behavioural output by adapting neural activity to particular situations. One way of providing this adaptability is through neuromodulation of the CPGs underlying locomotion.

Neuromodulation describes the alteration of CPG activity patterns through the activity of neuromodulators (often biogenic amines such as serotonin, dopamine and octopamine). These neuromodulators are able to significantly alter a variety

of CPG activity pattern properties including the frequency at which neural activity oscillations (or ‘bursts’) occur and the minimum thresholds that need to be reached for a CPG to begin to produce rhythmic bursts. Mechanistically, these changes to CPG activity patterns can be facilitated by neuromodulator-induced alterations to the sensitivity of ion channels, the production of neurotransmitters or the strength of synaptic connections between the neurons comprising a CPG (Harris-Warrick & Marder, 1991).

The relevance of CPG neuromodulation to behaviour is in the dynamic and constant adaptation of neural networks of fixed structure to produce multiple, separate rhythmic behaviours. Decapod crustaceans have served as key model organisms for the investigation of CPG neuromodulation and the stomatogasric ganglion (or ‘STG’) systems of these animals have been particularly useful due to their modulatory structures. The STG systems of these animals composed of several independent neural circuits that are able to generate multiple variations of their base oscillatory patterns (reviewed in Marder and Bucher, 2007).

The work of Harris-Warrick and Marder has been instrumental in the sequential categorisation and characterisation of these circuits and the models produced during the investigation of neuromodulatory dynamics in decapod crustacea have been fundamental for the analysis of this process in other organisms (Marder, 2012).

Regarding the systems controlling locomotor behaviour specifically, the biogenic amines dopamine and serotonin have been particularly heavily implicated in regulation of both mammalian and non-mammalian locomotion. For example, in the mouse, the role of the dopaminergic signalling system in

regulation of locomotion has been well-characterised (Krezel *et al.,* 1998; Kelly *et al.,* 1998; Medvedev *et al.,* 2013) and in the larval zebrafish, the CPG underlying swimming behaviour has been shown to be modulated by both serotonin (Brustein *et al.,* 2003) and dopamine (Thirumalai *et al.,* 2008; Jay *et al.,* 2015) expression. In *D. melanogaster* larvae, tyramine and octopamine have been shown to work in conjunction to adjust locomotor behaviour in situations of starvation by increasing excitability (Schützler *et al.,* 2019) and even in animals such as the mollusc *Pleurobranchae californica*, the A1/C2 neuron (which acts the swim central pattern generator) has been shown to be dependent on the serotonergic system via the modulation of synaptic strength through the 5HT2a and 5-HT7 receptors (Tamvacakis *et al.,* 2018). In addition to these examples, in *D. melanogaster larvae*, it has been demonstrated that mutations in the DvMAT gene (encoding a protein responsible for the transport of biogenic amines such as dopamine and serotonin) can also significantly reduce locomotion (Simon *et al.,* 2009).

1.5 *Drosophila melanogaster* as a model organism for the study of behaviour

1.5.1 The *Drosophila melanogaster* life cycle

Investigating aspects of the neural control of behaviour such as the structure of CPGs and the nature of neuromodulation requires the use of model organisms and, in particular, the fruit fly *D. melanogaster* presents many advantages.

The fruit fly life cycle at 25˚C (Figure 1.2A) consists of a 21-hour period of embryonic development followed by the hatching of the first instar (or ‘L1’) larva

(Chong *et al.,* 2018). The L1 larva constantly feeds and grows and, after 24 hours, a pulse of the hormone ecdysone triggers moulting of the cuticle and the larva begins the next stage of development as a larger, second instar (or 'L2') larva.

As with the L1, the L2 larva continuously feeds for 24 hours until another pulse of ecdysone triggers a second moult, and the larva begins the final stage of larval development as a third instar (or 'L3' larva). The L3 stage lasts for 48 hours but is split into two distinct sections. Early L3 larvae continue to constantly feed but a sudden high-titre pulse of ecdysone results in a stark behavioural change and larvae cease to feed, instead beginning to search for a suitable place to pupate (giving this stage of development the nickname of the "wandering" stage) (Andres *et al.,* 1993). Pupation lasts for approximately 3 to 4 days, in which time stark remodelling of the CNS occurs (Truman, 1990) as well as the development of adult appendages such as eyes, legs and wings before eclosion. In a lab setting *D. melanogaster* is relatively easy to culture and the overall length of the life cycle described above can be extended or shortened by temperature adjustment as convenient.

1.5.2 The genetic amenability of *Drosophila melanogaster*

It has been estimated that 65% of genes responsible for human diseases have homologues in flies (Ugur *et al.,* 2016) making insights gained about behavioural control (and particularly, how this is affected by neurodegenerative disease) extremely relevant for our understanding of this process in human beings. Above all, however, the main advantage of *D. melanogaster* is its

genetic amenability. The pioneering of *D. melanogaster* as a model organism by T.H. Morgan in the early 20th Century occurred in the context of his identification of the famous “white” mutation, and his subsequent studies of its heritability (Morgan, 1910). A century later, the ease with which mutations can be imposed onto *D. melanogaster* and the efficiency with which the effects of these mutations can be investigated have led to *D. melanogaster* becoming an organism of choice for genetic studies.

In the context of the neural control of behaviour, this genetic amenability is even more advantageous when the small size of the *Drosophila* CNS is considered. While the human brain is made up of approximately 86 billion neurons (Herculano-Houzel, 2012) and the mouse brain has been estimated at 71 million neurons (Herculano-Houzel *et al.,* 2006), the adult *Drosophila* CNS is made up of 100,000 neurons (Zheng *et al.,* 2018) and the larval CNS has been estimated to comprise 10,000 neurons at its largest extent during the L3 stage (Schleyer *et al.,* 2015).

1.5.3 The structure of the *Drosophila melanogaster* larval central nervous system

Structurally, the larval CNS is composed of two brain lobes and a ventral nerve cord (or ‘VNC’) (Figure 1.2B) which itself is divided into the suboesophageal zone, three thoracic neuromeres and eight abdominal neuromeres. The order of the neuromeres of the VNC corresponds to the order of the thoracic and abdominal segments of the larval body with motor output largely regulated in each segment by the motor neurons of each neuromere (Landgraf *et al.,* 1997).

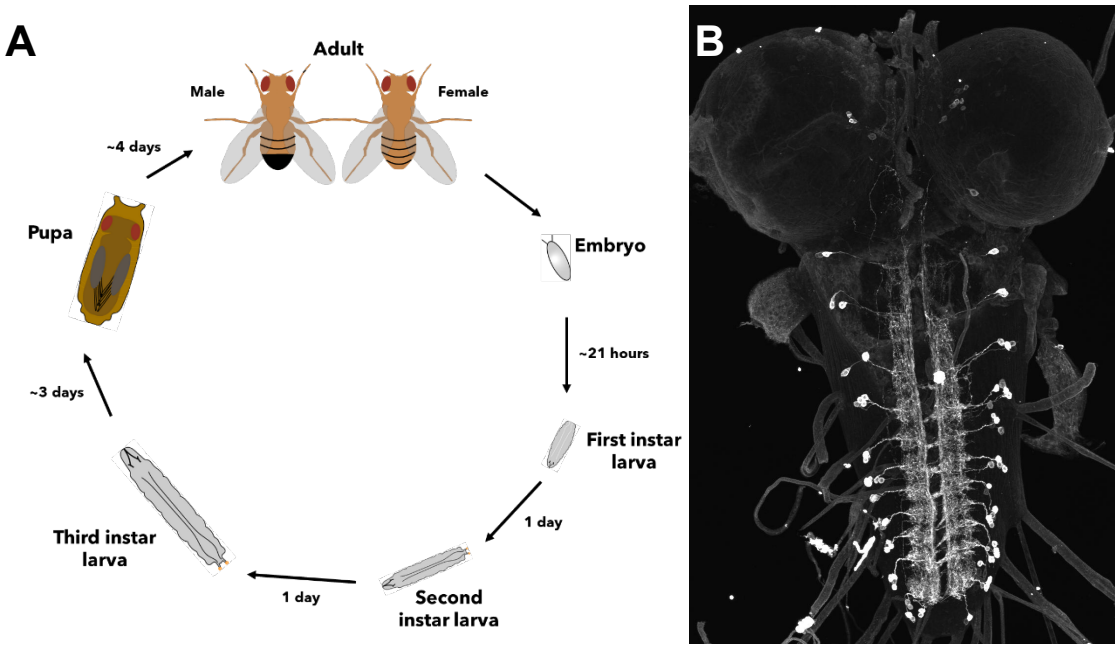

Figure 1.2 *Drosophila melanogaster* is a widely-used model organism to study the neural control of behaviour

(A) The *Drosophila melanogaster* life cycle. At 25˚C, the *D. melanogaster* life cycle lasts for approximately 10 days and begins with a period of embryonic development followed hatching. Hatched larvae then constantly feed and grow through three larval stages (or 'instars') before searching for a place to pupate once a critical weight has been reached. During pupation, the central nervous system is remodelled, and larval appendages grow before the eclosion of the adult fly. **(B) The larval central nervous system.** The larval central nervous system (or 'CNS') consists of two brain lobes and a ventral nerve cord (or 'VNC') which is analogous to the human spine. In this image, the Basin interneurons are highlighted in white and motor axons can be seen surrounding the VNC (Credit: Janelia FlyLight).

At the sensory level, the dendritic projections of multidendritic sensory neurons tile the body wall and eventually project into the neuropil where they contact downstream interneurons providing a route for sensory information to be processed internally (Grueber *et al.,* 2002). In addition to the multidendritic sensory neurons, sensory organs such as the chordotonal organs also have projections extending into the neuropil where they also contact downstream interneurons. The interneurons of the larval CNS act as signalling centres, facilitating the flow of information between sensory elements interacting with external stimuli and the motor components acting to facilitate behavioural output. These interneurons can produce excitatory or inhibitory neurotransmitter and are commonly present in a hemisegmentally repeated manner (i.e., one per hemineuromere of the VNC) but sometimes exist as large pairs of individual neurons with longer projections contacting upstream and downstream neurons along the length of the entire VNC and occasionally linking with the brain (Ohyama *et al.,* 2015; Tastekin *et al.,* 2015; 2018).

Information flow to the motor components flows via a group of interneurons termed ‘premotor’ interneurons (Zarin *et al.,* 2019) and motor output is facilitated by the co-ordinated innervation of body wall muscles in each segment by motor neurons (Landgraf *et al.,* 1997). The arrangement of the body wall muscles in each of the segments has been well characterised (Figure 1.3) and myotopic maps have been produced demonstrating how each motor neuron contacts its target muscle (Bate and Martinez Arias, 1993).

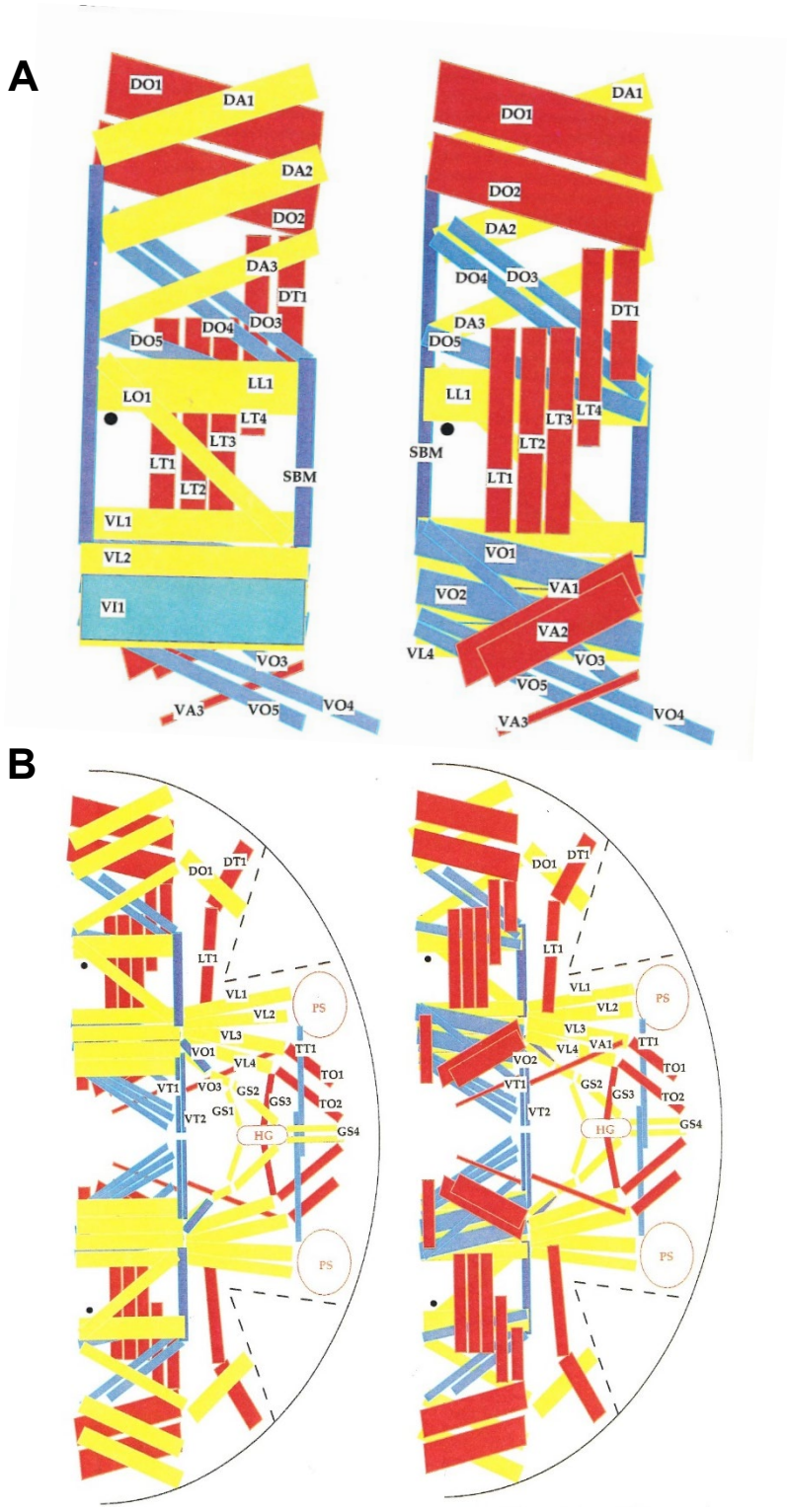

Figure 1.3 The internal arrangement of the larval body wall muscles (adapted from Bate and Martinez Arias, 1993)

(Legend on the following page)

(A) The arrangement of the body wall muscles in abdominal segments A1 to A7 (left, interior view; right, exterior view). The arrangement of the body wall muscles in the first seven abdominal segments of the larval body is consistent with muscles extending along longitudinal and transverse axes. Each muscle is innervated by a single “big bouton” motor neuron while groups of functionally-related muscles are simultaneously innervated by “small bouton” motor neurons. **(B) The arrangement of the body wall muscles in the posterior abdominal segments A7 and A8 (left, interior view; right, exterior view).** The arrangement of the body wall muscles in the terminal segment A8 is shown by the annotated muscles in the diagram. Although a similar arrangement that of the body wall muscles in segment A7, in A8 some muscles are not present including the lateral transverse muscles 2-4. (PS) Posterior spiracle. (HG) Hindgut.

The motor neurons are divided into big bouton (that contact one muscle) and small bouton (that contact groups of functionally related muscles) neurons are named according to the muscle they contact (which is, in turn, named according to its dorsoventral position in the segment).

The six major motor nerves present in each segment are the intersegmental nerve (or ISN), the transverse nerve (or TN) and the four branches of the segmental nerve (SNa, SNb, SNc and SNd) and the axons of each of the motor neurons in each abdominal segment (excluding A1) leave the CNS to contact target muscles via one of these (Landgraf *et al.,* 1997).

1.5.4 Binary expression systems for targeted gene expression in *Drosophila*

Although complex, the small size of the larval CNS therefore presents a good opportunity for direct circuit-to-behaviour correlation as well as the ability to examine the results of genetic manipulations relatively easily using binary expression systems for the targeting of functional effectors to specific neurons of interest.

The most widely used of these binary expression systems is the GAL4-UAS system developed by Brand and Perrimon in 1993 (Brand and Perrimon, 1993). The GAL4-UAS system consists of the yeast transcriptional activator protein GAL4 and its target enhancer sequence, termed the Upstream Activation Sequence (or ‘UAS’). In *Drosophila,* the expression of the GAL4 protein can be targeted to particular neurons via the linking of the GAL4 coding sequence to a cell-specific promoter sequence. Through genetic crosses, progeny is produced

carrying sequences encoding functional effectors downstream of UAS sequences in all cells, however in cells where GAL4 is also expressed, the interaction of GAL4 and the UAS sequence leads to the expression of the functional effector in a targeted manner. These functional effectors comprise a large toolkit with which researchers can manipulate neurons and dissect neuronal circuits. For example, the expression of fluorescent proteins can be targeted to the membranes (Lee and Luo, 1999) and cell bodies (Davis *et al.,* 1995) of neurons of interest as well as calcium indicators (Tian *et al.,* 2009; Akerboom *et al.,* 2012), channelrhodopsins (Zhang *et al.,* 2007), thermosensitive ion channels (Berni *et al.,* 2010) and permanent inhibitors of neural activity (Sweeney *et al.,* 1995).

One disadvantage of the GAL4-UAS system is the potential for off-target expression of GAL4 due to the shared expression of a particular promoter sequence. To address this issue, the intersectional “split-GAL4” system has been developed in which the activation domain (or ‘AD’) of the GAL4 protein is linked to a different promoter sequence to that of the GAL4 DNA-binding domain (or ‘DBD’) (Luan *et al.,* 2006; Pfeiffer *et al.,* 2010). When expressed in the larva, functional GAL4 protein is only reconstituted in cells expressing both the AD and DBD of GAL4 providing more specific spatial control over its expression (often down to the level of the single neuron).

Alternative binary expression systems more recently developed include the LexA-LexAop system developed in 2006 (Lai and Lee, 2006) and the Q system developed in 2010 (Potter *et al.,* 2010). These systems have been used in conjunction with the GAL4-UAS system to facilitate the simultaneous expression of multiple functional effectors and this strategy has been widely

adopted in the investigation of neural circuits via expression of optogenetic/thermogenetic stimulators of neural activity in conjunction with calcium indicators (Kim *et al.,* 2017; Simpson *et al.,* 2018).

In the *Drosophila* larva, the GAL4-UAS system has been used to demonstrate that the neuronal network underlying crawling behaviour forms in the absence of sensory input during embryonic development (Suster and Bate, 2002). Upon the abolishment of sensory input by the authors, embryos were found to still be capable of generating peristaltic waves in both directions during late development. In addition, although there was a marked shift in the proportion of forward to backward waves generated in sensory-deprived embryos – the fact that waves in both directions could still be generated supported the idea of a larval locomotor CPG able to function (even if not perfectly) without external input.

1.6 Neural circuits underlying *Drosophila* larval locomotor behaviour

1.6.1 Neural circuits underlying intersegmental co-ordination during crawling

More recently, approaches based on genetic screens have become progressively more commonly used to dissect the neuronal circuits underlying locomotor behaviours in adult and larval *Drosophila*. Typically, these genetic screens consist of the targeted expression of functional effectors to a collection of individual neuronal subsets using the GAL4-UAS system and large-scale, high-throughput analysis of the behavioural impact of activating these effectors. Where the manipulation of a neuron results in an interesting behavioural

change, the neurons involved are typically examined in more detail and their exact role in facilitating the behaviour of interest is determined (Ohyama *et al.,* 2015; Robie *et al.,* 2017; Tastekin *et al.,* 2018; Hiramoto *et al.,* 2021).

The application of this strategy, as well as the targeting of the expression of calcium imaging tools to motor neurons to demonstrate spontaneous nervous activity (Pulver *et al.,* 2015), has led to the identification of several neurons that communicate with each other to form circuits which, in turn, communicate with each other to form the locomotor CPG in the larva.

The propagation of peristaltic waves of muscular contraction throughout the larval body during locomotion requires the co-ordinated contraction and relaxation of each specific muscles in each segmental muscle group. A fundamental neural circuit that has been identified to facilitate this co-ordination is the A27h-GDL circuit. The A27h-GDL circuit comprises a hemisegmentally repeated pair of interneurons that function as an overall inhibitory network to prevent premature contraction of muscles in adjacent segments of the larval body (Fushiki *et al.,* 2016). In addition to this circuit, intersegmental co-ordination has also been shown to be facilitated by the activity of Ifb-Fwd and Ifb-Bwd neurons that act to regulate premotor neuron activity during forward and backward locomotion respectively (Kohsaka *et al.,* 2019) and the very recently identified Canon neurons which act as key intersegmental co-ordinators of sequential muscle relaxation (Hiramoto *et al.,* 2021).

1.6.2 Neural circuits underlying intrasegmental co-ordination during crawling

At the intrasegmental level, the co-ordination of muscular activity is also tightly regulated by specific neural circuits. During the period between late 2014 and mid-2016, four sets of interneurons key for facilitating this co-ordination of intrasegmental co-ordination were identified in work primarily led by the lab of Akinao Nose (University of Tokyo, Japan). Firstly, the activity of the inhibitory, period-positive median segmental interneurons (also known as “PMSIs” or “Loopers”) was found to facilitate intrasegmental co-ordination via the negative regulation of motor activity post muscular contraction. This inhibitory activity acts to limit the duration of motor neuron activity and promote a temporally precise sequence of muscle contraction (Kohsaka *et al.,* 2014). Subsequently, in 2015, the Glutamatergic Vento-Lateral Interneurons (or ‘GVLIs’) were identified via a screen of GAL4 lines for neurons showing fictive neural activity similar to the peristaltic waves observed during larval locomotion and were proposed to play a similar role to the PMSIs previously discussed. A key difference between the PMSIs and GVLIs, however, was that instead of solely temporal regulation, the GVLIs were proposed to also facilitate spatial regulation of intrasegmental motor neuron activity via the inhibition of motor activity once it reaches anterior segment borders (Itakura *et al.,* 2015).

The lateral locomotor neurons (or ‘LLNs’) were then identified by Yoshikawa and colleagues in early 2016 using a different approach to the previous studies (Yoshikawa *et al.,* 2016). Rather than the screening of neurons showing wave-like activity during fictive locomotion applied in the aforementioned studies, Yoshikawa and colleagues screened GAL4 lines based on whether

thermogenetic inhibition of neuronal activity with the temperature-sensitive allele of the gene, *shibire* (shi^{ts}) led to significant changes to the propagation of peristaltic waves in the L1 larva. The decision to use the L1 larva (as opposed to the more generally favoured L3 larva) stemmed from the reduced number of neurons facilitating easier identification of neurons producing the motor output as well as the potential for investigations of neuronal development during the temporally-proximal embryonic development stage. The expression of the calcium indicator GCaMP in the LLNs, revealed that their fictive activity occurs in a wave-like pattern similar to that of the PMSIs and GVLIs, and that this matched the overall propagation of the wave of intrasegmental motor activity during fictive locomotion suggesting a link between LLNs and the behaviour.

Finally, the cholinergic lateral interneurons 1 and 2 (or CLI1 and CLI2) were identified to be a member of the group of interneurons with wave-like fictive activity via a screen of calcium reporter expression in mid-2016. Hasegawa and colleagues identified the production of the excitatory transmitter acetylcholine by CLI1/2 as well as directly observing muscular contraction as a result of artificial CLI activation (Hasegawa *et al.,* 2016). In addition to these discoveries, the temporal proximity of motor neuron activity to CLI activation suggested that CLIs provide excitatory drive to motor neurons during locomotion however, the authors note that no behavioural effect is observed upon CLI inhibition suggesting a potential level of redundancy between CLIs and other premotor interneurons in the CNS.

1.6.3 Neural circuits underlying other locomotor behaviours

As well as forward/backward crawling, the neural substrates of behaviours also exhibited during locomotion such as bending and pausing have also been characterised to a degree. A key example of this is a study in which Heckscher and colleagues provide data implicating the asymmetrical activity of the eve-positive (or EL) interneurons in the regulation of body posture. The authors of the study demonstrate that the ablation of EL interneurons leads to a "randomised left-right asymmetric body posture" via the dysregulation of symmetrical muscle contraction between the two mediolateral halves of the larva and this significantly increases bending behaviour (Heckscher *et al.,* 2015). At the level of the neural circuit, a small group of EL interneurons was reconstructed using CATMAID and found to receive substantial input from proprioceptive sensory neurons and provide substantial output to dorsal motor neurons such as the U and RP2 motor neurons.

A sensorimotor neural circuit responsible for the regulation of larval pausing behaviour was subsequently identified by Tastekin and colleagues in 2018 (Tastekin *et al.,* 2018). The authors of the study firstly applied the genetic screen and high-throughput tracking of larval locomotion approach described above to identify the two descending PDM-DN neurons as neurons key for cessation of locomotion during chemotactic locomotion. They showed that at the behavioural level, the PDM-DN neurons promote the activity of the SEZ-based inhibitory interneuron SEZ-DN1 which in turn inhibits the generation of new peristaltic waves of muscular contraction from the posterior segments. In the context of a neural circuit, the study applies a CATMAID-based approach to reveal indirect inhibitory output to the A27h premotor neurons of the posterior

segments (part of the previously-described GDL-A27h network) and anatomical observations reveal likely input from the lateral horn and mushroom bodies of the brain.

1.7 Methodological approaches for investigating *Drosophila* larval locomotion

Although the repertoire of motor behaviour performed by the *Drosophila* larva comprises several distinct behaviours (Green *et al.,* 1983), the larva spends the majority of its time performing exploratory searches for food in an attempt to grow and reach a critical weight necessary for the process of metamorphosis (Mirth *et al.,* 2005). The locomotor behaviour that underpins these searches comprises a combination of forward/backward crawling, turning and pausing (Berni *et al.,* 2012) and the predominance of locomotor behaviour has led to the neural substrates underlying these behaviours being investigated at length (reviewed in Kohsaka *et al.,* 2017 and Clark *et al.,* 2018).

At between 0.5 and 5mm in length (depending on developmental stage) (Schumann and Triphan, 2020), the relatively small size of the *Drosophila* larva has enabled the development of high-throughput, tracking-based approaches designed to analyse videos of groups of free crawling larvae in detail and extract information on several locomotor parameters simultaneously. Examples of these softwares include JAABA (Kabra *et al.,* 2013), and FIMTrack (Risse *et al.,* 2017) however, softwares originally designed for tracking *C. elegans* locomotion such as wrMTrck (Brooks *et al.,* 2016) and the “Multi Worm Tracker” (Swierczek *et al.,* 2011) have also increasingly been adapted for use with

Drosophila larvae. Several large-scale studies have taken advantage of these high-throughput tracking methods to reveal statistically significant insights about stimulus-driven decision making and various other locomotor behaviours (Ohyama *et al.,* 2013; Almeida-Carvalho *et al.,* 2017; Masson *et al.,* 2020).

The application of these tracking approaches often results in the production of large datasets, containing information on several locomotor parameters for each of the larvae tracked and this presents an opportunity to further characterise the relationships between these parameters. One of the methods that can be used to gain insight into these relationships is principal component analysis (or 'PCA'). PCA is a technique used to reduce the dimensionality of large datasets and identify specific variables which contribute disproportionately to the overall variance of large datasets (Jolliffe and Cadima, 2016). In the context of behavioural control, PCA has been used to reveal insights about the body shape of the *Drosophila* larva during locomotion (Szigeti *et al.,* 2015) as well as in other, similar animals, such as *C. elegans* (Stephens *et al.,* 2008).

1.8 Mathematical and physical descriptions of *Drosophila* larval locomotion

The use of high-throughput tracking (and subsequent analysis) has also facilitated the production of physical descriptions of larval locomotion (Loveless *et al.,* 2021). These physical descriptions can then guide subsequent investigations into the neural basis of the behaviour by informing predictions about the architecture of the underlying neuronal network which can then be consolidated into larger mathematical models.

One mathematical model that has been used to characterise larval locomotion in *D. melanogaster* is the “Lévy Walk”. A Lévy Walk (sometimes called a Lévy Flight) is a random walk model in which search behaviour is optimised when the distribution of flight lengths (or in the case of the larva, run lengths) follows an inverse square power-law (Viswanathan *et al.,* 1999). In practice, foraging behaviour fitting a Lévy Walk model is characterised as containing periods of movement in a limited area containing smaller “steps” occasionally interspersed with periods of longer “steps” in which the animal travels to a new area (Viswanathan *et al.,* 2001).

Although it has been suggested that the Lévy Walk model best explains *Drosophila* larval locomotion, it has been proposed in a study by Gunther and colleagues that, in fact, larval locomotion is best characterised by a bimodal persistent random-walk model, in which the direction of each crawling “run” is constantly influenced by the direction of the previous run and not by a consistent power-law (Günther *et al.,* 2016).

Following this, Sims and colleagues demonstrated that the blocking of synaptic activity in the brain leads to a state in which intrinsically generated motor patterns drive substrate exploration that closely match the optimal Lévy walk model (Sims *et al.,* 2019) and thus the mathematical model best describing larval locomotion remains a topic of debate.

1.9 The genetic control of behaviour

At the level of the neural control of locomotion, while the activities of groups of neurons forming CPGs are instrumental for regulation of behavioural output, the genomic content of each neuron as an individual is also fundamental.

Only a year after the publication of the Hodgkin-Huxley model in 1952, the crystal structure of DNA was resolved through the combined work of James Watson, Francis Crick and Rosalind Franklin (Watson and Crick, 1953). In relation to behavioural study, this discovery prompted questions about how the expression of genes within the cells specifically underlying the exhibition of behaviour related to functional behavioural output. In microscopic, unicellular organisms such as the bacteria *Escherichia Coli* and the protist *Paramecium aurelia*, for both of whom locomotor behaviour is key as it facilitates the search for nutrition, genetic mutation has been shown to significantly alter chemotactic and directional locomotion, respectively (Adler, 1969; Kung, 1971). Work in more complex, multicellular organisms on the genetic control of behaviour was then pioneered throughout the 1970s by Seymour Benzer (based the California Institute of Technology) and Sydney Brenner (based at the University of Cambridge).

Using *D. melanogaster* as a model system, work led by the lab of Seymour Benzer developed a pioneering mosaic system that led to the elucidation of the relationships between the control of behaviour in the adult fly and the spatial expression domains of specific genes (Hotta and Benzer, 1970; 1972; 1976). Simultaneously, through a large-scale screen of mutations imposed upon the (then new) model organism *C. elegans* carried out by Sydney Brenner, 77

mutations were identified that significantly affected the control of locomotor behaviour (Brenner, 1974). The results of these studies were foundational for the burgeoning field of “behavioural genetics” demonstrating that, in complex organisms, gene expression had a direct role in the regulation of functional behavioural output.

At the level of the process of gene expression itself, the concept of the so-called “central dogma” of molecular biology had originally been postulated by Crick in a, now famous, 1957 lecture (Cobb, 2017). The subsequent discovery of the reverse transcriptase enzyme by Baltimore (Baltimore, 1970) and Temin (Temin and Mizutami, 1970) therefore, resulted in some controversy but the central principle of irreversible information flow from DNA to protein remained valid, even if via the intermediate molecule RNA. The addition of the reverse transcription step to the understood process of gene expression opened more questions about the fine-tuning of gene expression and multiple routes through which gene expression could be regulated at the “post-transcriptional” level were subsequently identified.

For example, the formation of ribonucleoprotein (or ‘RNP’) complexes between mRNA transcripts and RNA-binding proteins (reviewed in Glisovic, 2008) can alter gene expression through the prevention of secondary mRNA structure formation (Portman and Dreyfuss, 1994) and, in the context of disease, mutations that affect RNP formation have been shown to lead to dysregulated mRNA trafficking and translation which, in turn, contribute to disease pathologies (reviewed in Thelen and Kye, 2020). In addition to RNA binding proteins, the alternative splicing of mRNA transcripts (reviewed in Kim *et al.,* 2008), alternative polyadenylation (reviewed in Tian and Manley, 2017) and

RNA editing (reviewed in Gott and Emeson, 2000) have all also been identified as mechanisms through which the levels of gene expression within a cell are regulated according to context. One mechanism for post-transcriptional regulation of gene expression that has been shown to be evolutionarily conserved, functionally important and key for organism development, however, is microRNA (or 'miRNA) based regulation of gene expression.

1.10 microRNAs

1.10.1 The discovery of microRNAs

miRNAs are small, non-coding RNA molecules that are typically 20-22 nucleotides long (Bartel, 2004) and were first discovered in 1993 (described in a study led by the lab of Victor Ambros based at Harvard University, USA). In this study, Lee and colleagues performed a genetic screen investigating the temporal control of development in *C. elegans* and cloned the *lin-4* gene (which was already known to negatively regulate the larval development regulator *lin-14* (Ambros and Horvitz, 1987; Ambros 1989)). After cloning the *lin-4* gene, however, Lee and colleagues discovered that it did not encode a protein and, in fact, encoded a pair of small (22 and 61 nt) RNA transcripts that were complementary to a sequence in the *lin-14* transcript's 3' untranslated region (or 'UTR'). This, in combination, with the previous identification of *lin-4* as a negative regulator of *lin-14* expression, led the authors to suggest that "*lin-4* regulates *lin-14* translation via an antisense RNA-RNA interaction" (Lee *et al.,* 1993). The regulation of gene expression via antisense mechanisms involving RNA transcripts had been previously identified in the natural world but it was

noted by Lee and colleagues that these mechanisms were mainly confined to antisense RNA interactions at the 5 ’UTR end of target mRNA transcripts. They, therefore, suggested that this *lin4-lin14* interaction may represent a novel mechanism for regulation of gene expression.

Indeed, the level of conservation of this particular mechanism in other animals remained unknown for years as *lin-4* itself was initially not found to be conserved in other organisms. The later discovery of the *let-7* gene however, and its regulation of developmental transition in *C. elegans* in a similar fashion to *lin-14*, revolutionised the field of small RNA biology. *Let-7* was the first of these 3’ UTR targeting, small RNAs shown to be evolutionarily conserved in other organisms (including *Drosophila*) via the work of Pasquinelli and colleagues (Pasquinelli *et al.,* 2000) and these particular small RNAs were eventually termed microRNAs (or ‘miRNAs’) (Lagos-Quintana *et al.,* 2001; Lau *et al.,* 2001; Lee and Ambros*,* 2001).

1.10.2 Canonical and non-canonical microRNA biogenesis

The majority of miRNA biogenesis begins with the transcription of the primary miRNA transcript (or ‘pri-miRNA’) by RNA polymerase II. This transcript contains a self-complementary sequence that spontaneously forms a hairpin loop structure when cleaved from the primary miRNA transcript by the Drosha-DGCR8 (or ‘Pasha’ in *Drosophila* (Landthaler *et al.,* 2004)) microprocessor complex, resulting in a free ‘pre-miRNA’ hairpin loop. After export from the nucleus via the nucleocytoplasmic shuttler protein Exportin 5 (Lund *et al.,* 2004), the cytoplasmic Dicer enzyme then cleaves this hairpin loop, resulting in

a duplex of complementary miRNAs (these miRNAs, when separate, are referred to as the 3p- and 5p- variants of a miRNA according to the arm of the hairpin that the miRNA comes from). Mature 3p- or 5p- miRNA then associates with the Argonaute protein which, in turn, associates with a variety of proteins (Kawamata and Tomari, 2010) to form the RNA-induced silencing complex (or 'RISC'). The remaining 3p or 5p miRNA is degraded simultaneously and the activated miRNA-RISC then targets complementary seed sequences mostly found in the 3 'UTRs of mRNA transcripts. For years, it remained unclear exactly how active small RNA-RISC complexes (referred to here as 'loaded' RISC complexes) were able to specifically target mRNAs containing complementary sequences however, in 2007, Ameres and colleagues demonstrated that the loaded RISC complex transiently contacts several single-stranded RNAs in the cytoplasm. RNAs that have folded to form secondary structures are unable to be unfolded by the loaded RISC complex and this greatly reduces the chance for off-target interactions. When contact between loaded RISC complexes and single-stranded mRNA is successful, however, a minimal thermodynamic threshold for stable association is determined by the 5' section of the small RNA in the RISC complex (Ameres *et al.,* 2007).

While the aforementioned steps of miRNA biogenesis represent the majority of cases (and, therefore, comprise the 'canonical' pathway (Figure 1.4), alternative biogenesis mechanisms have also been identified that, for example, use different RNA polymerases or do not require cleavage of the pri-miRNA transcript by the Drosha-DGCR8 microprocessor complex (Ruby *et al.,* 2007).

The first 'non-canonical' pathway for miRNA biogenesis discovered facilitated the biogenesis of the miRNAs known as 'miRtrons'. MiRtrons are miRNAs that

are produced from the splicing of particular introns from mRNA transcripts (which themselves, encode functional proteins). During miRtron biogenesis, these spliced introns (which contain complementary sequences) spontaneously form a lariat structure in which the 5' splice junction is linked to the 3' branch point (Okamura *et al.,* 2007). This lariat is debranched by the lariat debranching enzyme, Ldbr and subsequently adopts the folded hairpin pre-miRNA structure which is exported via Exportin-5 and undergoes the final steps of the canonical miRNA biogenesis pathway. It has been suggested that the independent evolution of the miRtron biogenesis pathway in mammals, *C. elegans* and the Drosophilds occurred as independent parasitisations of an existing miRNA biogenesis pathway (Westholm and Lai, 2011) and this suggests a potential functional significance to the development of this method of miRNA production.

1.10.3 The functional role of microRNAs

At the functional level, miRNAs act as post-transcriptional, negative regulators of gene expression (Bartel, 2004). By binding to complementary sequences mostly found in the 3'UTR of target mRNA transcripts, they prevent the translation of these transcripts into protein. These complementary sequences (or 'binding sites') can be fully or partially complementary to the mature miRNA sequences and, in fact in animals, partial complementarity is more common. It has been shown that of the approximately 22 nucleotides usually comprising a mature miRNA sequence, only the first 8 or so are highly complementary to the binding site of a target mRNA transcript. These 8 nucleotides are, therefore, known referred to as the 'seed sequence' of the miRNA.

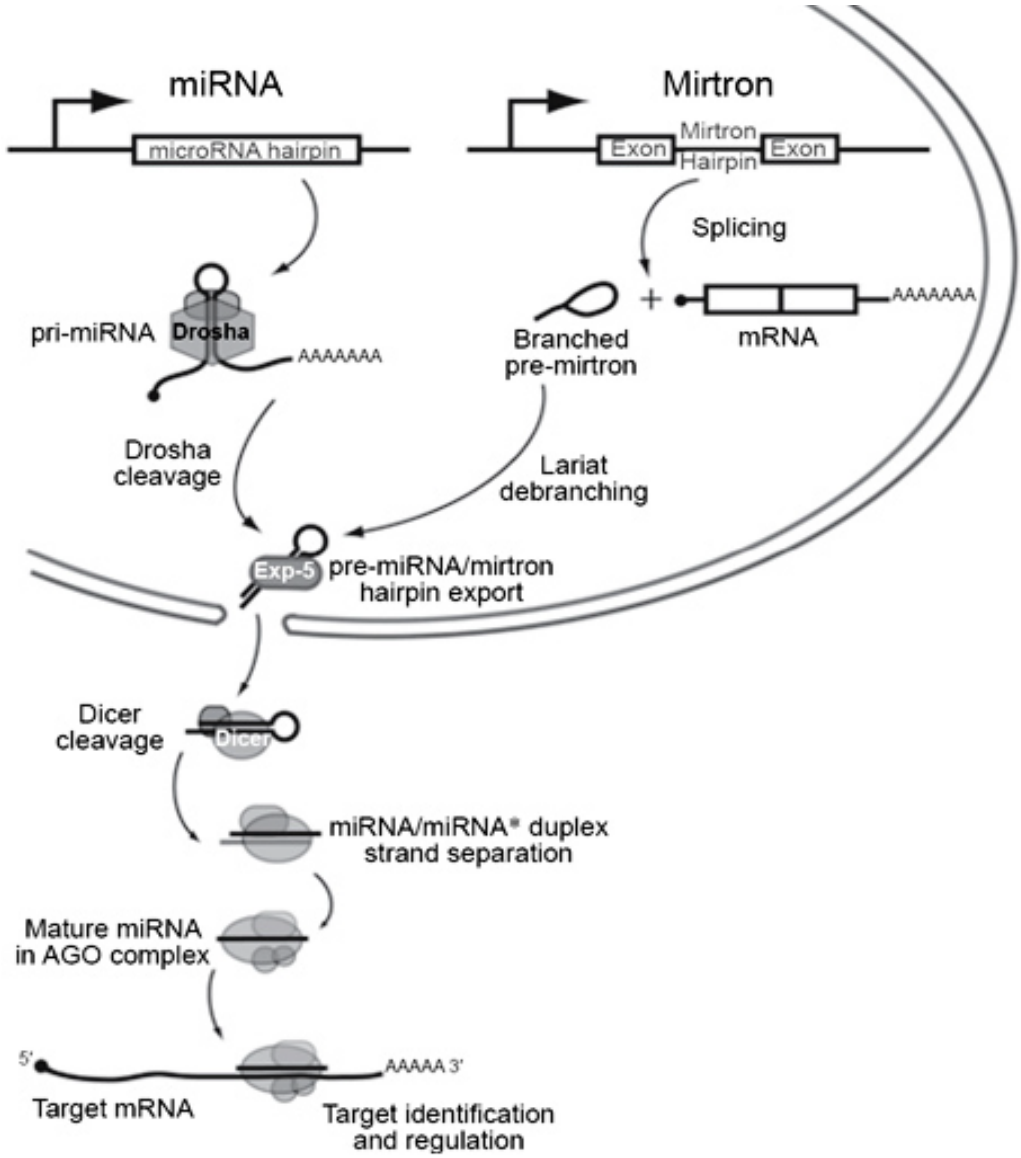

Figure 1.4 The canonical and non-canonical miRNA biogenesis pathways (adapted from Liu *et al.,* 2008)

A schematic demonstrating the canonical biogenesis of miRNAs as well as the non-canonical biogenesis of miRNAs from miRtrons. Before export from the nucleus, pri-miRNAs in the canonical pathway are cleaved by the Drosha-DGCR8 complex whereas miRtrons produced via mRNA splicing spontaneously adopt lariat conformations which are debranched. After export from the nucleus into the cytoplasm, miRNAs are processed in the same way in both biogenesis pathways.

The methods by which miRNAs (once bound to target mRNAs) prevent translation remain a topic of investigation. It has been shown that, once bound to target mRNA transcripts, miRNAs inhibit the initiation of translation which then results in the subsequent degradation of mRNAs (Thermann and Hentze, 2007; Bazzini *et al.,* 2012).

It has also been postulated however that the inhibition of gene expression by miRNAs is not directly related to translational machinery but rather, that translation is prevented by an increase in the likelihood of mRNA degradation by surrounding nucleases before the miRNA-bound transcript can even interact with ribosomes (reviewed in Ameres and Zamore, 2013). Finally, Tat and colleagues have identified a potentially overlooked mechanism in which miRNA-associated mRNAs are degraded by cellular machinery while active translation is occurring. In this model, once ribosome-associated mRNAs are decapped, the Argonaute protein of the RISC associated with the bound miRNA recruits the GW182 protein which, in turn, recruits cellular machinery for deadenylation; increasing the likelihood of mRNA degradation by the exonuclease XRN1 (Tat *et al.,* 2016).

1.10.4 The genomic context of microRNAs

Within the genome, miRNAs exist as standalone genes or as part of co-transcribed ‘clusters’ (Kabekkodu *et al.,* 2018). These co-transcribed miRNA ‘clusters’ may serve to reinforce repression of gene activity by combinatorial repression of single host genes, or the simultaneous repression of functionally-related genes expressed by host cells. The co-transcription of miRNA clusters

in this way can lead to the construction of vast gene regulatory networks with the multiple interactions of miRNAs with target mRNAs leading to domino effects that overall serve to regulate key processes within the cell itself.

In *Drosophila*, for example, the miRNA *let-7* is part of a co-transcribed cluster with *miR-100* and (the later identified fly homologue of *lin-4*, *miR-125* (Lagos-Quintana *et al.,* 2002)). These miRNAs have been shown to regulate a variety of biological processes across different tissues and stages of *Drosophila* life. Interestingly, this includes the demonstration of a role for *let-7* and *miR-125* in the temporal regulation of development during fly metamorphosis suggesting a conservation of its role between *C. elegans* and *D. melanogaster*. Even when miRNAs are not co-transcribed in these clusters, evidence exists to suggest that genetically distanced but sequentially related miRNAs can act to simultaneously repress functionally-related genes (Smibert and Lai, 2010).

1.10.5 microRNA conservation

miRNAs have also been found to be widely conserved between species and in humans, over 60% of protein-coding genes form miRNA-mRNA target interactions that are conserved between vertebrates (Friedman *et al.,* 2009). In addition, over half of *C. elegans* miRNAs (identified at the time of publication in 2008) have been shown to also be conserved in *D. melanogaster* and humans (Ibáñez-Ventoso *et al.,* 2008). In combination with results showing that miRNAs comprise about 1% of predicted genes in these three species (Lai *et al.,* 2003; Lim *et al.,* 2003a; Lim *et al.,* 2003b), regulation of gene regulatory networks by

miRNAs has been shown to be a fundamental process by which gene expression is tightly co-ordinated in evolutionarily distinct organisms.

In terms of *D. melanogaster,* the advent of high-throughput sequencing approaches has led to the number of identified miRNAs in the *Drosophila* genome steadily rising over time from 21 in 2001 (Lagos-Quintana *et al.,* 2001) to 258 as of 2018 (miRBase Release 22.1, 2018). These 258 miRNA sequences, in turn, encode 469 mature miRNA sequences (via the production of 3p and 5p sequences in most cases) (Kozomara & Griffiths-Jones, 2014) with vast regulatory influence over *Drosophila* cellular development and function (reviewed in Enright *et al.,* 2003; Jones and Newbury, 2010 and Carthew *et al.,* 2017).

1.10.6 microRNA target prediction algorithms

The identification of miRNAs has also led to the development of *in silico* platforms, designed to enable researchers to efficiently predict the likelihood of *in vivo* binding between a miRNA and its target mRNA transcript. By combining algorithms that consider factors such as the number of sequences present in a 3' UTR which are complementary to a given, the theoretical free energy released during miRNA-mRNA binding and the level of conservation of each miRNA-mRNA interaction – numerous target prediction softwares have been created.

Relatively quickly after the identification of the *let-7* miRNA cluster, *D. melanogaster* became the first organism for which large-scale prediction of miRNA targets was developed (Stark *et al.,* 2003). After preparing a database

of 3’ UTR sequences conserved between the Drosophilids *D. melanogaster and Drosophila pseudoobscura,* Stark and colleagues screened these sequences for potential miRNA targets (considering the aforementioned features of miRNA-mRNA interaction) and identified experimentally provable interactions.

Since this publication, a multitude of target prediction algorithms have been developed including miRanda (Enright *et al.,* 2003), TargetScan (Lewis *et al.,* 2003) and PITA (Kertesz *et al.,* 2007). These algorithms all apply distinct methodologies to the prediction of miRNA-mRNA target interactions (reviewed in more detail by Mazière *et al.,* 2007). miRanda, for example, primarily takes base pairing and conservation into account over predicted thermodynamic stability while PITA relies heavily upon predicted thermodynamics to determine the likelihood of a predicted interaction *in vivo.* The application of target prediction softwares in general, however, has proven to be useful in the identification of *in vivo* interactions with functional consequences for the fly (and other organisms) and algorithms are being continually refined to the current day (Agarwal *et al.,* 2015; Bertolazzi *et al.,* 2020; Mohebbi *et al.,* 2021).

1.11 The roles of microRNAs in the central nervous system

In the context of neural development, miRNA-based regulation of gene expression has been shown to play a role in the normal development of a functioning CNS in a variety of vertebrate and invertebrate organisms.

At the level of cell fate determination during the earliest stages of life, the conserved miRNAs *miR-9* and *miR-124* have both been well characterised as repressors of neural differentiation and growth regulators in mice (Zhao *et al.,*

2009; Mokabber *et al.,* 2019), zebrafish (Leucht *et al.,* 2008) and the western clawed frog *Xenopus tropicalis* (Bonev *et al.,* 2011; Baudet *et al.,* 2011). It has also been shown that in the *Drosophila* genome*,* the removal of *miR-9a* expression (and subsequent upregulation of the expression of the transcription factor, *senseless*) leads to the ectopic development of sensory organ precursors (Li *et al.,* 2006).

The apparent ubiquity of gene regulation in the nervous systems of the aforementioned animals by *miR-9* homologues (and the subsequent discovery of *miR-9* in the nervous cells of the amphioxus (Candiani *et al.,* 2011) and Platynereis (Christodoulou *et al.,* 2010)) has led to its suggestion as a potential "ancestral characteristic of bilaterian animals" (Coolen *et al.,* 2013). In addition to *miR-9* homologues, several other miRNAs including *bantam* (Parrish *et al.,* 2009), *miR-124* (Sun *et al.,* 2012) and *miR-7* (Li *et al.,* 2009; Caygill and Brand, 2017) have all also been shown to play key roles in neural differentiation and specification.

1.12 microRNA-based regulation of behaviour

It follows, therefore, that removal or alteration of miRNA expression can lead to significant changes to animal behaviour.

In the African clawed frog *Xenopus laevis*, for example, miRNA-based negative regulation of the transcription factors *Pax6* and *Bcl11b* has been shown to facilitate the switching of neurotransmitter production in accessory olfactory bulb neurons necessary for development of kin attraction during early life (Dulcis *et al.,* 2017). In the mouse, miRNA regulation of behaviour has been more

thoroughly studied in the context of disease and several changes to miRNA expression that occur during the exhibition of disease-associated behaviours have been identified (reviewed in Bushati and Cohen, 2008 and Issler and Chen, 2015). An example of miRNA-based behavioural regulation in mice that is not related to disease has recently been identified by Watts and colleagues, who have examined the role of the conserved miRNA *miR-210* in neuronal function and cognitive behaviour (Watts *et al.,* 2021). The results of this study found that at the behavioural level, flexibility (i.e., the ability to adapt behaviour to match changes in the external environment) was significantly increased in *miR-210* knockout mice and the authors suggest that the behavioural change may occur as a result of derepression of the HIF-1α transcription factor.

1.13 microRNA-based regulation of neuromodulation

The role of miRNAs in the regulation of CPG neuromodulation (which itself is necessary to provide behavioural flexibility in the face of changing external circumstances) has been examined in few studies and to date, none have demonstrated conclusive mechanistic links between the two although links have been postulated.

For example, in songbirds, the neurons controlling song produce spontaneous activity at different rates in the spring and summer (Meitzen *et al.,* 2007) and this has been hypothesised to be linked to high expression of the miRNA *miR-135* in these neurons (Larson *et al.,* 2015). *miR-135* in other systems has been shown to regulate components of the serotonergic system (Issler *et al.,* 2014), a system which has itself been linked to the modulation of song characteristics in

the zebra finch (Wood *et al.,* 2013). Larson and colleagues suggest, therefore, that *miR-135* may regulate changing song throughout the year by regulating the serotonergic system in a season-dependent manner.

Building on this, in mice, the removal of the HTR1B serotonergic receptor significantly increases aggressive behaviours (Saudou *et al.,* 1994) and evidence exists to suggest that in humans, expression of the receptor is regulated by the conserved miRNA *miR-96* and that modulation of this mRNA-miRNA target interaction also correlates with aggressive behaviours (Jensen *et al.,* 2008).

1.14 microRNAs and the control of motor behaviour

At the level of miRNA-based regulation of the systems driving motor behaviour specifically, examples are present throughout the animal kingdom of alterations to this regulation affecting the ability to perform stereotyped locomotor behaviour.

miR-143 has been shown to be involved in the control of motor behaviour related to schizophrenia in mice. *miR-143* normally inhibits the expression of the signalling protein neuregulin-1 in neuronal cells but upon activation of the D2 dopamine receptor (which is commonly activated by the hallucinogen, PCP), *miR-143* levels fall, and neuregulin-1 expression is derepressed. At the behavioural level, this leads to hyperlocomotion and the authors suggest that this mechanism could be a target for the development of antipsychotic drugs (Wang *et al.,* 2019b).

In *C. elegans*, a study led by Sun and colleagues has identified a group of 9 miRNAs that are required for the suppression of locomotion behaviour after exposure to simulated microgravity (Sun *et al.,* 2020) and in zebrafish, locomotor behaviour at the larval and juvenile stages has been shown to be regulated by the activities of the neurally-expressed *miR-9/9** and *miR-153c* (Tal *et al*. 2012).

1.15 microRNAs and the control of *Drosophila* motor behaviour

In the fruit fly *D. melanogaster,* studies of miRNA-based regulation of motor behaviours have mostly demonstrated links between the control of circadian locomotion and the expression of miRNAs. To date, *let-7* (Chen *et al.,* 2014a), *miR-124* (Zhang *et al.,* 2016), *miR-92a* (Chen *et al.,* 2017) *miR-210* (Niu *et al.,* 2019) and *miR-263a* (Nian *et al.,* 2020) have all been shown to regulate circadian locomotion in the adult fly through the regulation of genetic targets in the neural substrates controlling the overall circadian rhythm.

At the larval stage, the first links between the control of locomotion and miRNA expression were drawn in a 2005 study by Sokol and Ambros in which it was shown that the removal of the miRNA *miR-1* was sufficient to severely reduce the growth of body wall muscle upon food consumption post-hatching. *miR-1* mutant larvae therefore exhibited severe locomotor defects, often becoming paralysed and dying (Sokol and Ambros, 2005) however, the exact target gene regulating this process remains unidentified.

In terms of the neural control of larval locomotion, *miR-8* and *miR-1000* have also both been shown to affect the development of the neural components

underlying locomotion in larvae. *miR-1000*, for example, has been shown to negatively regulate the expression of the glutamate transporter, VGlut. Verma and colleagues demonstrate that derepression of Vglut expression leads to excessive glutamate intake and subsequent early-onset neuronal death through excitotoxicity. In addition to this, at the larval neuromuscular junction (or 'NMJ'), derepression of Vglut by removal of *miR-1000* leads to an excess of synaptic glutamate release (Verma *et al.,* 2015). In a similar fashion, Loya and colleagues have demonstrated that *miR-8* regulates the development of synapses at the NMJ and that modulation of *miR-8* expression using a miRNA "sponge" results in severe defects in the morphological complexity of a representative neuron-to-muscle connection (Loya *et al.,* 2009). In a later study, Loya and colleagues build on this to demonstrate that *miR-8* directly regulates synapse structure through repression of *enabled* (or '*VASP'*) expression and that this process, in turn, regulates excitatory synapse potential production (Loya *et al.,* 2014). Finally, the miRNAs of the 310 cluster have also been shown to negatively regulate synaptic strength at the NMJ (Tsurudome *et al.,* 2010) however, the behavioural consequence of this is unclear.

At the level of development, miRNAs had, therefore, been shown to play important roles in the control of the systems underpinning behaviour. Examples of fully-elucidated mechanisms for miRNA-based regulation of functional behavioural output in the larva, however, have remained rare. One example that has been discerned is the mechanism by which the miRNA, *miR-iab-4* regulates the complex self-righting response in L1 and L3 larvae (Picao-Osorio *et al.,* 2015; Issa *et al.,* 2019). Through regulation of the Hox gene *Ultrabithorax*, *miR-iab-4* has been shown to regulate the neural activity of the LT-1/2 motor

neurons in larvae to facilitate timely self-righting behaviour. In addition to *miR-iab-4*, *miR-263b* has also been shown to regulate self-righting behaviour through repression of expression of the transcription factor atonal in the sensory components of the larval peripheral nervous systems (Klann *et al.,* 2020). The identification of several other miRNAs that purportedly play a role in the control of this motor response through a genetic screen carried out by Picao-Osorio, Lago-Baldaia and colleagues also suggests that the role of miRNAs in the regulation of motor behaviour in the larva is more pervasive than previously considered (Picao-Osorio *et al.,* 2017).

1.16 A previous investigation of the role of microRNAs in the control of *Drosophila* larval locomotor behaviour

Building on this idea, during the production of this thesis, a study was produced by Donelson and colleagues in which the roles of miRNAs in the control of locomotor behaviour was examined in the adult fly and the L2 larva. Using the aforementioned miRNA “sponge” technique to remove miRNA expression in different spatial domains and at different times during development, the authors remark that 20 of the “miR-SP” lines tested showed significant changes to average crawling speed and that significant changes were also observed to other locomotor parameters such as the average length of activity bouts and average rates of acceleration. The authors of the study suggest that their methodology may have resulted in the underestimation of the pervasiveness of miRNA effects on locomotion and this is an idea explored further in Section 5.3 after our own screen for locomotor defects in miRNA mutant *Drosophila* larvae.

1.17 Aims and outcomes of the thesis

This thesis aims to answer the following questions:

1) What is the structure of the minimal neuronal circuit underlying larval self-righting behaviour?
2) Do the neurons of the self-righting wiring diagram function as a circuit to control self-righting *in vivo*?
3) What is the impact of miRNAs on the regulation of larval locomotion?
4) Through what mechanisms do miRNAs regulate larval pausing behaviour?

To address our first question, we used the CATMAID tool (Saalfeld *et al.,* 2009) to facilitate a combination of *in silico* neuronal reconstruction and connectomic analysis which, in turn, resulted in the production of a complex wiring diagram of neurons connected to the LT-1/2 motor neurons (previously identified as key for self-righting behaviour by Picao-Osorio and colleagues) (Picao-Osorio et al. 2015).

Building on this, we addressed the question of the wiring diagram's *in vivo* function as a circuit by performing a screen of thermogenetic inhibition, inhibiting the activity of each neuron in the wiring diagram, and analysing the effects on the time taken by larvae to self-right. The results of this screen revealed that the vast majority of neurons in the wiring diagram play crucial roles in the control of self-righting behaviour – validating the wiring diagram as a functional neural circuit *in vivo*.

Having established this cellular map, we then built on a previously reported study from this lab in which self-righting behaviour was shown to require the normal expression of several miRNAs (Picao-Osorio *et al.,* 2017), investigating the impact of miRNAs on the regulation of larval locomotion. This investigation consisted of a screen of 84 *Drosophila* miRNA mutants for locomotor defects at the L1 stage with 17 of these mutants also being tested for locomotor defects at the L3 stage. The results of this screen revealed an extremely pervasive reduction in average crawling speed among the mutants as well as significant changes to bending and pausing behaviours.

With such widescale effects, we used principal component analysis to establish that changes to pausing behaviours represented the majority of variance in our locomotor dataset. This prompted us to examine mechanisms through which miRNAs regulate pausing behaviour and for this, we examined *ΔmiR-133* mutant larvae in detail, revealing that significant changes to the serotonergic system in the mutant lead to aberrant head-rearing behaviour.

Chapter 2

Materials and Methods

2.1 CATMAID

2.1.1 Neuronal reconstruction using CATMAID

Reconstruction of neurons was performed using the Collaborative Annotation Toolkit for Massive Amounts of Image Data (CATMAID) approach developed by Pavel Tomančák and colleagues (Saalfeld *et al.,* 2009; Schneider-Mizell *et al.,* 2016). Briefly, neurons were identified in electron microscopy (EM) images based on the shape of their outlines as well as features including mitochondria, smooth endoplasmic reticulum and microtubules. When a neuron was identified in a single EM image, a “node” was placed by clicking once. Scrolling through EM images, the location of the neuron of interest was tracked and a skeletonised version of the neuron’s morphology was built by placing nodes on each EM image (“tracing”). Where neuronal projections followed a single direction across several images, nodes were occasionally placed on non-consecutive images with CATMAID automatically annotating the intervening images with “virtual” nodes.

2.1.2 Reconstruction of synapses using CATMAID

Synapses were identified in EM images by their characteristic features including a dark, T-shaped synaptic cleft, pre/post-synaptic vesicles and the common presence of a mitochondrion near the pre-synaptic site. When a synapse was identified between neurons, the pre-synaptic neuron’s node was connected to the node of its post-synaptic counterpart by the addition of a “connector”.

2.2 Extracting information on general features and specific neuronal connectivity using CATMAID

Information on general neuronal features (Raw cable length, number input/output synapses) was extracted using the “Measurements” widget in CATMAID. Cable length per synapse number was calculated by dividing the raw cable length of a neuron by the number of input/output synapses as appropriate.

Information on the number of self-righting circuit-specific input/output synapses between the neurons of the self-righting circuit was extracted using the “Connectivity” widget in CATMAID. Information on percentage input/output between specific neurons of interest (e.g. A26f and LT-1/2 neurons) was extracted using the “Synapse Fractions” widget in CATMAID. A neuron of interest was appended to the widget as an upstream or downstream neuron while neurons to be queried for connectivity to this neuron were appended as a named “Partner group”.

All graphs were plotted using GraphPad Prism 8.0 (GraphPad).

2.3 Building a connectivity matrix for the neurons of the self-righting circuit

Spreadsheets detailing all downstream synaptic partners of a neuron of interest (and the number of connections per neuron) were exported from CATMAID. These files were then edited to only include neurons belonging to the self-

righting circuit. The matrix was created by combining these files into one large spreadsheet and arranging the downstream neurons by name followed by the merging of duplicate rows to ensure that each downstream neuron's connections was only represented once.

2.4 Building the self-righting wiring diagram

The self-righting circuit (SRC) wiring diagram (Figure 3.2.9) was created by arranging all of the observed connections within the SR circuit matrix (Figure 3.2.8) by whether they fit into one of four groups. Ipsilateral connections between neurons on the left of the ventral nerve cord (VNC), contralateral connections originating from the left of the VNC, ipsilateral connections between neurons on the right of the VNC and contralateral connections originating from the right of the VNC. The number of synapses between SRC neurons of a given class was then averaged across the first six abdominal segments of the VNC to ascertain average strength.

2.5 Self-righting tests with thermogenetic inhibition of neural activity

A 1.5% agar plate (2mm thickness) was placed onto a custom-built temperature controller-Peltier module and its temperature was adjusted to 25±0.5˚C. Freshly-hatched larvae (≤30 minutes post-hatching) were placed onto this agar plate and allowed to acclimatise for 1 minute before being rolled onto their dorsal sides using a single-bristled paintbrush. Larvae were allowed to self-right (SR) and the temperature was raised to 36±0.5˚C. After 2 minutes of exposure to this temperature, larvae were rolled onto their dorsal sides again and allowed

to self-right. After successful self-righting or 5 minutes of attempting, larvae were transferred to a new agar plate kept at 25˚C and allowed to rest for 5 minutes before being rolled onto their dorsal sides and allowed to self-right for a third time (recovery testing). Movies of SR testing were filmed using a Leica DFC 340 FX camera (Leica Microsystems) mounted on a Leica M165 FC microscope (Leica Microsystems) and Leica Application Suite 4.5 (Leica Microsystems).

A minimum of 22 larvae and a maximum of 24 larvae were tested per genotype and statistical significance was ascertained using a Wilcoxon matched-pairs signed-rank test. All experiments were done in a room maintained at 25˚C with constant light and odour conditions.

2.6 Rearing of *Drosophila melanogaster* strains

Fruit flies were raised on molasses food using standard procedures at 25˚C. Flies were kept on a 12-hour light/dark cycle and at 50-60% humidity.

2.7 Collection of *D. melanogaster* embryos

Adult flies were anaesthetised and transferred into an egg-collection chamber. Apple juice plates smeared with yeast paste were attached to the egg-collection chambers with elastic bands and changed twice daily. When necessary for collection, fresh apple-juice plates were applied and flies were allowed to lay eggs for two hours before the plates were replaced.

Table 2.1 microRNA mutant stocks

Stock Name	BDSC number/Origin	Detailed genotype
w^{1118}	**5905**	w[1118]
yw	**1495**	y[1] w[1]
ΔmiR-1	**58879**	w[*]; mir-1[KO]/CyO, P{w[+mC]=GAL4-twi.G}2.2, P{UAS-2xEGFP}AH2.2
ΔmiR-10	**58880**	w[*]; TI{w[+mW.hs]=GAL4}mir-10[KO]
ΔmiR-100/let-7/125	**58881**	w[*]; Df(2L)let-7-C[KO1], TI{w[+m*]=TI}CG10283[K01]/CyO, P{w[+mC]=GAL4-Kr.C}DC3, P{w[+mC]=UAS-GFP.S65T}DC7
ΔmiR-1000	**58882**	w[*]; TI{TI}mir-1000[KO]/TM3, P{w[+mC]=GAL4-twi.G}2.3, P{UAS-2xEGFP}AH2.3, Sb[1] Ser[1]
ΔmiR-1003	**58883**	w[*]; TI{TI}mir-1003[KO]/TM3, P{w[+mC]=GAL4-twi.G}2.3, P{UAS-2xEGFP}AH2.3, Sb[1] Ser[1]
ΔmiR-1010	**58886**	w[*]; TI{TI}mir-1010[KO]/TM3, P{w[+mC]=GAL4-twi.G}2.3, P{UAS-2xEGFP}AH2.3, Sb[1] Ser[1]
ΔmiR-1017	**58889**	w[*]; TI{TI}mir-1017[KO]/TM3, P{w[+mC]=GAL4-twi.G}2.3, P{UAS-2xEGFP}AH2.3, Sb[1] Ser[1]
ΔmiR-11	**58890**	w[*]; TI{TI}-mir11[KO.w-]
ΔmiR-124	**(*)(1)**	w[*]; TI{w[+mW.hs]=TI}mir-124[w+]6623-6/CyO
ΔmiR-133	**58892**	w[*]; TI{w[+mW.hs]=TI}mir-133[KO]/CyO, P{w[+mC]=GAL4-twi.G}2.2, P{UAS-2xEGFP}AH2.2
ΔmiR-137	**58893**	w[*]; TI{w[+mW.hs]=TI}mir-137[KO]
ΔmiR-13b-2	**58894**	y[1] w[*] TI{TI}mir-13b-2[KO]
ΔmiR-14	**58895**	w[*]; mir-14[Delta1]/CyO, P{w[+mC]=GAL4-Kr.C}DC3, P{w[+mC]=UAS-GFP.S65T}DC7
ΔmiR-184	**58896**	w[*]; TI{w[+mW.hs]=TI}mir-184[KO]/CyO, P{w[+mC]=GAL4-twi.G}2.2, P{UAS-2xEGFP}AH2.2
ΔmiR-190	**58897**	w[*]; TI{TI}mir-190[KO]/TM3, P{w[+mC]=GAL4-twi.G}2.3, P{UAS-2xEGFP}AH2.3, Sb[1] Ser[1]
ΔmiR-193	**58898**	w[*]; TI{w[+mW.hs]=GAL4}mir-193[KO]/TM3, P{w[+mC]=GAL4-twi.G}2.3, P{UAS-2xEGFP}AH2.3, Sb[1] Ser[1]
ΔmiR-210	**58899**	y[1] w[*] TI{w[+mW.hs]=GAL4}mir-210[KO]
ΔmiR-219	**58900**	w[*]; TI{w[+mW.hs]=TI}mir-219[KO]/TM3, P{w[+mC]=GAL4-twi.G}2.3, P{UAS-2xEGFP}AH2.3, Sb[1] Ser[1]
ΔmiR-252	**58901**	w[*]; TI{TI}mir-252[KO]/TM3, P{w[+mC]=GAL4-twi.G}2.3, P{UAS-2xEGFP}AH2.3, Sb[1] Ser[1]
ΔmiR-263a	**58902**	w[*]; TI{w[+mW.hs]=TI}bft[Delta263a]/CyO, P{w[+mC]=GAL4-twi.G}2.2, P{UAS-2xEGFP}AH2.2
ΔmiR-263b	**58903**	w[*]; TI{TI}mir-263b[Delta]
ΔmiR-274	**58904**	w[*]; TI{TI}mir-274[KO]/TM3, P{w[+mC]=GAL4-twi.G}2.3, P{UAS-2xEGFP}AH2.3, Sb[1] Ser[1]

ΔmiR-275/305	**58905**	w[*]; Df(2L)mir-275-305-KO, TI{w[+mW.hs]=TI}mir-275-305-KO/CyO, P{w[+mC]=GAL4-twi.G}2.2, P{UAS-2xEGFP}AH2.2
ΔmiR-276a	**58906**	w[*]; TI{w[+mW.hs]=TI}mir-276a[KO]/TM3, P{w[+mC]=GAL4-twi.G}2.3, P{UAS-2xEGFP}AH2.3, Sb[1] Ser[1]
ΔmiR-276b	**58907**	w[*]; TI{TI}mir-276b[KO]/TM3, P{w[+mC]=GAL4-twi.G}2.3, P{UAS-2xEGFP}AH2.3, Sb[1] Ser[1]
ΔmiR-277/34	**58908**	w[*]; Df(3R)mir-277-34-KO, TI{w[+mW.hs]=TI}mir-277-34-KO/TM3, P{w[+mC]=GAL4-twi.G}2.3, P{UAS-2xEGFP}AH2.3, Sb[1] Ser[1]
ΔmiR-278	**58909**	w[*]; TI{w[+mW.hs]=TI}mir-278[KO]
ΔmiR-281-1/2	**58910**	w[*]; Df(2R)mir-281-1-281-2-KO/CyO, P{w[+mC]=GAL4-twi.G}2.2, P{UAS-2xEGFP}AH2.2
ΔmiR-282	**58911 (2)**	w[*]; TI{w[+mW.hs]=TI}mir-282[KO]/TM6B, Tb[1]
ΔmiR-283	**58912**	w[*] TI{TI}mir-283[KO]
ΔmiR-284	**58913**	w[*]; TI{w[+mW.hs]=TI}mir-284[KO]/TM3, P{w[+mC]=GAL4-twi.G}2.3, P{UAS-2xEGFP}AH2.3, Sb[1] Ser[1]
ΔmiR-285	**58914**	w[*]; TI{w[+mW.hs]=TI}mir-285[KO]
ΔmiR-2a-2/2a-1/2b-2	**59032**	w[*]; Df(2L)mir-2a-2-2a-1-2b-2-KO/CyO, P{w[+mC]=GAL4-twi.G}2.2, P{UAS-2xEGFP}AH2.2
ΔmiR-2b-1	**58915**	w[*]; TI{w[+mW.hs]=TI}mir-2b-1[KO]
ΔmiR-2c/13a/13b-1	**58916**	w[*]; Df(3R)mir-2c-13a-13b-1-KO, TI{w[+mW.hs]=TI}mir-2c-13a-13b-1-KO
ΔmiR-303	**58917**	w[*] TI{w[+mW.hs]=TI}mir-303[KO]
ΔmiR-304	**58918**	w[*] TI{TI}mir-304[KO]
ΔmiR-306/79/9b	**58919**	w[*]; Df(2L)mir-306-79-9b-KO/CyO, P{w[+mC]=GAL4-twi.G}2.2, P{UAS-2xEGFP}AH2.2
ΔmiR-307a/b	**58920 (1)**	w[*]; Df(2R)mir-307a-307b-KO/CyO
ΔmiR-309/286/3/4/5/6-1/6-2/6-3	**58922**	w[*]; Df(2R)mir-309-6[Delta1], TI{w[+mW.hs]=GFP}Df-mir-309-6[Delta1]/CyO, P{w[+mC]=GAL4-twi.G}2.2, P{UAS-2xEGFP}AH2.2
ΔmiR-310/311/312/313	**58923**	w[*]; Df(2R)mir-310-311-312-313 P{ry[+t7.2]=neoFRT}42D/CyO, P{w[+mC]=GAL4-twi.G}2.2, P{UAS-2xEGFP}AH2.2
ΔmiR-314	**58924**	w[*]; TI{w[+mW.hs]=TI}mir-314[KO]
ΔmiR-316	**58925**	w[*]; TI{w[+mW.hs]=TI}mir-316[KO]/TM3, P{w[+mC]=GAL4-twi.G}2.3, P{UAS-2xEGFP}AH2.3, Sb[1] Ser[1]
ΔmiR-317	**58926 (2)**	w[*]; TI{w[+mW.hs]=TI}mir-317[KO]/TM3, Sb[1]
ΔmiR-318	**58927**	w[*]; TI{w[+mW.hs]=TI}mir-318[KO]/TM3, P{w[+mC]=GAL4-twi.G}2.3, P{UAS-2xEGFP}AH2.3, Sb[1] Ser[1]
ΔmiR-31a	**58928**	w[*]; TI{w[+mW.hs]=TI}mir-31a[KO]
ΔmiR-31b	**58929**	w[*] TI{TI}mir-31b[KO]
ΔmiR-33	**58930**	w[*]; TI{TI}mir-33[KO]

ΔmiR-375	**58931**	w[*]; TI{w[+mW.hs]=GAL4}mir-375[KO]/CyO, P{w[+mC]=GAL4-twi.G}2.2, P{UAS-2xEGFP}AH2.2
ΔmiR-8	**58932**	w[*]; mir-8[Delta2]/CyO, P{w[+mC]=GAL4-Kr.C}DC3, P{w[+mC]=UAS-GFP.S65T}DC7
ΔmiR-87	**58934**	w[*]; TI{w[+mW.hs]=TI}mir-87[KO]/CyO, P{w[+mC]=GAL4-twi.G}2.2, P{UAS-2xEGFP}AH2.2
ΔmiR-927	**58935**	y[1] w[*] TI{TI}mir-927[KO]
ΔmiR-929	**58936**	w[*]; TI{TI}mir-929[KO]/TM3, P{w[+mC]=GAL4-twi.G}2.3, P{UAS-2xEGFP}AH2.3, Sb[1] Ser[1]
ΔmiR-92a	**58937**	w[*]; TI{TI}mir-92a[KO]
ΔmiR-92b	**58938 (2)**	w[*]; TI{w[+mW.hs]=TI}mir-92b[KO]/TM3, Sb[1]
ΔmiR-932	**58939**	w[*]; TI{TI}mir-932[KO]/CyO, P{w[+mC]=GAL4-twi.G}2.2, P{UAS-2xEGFP}AH2.2
ΔmiR-955	**58940**	w[*]; TI{w[+mW.hs]=GAL4}mir-955[KO]
ΔmiR-956	**58941**	w[*]; TI{w[+mW.hs]=GAL4}mir-956[KO]/TM3, P{w[+mC]=GAL4-twi.G}2.3, P{UAS-2xEGFP}AH2.3, Sb[1] Ser[1]
ΔmiR-957	**58942**	w[*]; TI{w[+mW.hs]=TI}mir-957[KO]
ΔmiR-958	**58943**	w[*]; TI{w[+mW.hs]=TI}mir-958[KO]
ΔmiR-959/960/961/962	**58944**	w[*]; Df(2L)mir-959-960-961-962-KO
ΔmiR-965	**58946 (1)**	w[*]; TI{TI}mir-965[KO1]/CyO
ΔmiR-966	**58947**	w[*]; TI{TI}mir-966[KO]/CyO, P{w[+mC]=GAL4-twi.G}2.2, P{UAS-2xEGFP}AH2.2
ΔmiR-967	**58948**	w[*]; TI{TI}mir-967[KO]/CyO, P{w[+mC]=GAL4-twi.G}2.2, P{UAS-2xEGFP}AH2.2
ΔmiR-968/1002	**58949**	w[*]; Df(2L)mir-968-1002-KO, TI{w[+mW.hs]=GAL4}mir-968-1002-KO/CyO, P{w[+mC]=GAL4-twi.G}2.2, P{UAS-2xEGFP}AH2.2
ΔmiR-969	**58950**	w[*] TI{w[+mW.hs]=GAL4}mir-969[KO]/FM6
ΔmiR-970	**58951**	w[*] TI{TI}mir-970[KO]
ΔmiR-971	**58952**	w[*] TI{w[+mW.hs]=GAL4}mir-971[KO]
ΔmiR-972/973/974	**58953**	Df(1)mir-972-973-974-KO, y[1] w[*] TI{w[+mW.hs]=GAL4}mir-972-973-974-KO
ΔmiR-975/976/977	**58954**	Df(1)mir-975-976-977-KO, w[*] TI{w[+mW.hs]=GAL4}mir-975-976-977-KO
ΔmiR-980	**58955**	TI{TI}mir-980[KO] w[*]
ΔmiR-981	**58956 (3)**	TI{TI}mir-981[KO] w[*]/FM6
ΔmiR-982/303	**58957**	Df(1)mir-982-303-KO, w[*] TI{w[+mW.hs]=TI}mir-982-303-KO
ΔmiR-984/983-1/983-2	**58958**	Df(1)mir-984-983-1-983-2-KO, w[*]
ΔmiR-986	**58959**	w[*]; TI{TI}mir-986[KO]/CyO, P{w[+mC]=GAL4-twi.G}2.2, P{UAS-2xEGFP}AH2.2
ΔmiR-987	**58960**	w[*]; TI{w[+mW.hs]=GAL4}mir-987[KO]/CyO, P{w[+mC]=GAL4-twi.G}2.2, P{UAS-2xEGFP}AH2.2

ΔmiR-988	**58961**	w[*]; TI{TI}mir-988[KO]
ΔmiR-989	**58962**	w[*]; TI{w[+mW.hs]=TI}mir-989[KO]/CyO, P{w[+mC]=GAL4-twi.G}2.2, P{UAS-2xEGFP}AH2.2
ΔmiR-990	**58963**	w[*]; TI{TI}mir-990[KO]/CyO, P{w[+mC]=GAL4-twi.G}2.2, P{UAS-2xEGFP}AH2.2
ΔmiR-995	**58965**	w[*]; TI{TI}mir-995[KO]/TM3, P{w[+mC]=GAL4-twi.G}2.3, P{UAS-2xEGFP}AH2.3, Sb[1] Ser[1]
ΔmiR-999	**58966**	w[*]; TI{TI}mir-999[KO]
ΔmiR-9c	**58967**	w[*]; TI{TI}mir-9c[KO]/CyO, P{w[+mC]=GAL4-twi.G}2.2, P{UAS-2xEGFP}AH2.2
ΔmiR-iab-4/iab-8	**(Bender, 2008)**	w1118;; iab-4/iab-8[KO]/TM3, P{w[+mC]=GAL4-twi.G}2.3, P{UAS-2xEGFP}AH2.3, Sb[1] Ser[1]

(*) Stock kindly donated by Patrick Emery (Neurobiology department, University of Massachusetts Medical School, USA)
(1) Stocks re-balanced with the fluorescent balancer: CyO, P{w[+mc]=GAL4-twi.G}2.2, P{UAS-2xEGFP}AH2.2 (BDSC #6662)
(2) Stocks re-balanced with the fluorescent balancer: TM3, P{w[+mc]=GAL4-twi.G}2.3, P{UAS-2xEGFP}AH2.3, Sb[1] (BDSC #6663)
(3) Stock re-balanced with the fluorescent balancer: FM7c, P{w[+mc]=GAL4-twi.G}108.4, P{UAS-2xEGFP}AX (BDSC #6873)

Table 2.2 Other *D. melanogaster* stocks used

Stock Name	BDSC number/Origin	Detailed genotype
412-GAL4	63300	w[1118]; PBac{w[+mC]=IT.GAL4}CG7634[0412-G4]
iav-GAL4	52273	w[*];; P{w[+mC]=iav-GAL4.K}3
ppk1.9-Gal4	(Ainsley *et al.,* 2003) (*)	w;ppk1.9-Gal4
R16E11-GAL4	48729	w[1118]; P{y[+t7.7] w[+mC]=GMR16E11-GAL4}attP2
R16E12-GAL4	48730	w[1118]; P{y[+t7.7] w[+mC]=GMR16E12-GAL4}attP2
R47D07-GAL4	50304	w[1118]; P{y[+t7.7] w[+mC]=GMR47D07-GAL4}attP2
R58E05-GAL4	39182	w[1118]; P{y[+t7.7] w[+mC]=GMR58E05-GAL4}attP2
R61A01-GAL4	39269	w[1118]; P{y[+t7.7] w[+mC]=GMR61A01-GAL4}attP2
R72F11-GAL4	39786	w[1118]; P{y[+t7.7] w[+mC]=GMR72F11-GAL4}attP2
R75H04-GAL4	39909	w[1118];; P{y[+t7.7] w[+mC]=GMR75H04-GAL4}attP2
ss01411-GAL4	(Zwart *et al.,* 2016) (**)	w-1118; GMR_45A08/-p65ADZp in attP40 CyO, Tb RFP; GMR_83H09-ZpGdbd in attP2 (S)

ss01970-GAL4	(Zwart *et al.,* 2016) (**)	w-1118; VT059793-p65ADZp in attP40; GMR_58F03-ZpGdbd in attP2
TRH-GAL4	38388	w[1118]; P{w[+mC]=Trh-GAL4.long}2
UAS-myrGFP	32198	w[*]; P{y[+t7.7] w[+mC]=10XUAS-IVS-myr::GFP}attP40
UAS-shi^{ts}	44222	w[*]; P{w[+mC]=UAS-shi[ts1].K}3
UAS-Trh	27638	y[1] w[*]; P{w[+mC]=UAS-Trh.Y}2

(*) Stock kindly donated by Matthias Landgraf (Department of Zoology, University of Cambridge, UK)
(**) Stocks kindly donated by Akira Fushiki (Mortimer B. Zuckerman Mind Brain Behaviour Institute, Columbia University in the City of New York, USA)

2.8 Analysis of larval locomotion

2.8.1 Recording larval locomotion with the FIMTable

Embryos were collected as explained above and raised at 25˚C (50-60% humidity) for 21 hours. If necessary, embryos were selected against GFP balancer expression, no more than 2 hours before hatching. Freshly hatched larvae (≤30 minutes post-hatching) were placed onto a 1.5% agar plate (4mm thickness) and allowed to acclimatise for one minute. The agar was removed from the dish and placed on top of the FIMTable (Risse *et al.,* 2013, 2017). Larvae were then recorded using a Basler acA2040-90um camera (Basler) and pylon Viewer 5.0.11 (Basler) to create a 7.5fps .avi movie of 3 minutes 14 seconds.

For experiments on third instar larvae, larvae (120h AEL) were removed from molasses food, transferred to fresh 1.5% agar plates and cleaned using a moist paintbrush. After cleaning, larvae were transferred with a paintbrush to a 25x25cm layer of 1.5% agar on top of the FIMTable. Larvae were then recorded using Basler acA2040-90um camera (Basler) and pylon Viewer 5.0.11 (Basler) to create a 10fps .avi movie of 2 minutes.

2.8.2 Analysing larval locomotion videos using FIMTrack

Behavioural videos were imported into FIJI (Schindelin *et al.,* 2012) and converted into sequences of 1459 .tif image files (1200 .tif files when third instar larvae were analysed). These .tif files were imported into FIMTrack v2 (Risse *et al.,* 2013, 2017) and the program was used to extract behavioural information from the recordings.

2.8.3 Analysing cumulative time spent turning by larvae

Analysis of time spent in a bent conformation was performed using a custom Microsoft Excel for Mac 16.22 (Microsoft) macro on .csv files produced by FIMTrack. Briefly, the “left_bended” or “right_bended” variables in FIMTrack .csv files were assigned a binary value (1 = affirmative or 0 = negative) depending on whether a larva’s body was bent >30˚ in either direction for a single frame. The custom Microsoft Excel macro summed these values for each larva and reported the total as a percentage of 1459 frames (1200 for third-instar larvae).

2.8.4 Analysis of other behavioural variables using PyFIM

Analysis of average pause duration, pause frequency and bending frequency were carried out by using the custom package PyFIM (Developed by Philipp Schlegel (MRC Laboratory of Molecular Biology, Cambridge, UK) and others) on FIMTrack-derived .csv files. The PyFIM package was run in Terminal 2.9.5 (Apple).

2.9 Statistical analysis of behavioural variables

Comparisons between all behavioural variables of microRNA mutant (*ΔmiRNA*) larvae and controls were carried out using the Mann-Whitney U Test with Bonferroni correction for multiple comparisons in GraphPad Prism 8.0 (GraphPad).

Where correlation analyses were performed, median values for each genotype were used to reduce the impact of outliers.

2.10 Principal component analysis and clustering analysis

Principal component analysis (PCA) was performed using the *prcomp* function in R while the biplot shown (Figure 5.2.16B) was plotted using the *ggbiplot* R package developed by Vincent Q. Vu (The Ohio State University, Columbus, USA). The eigenvalues from the PCA were plotted (Figure 5.2.16A) using the *factoextra* R package developed by Alboukadel Kassambara (HalioDx, Marseille, France) and Fabian Mundt (Karlsruhe University of Education, Karlsruhe, Germany). *K*-means clustering analysis (Figure 5.2.17) was carried out using the *kmeans* function in R with 10 initial centers tested for stability. All analysis was run in RStudio 4.0.0.

2.11 Assaying larval rearing behaviour

Embryos of appropriate genotype were collected and raised at 25˚C (50-60% humidity) for 21 hours. If necessary, embryos were selected against a GFP balancer no more than 2 hours before hatching. Freshly hatched larvae (≤30

minutes post-hatching) were placed onto a 1.5% agar plate (4mm thickness) and allowed to acclimatise for one minute. Larvae were filmed for three minutes using a Leica DFC 340 FX camera (Leica Microsystems) mounted on a Leica M165 FC microscope (Leica Microsystems) and Leica Application Suite 4.5 (Leica Microsystems). Events in which the larvae raised the anterior half of the body from the substrate were noted and tallied by observers during the three minutes of recording. Comparisons between the number of rears by *ΔmiRNA* mutant larvae and controls were carried out using the Mann-Whitney U test and, in the case of *Trh* overexpression tests, the Kruskal-Wallis ANOVA test was used. All experiments were done in a room maintained at 25˚C with constant light and odour conditions.

2.12 Total RNA extraction from *Drosophila* embryos

Embryos were collected and placed into 500µl of DEPC-treated 1X PBS. PBS was removed and replaced with 50µl TRI Reagent (Ambion) and embryos were homogenized in this solution with a mechanical homogenizer and pestle. 450µl of TRI Reagent was added and the solution was left to incubate at room temperature for 5 minutes before being centrifuged at 12000*x g* for 10 minutes at 4˚C. Supernatant was removed and transferred to a fresh Eppendorf tube before 100µl chloroform was added to separate RNA from DNA and shaken for 15 seconds. The salutation was transferred to a pre-spun (90 seconds, 10,000*x g*) 5PRIME phase-lock tube (QuantaBio) and left to incubate for 15 minutes at room temperature before the aqueous phase (containing RNA) was separated from other phases by centrifugation at 12,000*x g* for 15 minutes at 4˚C. This

aqueous phase was transferred to a fresh Eppendorf tube for RNA precipitation with 250µl isopropanol and 1µl glycogen (Invitrogen). The solution was shaken and left to incubate at -20˚C for 30 minutes before being centrifuged at 12000*x g* for 8 minutes at 4˚C. Supernatant was discarded and the remaining pellet was dislodged from the tube with 500µl 70% RNAse-free ethanol before being centrifuged at 7500*x g* for 5 minutes at 4˚C. All ethanol was removed and the RNA pellet was left to air-dry before being resuspended in 20µl nuclease-free water. RNA was then measured for concentration using a Nanodrop 2000 (Thermo Fisher Scientific), treated with TurboDNAse (Invitrogen) following the manufacturer's instructions and stored at -80˚C if not immediately used in downstream applications.

2.13 Reverse transcription of embryonic RNA

500ng of extracted total RNA (see 2.12), 1µl of Oligo$(dT)_{18}$ primers (Thermo Scientific), 1µl 10mM dNTP Mix (New England Biolabs) was combined and DEPC-treated H_2O was added to 12µl final volume. RNA was denatured at 65˚C for 5 minutes and chilled on ice for ≥1 minute. 4µl 5x First-strand Buffer (Invitrogen), 0.1M DTT (Invitrogen), 1µl RNAse inhibitor (Invitrogen) and 1µl MMLV Reverse Transcriptase (Invitrogen) (or DEPC-treated H_2O for non-template controls) were added per sample and cDNA was synthesised at 37˚C for 50 minutes. The RT enzyme was deactivated by incubating the sample at 70˚C for 15 minutes before synthesised cDNA was stored at -20˚C. All incubations were carried out in a Bio-Rad PCR Thermocycler.

2.14 RT-PCR and analysis

2.14.1 RT-PCR reactions

A mix of 18µl of DEPC-treated water, 2.5µl 10X Taq buffer (New England Biolabs), 1µl 10mM DNTP mix, 1µl cDNA (see 2.13), 1µl 10µM forward primer, 1µl 10µM reverse primer and 0.5µl Taq polymerase (New England Biolabs) was combined per reaction. To amplify the *Trh* gene, the following conditions were used for PCR in a Bio-Rad PCR Thermocycler: Extended DNA denaturation at 95˚C for 3 minutes before 33 cycles of DNA denaturation at 95˚C for 30 seconds, primer annealing at 60˚C for 30 seconds and extension at 72˚C for 45 seconds. A final extension was performed at 72˚C for 10 minutes and the sample was held at 4˚C.

2.14.2 Agarose gel electrophoresis and band intensity quantification

The PCR product was visualised using agarose gel electrophoresis. Briefly, agarose gels of 2% (w/v) were made by dissolving 2g of agarose (Fisher Chemical) in 100ml 1X TAE Buffer (0.4M Tris acetate, 0.01M EDTA in dH_2O). The buffer was heated in a microwave until all agarose had dissolved at which point it was removed, allowed to cool slightly and 400ng/ml ethidium bromide (Roche) was added to aid visualisation. This liquid agarose was then poured into a gel cast and allowed to set. Samples were mixed with 1X loading buffer (New England Biolabs) before being loaded into the gel and electrophoresed in 1X TAE Buffer alongside a 100bp ladder (New England Biolabs). Pictures of gels were taken using the UVP BioDoc-It Imaging System and printed using a Video Graphic Printer (Sony). Quantification of band intensity was carried out

using the Label Peaks function in FIJI (Schindelin *et al.,* 2012) with all bands quantified with a consistent region of interest surrounding them. Expression levels were normalised to the band intensity of the reference gene, *actin*.

Table 2.3 Primers used in RT-PCR

Target		Primer sequence (5' to 3')
Trh	Fw	CCTGTGGCTCTACAGGAGTG
	Rv	ATCGCCGAAGTCAAAACTGGA
Actin (*)	Fw	GAGCGCGGTTACTCTTTCAC
	Rv	ATCCCGATCCTGATCCTCTT

(*) Primers designed in Stacey *et al.,* 2010

2.15 Fixation of larval tissues

Embryos were collected and raised at 25˚C (50-60% humidity) for 21 hours. If necessary, embryos were selected against a GFP balancer no more than 2 hours before hatching. In a glass dish with cold PBS, freshly-hatched larvae (≤30 minutes post-hatching) were opened to expose the central nervous system before being transferred to an Eppendorf tube with 500µl cold PBS. Larvae were then fixed in 500µl 4% formaldehyde/PBS (200µl of 10% ultrapure formaldehyde (Polysciences Inc.) and 300µl 1X PBS) for 20 minutes on a rotation shaker set to 300rpm.

2.16 Immunohistochemistry and analysis

2.16.1 Antibody staining of the larval CNS

Fixed, dissected larvae (see 2.15) were washed 3 times for 10 minutes in PBTx (1X PBS, 0.3% Triton X-100) before being incubated overnight at 4˚C in 100µl of PBTx/polyclonal rabbit anti-serotonin antibody (S5545, Sigma-Aldrich, 1:1000) solution. Larvae were then rinsed 3 times and washed 3 times in PBTx before being incubated in 100µl of a PBTx/Alexa Fluor® 488 Goat anti-rabbit antibody (A-11008, Invitrogen, 1:500) solution for 2 hours at room temperature. All larvae were also counterstained with 4′,6-diamidino-2-phenylindole (DAPI). Larvae were then rinsed 3 times and washed 4 times for 15 minutes in PBTx. Intact central nervous systems were then removed from the larval body before being mounted in Vectashield anti-fade medium (Vector Laboratories).

2.16.2 Imaging and protein quantification

Z-stacks of larval central nervous systems stained with DAPI and an anti-serotonin antibody were taken using a Leica SP8 confocal microscope (Leica Microsystems). Central nervous systems from control larvae and miRNA mutant larvae were taken using the same settings during the same imaging session. Quantification of serotonin levels was analysed in FIJI (Schindelin *et al.,* 2012) by collapsing confocal stacks of the central nervous system into a singly projection with the “Sum Slices” tool. ROIs were added around the serotonergic neurons in each hemisegment and the “Measurements” tool was then used to measure the intensity of fluorescence emitted (their “average gray value”) along the A-P axis. Before comparison between genotypes, these gray values were

normalised to background fluorescence in the CNS. Gray values were plotted (mean ± SEM) in GraphPad Prism 8.0 (GraphPad).

2.17 Dissociation of larval tissues

Embryos were collected and raised at 25˚C (50-60% humidity) for 21 hours. In a glass dish with cold Schneider's Drosophila medium (Gibco), freshly-hatched larvae (≤30 minutes post-hatching) were opened to expose the central nervous system. Dissected larvae were transferred to an Eppendorf tube with cold 1X Rinaldini's solution (8mg ml $^{-1}$ NaCl, 0.2mg ml $^{-1}$ KCl, 0.05mg ml $^{-1}$ Na_2HPO_4, 1mg ml $^{-1}$ $NaHCO_3$, 1mg ml $^{-1}$ Glucose in dH_2O) before being dissociated in dissociation solution (1 mg ml $^{-1}$ Collagenase I (Sigma-Aldrich), 1mg ml $^{-1}$ papain (Sigma-Aldrich)) in Schneider's Drosophila medium at 30˚C for 1 hour. Dissociation solution was removed slowly and replaced with 500µl Rinaldini's solution which in turn was removed and replaced with 500µl Schneider's Drosophila medium. Larvae were mechanically dissociated in 200µl fresh Schneider's Drosophila medium by pipetting up and down and kept on ice.

2.18 Fluorescence-activated cell sorting (FACS) of serotonergic neurons

All FACS experiments were carried out using a BD FACS Melody Cell Sorter. Immediately prior to cell sorting, the cell suspension (see 2.17) was passed through a 100µm cell strainer (Fisher Scientific) into a 5ml round-bottom tube (Falcon). A few control cells were sorted briefly to establish a fluorescence threshold above which GFP signal could be reliably identified. GFP-positive and an equivalent number of control cells were then sorted into Eppendorf tubes

with 300µl TRI Reagent and cells were immediately lysed by vortexing for 30 seconds before being kept on ice.

2.19 RNA extraction from sorted cells

The volume of TRI reagent in a previously-sorted cell solution (see 2.18) was brought to 500µl before RNA was separated from DNA by addition of 100µl RNase-free chloroform and immediate vortexing for 30 seconds. The lysate was poured into a pre-spun (90 seconds, 10000*x g*) gel-lock tube and the aqueous phase (containing RNA) was separated from other phases by centrifugation at 12000*x g* for 10 minutes at 4˚C. This aqueous phase was transferred to a fresh Eppendorf tube for RNA precipitation with 250µl isopropanol and 1µl glycogen. The solution was shaken and left to incubate at room temperature for 10 minutes before being centrifuged at 12000*x g* for 10 minutes at 4˚C. Supernatant was discarded and the remaining pellet was dislodged from the tube with 750µl 70% RNAse-free ethanol before being centrifuged at 7500*x g* for 5 minutes at 4˚C. All ethanol was removed, and the RNA pellet was left to air-dry before being resuspended in 14µl nuclease-free water.

2.20 Expression profiling of *miR-133*

2.20.1 Poly(A) tailing of extracted RNA

Poly-A tailing of RNAs extracted from sorted cells was performed by combining 1µl 5X EPAP buffer (Invitrogen), 0.5µl 25mM Cl_2 (Invitrogen). 0.5µl 10mM ATP

(Invitrogen), 1µl EPAP (Invitrogen) and 14µl extracted RNA per tube. This mix was then incubated at 37˚C for 30 minutes in a Bio-Rad PCR thermocycler.

2.20.2 Real-time quantitative PCR

Real-time quantitative PCR (qPCR) was carried out on cDNA synthesised from RNA extracted from sorted serotonergic neurons. 1µl of cDNA (or dH_2O for non-template controls) was added to the wells of a MicroAmp™ Optical 96-well plate (Applied Biosystems). A master mix containing 5µl 2X LightCycler®480 SYBR Green I Master (Roche), 2µl H_2O, 1µl forward primer and 1µl reverse primer per well was created. 9µl of this master mix was added to each well containing cDNA or water and briefly mixed by pipetting before plates were sealed with MicroAmp™ Optical Adhesive Film (Applied Biosystems). Triplicates of reactions were run concurrently using the comparative C_T with melting curve program in a QuantStudio 3 Real-Time PCR System (Applied Biosystems).

Primer efficiencies were determined by plotting standard curves using cDNA dilution factor 5.

Efficiencies for primers used ranged from 0.7 – 2.1 and were calculated using the following equation (Pfaffl, 2001):

$$E = d^{-1/-s}$$

Differential gene expression was calculated using the extracted C_T values and the following equation for fold-change (Pfaffl, 2001):

$$FC = \frac{2^{CT}\ gene\ of\ interest\ (control - mutant)}{2^{CT}\ reference\ gene\ (control - mutant)}$$

Table 2.4 Primers used in qPCR

Target		Primer sequence (5' to 3')
Actin (*)	Fw	GCGTCGGTCAATTCAATCTT
	Rv	AAGCTGCAACCTCTTCGTCA
GFP	Fw	CATTCATCAGCCGTCTTCCG
	Rv	GAGTGCCCAAGAAAGCTACC
miR-133	Fw	CTGTGTGTAGCTGGTTGACAT
	Rv	TTGTCATCAACCACTGGCTAC
Trh	Fw	AGCCAAGATGCTCCCTCTG
	Rv	CGGCACTTTTTAGCTTACTGCT
VGlut	Fw	AGGAAACCTCATTCGGTGCC
	Rv	GCCGTAGCTAATGGCAGTCG

(*) Primers designed in Ponton *et al.,* 2011

Chapter 3

The cellular basis of larval self-righting behaviour

3.1 Chapter overview

The ability to perform complex behaviour relies upon communication between multiple neurons in discrete groups termed ‘circuits’. Elucidation of the exact structures of these neural circuits and their relationships to the exhibition of specific behaviours is a fundamental aspect of neuroscientific research in mammalian and non-mammalian model organisms. Neural circuit structure can be examined indirectly, using genetically-encoded tools to monitor how predicted downstream neurons respond to artificial stimulation of predicted upstream neurons (reviewed in Bernstein *et al.,* 2012). Neural circuit structure can also be investigated via the specific ablation of neural activity and analysis of subsequent behavioural output (Renn *et al.,* 1999; Tsalik & Hobert, 2003).

The use of electron microscopy (or ‘EM’), however, enables researchers to directly visualise the synaptic connections between the neurons of a circuit. One outcome of this has been the enhancement of the ‘serial reconstruction’ approach, in which researchers use a microtome to produce ultrathin sections of an animal’s central nervous system (or ‘CNS’) and produce collections (or ‘volumes’) of consecutive EM images taken of these sections.

When the approach was first developed, these images would then be magnified by thousands of times and researchers would manually reconstruct the three-dimensional morphologies of neurons of interest by ‘tracing’ their positions through consecutive EM images (Ware and Lopresti, 1975). As time progressed, however, this process was improved with EM images obtained at higher resolution and the development of *in silico* neuronal reconstruction (Stevens *et al.,* 1980). For decades, however, a substantial drawback remained

the handling of large amounts of images and the time-consuming nature of neuronal reconstruction.

To address these drawbacks and facilitate the use of reconstruction methods in the *Drosophila* CNS, Stephan Saalfeld and colleagues developed the computer-based Collaborative Annotation Toolkit for Massive Amounts of Image Data (or 'CATMAID') in 2009 (Saalfeld *et al.,* 2009). The development of CATMAID provided a platform for researchers to work collaboratively (via the internet) on reconstructing neurons in large online volumes of EM images and here, we use the tool to investigate the structure of the neuronal network underlying self-righting behaviour in the first instar (L1) *Drosophila* larva.

Previous work by our lab demonstrated that the normal neuronal activity of the LT-1/2 motor neurons (or 'LT-1/2 MNs') is necessary for self-righting behaviour (Picao-Osorio *et al.,* 2015) and we begin by using CATMAID to produce skeletonised reconstructions of the LT-1/2 MNs in the first seven abdominal segments of the larval ventral nerve cord (or 'VNC'). Connectomic analysis of these neurons reveals fluctuations in various morphological and connectivity-related parameters along the anteroposterior (or 'AP') axis as well as an increase in the rarity of input synapses towards the posterior of the VNC.

We then identify five segmentally-repeated premotor interneurons (or 'pre-LT' interneurons) strongly connected to the LT-1/2 MNs in each of the first six abdominal segments of the VNC and demonstrate that segment-specific refinement has an impact on pre-LT interneuron connectivity. As a previously uncharacterised premotor interneuron, we investigate the pre-LT interneuron A26f in greater detail and find a high degree of symmetry between the

mediolateral connectivity of the neurons on both sides of the VNC as well as a tight balance between anterior, intrasegmental and posterior output to the rest of the self-righting circuit (or ‘SRC’).

Further upstream of the pre-LT interneurons, we identify strong connections between the A27k and Down-and-Back interneurons and premotor/motor components and identify the interneuron A19f as a ‘premotor integrator’, integrating signals between the pre-LT interneurons A26f and eIN-2. Building on this, we investigate how the neurons of the previously identified rolling circuit are connected to the SRC and find that the two are linked via a pair of nociceptive integrator neurons, TePn05 and A02o ‘Wave’.

Having created a putative map for the neurons of the SRC, we examine the average strength of connections between SRC and summarise this information in a connectivity matrix, subsequently using this matrix to create a neural wiring diagram displaying average synaptic strength and routes for information flow. The finding that there is an almost equal balance between the number of intrasegmental and intersegmental synapses between SRC neurons leads us to investigate how consistently the neural wiring diagram is repeated intrasegmentally. We examine intrasegmental connections in each of the first six abdominal segments of the VNC and find that the level of intrasegmental connection between SRC neurons reduces towards the posterior segments.

Finally, we perform a detailed characterisation of anteroposterior information flow between SRC neurons, and our investigation of mediolateral connection symmetry reveals that while SRC neurons mostly receive symmetrical inputs on both sides of the VNC, SRC-specific output occurs asymmetrically.

We present the results of this chapter as the first neural wiring diagram for the control of larval self-righting behaviour and in the following chapter, functionally test the relevance of this for self-righting behaviour *in vivo*.

3.2 Results

3.2.1 Description of the methodological approach

3.2.1.1 Identification and tracing of neurons using CATMAID

At approximately 10,000 neurons (Schleyer *et al.,* 2015), the *Drosophila* larval central nervous system (or 'CNS') is relatively small and the connections between neurons that facilitate behaviour can be investigated via a variety of genetically-encoded tools such as GFP Reconstitution Across Synaptic Partners (or 'GRASP') (Feinberg *et al.,* 2008) or the simultaneous expression of genetically encoded calcium indicators and channelrhodopsins (Kim *et al.,* 2017). The polyadic nature of insect synapses, however, means that although the use of these tools provides binary information (i.e., whether two neurons are synaptically connected or not), it remains difficult to gather more detailed information on the strength of these connections in terms of synapse number. To better characterise synaptic connectivity between neurons in the circuits underlying behaviour therefore, an efficient approach is required that allows the direct observation of synaptic connections at high-resolution and subsequent examination of neural circuit structure.

Here, we adopt a 'serial reconstruction' approach, reconstructing neuronal morphologies from a volume of electron microscopy (or 'EM') images. The volume we use consists of a series of transmission electron microscopy images taken of 45nm sections produced from an early, wild-type, first instar (L1) larval *Drosophila* CNS (Schneider-Mizell *et al.,* 2016; Eschbach *et al.,* 2020) (Figure 3.2.1A) and we use the computer-based Collaborative Annotation Toolkit for

Massive Amounts of Image Data (or ‘CATMAID’) (Saalfeld *et al.,* 2009) for neuronal and circuit reconstruction.

In the EM volume used for our analysis, neurons are identified by a combination of features including the shape of their outlines, the presence of microtubules and the presence of other organelles such as mitochondria and smooth endoplasmic reticulum. An identified neuron of interest is “traced” by the placing of a “node” annotation on the location of a single neuron of interest in consecutive EM images. This “tracing” process (Figure 3.2.1B) results in the automatic construction of a virtual 3D skeletonised version of a neuron’s morphology with the neuron’s cell body, axon, and dendritic projections visible within a virtual CNS.

3.2.1.2 Annotation of synapses and connectomic analyses using CATMAID

In addition to neuronal morphology, CATMAID also the provides the ability to annotate EM images with the locations of synapses between neurons (Figure 3.2.1C’). Synapses are identified by a group of characteristic features including a dark, T-shaped synaptic cleft and pre/post-synaptic vesicles (Figure 3.2.1C’’). Researchers are able to label the pre- and post-synaptic neurons of a synapse using “connector” links between the “nodes” of the respective neurons and the locations of the pre/post-synaptic connections of a given neurons are visible as coloured markers on the 3D skeletonised version of the neuron’s morphology.

A key feature of CATMAID is the automatic storing of the locations of these annotated synapses and calculation of various connectivity metrics. The results

of these automatic connectomics analyses can then be accessed by researchers using various sub-menus or “widgets”. For example, the “Connectivity” widget provides users with a list of neurons that are “upstream” and “downstream” from a neuron of interest and the number of synapses comprising each connection. The “Graph” widget (Figure 3.2.1D) allows users to visualise connections between neurons (and their strengths), quickly identifying the direction of information flow while the “Synapse fractions” widget provides users with the ability to quickly determine what percentage of a neuron’s total synaptic input or output is represented by connections of interest.

These, and other, features provide the means to perform powerful, large-scale connectomics analysis and here, we use CATMAID to investigate the structure of the neuronal network underlying self-righting behaviour in the L1 larva.

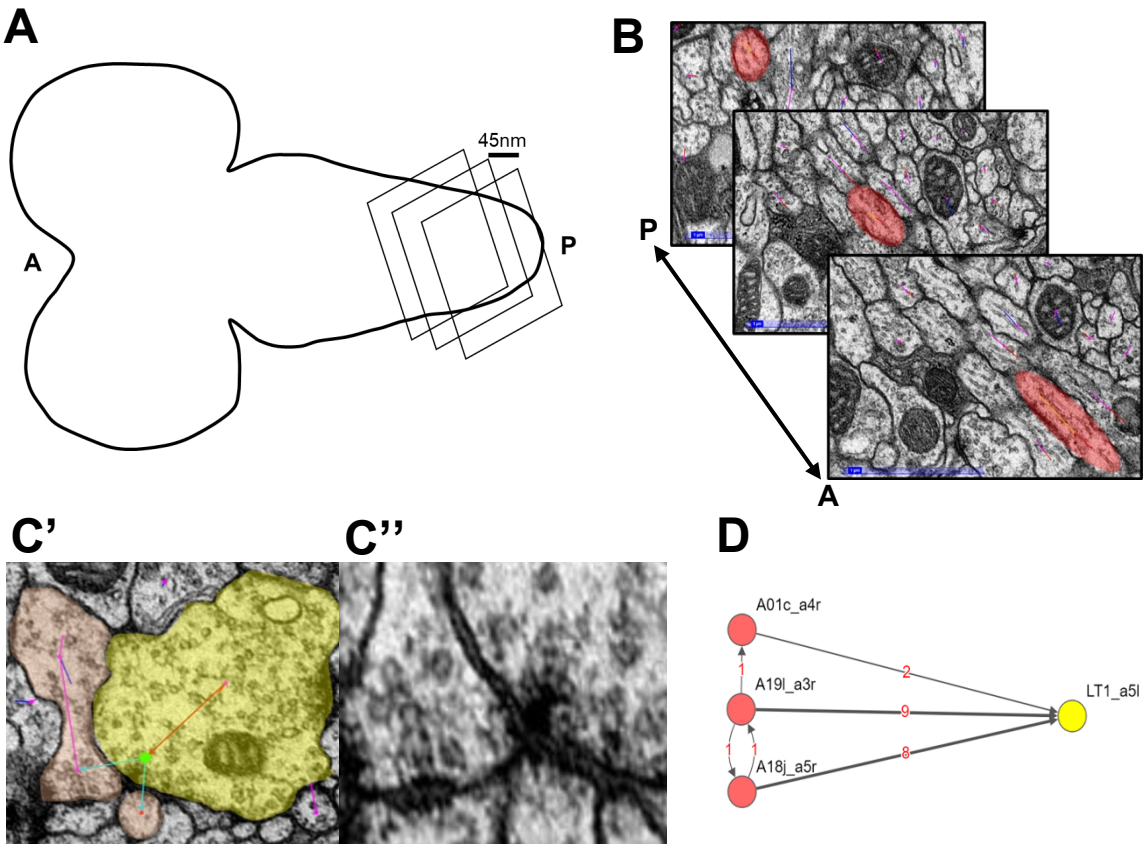

Figure 3.2.1 CATMAID is used to virtually reconstruct neurons and analyse their connectivity

(A) A 6 hour old larval central nervous system (CNS) was frozen and sliced into 45nm sections using a microtome. **(B)** Transmission electron microscope images of sections can be annotated using CATMAID allowing users to "trace" the 3-dimensional morphology of neurons (red). **(C) (')** Pre-synaptic (yellow) and post-synaptic (red) neurons can be annotated using a connector link. **(")** Synapses are typically identified in CATMAID EM images by the presence of dark, T-shaped clefts as well as the presence of pre- and post-synaptic vesicles. **(D)** The "Graph" widget in CATMAID allows users to identify the connections between neurons as well as the strength of these connections (as measured by the number of synapses).

3.2.2 Reconstruction of the LT-1/2 motor neurons using CATMAID

Self-righting behaviour (or 'SR') consists of a stereotyped behavioural sequence in which the larva, when inverted along the dorsoventral axis, struggles, and eventually performs a full 180˚ rotation to return its ventral surface to contracting the substrate (Picao-Osorio *et al.,* 2015; 2017). Previous work by our lab has identified the Lateral Transverse 1 and 2 motor neurons (or 'LT-1/2 MNs') as key cellular substrates of SR behaviour and shown that their normal activity is necessary for timely SR behaviour (Picao-Osorio *et al.,* 2015).

The identification of the role of LT-1/2 MNs in control of SR behaviour occurred as part of a wider study into the control of motor behaviour by the miRNA, *miR-iab-4*. In this study, Picao-Osorio and colleagues showed that the expression of *miR-iab-4* was highest in abdominal segments A4, A5 and A6 and that repression the expression of the Hox gene, *Ultrabithorax* by *miR-iab-4* was necessary to facilitate normal LT-1/2 activity and normal self-righting behaviour.

In order to further investigate the cellular substrates underlying SR behaviour therefore, we began by using CATMAID to reconstruct the LT-1/2 MNs in abdominal segments A4 and A5 of the VNC.

The LT-1/2 MNs innervate a pair of transverse muscles of the same name (Landgraf *et al.,* 1997) and form part of a group of 4 LT motor neurons present in each of the seven abdominal hemisegments of the larval ventral nerve cord. Myotopic maps produced by Bate and colleagues have shown that in the most posterior abdominal segment (A8), only LT1 is present (Bate & Martinez Arias, 1993) (Figure 1.3).

Our reconstruction of the LT-1/2 MNs began with the identification of the segmental nerve from which they branch (Landgraf *et al.,* 1997). After identifying this branch in the CATMAID volume, we systematically reconstructed neurons branching from it in the neuropil until we identified the LT-1/2 MNs by their distinctive morphologies (Figure 3.2.2B). As the LT-1/2 MNs had already been reconstructed by other researchers in more anterior segments such as A1 and A2, we then continued towards the posterior also reconstructing the LT-1/2 MNs in segments A6 and A7.

The identification and reconstruction of the LT-1/2 MNs in each of the first 7 abdominal segments (Figure 3.2.2A) allowed us to address various questions about how anteroposterior location may be related to changes in neuronal morphology. As a Hox gene involved in anteroposterior patterning, *Ultrabithorax* is expressed in a specific domain along the larval VNC (Struhl and White, 1985) and its role in facilitating the normal neuronal activity of the LT-1/2 MNs (Picao-Osorio *et al.,* 2015) led us to question how this may be related to segment-specific morphological and connectivity-related characteristics.

3.2.3 Connectomic analysis of the LT-1/2 motor neurons

3.2.3.1 Analysis of LT-1/2 motor neuron morphology

Firstly, we examine whether there is any significant difference between the overall morphology of the LT1 and LT2 motor neurons. We predicted that although LT2 has a slightly longer main axon than LT1, the two neurons show similar dendritic branching patterns and therefore overall morphology would not be significantly different. The results of our analysis validate this prediction,

finding that the total raw cable length of LT1 and LT2 is not significantly different (Figure 3.2.2C). Along the AP axis, however, we find that the raw cable length of both neurons fluctuates (Figure 3.2.2D) in tandem suggesting a degree of segment-specific influence on their morphologies. Between the anterior abdominal segments A1 and A2, the raw cable length of both LT1 and LT2 MNs fall before the raw cable length of both neurons increases in abdominal segment A3. A reduction in raw cable length is also observed in both neurons in A4 before another increase in A5. In the two most posterior segments analysed (abdominal segments A6 and A7), the raw cable length of both LT1 and LT2 are both slightly reduced. Initially, we predicted that although there may be some differences, the raw cable length of LT1 and LT2 would remain relatively consistent along the anteroposterior axis to facilitate consistent motor output along the larval body. Our observation of such severe fluctuations in raw cable length, however, was unexpected and suggests that the systems directly responsible for motor output are morphologically refined in each segment of the VNC and prompts questions surrounding the relevance of this to behavioural output.

3.2.3.2 Analysis of LT-1/2 motor neuron upstream connectivity

Building on the identification of anteroposterior fluctuations in LT-1/2 morphology, we then examine whether any changes in overall synaptic connectivity are evident. We predicted that synaptic connectivity and morphology would be intrinsically linked and firstly analysed the total synapse number of LT1 and LT2 motor neurons along the AP axis. The results of our

analysis show that the relationships in the total synapse number of LT1 and LT2 motor neurons in each segment (Figure 3.2.2E) are largely the same as the relationships between the raw cable length of the two neurons, validating our prediction and suggesting that segment-specific changes to overall morphology are related to changes in overall connectivity.

Finally, we analyse whether the previously observed fluctuations manifest in changes to the scarcity of LT-1/2 input synapses (i.e., the number of these synapses per nm of cable length). We hypothesised that synapse scarcity would fluctuate in a similar fashion to total synapse number (Figure 3.2.2E) and raw cable length (Figure 3.2.2D) however we observe that moving from the anterior segments to the posterior segments, input synapses to LT1 and LT2 become rarer from A1 to A7 (Figure 3.2.2F). This suggests that although raw cable length and total number of input synapses fluctuate in tandem, synapses become more spread out over the dendritic portions of the LT-1/2 MNs from anterior to posterior.

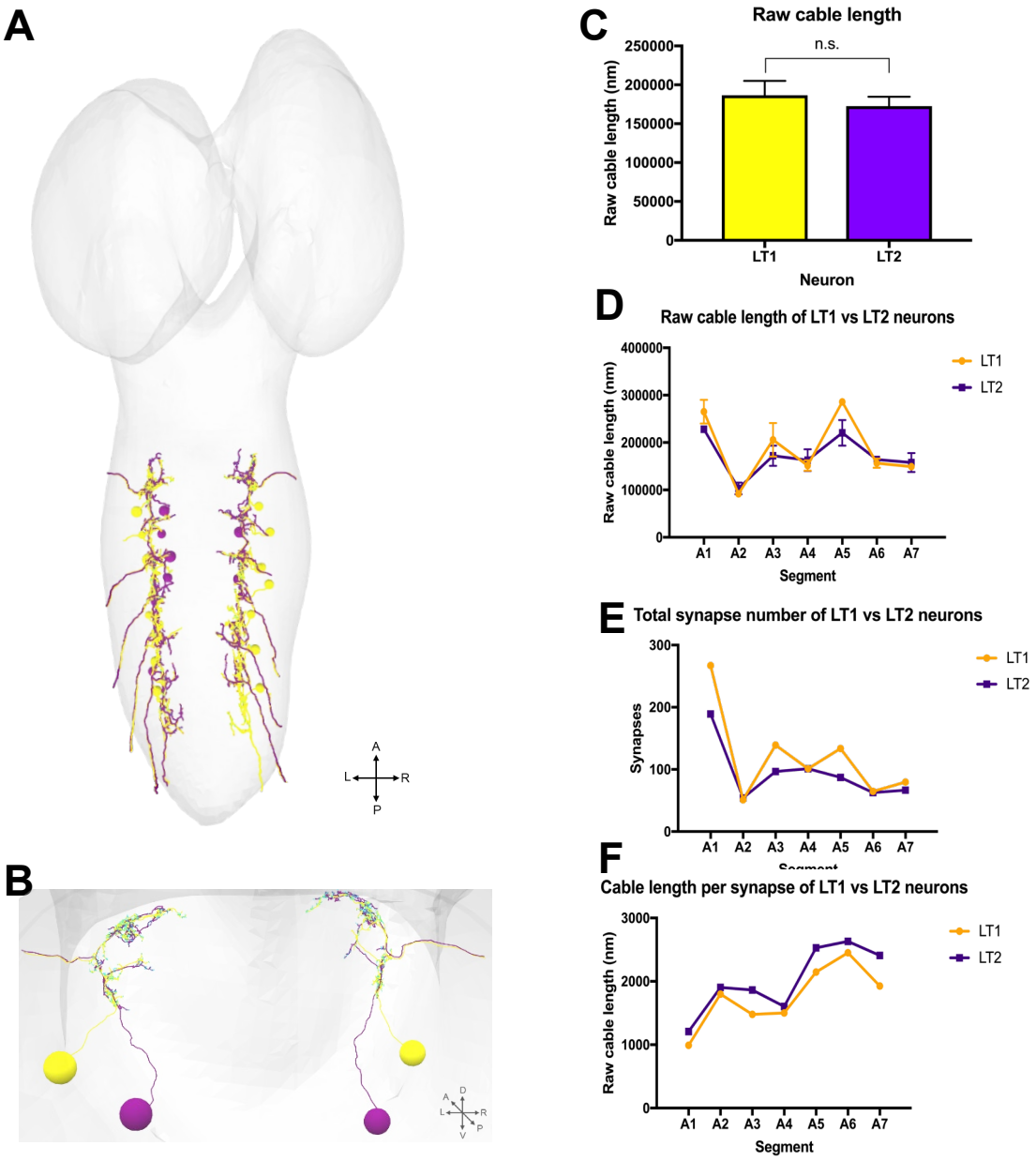

Figure 3.2.2 The morphology and upstream connectivity of the LT-1/2 MNs fluctuates along the AP axis

(A) The LT1 (yellow) and LT2 (purple) motor neurons were reconstructed in the first seven abdominal segments of the larval ventral nerve cord using CATMAID. **(B)** A transverse view of the LT-1/2 MNs on either side of abdominal segment A1. Both neurons have cell bodies located ventrally and arborise in the dorsal region of the VNC where they receive synaptic input from premotor

components. **(C)** No signifcant difference is observed between the average raw cable length of the LT1 and LT2 motor neurons along the first seven abdominal segments. **(D)** The average raw cable length of the LT1 and LT2 motor neurons fluctuate in tandem along the anteroposterior axis. **(E)** The total synapse number of the LT1 and LT2 motor neurons falls substantially between abdominal segments A1 and A2 before fluctuating across abdominal segments A3-A7. **(F)** The scarcity of synapses (measured as the cable length per synapse) increases overall in both LT1 and LT2 motor neurons towards the posterior segments of the VNC. Please note, Dr. Joao Picao-Osorio reconstructed the LT-1/2 motor neurons in segment A4.

3.2.4 Five interneurons provide strong and consistent input to the LT-1/2 MNs

The identification and characterisation of the LT-1/2 MNs in the first seven abdominal segments of the VNC, allowed us to use CATMAID to identify and investigate upstream interneurons providing premotor input as part of our investigation of the cellular substrates of SR behaviour (Figure 3.2.3A). Building on the work of others in the field (Schneider-Mizell *et al.,* 2016), we applied a threshold of 3 synapses for meaningful (or "strong") connections between 2 neurons and reviewed our connectomics data for neurons providing consistent (i.e., in several abdominal segments) and strong synaptic input to the LT-1/2 MNs.

We identify a group of five neurons, consistently providing strong contralateral input to the LT-1/2 MNs along the first six abdominal segments of the VNC (which we term the 'pre-LT interneurons') (Figure 3.2.3B). Four of these neurons (A18j, A01c, A14a and A19l) belong to a group of previously characterised premotor interneurons that facilitate timely contraction of transverse muscles during larval locomotion (Zwart *et al.,* 2016). Zwart and colleagues have termed the A18j (Figure 3.2.3Bi) and A01c (Figure 3.2.3Bii) interneurons "excitatory interneuron 1" (or eIN-1) and "excitatory interneuron 2" (or eIN-2) respectively, due to their production of the excitatory neurotransmitter, choline acetyltransferase. Zwart and colleagues have also termed the A14a (Figure 3.2.3Biii) and A19l (Figure 3.2.3Biv) interneurons "inhibitory interneuron 1" (or iIN-1) and "inhibitory interneuron 3" (or iIN-3), respectively due to their production of the inhibitory neurotransmitter, GABA. In

this chapter, we use the nomenclature developed by Zwart and colleagues to describe these four neurons.

During our reconstruction work, we were able to identify singular eIN-1, eIN-2, and iIN-1 interneurons in each of the first 12 abdominal hemisegments of the larval VNC, however, we remain unable to identify iIN-3 neurons in segments posterior to A3 (and even within A3, we only identify an iIN-3 interneuron on the right-hand side of the VNC). The unusual morphology of the iIN-3 interneurons however (in which projections extend into anterior and posterior segments) still provides the ability for these neurons to contact LT-1/2 MNs in distant segments and so we continue to analyse iIN-3 as part of the group of five pre-LT interneurons. Our identification of the A26f neuron (Figure 3.2.3Bv) as a pre-LT interneuron is particularly interesting as it was previously uncharacterised, and we discuss this in more detail in Section 3.2.6.

3.2.5 Analysis of pre-LT interneuron connectivity using CATMAID

Our connectomics analysis of the pre-LTs began with an investigation of how much of the total synaptic input received by LT-1/2 MNs was comprised of input from each pre-LT interneuron (Figure 3.2.3C). We predicted that considering the study produced by Zwart and colleagues in which eIN-1, eIN-2 and iIN-1 were all shown to be functionally connected to the LT-1/2 MNs, we would observe that they represent large proportions of the LT-1/2 MN's total input. Unexpectedly, we observe that each of these neurons represents less than 10% of total synaptic input with eIN-1 on representing 9.12% on average, eIN-2 representing 7.13% on average and iIN-1 only representing 3.33% on average.

We observe that the inhibitory interneuron iIN-3 (which our reconstruction work could only identify in segments A1, A2 and A3) represents 8.45% but that the uncharacterised interneuron A26f represents 13.15% of LT-1/2 input, the highest amount of all five pre-LT interneurons.

Building on this and our previous identification of fluctuations in total LT-1/2 input along the anteroposterior axis (Figure 3.2.2E), we examined how the proportion of total LT-1/2 input that the five pre-LT interneurons contributed changed along the AP axis (Figure 3.2.3D). Our results indicate that iIN-1 neurons provide a consistently low proportion of LT-1/2 input (ranging from 2.32% to 5.6%), however we observe large fluctuations in the proportion of LT-1/2 input provided by the other four pre-LT interneurons. In the cases of A26f and eIN-1, the proportion of LT-1/2 input in abdominal segments A1-A6 ranges by 9.7% and 10% respectively while in the cases of eIN-2 and iIN-3, ranges increase to 13.15% and 14.33%. Along the AP axis, we also observe decreases in the proportion of LT-1/2 input from eIN-1, A26f and iIN-3 in the more posterior segments (A4-A6).

We suggest therefore that segment-specific factors refine communication between motor and premotor elements of the CNS and to further investigate this we have also analysed how much of the total synaptic output provided by the five pre-LT interneurons is represented by synaptic connections to LT-1/2 MNs (Figure 3.2.3E). We observe that in A26f, eIN-1 and eIN-2, this value is relatively consistent on average at 15.13%, 14.21% and 13.54% respectively. We also observe that (similar to the proportion of LT-1/2 input provided by iIN-1) the proportion of total iIN-1 output provided to LT-1/2 is the lowest of the five pre-LT interneurons at 6.57%, We do, however, observe a large imbalance

between the same statistics when analysed for the iIN-3 interneurons. We note that although LT-1/2 MNs receive 8.45% of their input from iIN-3 neurons on average, 21.96% of iIN-3 output is represented by LT-1/2 MNs suggesting a key role for iIN-3 input to LT-1/2 interneurons.

Finally, we examine how the proportion of total pre-LT synaptic output provided to the LT-1/2s changed along the AP axis (Figure 3.2.3F) and find that although we observe cases of large fluctuations (for example, 22.9% of eIN-2 output is to LT-1/2 MNs in A1 and this falls to 13.2% in A2), for the most part fluctuations are mild (on average, less than 5%).

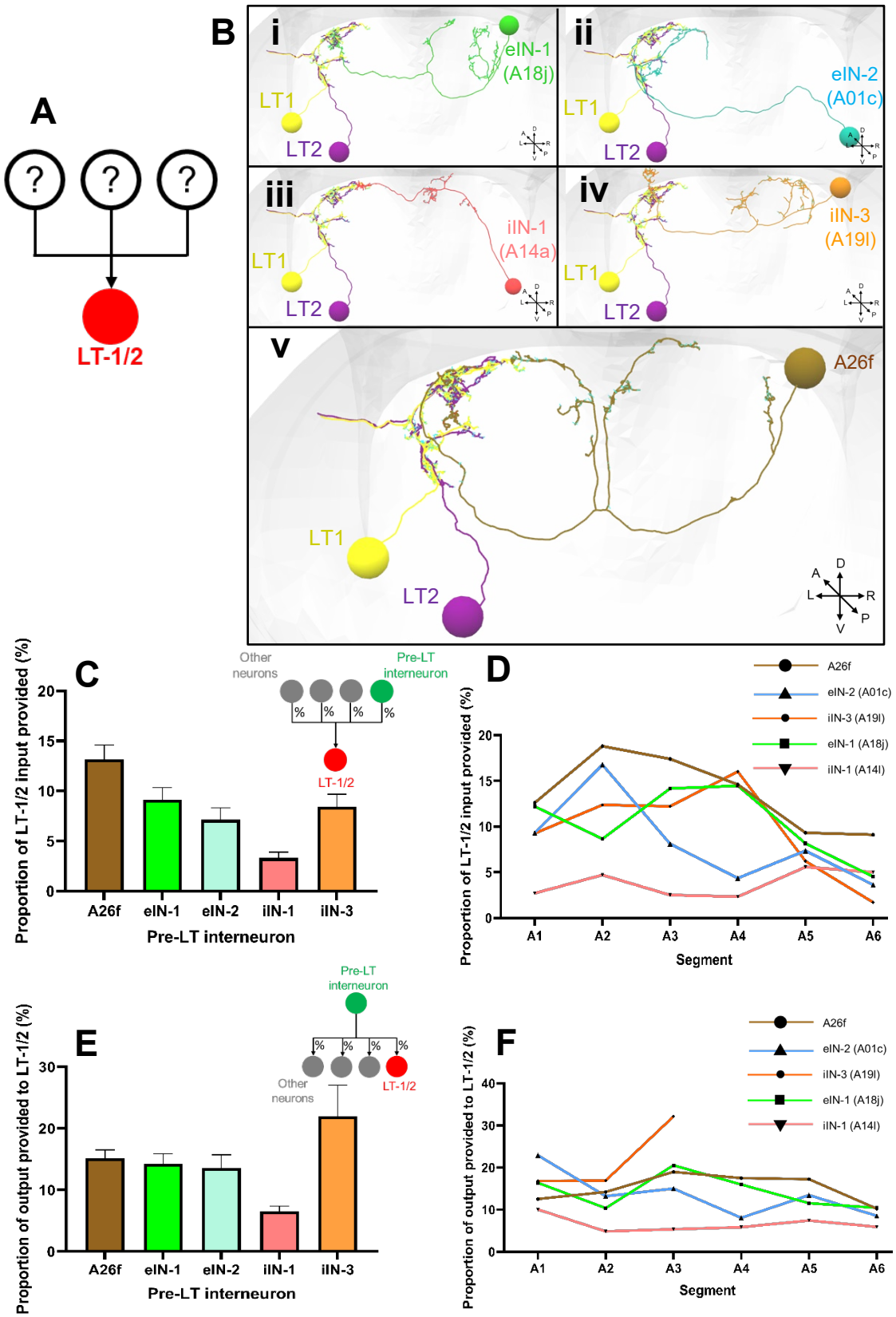

Figure 3.2.3 Five premotor interneurons provide strong, consistent input to the LT-1/2 MNs along the AP axis

(Legend on the following page)

(A) Having previously identified the LT-1/2 MNs as key cellular substrates of self-righting behaviour, we investigated premotor components providing upstream input. **(B)** The five pre-LT inteneurons provide contralateral input to the LT1 (yellow) and LT2 (purple) motor neurons in a strong and hemisegmentally-repeated fashion (i) A skeletonised representation of an eIN-1 interneuron (green) interacting with the LT-1/2 MNs. (ii) A skeletonised representation of an eIN-2 interneuron (blue) interacting with the LT-1/2 MNs. (iii) A skeletonised representation of an iIN-1 interneuron (pink) interacting with the LT-1/2 MNs. (iv) A skeletonised representation of an iIN-3 interneuron (orange) interacting with the LT-1/2 MNs. (v) A skeletonised representation of an A26f interneuron (brown) interacting with the LT-1/2 MNs. **(C)** On average, A26f interneurons provide the highest proportion of total LT-1/2 motor neuron input of the five pre-LT interneurons identified. **(D)** The proportion of total input that LT-1/2 MNs receive from the A26f, eIN-1, eIN-2 and iIN-3 pre-LT interneurons substantially varies along the anteroposterior axis. **(E)** On average, iIN-3 interneurons provide the highest proportion of their output to LT-1/2 MNs of the five pre-LT interneurons identified. **(F)** The proportion of total output provided to LT-1/2 MNs by the five pre-LT interneurons remains relatively consistent along the anteroposterior axis with the exception of iIN-3.

3.2.6 The A26f pre-LT interneurons

3.2.6.1 Reconstruction of the A26f pre-LT interneurons

As previously mentioned, our investigation of strongly connected pre-LT interneurons, led to the identification of the previously uncharacterised interneuron, A26f. A26f neurons exhibit a characteristic morphology in which the cell body is located in the dorsolateral region of the VNC (Figure 3.2.4A). The main axonal projection extends ventromedially from the cell body towards to centre of the VNC where two large projections branch off and extend dorsally where they arborise (forming dendritic arbors that are mainly post-synaptic). The main axonal projection continues to extend across the mid-line of the VNC and eventually dorsolaterally, arborising to form another dendritic region that extends in anterior and posterior segments and is mainly pre-synaptic.

We were able to reconstruct the A26f interneurons in the posterior abdominal segments A4-A6 and, combined with previous reconstruction work in more anterior segments, this reveals that the A26f interneurons exist as single hemisegmentally-repeated neurons (Figure 3.2.4C). We do, however, note that the presence of large sections of missing EM images hampered our ability to fully reconstruct the central pre-synaptic hubs of the A26f neurons in segments A4 and A5.

3.2.6.2 The A26f pre-LT interneurons provide strong contralateral input the LT-1/2 MNs and interact with iIN-3 ipsilaterally

Regarding the interaction between A26f interneurons and LT-1/2 MNs, we have identified strong connection between A26f interneurons and LT-1/2 MNs on

both sides of each of the first six abdominal segments (Figure 3.2.4D) and our connectomics analysis reveals that all synaptic interaction between A26f interneurons and LT-1/2 MNs is contralateral (similar to the other four pre-LT interneurons) (Figure 3.2.3B).

Our connectomics analysis also reveals strong ipsilateral connection between the iIN-3 pre-LT interneurons and the A26f interneurons (Figure 3.2.4E). On average, individual iIN-3 interneurons provide 2.7 synapses onto ipsilateral A26f interneurons and A26f interneurons provide 5.1 synapses onto ipsilateral iIN-3 interneurons suggesting the existence of a strong feedback loop between the two neurons in addition to their individual connections to LT-1/2 MNs.

3.2.6.3 Analysis of A26f connectivity along the mediolateral and anteroposterior axes

Having identified this ipsilateral feedback loop between A26f and iIN-3 interneurons, we were prompted to perform connectomic analysis to analyse the proportion of contralateral to ipsilateral connection provided by A26f to other circuit neurons (i.e., the LT-1/2 MNs and pre-LT interneurons) (Figure 3.2.4F). We find that the proportion of contralateral to ipsilateral connection is similar on both sides of the VNC with 81% of A26f circuit-specific output connections being contralateral on the left of the VNC and 86% of A26f circuit-specific output connections being contralateral on the right. This suggests a high degree of symmetry to the roles of the LT-1/2 MNs and implies the need for left-right co-ordination in output, something is particularly key in self-righting for successful completion of the behavioural sequence.

Finally, considering the morphology of the A26f interneurons (in which we noted that the dendritic arbors representing the pre-synaptic hub of the neurons often extended into anterior and posterior segments), we analysed the directionality of A26f information flow in an attempt to shed light on the potential functional roles of the neurons (Figure 3.2.4G). The results of our analysis indicate that, of all synaptic output provided by A26f interneurons to other neurons in the putative circuit, 35% of synapses are between A26f interneurons and neurons in anterior segments. In addition to this, 31% of A26f output to these neurons is intrasegmental while 34% is provided to neurons in posterior segments. The finding that anterior, intrasegmental and posterior output is nearly equal was unexpected as we predicted that A26f synaptic output would mainly be to LT-1/2 MNs in the same segment. This finding suggests that A26f may play an important role in the co-ordination of downstream LT-1/2 MN activity across abdominal segments.

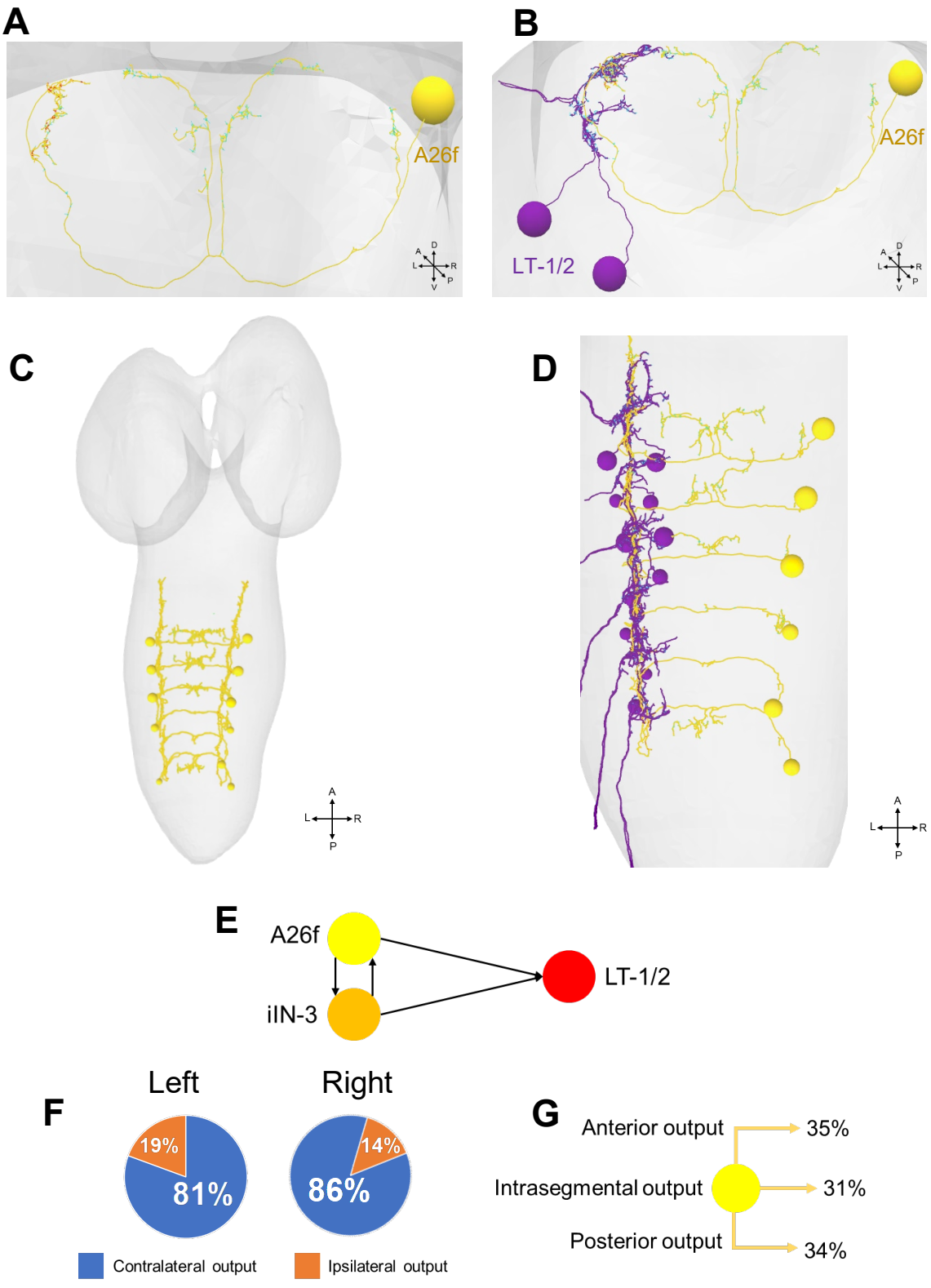

Figure 3.2.4 The A26f interneurons provide strong, contralateral input to to LT-1/2 MNs intrasegmentally and intersegmentally

(Legend on the following page)

(A) A transverse view of the skeletonised A26f interneuron in segment A1. The A26f neuron has a long projection extending across the mid-line from which two branches extend dorsally that contain many of the neuron's post-synaptic inputs (blue). Contralateral to the cell body, a large dendritic projection containins many of the neuron's pre-synaptic outputs (red). **(B)** A transverse view of the contralateral interaction between the A26f interneurons (yellow) and the LT-1/2 MNs (purple). **(C)** The A26f interneurons (yellow) were reconstructed in each of the first six abdominal segments of the VNC. **(D)** A dorsal view of the interaction between the A26f interneurons (yellow) and the LT-1/2 MNs (purple) in each of the first six abdominal segments. **(E)** Our connectomics analysis reveals the existence of a feedback loop between the A26f and iIN-3 pre-LT interneurons in additon to their shared connection to the LT-1/2 MNs **(F)** On both sides of the VNC, A26f interneurons provide nearly equal amounts of contralateral and ipsilateral output to the LT-1/2 MNs and other pre-LT interneurons. **(G)** On average, the percentage of output to LT-1/2 and other pre-LT interneurons in the same segment, anterior segments and posterior segments is nearly equal.

3.2.7 The A27k, A19f and Down-and-Back interneurons provide synaptic input to premotor and motor elements of the SRC

3.2.7.1 The A27k interneurons are key for mediolateral co-ordination of motor and premotor elements

Having identified five pre-LT interneurons providing substantial premotor input to the LT-1/2 MNs, we moved on to identify upstream neuronal components that may provide a link between these neurons and sensory components – allowing the completion of a sensorimotor pathway as part of the neural diagram underlying self-righting (Figure 3.2.5A).

We firstly identify that the A27k interneurons provide strong and consistent connection to both the eIN-1 and eIN-2 pre-LT interneurons as well as the LT-1/2 MNs along the length of the VNC (Figures 3.2.5Bi to 3.2.5Bvi, dark blue). The A27k interneurons (otherwise known as the “Ifb-Bwd” neurons) have recently been characterised by Kohsaka and colleagues (Kohsaka *et al.,* 2019) who described their functional role in the mediation of intersegmental feedback signalling. Morphologically, the cell bodies of A27k neurons are located in the dorsolateral region of the VNC from where axonal projections extend ventrally. Unlike the pre-LT interneurons however (which have axonal projections extending across the mid-line of the VNC), axonal projections from A27k interneurons extend towards the anterior of the VNC into the adjacent anterior segment before extending dorsally again to form a characteristic looping shape (Figure 3.2.5Biii).

Our connectomics analysis reveals that all connections from A27k interneurons to eIN-1 interneurons (as well as to LT-1/2 MNs) are ipsilateral whereas all

connections between A27k interneurons and eIN-2 interneurons are contralateral. We suggest, therefore, that A27k not only plays a role in anteroposterior co-ordination as highlighted by Kohsaka and colleagues but also in mediolateral co-ordination of motor and premotor elements, potentially strengthening overall connection between motor elements on both sides of the VNC.

3.2.7.2 The first order Down-and-Back interneurons provide input to downstream pre-LT and LT-1/2 MNs

Upstream of the A27k interneurons, we also identify substantial connection to a well-characterised set of interneurons directly downstream of sensory components named the Down-and-Back interneurons (Figure 3.2.5Biv to Figure 3.2.5Bvi, red). The Down-and-Back interneurons were reconstructed in the first five abdominal segments by Burgos and colleagues who identified their functional role in the promotion of larval C-bending behaviour (Burgos *et al.,* 2018). Morphologically, they project from the mediolateral cell body towards the ventromedial neuropil where arborisation occurs. A second large projection then extends dorsolaterally back towards the cell body.

Our connectomics analysis shows that, in agreement with analysis produced by Burgos and colleagues, the Down-and-Back interneurons provide substantial input to ipsilateral A27k interneurons along the length of the VNC. Burgos and colleagues also refer to “modest” connections made by the Down-and-Back interneurons directly to ipsilateral LT1 MNs and we also observe these but note that we find only them to be above 3 synapses on average on the left hand side

of the VNC. On the right hand side, we find Down-and-Back connections to LT1 MNs to be relatively weak with an average of 1.75 synapses between the two neurons.

3.2.7.3 The A19f interneurons act as premotor integrators

Finally, our connectomics analysis reveals the presence of another integrator neuron connected to pre-LT interneurons in a similar fashion to A27k. The A19f interneurons (Figure 3.2.5Bvii to Figure 3.2.5ix, pink) provide substantial contralateral input to the pre-LT interneurons A26f while receiving substantial contralateral input from the pre-LT interneurons eIN-2, and we class A19f as a ‘premotor integrator’ neuron. Functionally uncharacterised, the A19f interneurons exhibit a similar morphology to the A27k interneurons with cell bodies also located in the dorsolateral region of the VNC and a ventrally-projecting main axon which gradually extends anteriorly into the adjacent segment before projecting dorsally again. A key difference between the A19f and A27k interneurons, however, is the length of the projection that extends anteriorly from the dorsal region of the immediately anterior segment. In A19f neurons, this projection is extremely long and can extend from A19f neurons in segment A8 to connect with neurons located in the first thoracic segment suggesting that, even though A19f plays a role in mediolateral co-ordination of premotor elements, it may also play an important role in general anteroposterior co-ordination.

3.2.7.4 Analyses of A27k, Down-and-Back and A19f SRC-specific connectivity

We applied similar connectomics analyses to the Down-and-Back, A27k and A19f interneurons to that previously applied to the pre-LT interneurons (Figure 3.2.3C). Firstly, we analysed how much of the Down-and-Back, A27k and A19f interneurons' total synaptic output was provided to other circuit neurons (Figure 3.2.5C) (Note, we included the output from the Down-and-Back interneurons to the nociceptive integrator neuron TePn05 in this analysis which is discussed further in Section 3.2.11.1).

The results of this analysis show that the Down-and-Back interneurons and A27k interneurons provide similar proportions of their total output to self-righting circuit neurons (or 'SRC-specific output'). 9% of Down-and-Back output is SRC-specific while 9.5% of A27k output is SRC-specific but this falls to 5.5% in A19f interneurons. While we initially postulated that this difference could be explained by the sheer difference in sizes between the A19f and Down-and-Back interneurons (in other words, that A19f neurons project into many more segments and therefore provide a much higher number of output synapses overall), we find that on average A19f neurons have 422 output synapses compared to 397 and 272 for Down-and-Back and A27k interneurons, respectively. This implies that the reduction in SRC-specific output in A19f neurons is not due to a large increase in overall output minimising the contribution of SRC-specific output. We suggest, though, that the A19f output connectome may be much more diversified than Down-and-Back, receiving and providing input to more classes of neuron in its function as a premotor integrator

as opposed to Down-and-Back/A27k neurons that have more strictly defined roles in passing signal from sensory to motor components.

Investigating changes to SRC-specific output along the length of the AP axis (Figure 3.2.5D), the results of our analysis reveal a decrease in the percentage of SRC-specific output provided by A27k as well as a slight increase in this metric for Down-and-Back neurons (particularly in the posterior abdominal segments A3-A5). For the A19f interneurons, we observe fluctuations in the percentage of SRC-specific output, however, the range of these values is relatively low at 6.6% suggesting a consistency of A19f SRC-specific output along the AP axis and that its role as a premotor integrator is maintained in a consistent fashion.

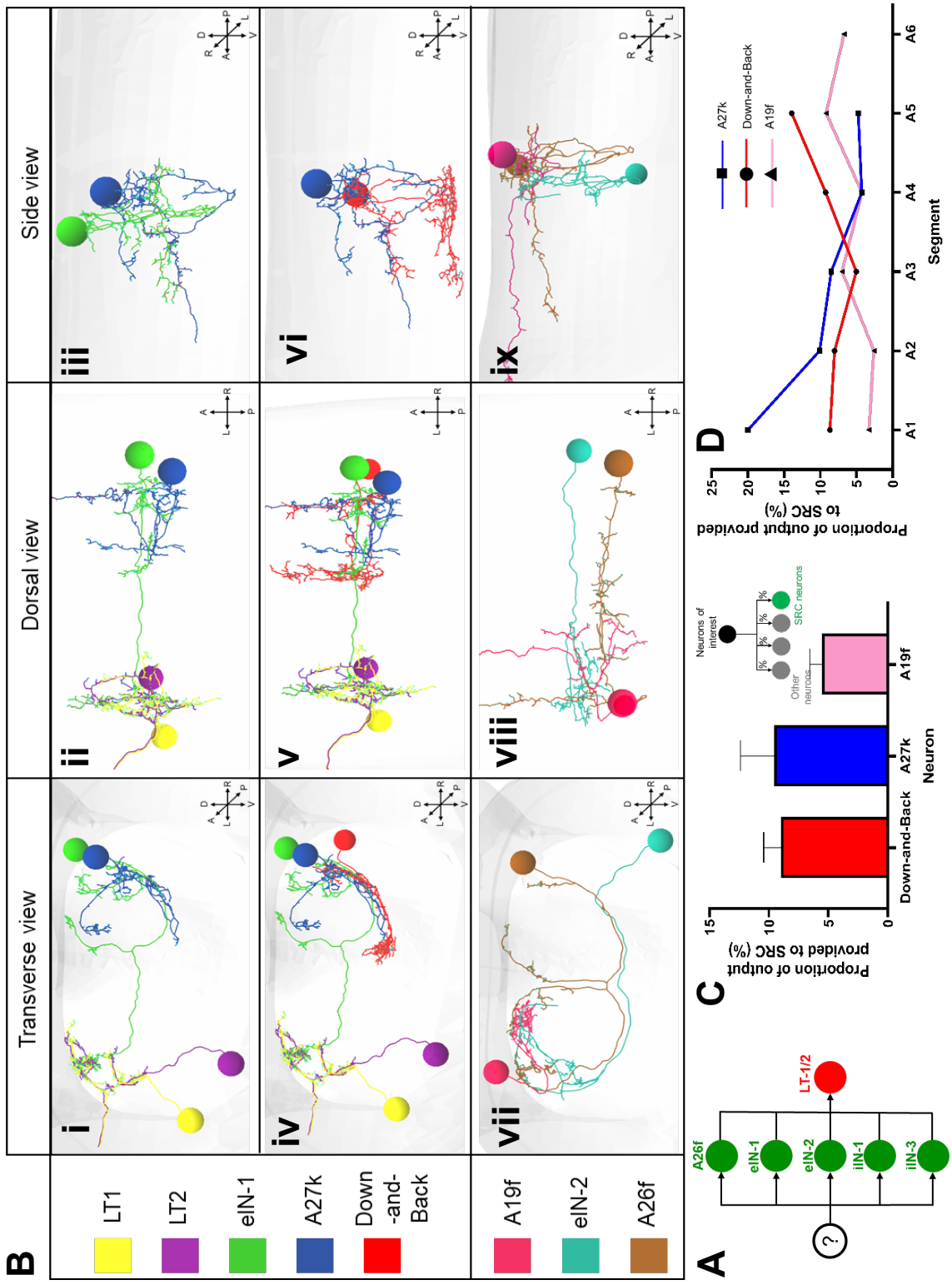

Figure 3.2.5 The Down-and-Back neurons communicate with pre-LT interneurons while the A27k and A19f neurons act as premotor integrators

(Legend on the following page)

(A) Building on the identification of premotor components providing substantial upstream input to the LT-1/2 MNs, we used CATMAID to investigate upstream neuronal components in an attempt to build a sensorimotor pathway. **(B)** We identify the A27k (dark blue) and A19f (pink) interneurons as integrators of premotor signalling within the SRC. We also identify indirect connections between the A27k interneurons and the Down-and-Back interneurons (red) with the LT1 (yellow) and LT2 (purple) motor neurons. (i) (ii) and (iii) Alternative views of the interaction between eIN-1 (green), A27k and LT-1/2 MNs in segment A1. (iv) (v) and (vi) Alternative views of the interaction between eIN-1 (green), A27k, Down-and-Back and LT-1/2 MNs in segment A1. (vii) (viii) and (ix) Alternative views of the interaction between A19f, eIN-2 (cyan) and A19f neurons in segment A1. **(C)** On average, the Down-and-Back and A27k interneurons provide similar proportions of their output to other neurons in the SRC while A19f provide a reduced amount. **(D)** The proportion of total input that other SRC neurons receive from the Down-and-Back interneurons slightly increases towards the posterior segment. From the A27k interneurons SRC-specific output steadily decreases while SRC-specific output from A19f interneurons remains relatively consistent.

3.2.8 The neurons of the rolling circuit share common sensory input with the SRC

Having identified the Down-and-Back and A27k interneurons as key upstream elements of the circuitry providing input to the pre-LT interneurons, we noted that Down-and-Back interneurons receive direct synaptic input from the multidendritic class IV (or ‘md class IV’) sensory neurons (as functionally proven by Burgos and colleagues) (Figure 3.2.6B). We validated this with our connectomics analysis however this prompted the question of whether other interneurons directly downstream of the md Class IV sensory neurons (i.e., ‘first-order’ interneurons) were also connected to the growing SRC (Figure 3.26A).

We noted that previous work by Ohyama and colleagues (in which the identity of a putative circuit for rolling behaviour in larvae was established) linked the md class IV sensory neurons to a master neuron for rolling named, ‘Goro’ (Ohyama *et al.,* 2015) (Figure 3.2.6C). Considering the shared dorsoventral rotational aspect of self-righting and rolling behaviours, we therefore investigated the nature of connection between the neurons of this rolling circuit and those of our SRC.

3.2.9 Reconstruction and connectomic analysis of the rolling circuit neurons

3.2.9.1 Identification and reconstruction of the Md Class IV-to-Goro sub-pathway

During our reconstruction work, we encountered previous reconstructions of neurons of the Md class IV subtype (v'ada, vdaB and ddaC) in each of the first six abdominal segments and noted that in the first five abdominal segments, they were connected to the ventromedially-projecting Basin-2 and Basin-4 interneurons (as reported in Ohyama *et al.,* 2015) (Figure 3.2.6Di). We also noted strong connections between the Basin-2/4 interneurons and dorsomedially projecting A05q interneurons (Figure 3.2.6Dii) as reported by Ohyama and colleagues.

Our reconstruction work was unable to identify neurons matching the morphology of A05q in abdominal segments posterior to A2 and we therefore exclude it from later analyses of SRC-specific output along the length of the AP axis (Figure 3.2.6G). Ohyama and colleagues demonstrated functional synaptic connection between the A05q and Goro interneurons *in vivo* and our connectomics analysis supports this showing that A05q provides strong synaptic input to Goro (Figure 3.2.6Diii).

The downstream Goro interneurons are a pair of interneurons functionally shown by Ohyama and colleagues to act as 'master' neurons for rolling behaviour, solely facilitating the rolling that occurs as part of the larval nociceptive escape response (Hwang *et al.,* 2007; Ohyama *et al.,* 2015). From the two cell bodies located in T2, long projections extend both anteriorly and

posteriorly along the entire length of the VNC providing input to and receiving input from neurons in all thoracic and abdominal segments (Figure 3.2.6E). Our connectomics analysis confirms that A05q provides strong contralateral input to the two Goro interneurons however we also observe weak ipsilateral input to each of the Goro interneurons.

3.2.9.2 Identification and reconstruction of the chordotonal organ-to-Goro sub-pathway

A second pathway between sensory components and the Goro interneurons was also identified by Ohyama and colleagues. This pathway stems from the mechanosensory chordotonal organs located in the peripheral nervous system and our connectomics analysis confirms segmentally-repeated, strong ipsilateral connection between the chordotonal organs and the Basin-3 interneurons in each of the first four abdominal segments (Figure 3.2.6Div). Downstream from the Basin-3 interneurons, we also confirm strong synaptic connections to ventromedially projecting A23g interneurons (as reported by Ohyama and colleagues) (Figure 3.2.6Dv). Similar to A05q, our reconstruction work was unable to identify neurons matching the morphology of A23g in abdominal segments posterior to A2 and we also exclude it from later analyses of SRC-specific output along the length of the AP axis.

Regarding synaptic connection between A23g and Goro, we find that the threshold for a strong connection is only met by A23g neurons on the right of the VNC providing contralateral input to the Goro interneuron on the left (Figure 3.2.6Dvi). In the opposite case, A23g neurons only provide a weak connection

(an average of 1.5 synapses) to the Goro on the right-hand side of the VNC. We hypothesise that this could represent a divergence in rolling behaviour according to the sensory trigger received. As mechanosensors, chordotonal organs respond to vibration (Ohyama *et al.,* 2015; Klann *et al.,* 2020) whereas the nociceptive md class IV neurons respond to changes in temperature (Burgos *et al.,* 2018) and external threats such as the ovipositors of parasitoid wasps (Hwang *et al.,* 2007; Robertson *et al.,* 2013). Differences in sensory input therefore could lead to different “versions” of rolling behaviour, one in which rolling is directionally biased and one in which rolling occurs with no directional bias.

3.2.9.3 Analyses of rolling circuit neuron SRC-specific connectivity

Analysing the amount of SRC-specific output that each of the ‘rolling circuit’ neurons provide as percentage of total synaptic output, we observe that the SRC-specific output of md class IV neurons far outweighs those of other rolling circuit neurons (Figure 3.2.26F). At 28.6% on average, nearly a third of the total synaptic output from md class IV neurons is dedicated to the Down-and-Back, Basin-2 and Basin-4 interneurons (with some contribution to the A02o ‘Wave’ interneurons discussed in the next section). Conversely, we only observe that, on average, only 1.6% of output synapses from chordotonal organs connect to neurons in the SRC (and that connections are solely made to the Basin interneurons). The large difference in the SRC-specific output of the two sensory components identified may reflect differences in the sensory processing of inversion during self-righting. In other words, the larva may

perceive a situation where it finds itself upside-down as a nociceptive threat rather than a mechanosensory stimulus.

In addition to this, we observe that the Basin-2 and Basin-4 interneurons dedicate similar amounts of their total synaptic output to other neurons in the SRC (7% and 6.3%, respectively) while Basin-3 dedicates 9.9%. We note that ‘second-order’ interneurons (i.e., neurons receiving input from the ‘first-order’ Basin interneurons and providing output to the Goro interneurons) differ in the amount of their total output that they provide to Goro. On average, 6.4% of A05q output is represented by connections to Goro as opposed to 2.2% of A23g output and we hypothesise that this may be a further indicator of differences in the processing of mechanosensory and nociceptive input.

Along the AP axis, we observe a general fall in SRC-specific output of Md class IV sensory neurons moving towards the posterior however overall, SRC-specific output remains much higher than from other rolling circuit neurons (Figure 3.2.6G). The SRC-specific output of the chordotonal organs remains consistently low along the AP axis (peaking at 3.7% in segment A1 and falling to 0% in segment A6) while we observe no large fluctuations in SRC-specific output from the Basin interneurons.

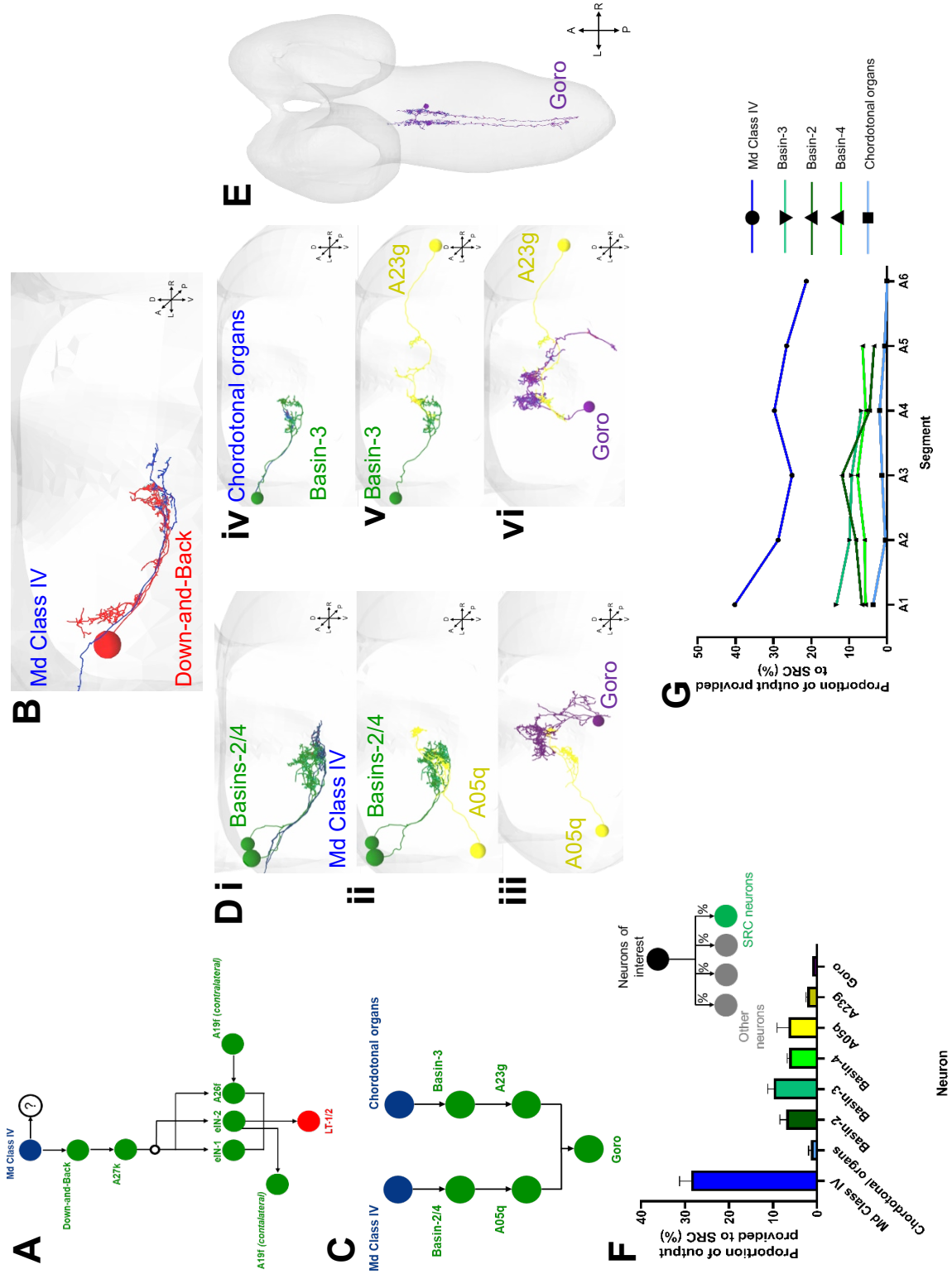

Figure 3.2.6 The neurons of the rolling circuit are connected to the SRC

(Legend on the following page)

(A) The Down-and-Back interneurons are first-order interneurons, directly receiving synaptic input from the Md class IV sensory neurons (blue). Building on this, we analysed how other first order neurons were also connected to the SRC. **(B)** A skeletonised representation of the interaction between the Md Class IV neurons ddaC, vdaB and v'ada (blue) and the Down-and-Back interneurons (red) in segment A1. **(C)** The neurons of the rolling circuit identfied by Ohyama and colleagues are also connected to the Md Class IV sensory neurons and we investigated their relationship to the other neurons of the SRC. **(D)** Transverse views of the interactions between the various neurons of the rolling circuit (i) The Md Class IV sensory neurons (blue) provide ipsilateral input to the Basin-2 and Basin-4 interneurons (green). (ii) The Basin-2 and Basin-4 interneurons (green) provide ipsilateral input to A05q interneurons (yellow) (iii) A05q interneurons (yellow) provide contralateral and ipsilateral input to the master neurons for rolling, Goro (purple). (iv) The chordotonal organs (blue) provide ipsilateral input to Basin-3 interneurons (green). (v) Basin-3 interneurons (green) provide contralateral input to A23g interneurons (yellow) (vi) A23g interneurons (yellow) provide contralateral input to the Goro interneurons (purple). **(E)** The two Goro interneurons (purple) have cell bodies located in the thoracic T2 segment and extend long projections throughout the entire larval VNC. **(F)** The proportion of total output provided by the Md Class IV sensory neurons to other neurons in the SRC far outweighs that provided by the other neurons of the SRC. **(G)** The proportion of SRC-specific output provided as a percetnage of total output from the rolling circuit neurons remains relatively consistent along the anteroposterior axis with the exception of the Md Class IV neurons where a slight decrease is observed towards the posterior.

3.2.10 The nociceptive integrator neurons TePn05 and A02o ‘Wave’ link the neurons of the rolling circuit with downstream SRC elements

Our connectomics work to this point had identified a group of pre-LT interneurons receiving input from A27k interneurons which, in turn, were receiving substantial input from the first-order Down-and-Back interneurons. We also validated the fact that Md Class IV sensory neurons were providing input to the Down-and-Back interneurons and that the neurons of the ‘rolling circuit’ identified by Ohyama and colleagues were also connected to our circuit.

We noted that the results of connectomic analysis of the TePn05 and A02o ‘Wave’ interneurons by Burgos and colleagues suggested that the pair of neurons belonged to a group that integrated nociceptive signals (Burgos *et al.,* 2018). Considering the inclusion of functionally validated nociceptive-processing elements such as the Basin and Down-and-Back interneurons, we therefore examined the nature of connections between these ‘nociceptive integrator’ neurons and the SRC (Figure 3.2.7A).

3.2.11 Reconstruction and connectomic analysis of the nociceptive integrator neurons

3.2.11.1 The TePn05 interneurons integrate signal between the Down-and-Back interneurons and the Basin interneurons

The TePn05 interneurons are a pair of interneurons based in segment A8 with long projections extending as far as the sub-oesophageal zone of the VNC (Figure 3.2.7B). Little is known about their functional role, but they have been implicated in decision-making when the larva is presented with a

mechanosensory cue (Masson *et al.,* 2020). Contacting neurons in all segments of the VNC, the results of our connectomics analysis indicate that SRC-specific output mainly comprises interaction with the Basin-2, Basin-3, and Basin-4 interneurons (Figure 3.2.7C) (with weak output provided to Md Class IV sensory, A05q, A02o 'Wave' and Down-and-Back neurons). Although TePn05 does receive some direct synaptic input from Md Class IV sensory neurons, we find that on average, these connections are weak at 1.5 synapses per connection. We also find that the only SRC neurons providing strong input to TePn05 interneurons are the Down-and-Back interneurons which provide ipsilateral connection at an average of 5.3 synapses per connection (Figure 3.2.7D).

3.2.11.2 The A02o 'Wave' interneurons receive SRC-specific signal from sensory and first-order neurons

The A02o 'Wave' interneurons are hemisegmentally-repeated interneurons with axonal projections that extend dorsally from the cell body before arborising in anterior segments (Figure 3.2.7E). At the functional level, they play a role in the decision to propagate forward or backward waves of muscular contraction during larval locomotion (Takagi *et al.,* 2017). Our connectomics analysis shows that SRC-specific output from A02o 'Wave' neurons is limited with the only connection we found to be above 3 synapses on average being ipsilateral connections between A02o 'Wave' and A05q neurons on the left of the VNC (Figure 3.2.7F). SRC-specific input, however, is substantial with Md class IV sensory neurons and Basin-2/4 interneurons providing a total of 168 and 94

synapses respectively to the A02o ‘Wave’ neurons of the first six abdominal segments.

3.2.11.3 Analysis of nociceptive integrator SRC-specific connectivity

Examining the SRC-specific output of both TePn05 and A02o ‘Wave’, we find that the output of the singular TePn05 interneurons is just over double that of the hemisegmentally-repeated A02o ‘Wave’ interneurons at 9.9% and 4.5% respectively (Figure 3.2.7G). We also find that along the AP axis, the amount of SRC-specific output provided by the A02o ‘Wave’ neurons steadily increases over the first four abdominal segments before falling in A5 and A6 (Figure 3.2.7H).

We hypothesise that this may indicate that the segment-specific nature of A02o ‘Wave’ communication (i.e., A02o ‘Wave’ stimulation in anterior segments produces fictive backward waves while Wave output in posterior segments produces fictive forward waves (Takagi *et al.,* 2017)) may also be relevant for the propagation of waves observed during larval self-righting behaviour (Picao-Osorio *et al.,* 2017).

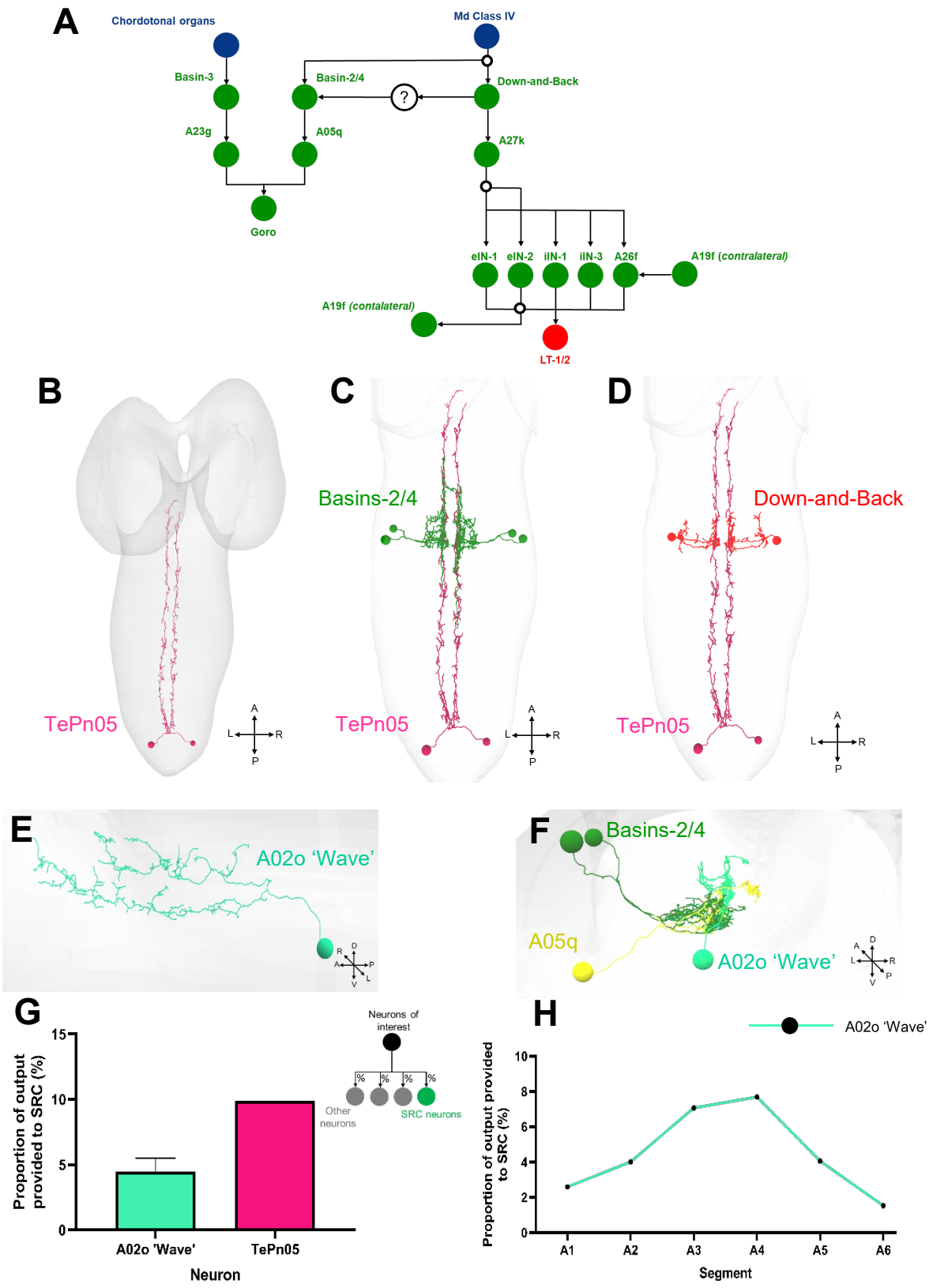

Figure 3.2.7 The nociceptive integrator neurons link the first-order neurons of the SRC

(Legend on the following page)

(A) Having established sensorimotor pathways for the control of self-righting behaviour, we investigated the scale of connection between the neurons of the SRC and the previously identified nociceptive integrator neurons **(B)** A skeletonised representation of the TePn05 interneurons (pink). The TePn05 interneurons are a pair of interneurons with cell bodies located in abdominal segment A8 that extend long projections throughout the entire larval VNC. **(C)** A skeletonised representation of the interaction between the TePn05 interneurons (pink) and the Basin-2 and Basin-4 interneurons (green) in segment A1. **(D)** A skeletonised representation of the interaction between the TePn05 interneurons (pink) and the Down-and-Back interneurons (red) in segment A1. **(E)** A side view of the skeletonised representation of the A02o 'Wave' interneuron in segment A1. A02o 'Wave' interneurons typically have a projection extending dorsally from a medially located cell body. This projection then extends towards the anterior segments where it arborises. **(F)** A transverse view of the interaction between Basin-2/4 interneurons (dark green), the A05q interneuron (yellow) and the A02o 'Wave' interneuron (light blue). **(G)** The proportion of total output provided by the TePn05 interneurons to other neurons in the SRC is more than double that that provided by the A02o 'Wave' interneurons. **(H)** The proportion of total output that A02o 'Wave' interneurons provide to other neurons in the SRC along the anteroposterior axis rises to a peak in segment A4 before falling in the posterior segments.

3.2.12 The SRC connectivity matrix

3.2.12.1 Insights into sensory and rolling circuit neuron SRC-specific connectivity

Having established a putative arrangement for the neurons of the SRC, including the directionality of their connectivity, we sought to consolidate the information gained from our connectomics analysis with the aim of revealing new insights about the architecture of the SRC. To do this, we analysed the average strength of all connections between the neurons of the SRC and created a matrix to display intra-SRC connection (Figure 3.2.8).

Our matrix reveals that sensory output to SRC neurons is not uniform with Md Class IV sensory neurons providing strong output to the first order Basin-2/4 and Down-and-Back interneurons (as well as the nociceptive integrator A02o 'Wave' interneurons). The chordotonal organs, on the other hand, exclusively provide strong output to Basin-2, Basin-3, and Basin-4 interneurons. As previously discussed, we suggest that this may reflect a bias towards the perception of larval dorsoventral inversion as a nociceptive stimulus rather than a mechanosensory input.

The first-order Basin interneurons also show differences in SRC-specific output with the Basin-2/4 interneurons providing strong input to the A05q, A02o 'Wave' and (unexpectedly) the chordotonal organs. Output from the Basin-2/4 interneurons to the chordotonal organs is solely comprised of 6 synapses between two individual neurons and we discuss this further in Section 3.2.13.3. We observe that the Basin-3 interneurons provide strong input to A23g (as well as to other Basin-3 interneurons) but nothing to neurons further downstream.

Moving further downstream, the second order A05q and A23g interneurons both provide strong input to Goro interneurons (as previously discussed) but although we observe strong A05q to A05q connection, interneuronal connection does not occur between individual A23g interneurons.

We observe no strong output from Goro to any premotor or motor components in the SRC suggesting that if Goro is exerting a motor influence in the SRC, it is either not via the LT-1/2 MNs or via, as of yet, unidentified pathways (Discussed further in Section 4.2.7).

3.2.12.2 Insights into nociceptive integrator neuron SRC-specific connectivity

Regarding the nociceptive integrator neurons TePn05 and A02o 'Wave', we note that both provide strong synaptic output to Basin interneurons but that the A02o 'Wave' interneuron also provides weak output to the premotor neurons eIN-1, eIN-2, and iIN-3. The fact that both nociceptive integrator neurons analysed provide strong output to the first-order components of the rolling circuit suggests that they do indeed serve to integrate nociceptive signals as suggested by Burgos and colleagues (Burgos *et al.,* 2018). At the behavioural level, this also suggests that they may integrate the Down-and-Back 'C-bending' pathway with the 'rolling' circuit pathway in order to facilitate a complete escape sequence and this idea is supported our identification of a strong output from Down-and-Back interneurons to the TePn05 interneurons.

3.2.12.3 Insights into first order and premotor integrator neuron SRC-specific connectivity

The Down-and-Back interneurons also provide strong input to the A27k and LT-1/2 MNs which, coupled with the strong input they receive from Md Class IV sensory neurons, confirms their role in transferring information from sensory components to the motor components in order to produce a behavioural response.

Further downstream, our matrix reveals that A27k and A19f both function as premotor integrator neurons as we observe strong connections between these neurons and pre-LT interneurons in the matrix.

3.2.12.4 Insights into premotor and LT-1/2 motor neuron SRC-specific connectivity

The 5 pre-LT interneurons themselves show strong connection to the LT-1/2 MNs as expected but, in our matrix, we observe the previously discussed strong connections between A26f interneurons and iIN-3 interneurons (as well as a strong reciprocal connection). We suggest that identification of the neurotransmitter produced by A26f could further elucidate the role of the A26f-iIN-3 connection at the premotor level.

Having identified neurons such as A19f and A26f providing strong intersegmental output in previous analyses, we also used the data from the matrix to calculate the percentage of intersegmental to intrasegmental output between the neurons of the SRC.

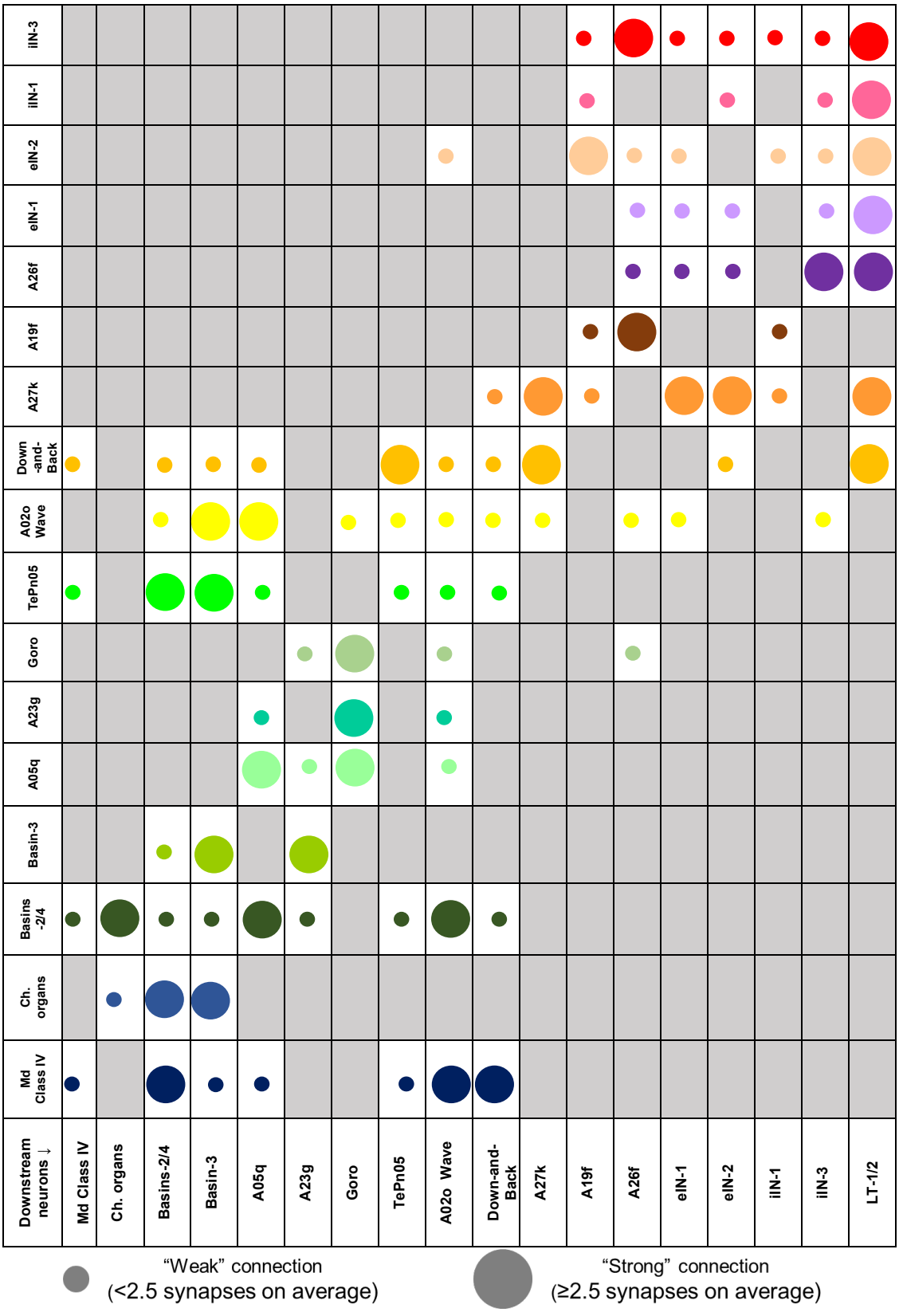

Figure 3.2.8 The condensed connectivity matrix for the neurons of the SRC

(Legend on the following page)

The condensed version of the SRC connectivity matrix displays a summary of all the connections found between the neurons of the SRC. The average strength of all connections between each class of neuron was calculated and is displayed as either a “weak” (<2.5 synapses on average, small circles) or “strong” (≥2.5 synapses on average, large circles) connection. We also observe from connectomics analyses that the intrasegmental and intersegmental connections displayed in the SRC connectivity matrix are almost equal in number.

The results of our analysis reveal that of the 3498 synapses included in the matrix, 1768 (50.5%) are intrasegmental while 1730 (49.5%) are intersegmental. This result suggests that inter and intrasegmental co-ordination between SRC neurons play almost equally vital roles, serving to ensure that overall co-ordination is maintained through a combination of both fine and gross motor control to ensure successful completion of the entire self-righting sequence.

3.2.13 The neural wiring diagram underlying larval self-righting

3.2.13.1 The neurons of the wiring diagram are arranged in a highly-symmetrical manner

Building on the creation of a matrix displaying connection strength between the neurons of the SRC, we were able to create the first version of an overall neural wiring diagram for self-righting (Figure 3.2.9). In this wiring diagram, we display how neurons are connected to each other and whether these arrangements are reflected on the left and right hand sides of the VNC. To create this wiring diagram, we arranged the neurons according to whether their cell bodies were located on the left or right of the VNC and indicated whether connections to other neurons of the SRC were “strong” on average (2.5 or more synapses) or “weak” on average (less than 2.5 synapses).

Initially, we expected to find a high degree of symmetry between the overall architecture of connections between SRC neurons on the left and right of the VNC. The creation of the neural wiring diagram reveals that this is the case with almost every strong connection on each side of the VNC having a counterpart

on the opposite side. Unexpectedly, however we observe differences in the average strength of these connections with several “strong” connections reflected by “weak” versions of the same connections on the opposite side of the VNC. Examples of this include the ipsilateral connection between chordotonal organs and the first order Basin-2/4 interneurons as well as the contralateral connection between the premotor integrator A19f and the pre-LT interneuron A26f.

Similar to our earlier suggestions regarding potential directional bias in rolling behaviour facilitated by asymmetrical differences in synaptic input to the Goro neurons, we suggest that the other asymmetries in synaptic strength identified may also create directional bias in self-righting behaviour. We note that the EM image volume used for the reconstruction and connectomics work presented in this study only comes from a single larval CNS, however, we suggest that the identification of synaptic strength asymmetries may provide basis for the future investigation of how this relates to behavioural output.

3.2.13.2 The neural wiring diagram reveals the existence of alternative routes for information flow between neurons

Our neural wiring diagram also reveals the existence of alternative routes for information flow that may provide communication redundancy within the VNC (Figure 3.2.9, black and white roundels). For example, the Basin-2/4 interneurons are strongly and directly connected to ipsilateral A05q interneurons, but we note that a route for information flow between the two neurons also exists via the A02o ‘Wave’ nociceptive integrator neurons. We

hypothesise that alternative routes can also serve to bolster co-ordination of neural activity between the left and right of the VNC as our wiring diagram reveals alternative routes that allow neurons to communicate with neurons of the same class on both sides of the VNC (e.g., Md Class IV neurons to Down-and-Back interneurons and Down-and-Back interneurons to TePn05 interneurons).

3.2.13.3 Chordotonal organs do not receive input from the Basin-2/4 interneurons

The sole connection we observe that does not have any counterpart on the opposite side of the VNC is synaptic input from the right-hand side Basin-2/4 interneurons to the right-hand side chordotonal organs (Figure 3.2.9, red arrow). We found this to be a highly unusual connection considering previous functional data showing that the Basin neurons are directly downstream of sensory components (Ohyama *et al.,* 2015). In addition to this, this aberrant connection implies that mechanosensory components could be receiving strong input from downstream interneurons (unusual as the role of sensory neurons is generally held to be providing information from the outside environment to interneurons). Upon deeper investigation of this connection, we identified that this Basin-to-chordotonal connection consisted of a singular 6-synapse interaction between Basin-4 on the right of segment A3 (referred to as ‘Basin-4 a3r’) and the lateral chordotonal organ “lch 5-1” on the right of segment A4 (referred to as ‘lch 5-1 a4r’).

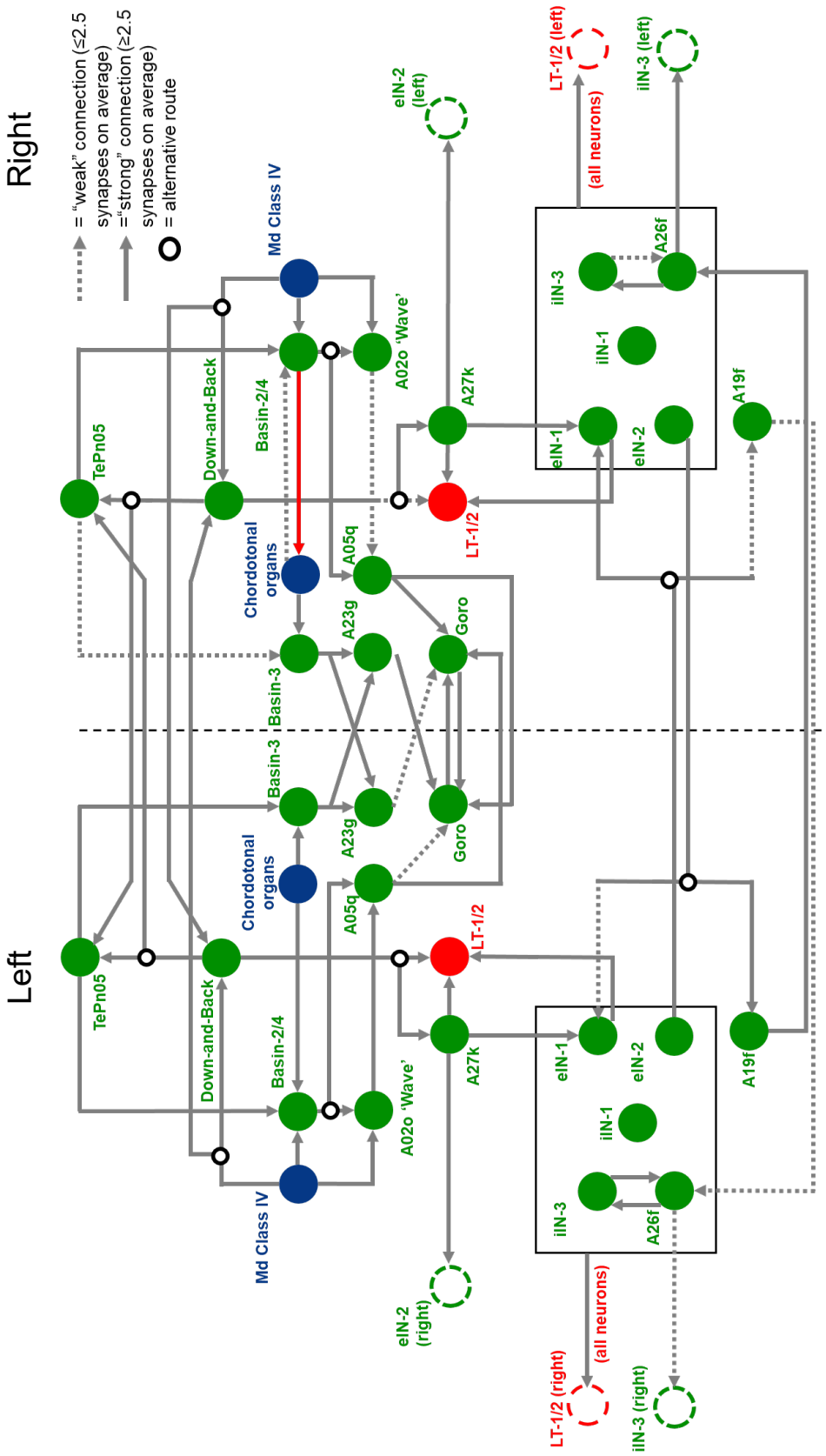

Figure 3.2.9 The neural wiring diagram underlying larval self-righting

(Legend on the following page)

The neural wiring diagram for self-righting behaviour displays the average of all connections observed between the neurons of the SRC in each of the first six abdominal segments. Connections that occur between two neurons with at least 2.5 synapses on average are displayed with solid lines with less than 2.5 synapses on average are displayed with dotted lines. Alternative routes for neuronal connection are also displayed with roundel markers while the only “strong” connection identified with no strong or weak counterpart identified on the opposite side of the VNC is indicated with a red arrow. For clarity, contralaterally connected neurons are occasionally displayed ipsilaterally as clear, dashed neurons. We find that the neural wiring diagram reveals alternative pathways for information flow as well as differences between the strength of synaptic connection on the left and right of the VNC. We note that the arrangement of neurons, however, is mostly reflected symmetrically including at the level of alternative information flow pathways.

We note that the previous reconstruction of Basin-4 a3r by other researchers includes a laterally-located branch that is not present in other Basin-4 interneurons but that the reconstruction of lch 5-1 matches the other lch 5-1 neurons. We also observed that the entirety of input provided to lch 5-1 a4r by Basin-4 a3r is located on this branch and we suggest that this branch was an erroneous addition to the Basin-4 a3r interneuron during reconstruction and does not represent the true architecture of the neuron in question.

We have investigated other synaptic connections along this branch and found none to (or from) other neurons in the SRC and therefore this does not affect the other results obtained from our connectomics analysis overall.

The creation of our neural wiring diagram, therefore, reveals a complex arrangement of neurons providing ipsilateral and contralateral input across both halves of the VNC to facilitate self-righting behaviour.

3.2.14 An investigation of intrasegmental connectivity between the neurons of the SRC

3.2.14.1 Intrasegmental connectivity between SRC neurons in abdominal segment A1

Considering the fact that the *Drosophila* larva is a metameric organism, we proceeded to investigate to what degree the exact neuronal arrangement described in the neural wiring diagram was maintained within in each of the first six abdominal segments. For this analysis, we quantified intrasegmental connections between SRC neurons and mapped them in a similar arrangement

to that of the neural wiring diagram. For clarity, we applied a threshold of 3 synapses as a minimum for a connection to be displayed on the map.

We firstly performed this analysis in abdominal segment A1 (Figure 3.2.10A). We note that, overall, there is a high degree of symmetry between the overall arrangement of intrasegmental neuronal connections on the left and right of the VNC with 74% of connections on the left of the segment reflected on the right of the segment. We also note that the cumulative synaptic strength of intrasegmental connections between the SRC neurons on each side of A1 is highly consistent at 425 synapses on the left and 429 synapses on the right, demonstrating coherence between SRC synaptic connectivity between the two halves of the segment.

At the sensory level, we see strong interaction between the Md Class IV sensory neurons and the Basin-2/4 interneurons, as well as strong input to both ipsilateral and contralateral Down-and-Back interneurons. We also observe strong interactions between the Chordotonal organs and the three Basin interneurons included in study.

At the level of the first order and nociceptive integrator neurons in A1, an asymmetrical ipsilateral interaction occurs between Basin-2/4 interneurons and Basin-3 interneurons on the right of A1 and Basin-2/4 interneurons and the TePn05 neurons on the left of A1 but note that overall connection symmetry is mostly maintained.

An interesting observation is the asymmetry between Basin-2/4 – to – A05q interactions on each side of A1. The work of Ohyama and others has shown a functional connection between the Basin interneurons and A05q interneurons

however we observe that in A1, Basin-2/4 is only strongly connected to A05q on the left-hand side (both directly and via A02o ‘Wave’).

Downstream connections between A05q and Goro interneurons are also asymmetrical with A23g and A05q neurons in segment A1 both providing contralateral inhibition to Goro interneurons but A05q only providing ipsilateral connection to Goro on the right of A1.

Finally, at the premotor level, we observe that all five pre-LT interneurons show strong contralateral, intrasegmental connections to the LT-1/2 MNs but that there are also strong pre-LT-to-pre-LT interactions present. The A26f neurons, for example, provide contralateral input to the iIN-3 neuron on the left of A1 as well as ipsilateral input to the iIN-3 neuron on the right of A1. We also note that eIN-2 on the left of A1 provides strong ipsilateral input to the iIN-1 neuron on the left of the segment as well as contralateral input to the eIN-1 on the right.

3.2.14.2 Intrasegmental connectivity between SRC neurons in abdominal segment A2

In segment A2 (Figure 3.2.10B), we observe some substantial changes to the arrangement of intrasegmental connections that we observed in A1. For example, we note that the chordotonal organs of segment A2 show markedly less intrasegmental output than in A1 with no intrasegmental connection to Basin-3 neurons on either side of the segment. We also note that, overall, Md Class IV connectivity is reduced from 99 intrasegmental output synapses on the left of A1 to just 21 intrasegmental output synapses on the left of A2. On the right-hand side, the reduction is smaller but the number of intrasegmental

output synapses still falls from 137 in A1 to 81 in A2 and contralateral output does not occur.

At the level of the first order and nociceptive integrator neurons, we observe little of the strong interaction between Down-and Back interneurons and TePn05 interneurons from A1 reflected in A2. In addition to this, we also observe the addition of new connections of reversed polarity between Basin-3 and Basin-2/4 interneurons as well as new, direct connections between the Md Class IV interneurons and the nociceptive integrator A02o ‘Wave’ interneurons. We do, however, note that the TePn05 neurons provide no input to the Basin-2/4 interneurons of segment A2 but rather that the opposite connection occurs.

Within the neurons of the rolling circuit, we note another interesting asymmetry between Basin-2/4-to-A05q interactions on each side of the VNC. We observe strong direct connection between Basin-2/4 interneurons and A05q on the right of A2 (whereas in A1, this connection was located on the left). We suggest therefore that the individual intrasegmental Basin-2/4-to-A05q connections on each side of A1 and A2 may compensate for the lack of a contralateral connection on the other side of each respective segment. We also note a total lack of A23g-to-Goro connection in segment A2.

Finally, at the premotor level, although we observe strong pre-LT-to-LT-1/2 output from the eIN-1 and eIN-2 neurons, we observe notable absences such as a lack of connection between iIN-1 and iIN-3 neurons on the left of A2 to LT-1/2 MNs. We also observe an absence of A26f-to-LT-1/2 connection on the right of A2. The overall strength of A26f interaction with iIN-3 is also reduced in A2

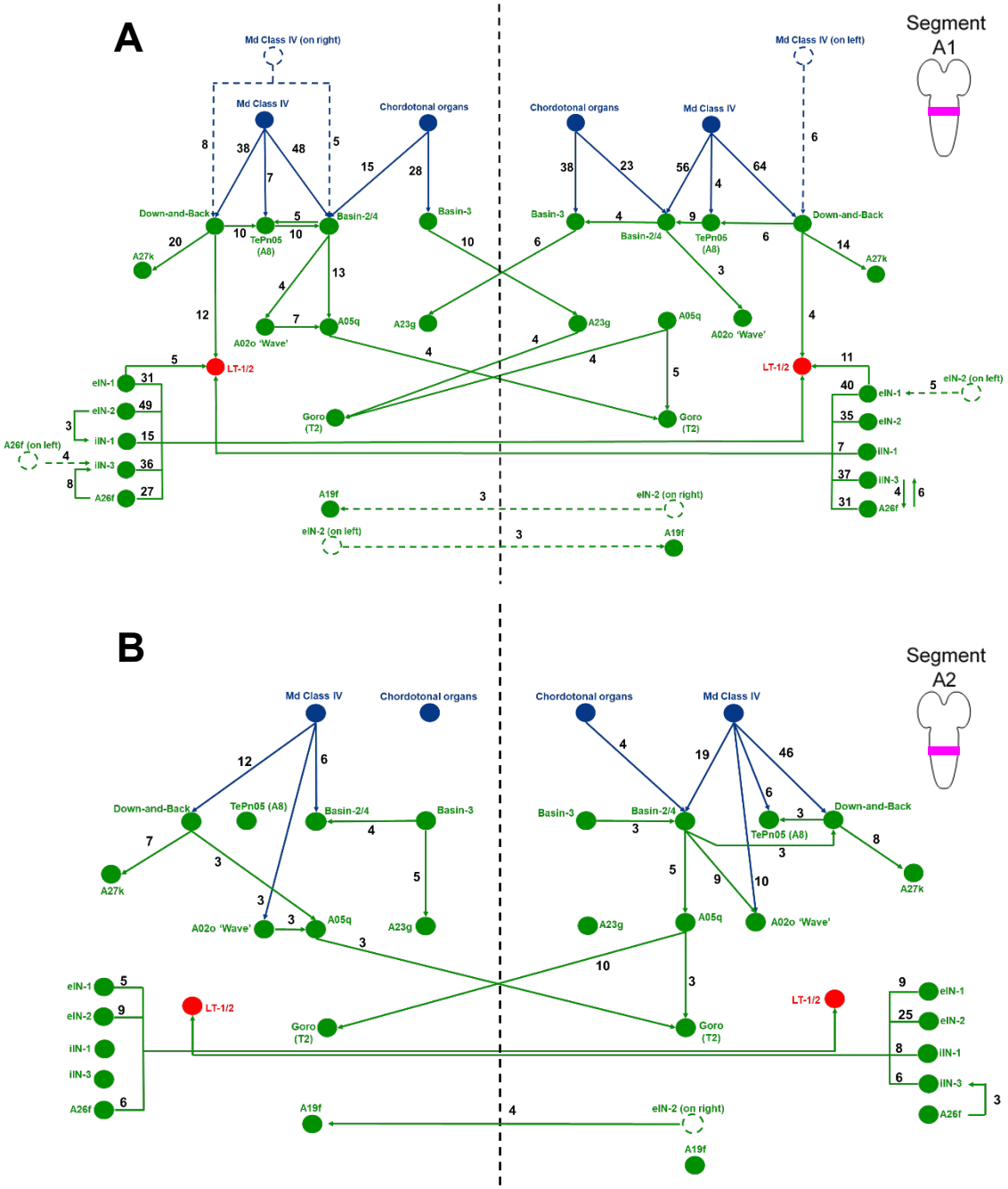

Figure 3.2.10 Maps of intrasegmental connection between the SRC neurons of segments A1 and A2

(A) A map of the intrasegmental connections present between the neurons of the SRC in abdominal segment A1. **(B)** A map of the intrasegmental connections present between the neurons of the SRC in abdominal segment A1.

compared to segment A1 as well as the overall strength of connections between the premotor integrator A19f and the pre-LT eIN-2.

3.2.14.3 Intrasegmental connectivity between SRC neurons in abdominal segment A3

In abdominal segment A3, we observe that general intrasegmental synaptic connectivity between the neurons of the circuit becomes reduced (Figure 3.2.11A). Although we still observe ipsilateral and contralateral input from Md Class IV sensory neurons to Basin-2/4 and Down-and-Back interneurons, we again observe no intrasegmental connection between the chordotonal organs and the Basin-3 interneurons. On the left of A3, we observe no connection between any of the first order and nociceptive integrators and, on the right of A3, only observe two strong connections between these neurons (Down-and Back to TePn05 and Basin-2/4 to A02o ‘Wave’).

Further downstream, neurons matching the morphologies of A05q and A23g were not identified in segment A3 (or any more posterior abdominal segments) and we hypothesise that if the Basin neurons in posterior segments still connect to Goro interneurons, they do so by alternative, unidentified routes. We note that the A02o ‘Wave’ neuron on the left of A3 provides a strong connection to Goro but can find no other example of this in any other segment to support the theory that A02o ‘Wave’ neurons may represent part of an alternative Basin-to-Goro route.

At the premotor level, the A19f neurons provide no intrasegmental integratory function between the pre-LT interneurons and we note that the intrasegmental

interactions between the A26f and iIN-3 pre-LT interneurons observed in anterior segments are also not present. Of the pre-LT interneurons that were identified during our reconstruction work in segment A3, a notable asymmetry exists between the iIN-3 interneurons with no neuron matching its morphology present on the right hand side of the segment. All other pre-LT interneurons in A3 (with the exception of iIN-1 on the right of A3) provide strong intrasegmental connection to the LT-1/2 MNs as expected. Most of this connection is contralateral, as previously described, however we do also note the existence of ipsilateral connection between eIN-1 and the LT-1/2 MNs in A3 (similar to A1).

3.2.14.4 Intrasegmental connectivity between SRC neurons in abdominal segment A4

Moving towards the posterior segments of the VNC, in abdominal segment A4, we observe that intrasegmental SRC synaptic connectivity is substantially increased overall compared to A3 (188 synapses in A3 to 302 synapses in A4) (Figure 3.2.11B).

We observe strong ipsilateral connections between the A4 chordotonal organs and Basin-3 interneurons that are not present in A2 or A3. In addition to this we note large increases in the numbers of synapses received by A4 Basin-2/4 interneurons from Md Class IV interneurons when compared to the same interactions in A3 (a total of 70 in A4 compared to 22 in A3). The strengthening of sensory-to-first order connections in A4 supports the idea that along the length of the larval body, there may be distinction made between the response to sensory input in anterior regions and posterior regions. This idea has been

discussed at length by Takagi and colleagues in the context of peristaltic wave propagation as an output of A02o ‘Wave’ stimulation (Takagi *et al.,* 2017) however, we propose that the A1 and A4 segments may act as strict boundaries for determining the larva’s response to sensory input. Sensory input to any segment between A1 and A3 may elicit the same response but that response may be different to the response to sensory input to A4 and more posterior segments as a result of the differing synaptic connectivity.

At the level of the first order interneurons and nociceptive integrators in A4, we also observe a general increase in the amount of intrasegmental connectivity including the presence of a direct connection between the Down-and-Back and LT-1/2 MNs not observed in A2 or A3.

Finally, we note that premotor connectivity is asymmetrical in A4 with the majority of connection between pre-LT interneurons and LT-1/2 MNs concentrated on the right hand side of the segment. On the left of A4, only eIN-1 and A26f provide direct contralateral intrasegmental connections to the LT-1/2 MNs however, we do note an ipsilateral connection between the pre-LT interneuron eIN-1 and LT-1/2.

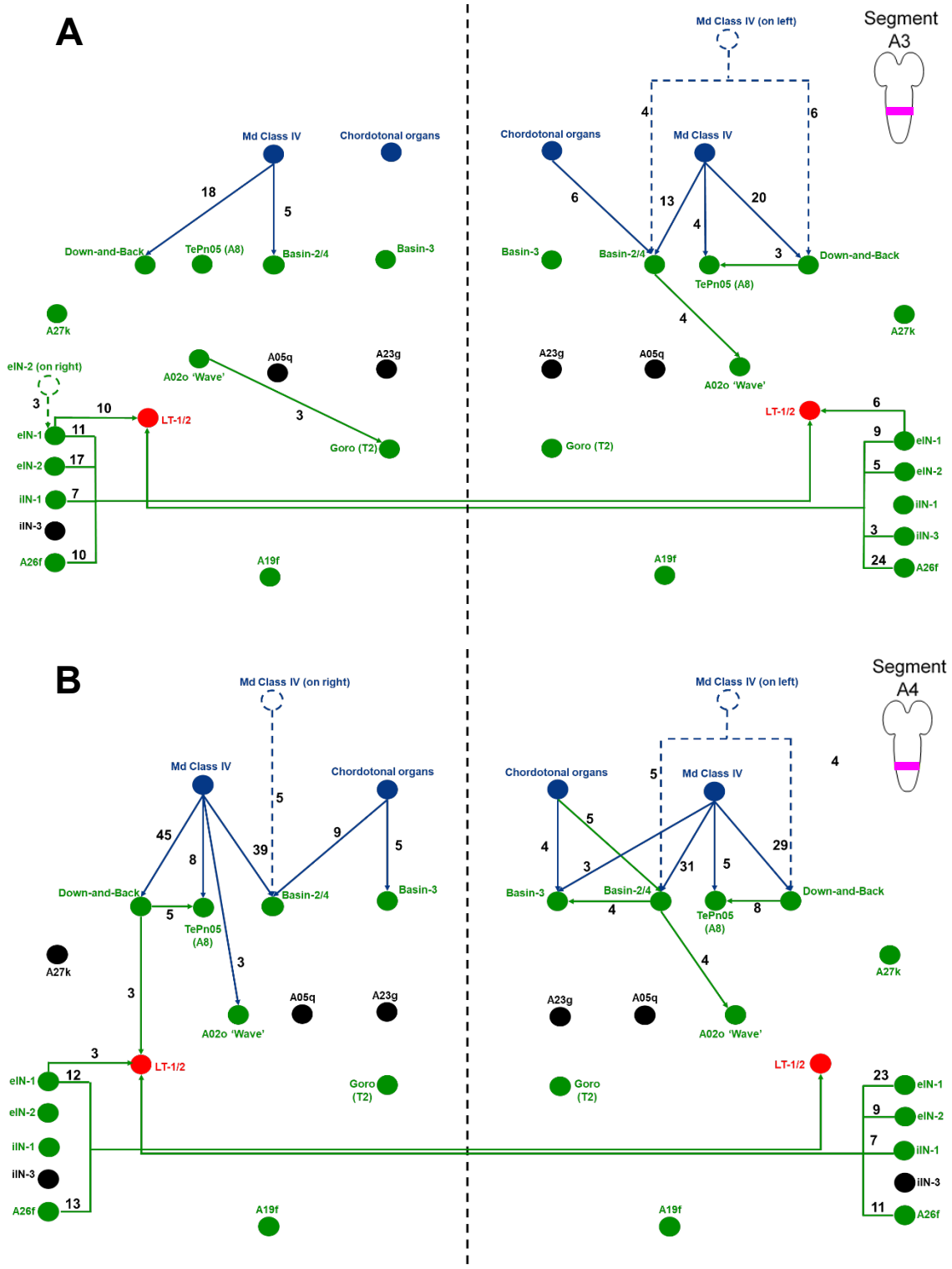

Figure 3.2.11 Maps of intrasegmental connection between the SRC neurons of segment A3 and A4

(Legend on the following page)

(A) A map of the intrasegmental connections present between the neurons of the SRC in abdominal segment A3. **(B)** A map of the intrasegmental connections present between the neurons of the SRC in abdominal segment A4.

3.2.14.5 Intrasegmental connectivity between SRC neurons in abdominal segment A5

In the posterior abdominal segments A5 and A6, we observe that intrasegmental connection between the SRC neurons is greatly reduced compared with the more anterior segments (Figure 3.2.12). Comparing overall connectivity in A5 to that of A4, we see that sensory-to-first order connections are reduced in both number and synaptic strength but note that we were unable to identify the Basin-3 interneurons in A5 and posterior segments and thus cannot comment on whether chordotonal organ-to-Basin-3 connectivity specifically is changed in this segment. In A5, we observe a unique contralateral connection between the md Class IV sensory neurons on the left of the segment and the A02o ‘Wave’ neurons on the right however the lack of this connection in other abdominal segments suggests that it may have little functional implication.

At the premotor level, we observe that eIN-1, eIN-2, and iIN-1 pre-LT interneurons all provide strong intrasegmental contralateral input to the LT-1/2 MNs as expected. We note that a section of missing EM images in A5 hampered efforts to fully reconstruct the A26f interneurons in this segment and thus areas of synaptic connectivity were missing from these neurons when this analysis was performed.

3.2.14.6 Intrasegmental connectivity between SRC neurons in abdominal segment A6

Our analysis of abdominal segment A6 and found very little intrasegmental SRC-to-SRC connection (Figure 3.2.12B). We note that while neurons that were identified and reconstructed in this segment (i.e., the pre-LTs, LT-1/2, A19f and A02o 'Wave') were revealed to contact other SRC neurons, the vast majority of this connection is intersegmental with these neurons predominantly communicating with neurons in more anterior locations. We do observe low levels of intrasegmental communication at the premotor level with each of the pre-LT interneurons identified in A6 providing strong contralateral input to the LT-1/2 MNs. The consistent repetition of this intrasegmental pre-LT-to-LT-1/2 connection along the length of the VNC therefore suggests that while upstream neurons serve to co-ordinate anteroposterior and mediolateral co-ordination of activity, at the level of premotor and motor neurons, final behavioural output is facilitated by intrasegmental activity.

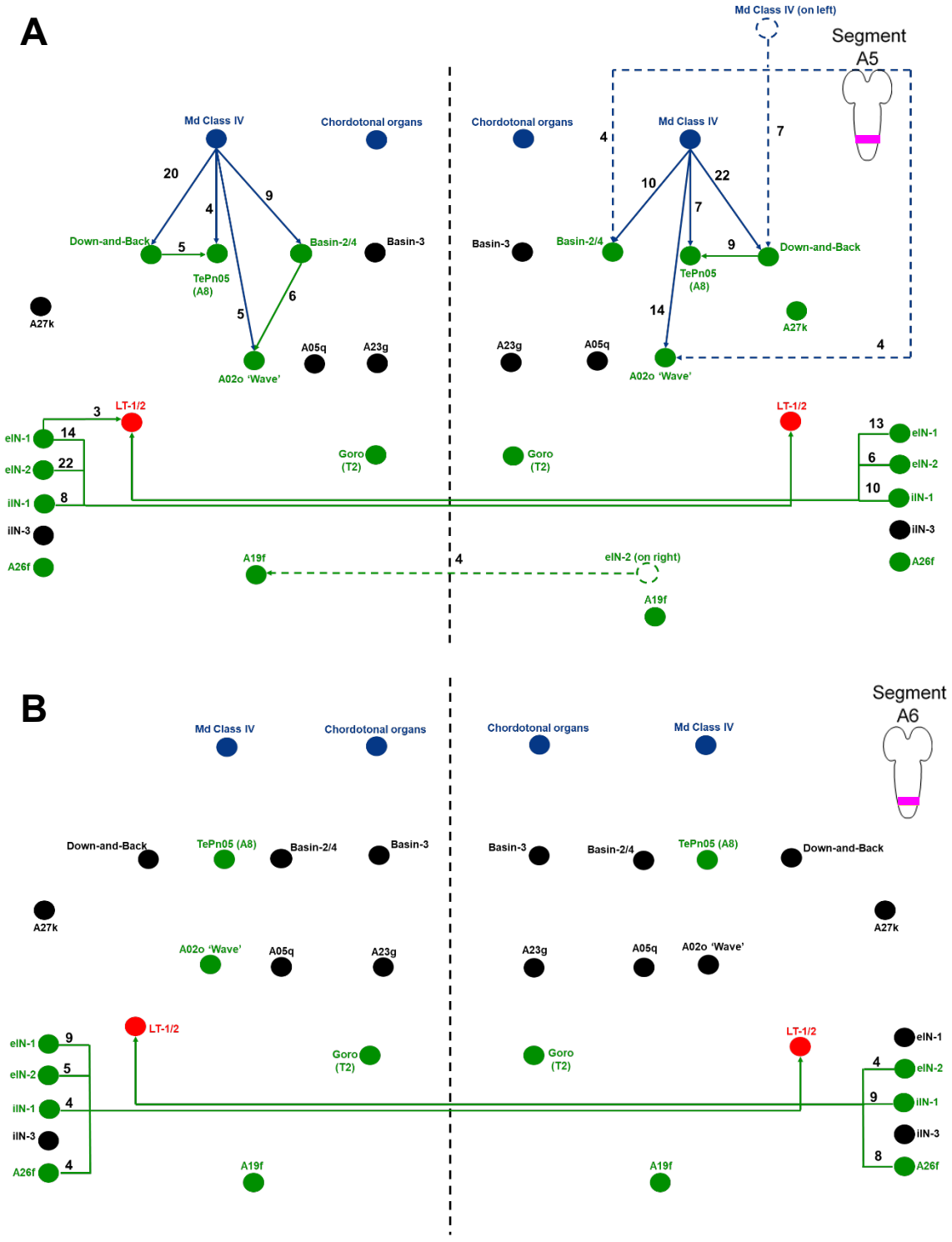

Figure 3.2.12 Maps of intrasegmental connection between the SRC neurons of segment A5 and A6

(Legend on the following page)

(A) A map of the intrasegmental connections present between the neurons of the SRC in abdominal segment A5. **(B)** A map of the intrasegmental connections present between the neurons of the SRC in abdominal segment A6.

3.2.15 Investigation of anteroposterior SRC-specific information flow between the neurons of the SRC

3.2.15.1 The anteroposterior information flow of the sensory and rolling circuit neurons

Building on the establishment of the neural wiring diagram for self-righting and our previous connectomics analysis showing that along the first six abdominal segments of the VNC, levels of intrasegmental connectivity fluctuate – we investigated the anteroposterior directionality of information flow to and from the SRC neurons (Figure 3.2.13). For this analysis, we analysed the percentage of input/output connectivity that was occurring with SRC neurons based in anterior segments, posterior segments, or the same segment (as defined by the location of a neuron's cell body). We then averaged these values for neurons of a given class across the first six abdominal segments.

The results of our analysis reveal that the Md Class IV sensory neurons predominantly communicate in an intrasegmental fashion. The vast majority of input to the Md Class IV sensory neurons is from other Md Class IV sensory neurons while output is mainly to Down-and-Back and Basin-2/4 first order interneurons. Chordotonal organs, however, display different information flow, predominantly receiving input from other chordotonal organs in anterior segments but providing output intrasegmentally (to Basin neurons).

Downstream of the sensory components, we note that all three Basin interneurons predominantly receive intrasegmental input but that each Basin neuron predominantly provides SRC-specific output to neurons in different anteroposterior locations. Basin-2 and Basin-4 interneurons, on average, show

strong connections with the same downstream neurons (e.g., A05q), but we note that Basin-2 output is predominantly intrasegmental while Basin-4 output is predominantly to neurons in posterior segments. In addition to this, Basin-3 interneurons predominantly communicate with neurons in the more anterior segments. Considering these results, we suggest that although they may play similar functional roles (i.e., integrating sensory information during the triggering of rolling behaviour), the Basin interneurons may each play roles which are subtly distinct from one another at the level of communication with downstream neurons.

Further downstream in the rolling circuit, the results of our analysis reveal that the A05q and A23g interneurons that connect the Basin neurons to Goro neurons also show distinct patterns of anteroposterior communication with other SRC neurons. As mentioned before, A05q input from SRC neurons mainly consists of synapses from Basin-2/4 interneurons and our analysis reveals that the majority of this input is from posterior neurons while the overwhelming majority of A05q SRC-specific output is to anterior neurons. In the case of the A23g neurons, our analysis shows that the majority of SRC-specific input to these neurons is intrasegmental (mainly from Basin-3 interneurons) while the majority of output is also to anterior neurons. Considering both neurons target the Goro neurons which have cell bodies in T2, we were not surprised by the findings that the majority of SRC-specific output in both A05q and A23g was to anterior neurons, however, the finding that A05q input was predominantly posterior while A23g input was predominantly intrasegmental was unexpected.

We note that both A05q and A23g neurons were only identified in segments A1 and A2 during our reconstruction work and considering the majority of their

input was coming from the segmentally-repeated Basin neurons, we expected to see that both neurons would show similar information flow patterns. We do note, however, that A05q neurons also receive input from A02o ‘Wave’ neurons and hypothesise that this could explain the increased posterior input.

The finding that Goro mainly receives SRC-specific input from posterior neurons was expected due to the location of Goro cell bodies in the anterior segment, T2. We noted, however, that the intrasegmental output representing the majority of SRC-specific output from Goro is confined to interaction between the two Goro neurons. We investigate in Section 4.2.7 how Goro may communicate with other motor neurons not identified as part of the SRC to exert influence on the motor system.

3.2.15.2 The anteroposterior information flow of the Down-and-Back and premotor integrator neurons

The information flow analysis of the first order Down-and-Back interneurons showed that information tends to flow through these neurons in an intrasegmental fashion, from Md class IV sensory neurons and to A27k (and occasionally LT-1/2 MNs) (Figure 3.2.9). The downstream A27k neurons, however, tend to receive this intrasegmental input from Down-and-Back interneurons and act as conduits for information to flow to neurons in more anterior segments. In this manner, A27k may act to link sensory information flow with motor components along the anteroposterior axis ensuring that the motor neuron response to sensory input is not confined to the segment where input occurred but rather co-ordinated intersegmentally.

3.2.15.3 The anteroposterior information flow of the nociceptive integrator neurons

Regarding the nociceptive integrator neurons TePn05 and A02o ‘Wave’, we predicted that SRC-specific information flow with the two TePn05 interneurons would be predominantly confined to anterior neurons considering the locations of their cell bodies in segment A8. Our analysis validates this prediction, showing that TePn05 solely interacts with SRC neurons in anterior segments with the exception of TePn05-to-TePn05 interactions. Our analysis of the A02o ‘Wave’ interneurons, however, reveals a bias towards communication with other SRC neurons in anterior segments. Considering the neuron’s morphology (which extends into the anterior segments) (Figure 3.2.7E), this was unsurprising however we note that our connectomics analysis reveals no strong downstream SRC partners and so the functional relevance of this bias towards anterior communication remains unclear.

The premotor integrator neuron A19f mainly receives SRC specific input from neurons in posterior segments and provides output to SRC neurons in anterior segments. Our connectomics analysis reveals that this SRC-specific input was mainly from eIN-2 interneurons and SRC-specific output was mainly to A26f interneurons and in a similar vein to A27k interneurons, we suggest that A19f interneurons serve to link information flow between motor components in an anteroposterior fashion to promote intersegmentally co-ordinated motor output.

3.2.15.4 The anteroposterior information flow of the pre-LT and LT-1/2 MNs

At the premotor level, we expected most output to be intrasegmental for the five pre-LT interneurons as (although we had observed examples of communication between pre-LTs) we expected the majority of these neurons' output to be focused on the LT-1/2 MNs in the same segments. For the pre-LTs eIN-1, eIN-2 and iIN-1, our prediction is validated however we do note that eIN-1 neurons predominantly receive input from anterior neurons. The upstream A27k interneurons predominantly provide input to anterior SRC neurons themselves but hypothesise that this could comprise interactions with eIN-2 and LT-1/2 MNs and that the 16% of A27k posterior SRC-specific output could be comprised of these interactions with eIN-1 interneurons. The iIN-3 interneurons do not have the same hemisegmentally-repeated, midline-crossing morphology as the other four pre-LTs but rather have long projections that extend towards the posterior segments facilitating connections with LT-1/2 MNs in these segments. The predominance of posterior output therefore was expected, and the predominance of posterior input may be explained by the lack of iIN-3 interneurons found in segments posterior to A3. The A26f interneurons are unique among the pre-LT interneurons as they are the only neurons with near equal amounts of SRC-specific output provided anteriorly, intrasegmentally and posteriorly. This is reflected by the morphology of the neurons with long projections acting as pre-synaptic hubs where input to LT-1/2 MNs in adjacent segments is provided (discussed in Section 3.2.6). Input to A26f interneurons is mainly from posterior neurons and this supports our model in which A19f acts

as a premotor integrator, receiving posterior input from eIN-2 neurons and providing anterior input to A26f interneurons.

Finally, the LT-1/2 MNs mostly receive input from pre-LT interneurons intrasegmentally. As shown in our intrasegmental maps, pre-LT to LT-1/2 connectivity is a consistent intrasegmental feature in each of the first six abdominal segments even when connections to upstream neurons such as Down-and-Back and A27k are not present. The remaining 51% of input (from anterior and posterior neurons combined) includes connections to these upstream neurons however as previously described, A26f provides a large amount of the intersegmental premotor input.

Figure 3.2.13 The anteroposterior flow of information between SRC neurons

(Legend on the following page)

The number of synapses between a given neuron and other neurons in the SRC was totalled and the percentage of synapses with neurons in the same segment, anterior segments and posterior segments was calculated. This figure was averaged across all neurons of that class identified within the CATMAID volume and an overall percentage calculated to demonstrate information flow. Regions with the largest input and output to and from each neuronal class are marked with coloured arrows as appropriate.

3.2.16 The proportion of contralateral to ipsilateral SRC-specific input is highly symmetrical between the two mediolateral halves of the VNC

Our neural wiring diagram demonstrated that, although there were fluctuations in synaptic strength, the existence of connections between SRC neurons was mostly symmetrical. This prompted the question of whether the proportion of contralateral to ipsilateral connections between SRC neurons was also symmetrically reflected across the VNC. We therefore analysed what proportion of the average SRC-specific input/output was contralateral or ipsilateral for each of the neurons of the SRC and compared the results for both sides of the VNC.

Regarding SRC-specific input, our analysis reveals that the proportion of contralateral to ipsilateral input among the neurons of the SRC is mainly symmetrical across the two halves of the VNC (Figure 3.2.14). We note that 4 of the 19 neurons examined (the chordotonal organs, Basin-3 interneurons, A05q interneurons and A27k interneurons) solely receive ipsilateral input on both sides of the VNC. For the other 15 neurons we took the difference between the percentage of contralateral and ipsilateral input that each neuron received and treated this figure as a ‘laterality index’.

We found that between the left and right of the VNC, 7 of the 19 neurons analysed (Basin-2, Basin-4, Goro, TePn05, Down-and-Back, Wave and iIN-3) showed a less than 5% difference between laterality indices on the left and right of the VNC. In other words, where contralateral/ipsilateral input is predominant in these neurons, this is reflected in a highly symmetrical manner on both sides of the VNC.

For the remaining 8 neurons, differences in the laterality indices on the left and right of the VNC range from 10.5% (LT-1/2) to 66% (iIN-1) and we note that of these 8 neuronal classes, 4 are premotor neurons (eIN-1, A26f, eIN-2 and iIN-1), one is the premotor integrator neuron A19f, and another is the LT-1/2 MNs. This suggests that (in the individual larva from which the CATMAID volume was formed, at least) there is an asymmetry in the way upstream neuronal components communicate with premotor neurons on the left and right hand sides of the VNC. This is particularly pronounced in the case of iIN-1 neurons where (on average) on the left of the VNC there is a 67% difference in the amount of ipsilateral and contralateral input but on the right hand side, ipsilateral and contralateral input occur in equal amounts.

3.2.17 Large differences are present between the proportion of contralateral to ipsilateral SRC-specific output on the two mediolateral halves of the VNC

Regarding SRC-specific output, our analysis reveals that the proportion of contralateral to ipsilateral input among SRC neurons is predominantly asymmetrical across the two mediolateral halves of the VNC (Figure 3.2.15). While chordotonal organs and Basin-2 interneurons solely provide ipsilateral output to SRC neurons on both sides of the VNC, only 3 other neurons (Basin-4, Down-and-Back and TePn05) show a less than 5% difference between the laterality indices on the left and right-hand sides. The other 12 neurons show substantial differences in laterality indices with the most pronounced difference

occurring between the A23g interneurons on the left (100% contralateral output) and right (50% contralateral output) of the VNC.

Overall, this suggests that although information input and processing may occur in a relatively symmetrical manner, it is at the level of output (and just before) that refinement occurs in order to produce directionally biased behavioural responses. For self-righting specifically, this may lead to biases in individual larvae towards rotation to the left or right during the execution of the behavioural sequence and we suggest that similar connectomic analyses in left/right-biased larvae could provide new insights into the relationship between the structure of neuronal circuits and exhibition of complex behaviours.

Left of VNC	
Neuron	Input from SRC
Chordotonal organs	
Md class IV	
Basin-2	
Basin-3	
Basin-4	
A05q	
A23g	
Goro	
TePn05	
A02o 'Wave'	
Down-and-Back	
A27k	
A19f	
eIN-1	
eIN-2	
iIN-1	
iIN-3	
A26f	
LT-1/2	

Right of VNC	
Neuron	Input from SRC
Chordotonal organs	
Md class IV	
Basin-2	
Basin-3	
Basin-4	
A05q	
A23g	
Goro	
TePn05	
A02o 'Wave'	
Down-and-Back	
A27k	
A19f	
eIN-1	
eIN-2	
iIN-1	
iIN-3	
A26f	
LT-1/2	

Contralateral input Ipsilateral input

Figure 3.2.14 The proportion of contralateral to ipsilateral SRC-specific input is mostly symmetrical between the two halves of the VNC

(Legend on the following page)

The proportion of contralateral to ipsilateral SRC-specific input was calculated for each neuronal class as an average across all individuals identified across the larval VNC. We observe that the majority of neurons (11/19) show less than 5% difference in contralateral: ipsilateral input difference between the left and right halves of the VNC.

Left of VNC	
Neuron	Output to SRC
Chordotonal organs	
Md class IV	
Basin-2	
Basin-3	
Basin-4	
A05q	
A23g	
Goro	
TePn05	
Wave	
Down-and-Back	
A27k	
A19f	
eIN-1	
eIN-2	
iIN-1	
iIN-3	
A26f	

Right of VNC	
Neuron	Output to SRC
Chordotonal organs	
Md class IV	
Basin-2	
Basin-3	
Basin-4	
A05q	
A23g	
Goro	
TePn05	
Wave	
Down-and-Back	
A27k	
A19f	
eIN-1	
eIN-2	
iIN-1	
iIN-3	
A26f	

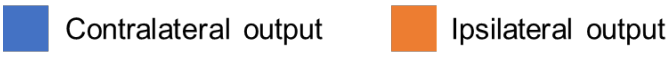

Figure 3.2.15 The proportion of contralateral to ipsilateral SRC-specific output is mostly asymmetrical between the two halves of the VNC

(Legend on the following page)

The proportion of contralateral to ipsilateral SRC-specific output was calculated for each neuronal class as an average across all individuals identified across the larval VNC. We observe that the majority of neurons (12/18) show more than 5% difference in contralateral: ipsilateral input differences between the left and right halves of the VNC suggesting a substantial difference in mediolateral communication between SRC neurons on the left and right of the VNC.

3.3 Discussion

In this chapter, we use a serial reconstruction approach combined with connectomic analysis to investigate the structure of the neuronal network underlying larval self-righting behaviour. Producing a neural wiring diagram for this network, we reveal a number of insights regarding the connectivity of neurons comprising the wiring diagram as well as the directionality of information flow between then.

A key observation is that, although connections tend to occur in a symmetrical manner across the two halves of the VNC, several asymmetries are present in terms of the strength of synaptic connection. We note that in the wiring diagram itself (Figure 3.2.9), there are several connections we find to be “strong” on average that are only reflected by “weak” versions of the same connections on the opposite side of the VNC. As the volume of EM images used to reconstruct the neurons of the wiring diagram only represents a single larva, we hypothesise that these synaptic strength asymmetries could represent a mechanism for subtle differences in the exhibition of behaviour between individual animals.

In the case of self-righting, individual larvae begin the self-righting sequence by exhibiting struggle behaviour in one of two directions and this may be the consequence of differing neuronal architectures. A potential approach for the investigation of this could be the application of the serial reconstruction approach to the central nervous systems of the “left-biased” and “right-based” larvae and the subsequent comparison of their neuronal architectures.

We also note the contribution of the neuronal circuit underlying rolling behaviour to the overall SRC. The two behaviours share the need for the larva to rotate along the dorsoventral axis and thus the sharing of neuronal components to achieve this part of each behavioural sequence is plausible. Contextually, however, self-righting and rolling differ and we suggest that the involvement of additional neurons processing nociceptive signals (e.g., the Down-and-Back interneurons) may serve to refine behavioural choice and distinguish the finite self-righting sequence from continuous rolling behaviour.

Indeed, Burgos and colleagues refer to the connections observed between the Down-and-Back interneurons and LT1 motor neurons as potentially representing links between Down-and-Back-mediated C-bending behaviour and self-righting behaviour (Burgos *et al.,* 2018).

Regarding the neural architecture of the wiring diagram underlying self-righting behaviour, we also note that we began its construction from the basis of investigating neurons providing strong upstream connection to the LT-1/2 MNs. While the necessity of LT-1/2 MN activity for normal self-righting behaviour has been shown (Picao-Osorio *et al.,* 2015), and therefore represents a logical place to begin the investigation, we suggest that future studies of other, related motor neurons may reveal further insights into self-righting control. For example, the five pre-LT interneurons found to provide strong output to the LT-1/2 MNs along the VNC also provide output to the Dorsal Transverse 1 motor neurons (or ‘DT1-MNs’) reconstructed in segment A1. This is mentioned by Zwart and colleagues in their study characterising the pre-LT interneurons (Zwart *et al.,* 2016), however, a future investigation could examine the DT1 premotor connectome and whether it also contains other neurons that may link

to alternative upstream components that facilitate normal self-righting behaviour.

Finally, our neural wiring diagram for self-righting identifies sensorimotor pathways for the control of the behaviour and presents routes by which information may flow between nociceptive sensory neurons and key motor components. We note that the LT-1/2 MNs, however, have also been linked (via a similar serial reconstruction and connectomics-based approach) to proprioceptive neurons, key for informing the larva's perception of its position in space during movement. The work of Zarin and colleagues (Zarin *et al.,* 2019) has linked the LT MNs in segment A1 to proprioceptive neurons via the inhibitory interneuron A02b (Kohsaka *et al.,* 2014) and the pre-LT interneuron eIN-1 (Zwart *et al.,* 2016). We suggest, therefore, that the investigation of this circuit in other abdominal segments of the VNC could provide further insights into the control of self-righting behaviour.

In conclusion, we identify a complex neuronal network that provides synaptic input to the LT-1/2 MNs and, that we hypothesise, facilitates anteroposterior and mediolateral co-ordination during the behavioural sequence. We then functionally validate the roles of the components of this network *in vivo* in the following chapter, converting the wiring diagram into a functional behavioural circuit.

Chapter 4

Functional validation of the self-righting circuit

4.1 Chapter overview

In order to convert the self-righting neural wiring diagram previously established (Figure 3.2.9) into a neural circuit for self-righting behaviour, it is necessary to functionally validate the roles of each cellular component *in vivo*. Binary expression systems such as the GAL4-UAS (Brand and Perrimon, 1993) and LexA-LexAop (Lai and Lee, 2006) systems provide the ability to target expression of various functional effectors to specific neurons of interest and this, in turn, opens many possibilities for functional validation of the neuronal subsets underlying larval behaviours.

One approach that has previously been used in the field for this validation is the targeted expression of tetanus toxin in neurons of interest to permanently eliminate synaptic vesicle transmission (Sweeney *et al.,* 1995; Suster *et al*, 2003; Hughes and Thomas, 2007). Although a valid strategy for determining whether a neuron's function is necessary for the performance of a behaviour of interest, it does not allow the manipulation of neuronal function in a reversible manner and the direct relation of changes in neural activity to changes in the ability of the animal to perform a certain behaviour.

Aiming to apply a more dynamic method to this study, we note that various approaches exist for conditional manipulation of neural activity including optogenetic manipulation of neural activity via targeted expression of channelrhodopsins such as ChR2 (Nagel *et al.,* 2003) and Chrimson (Klapoetke *et al.,* 2014). In addition to this, we also considered techniques for permanently labelling active neural circuits such as targeted expression of the photoconvertible fluorescent probe CAMPARI (Fosque *et al.,* 2015).

Finally, however, we opted to thermogenetically inhibit neural activity in selected neurons via targeted expression of the temperature-dependent allele of the gene, *shibire*. Exposure of neurons expressing temperature-sensitive *shibire* (or 'shi^{ts}') to a restrictive temperature results in the inhibition of synaptic vesicle recycling and thus a blocking of neuronal transmission (Kitamoto, 2001).

The results of our behavioural analyses show that the thermogenetic inhibition of all neuronal components tested (except iIN-3) results in significant delays to larval self-righting behaviour. We also perform connectomic analysis to examine the routes by which the pair of Goro interneurons (termed as master neurons for control of rolling behaviour) may exert their motor influence and identify specific dorsal motor neurons as candidates. The results of our behavioural testing, however, indicate that thermogenetic inhibition of these dorsal motor neurons has no effect on time to self-right in larvae and that, in fact, thermogenetic inhibition of motor neurons targeting ventral muscles significantly delays self-righting behaviour.

Overall, our findings establish the neural circuit underlying larval self-righting behaviour and reveal that the normal activity of a complex network of neurons is necessary for the larva to perform the behavioural sequence in a timely manner.

Please note that these experiments include contributions by others including Dr. Joao Picao-Osorio and Clare Hancock. Where this is the case, this is indicated at the end of each figure legend.

4.2 Results

4.2.1 Description of methodological approach

Having considered several options for the functional validation of the role of wiring diagram neurons (Figure 3.2.9) in *in vivo* self-righting behaviour, we chose to apply a strategy based on thermogenetic inhibition of activity in selected neurons.

This strategy consisted of targeting expression of the temperature-sensitive allele of the *shibire* gene (shi^{ts}) to neurons of interest using the binary GAL4-UAS system (Brand and Perrimon, 1993) (Figure 4.2.1A) and examining how thermogenetically inhibiting synaptic vesicle recycling in these neurons (Figure 4.2.1B) affected time to self-right in early (≤ 30 minutes post-hatching) first instar (or 'L1') larvae.

Throughout this chapter we functionally validate the roles of the majority of the neurons in the self-righting wiring diagram in the following manner (summarised in Figure 4.2.1C).

We place early L1 larvae (<30-minutes post-hatching) on a thin (2mm thick) agar plate which itself has been placed on top of a custom-built, Peltier-temperature controller module (Figure 4.2.1D) maintained at 25˚C (a permissive temperature). We then allow larvae to acclimatise to the crawling surface for 1 minute before performing the self-righting assay. Briefly, the self-righting assay consists of using a single-bristled paintbrush to gently rotate larvae so that their dorsal sides come into contact with the agar before removing the paintbrush and allowing larvae to perform a full 180˚ dorsal-ventral rotation – noting the time taken to 'self-right'.

We then raise the temperature of the agar to 36±0.5˚C (a restrictive temperature) and, after two minutes of exposure, perform the self-righting assay again. Finally, larvae are transferred to an alternate agar plate that has been maintained at 25˚C and allowed to recover for 5 minutes before the self-righting assay is performed a final time (the ‘recovery’ assay). All experiments are filmed under constant light and odour conditions using a Leica DFC 340 FX camera mounted on a Leica M165 FC microscope and Leica Application Suite software.

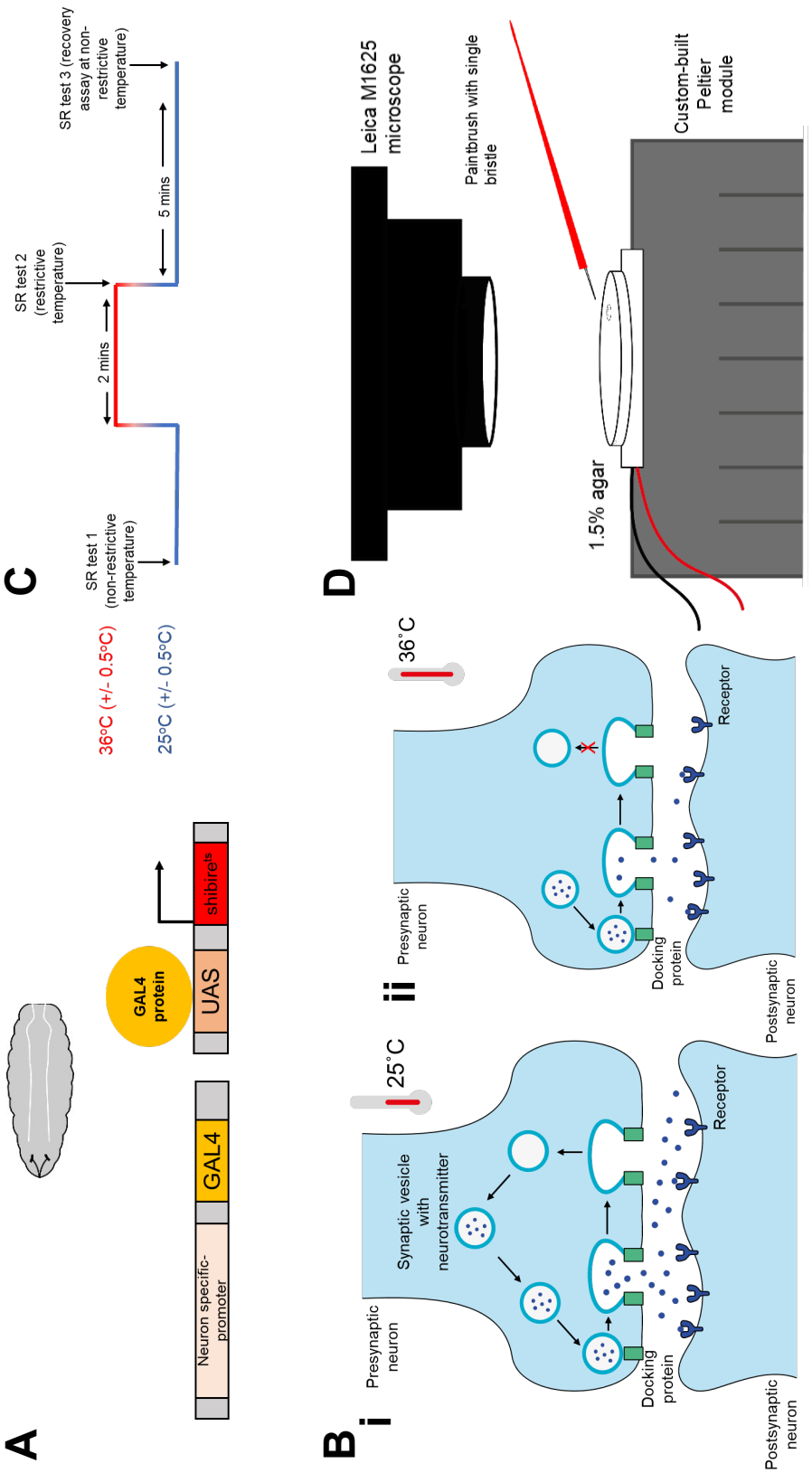

Figure 4.2.1 Thermogenetic inhibition was used to functionally validate the roles of wiring diagram neurons in larval self-righting behaviour

(Legend on the following page)

(A) To functionally validate the roles of the neurons in the neural wiring diagram for self-righting behaviour, we targeted expression of the temperature-dependent *shibire* (or '*shi^{ts}*') to specific neurons using the GAL4-UAS system. **(B**) (i) Exposure of neurons expressing shi^{ts} to the permissive temperature of 25˚C does not change the normal recycling of synaptic vesicles containing neurotransmitter after neurotransmitter release across the synaptic cleft. (ii) Exposure of neurons expressing shi^{ts} to the restrictive temperature of 36˚C blocks synaptic vesicle recycling, inhibiting neuronal transmission. **(C)** A schematic showing the experimental approach used for our thermogenetic inhibition experiments. Self-righting assays were performed after exposure to permissive and restrictive temperatures before five minutes of rest and a final self-righting assay at the permissive temperature. **(D)** A schematic showing the experiment set-up used for our thermogenetic inhibition experiments. Larvae were placed onto a thin 1.5% agar plate which was in turn placed onto a custom-built Peltier-temperature controller module. The temperature of the agar plate was adjusted as appropriate, and larvae were inverted using a single-bristled paintbrush. All experiments were recorded using a DFC 340 FX camera mounted on a Leica M165 FC microscope and Leica Application Suite software.

4.2.2 The role of the sensory neurons in self-righting behaviour

4.2.2.1 The multidendritic class IV neurons

We began by functionally testing the role of the sensory components of the SR wiring diagram, the multidendritic class IV neurons and the chordotonal organs.

The multidendritic class IV sensory neurons belong to an extensively-researched group of sensory neurons that tile the body wall of the *Drosophila* larva (Grueber *et al.,* 2002; 2007) (Figures 4.2.2A and 4.2.2B). The class IV neurons are so named due to their morphology, with extensive branching patterns that are more complex than the related multidendritic Class I, II and III sensory neurons (Grueber *et al.,* 2002). Functionally, the multidendritic class IV neurons play important roles in nociception – facilitating the larva's ability to sense changes in temperature (Burgos *et al.,* 2018) as well as escape external threats such as the ovipositors of parasitoid wasps from the *Leptopilina* genus (Hwang *et al.,* 2007; Robertson *et al.,* 2013). In the third instar (L3) larva, thermogenetic activation of multidendritic class IV neurons is sufficient to activate the 'rolling' motor program used by larvae to evade nociceptive stimuli (Ohyama *et al.,* 2015). Our connectomics work confirms that they provide synaptic input to the Basin-2 and Basin-4 interneurons as described by Ohyama and colleagues (Ohyama *et al.,* 2015) as well as the Down-and-Back interneurons as described by Burgos and colleagues (Burgos *et al.,* 2018) (Figure 4.2.2C). In our behavioural tests, we use the ppk1.9-GAL4 (Ainsley *et al.,* 2003) to target expression of *shibire* to the multidendritic class IV neurons.

4.2.2.2 The chordotonal organs

The chordotonal organs are stretch-sensing sensory elements that form part of the peripheral nervous system in *Drosophila* (Jarman *et al.,* 1995) (Figures 4.2.3A and 4.2.3B). The organs are classified according to their presence in lateral or ventral domains (Jarman *et al.,* 1995) and our connectomics work confirms that they provide synaptic input to Basin-3 interneurons as previously described by Ohyama and colleagues (Ohyama *et al.,* 2015) (Figure 4.2.3C). As mechanosensors, their arrangement along the larval body is key for the monitoring the movements of the body during locomotion (Field and Matheson, 1998) but they also respond to vibration (Ohyama *et al.,* 2015; Klann *et al.,* 2020) and even facilitate the ability to sense gravity (Kamikouchi *et al.,* 2009). Here we use the iav-GAL4 line (Kwon *et al.,* 2010) to target expression of *shibire* to the chordotonal organs.

4.2.2.3 Thermogenetic inhibition of sensory component activity delays self-righting behaviour

Our thermogenetic inhibition of these sensory components during self-righting reveals that their normal activity is essential for the larva to self-right in a timely fashion (Figures 4.2.2D and 4.2.3D). When tested after 2 minutes of exposure to a restrictive temperature, we observe that early L1 ppk>Shi^{ts} and iav> Shi^{ts} larvae both take significantly longer to self-right on average (Figures). We also observe that after a recovery period at 25˚C, self-righting time is returned to an average of 12 seconds in ppk1.9>Shi^{ts} larvae and 16 seconds in iav> Shi^{ts} larvae.

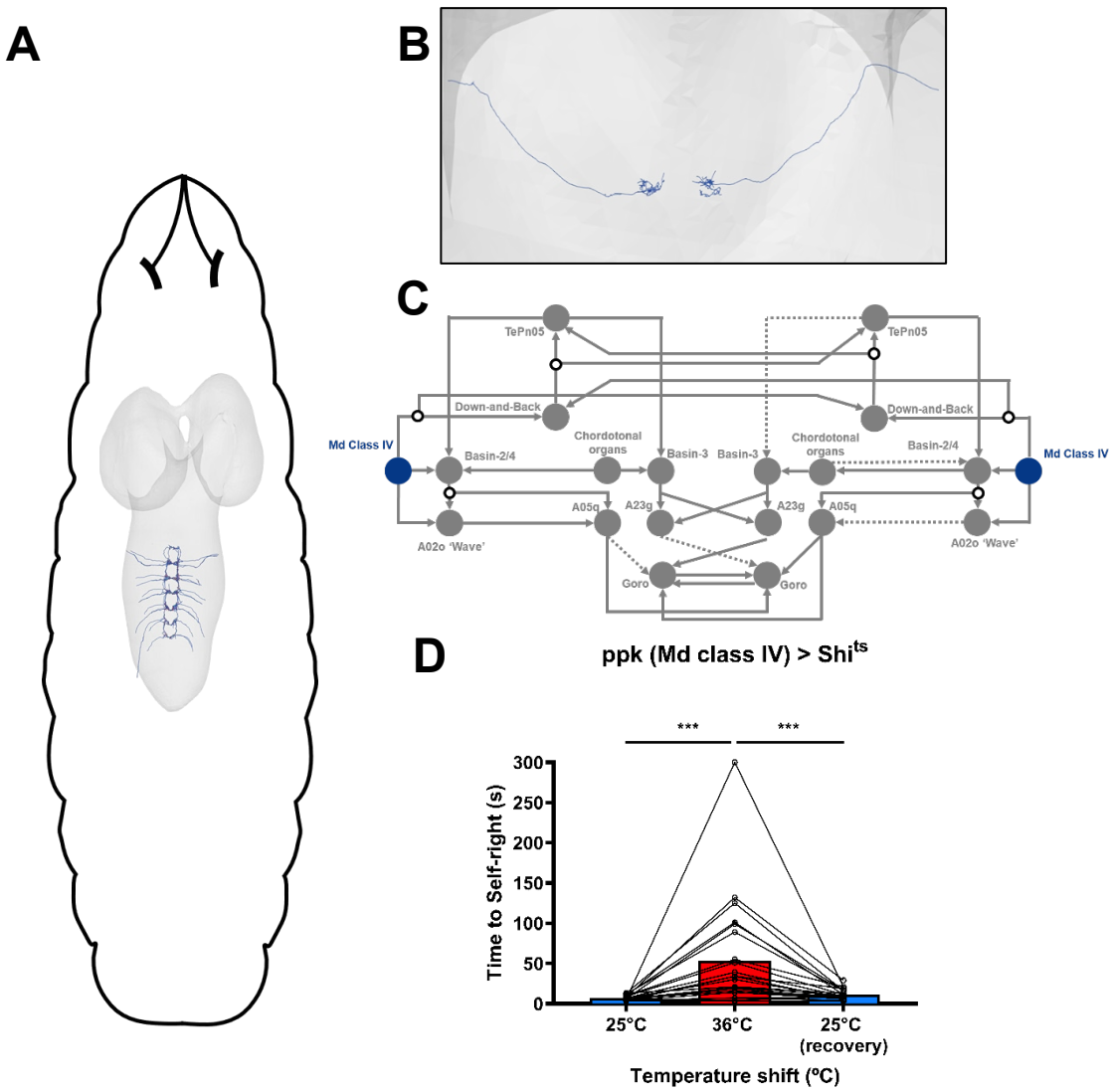

Figure 4.2.2 Thermogenetic inhibition of multidendritic class IV sensory neuronal activity results in delayed larval self-righting

(A) The multidendritic class IV (or 'Md class IV') sensory neurons (blue) comprise a group of three neurons (v'ada, vdaB and ddaC) that are hemisegmentally repeated along the length of the ventral nerve cord. **(B)** A transverse view of the v'ada sensory neurons in segment A1. All three Md class IV sensory neurons project into the neuropil from dorsolateral regions of the peripheral nervous system. **(C)** The Md Class IV sensory neurons (blue) provide output to the first-order Down-and-Back and Basin-2/4 interneurons in our neural wiring diagram. **(D)** Thermogenetic inhibition of multidendritic class IV

sensory neuronal activity results in significantly delayed self-righting at restrictive temperatures. Average self-righting times are raised from 6.8 seconds at 25˚C to 53 seconds at 36˚C. (n = 22. Average self-righting time is indicated by bar height and self-righting times of individuals are indicated by circles. Wilcoxon matched-pairs signed-rank test, *** $p < 0.001$). *Behavioural experiment performed by Clare Hancock.*

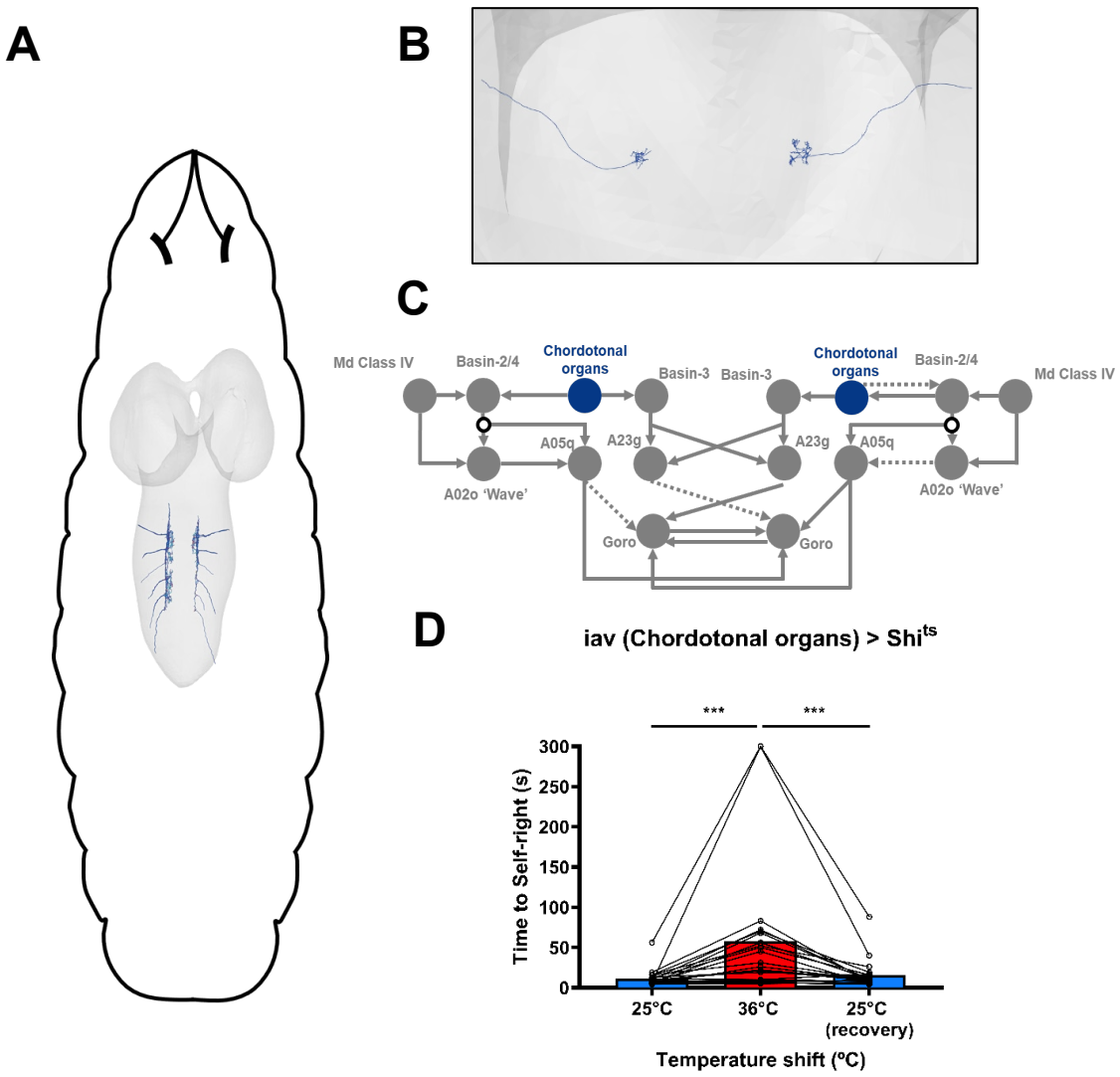

Figure 4.2.3 Thermogenetic inhibition of chordotonal organ activity results in delayed larval self-righting

(A) The chordotonal organs (blue) are lateral and ventral mechanosensory organs that are hemisegmentally repeated along the length of the ventral nerve cord. **(B)** A transverse view of the lateral 5-1 chordotonal organs in segment A1. All chordotonal organs project into the neuropil from dorsolateral regions of the peripheral nervous system however lateral chordotonal organs project less ventrally than ventral chordotonal organs. **(C)** The chordotonal organs (blue) provide output to the first-order Basin-2, Basin-3, and Basin-4 interneurons in our neural wiring diagram. **(D)** Thermogenetic inhibition of chordotonal organ

activity results in significantly delayed self-righting at restrictive temperatures. Average self-righting time is raised from 11.4 seconds at 25˚C to 57.7 seconds at 36˚C. (n = 22. Average self-righting time is indicated by bar height and self-righting times of individuals are indicated by circles. Wilcoxon matched-pairs signed-rank test, *** $p < 0.001$). *Behavioural experiment performed by Clare Hancock.*

Neither of these averages are significantly different to average self-righting times in larvae tested before neuronal inhibition, suggesting that neuronal function has been returned to normal.

We interpret this as evidence that sensory perception is fundamental for the larva's ability to self-right. We postulate that the removal of the larva's mechanosensory and nociceptive capabilities may hinder the larva's ability to sense when the dorsal side of its body has come into contact with the crawling surface and therefore initiate the self-righting motor program.

4.2.3 The role of first order interneurons in self-righting behaviour

4.2.3.1 The Basin interneurons

Having established the necessity of normal sensory component activity for timely self-righting behaviour in the early L1 larva, we built on this by functionally testing the involvement of neurons found to be directly downstream of sensory elements (termed 'first-order' interneurons) in self-righting. Here, we tested the roles of the Basin (previously identified as part of the circuit underlying rolling behaviour) (Ohyama *et al.,* 2015) and Down-and-Back interneurons (previously shown to be functionally linked to the class IV multidendritic sensory neurons) (Burgos *et al.,* 2018).

The Basin interneurons are a group of 4, lineage-related neurons repeated hemisegmentally along the length of the VNC (Figure 4.2.4A). They exhibit a characteristic morphology, projecting from the dorsolateral region of the VNC towards the ventromedial region of the neuropil where they arborise (Figure 4.2.4B). Pairs of Basin interneurons (Basin-1 and Basin-3; Basin-2 and Basin-4)

differ in connectivity to each other (Figure 4.2.4C) and although GAL4 lines exist that target each of the 4 neurons individually, we chose to test Basin involvement in self-righting using a GAL4 line targeting all 4 Basins simultaneously (R72F11-GAL4). Thermogenetic activation of the Basin neurons using this line is sufficient to initiate the rolling program (Ohyama *et al.,* 2015) and we confirm with our connectomics work that they receive synaptic input from the sensory elements that we have identified as fundamental neural substrates of self-righting behaviour (the chordotonal organs and multidendritic class IV neurons).

4.2.3.2 The Down-and-Back interneurons

The Down-and-Back interneurons exist are singular neurons in each hemisegment of the VNC (Figure 4.2.5A). Morphologically, the Down-and-Back neurons project from the cell body towards the ventromedial neuropil where arborisation occurs. A second large projection then extends dorsolaterally back towards the cell body (Figure 4.2.5B). After functionally demonstrating that the Down-and-Back interneurons are downstream of the class IV multidendritic sensory neurons, Burgos and colleagues identify their role in ‘C-bending’ prior to rolling (Burgos *et al.,* 2018). Our connectomics work confirms that the Down-and-Back interneurons receive substantial input from the class IV multidendritic sensory neurons (Figure 4.2.5C) and for our behavioural tests we use the 412-GAL4 line as opposed to the R70F01∩412 line developed by Burgos and colleagues for finer neuronal manipulation.

4.2.3.3 Thermogenetic inhibition of Basin and Down-and-Back neuronal activity delays self-righting

Our thermogenetic inhibition of the first order interneurons of the neural wiring diagram reveals that their normal activity is essential for larval self-righting behaviour (Figures 4.2.4D and 4.2.5D).

R72F11>shi^{ts} and 412>shi^{ts} larvae show significant delays to self-righting after exposure to a restrictive temperature and these delays are particularly severe upon inhibition of the Down-and-Back interneurons, with 30% of 412>shi^{ts} larvae tested failing to self-right within the maximum time limit we permitted of 5 minutes (as opposed to 5% of R72F11>shi^{ts} larvae). We also observe that thermogenetic inhibition of the Down-and-Back interneurons results in the highest average self-righting time of all lines tested at 104 seconds. The effects of thermogenetic inhibition of first order interneurons are reversible with average self-righting times of R72F11>shi^{ts} and 412>Shi^{ts} larvae returning to averages of 7 and 10 seconds respectively after a recovery period at 25˚C.

These results suggest that while sensory perception is fundamental to the larva's ability to self-right, the ability to relay that sensory information to the rest of the central nervous system is equally important. Considering the already established roles of the Basin and Down-and-Back interneurons in rolling/C-bending behaviours, these results also open the question of the degree of overlap between the motor systems controlling these behaviours and self-righting.

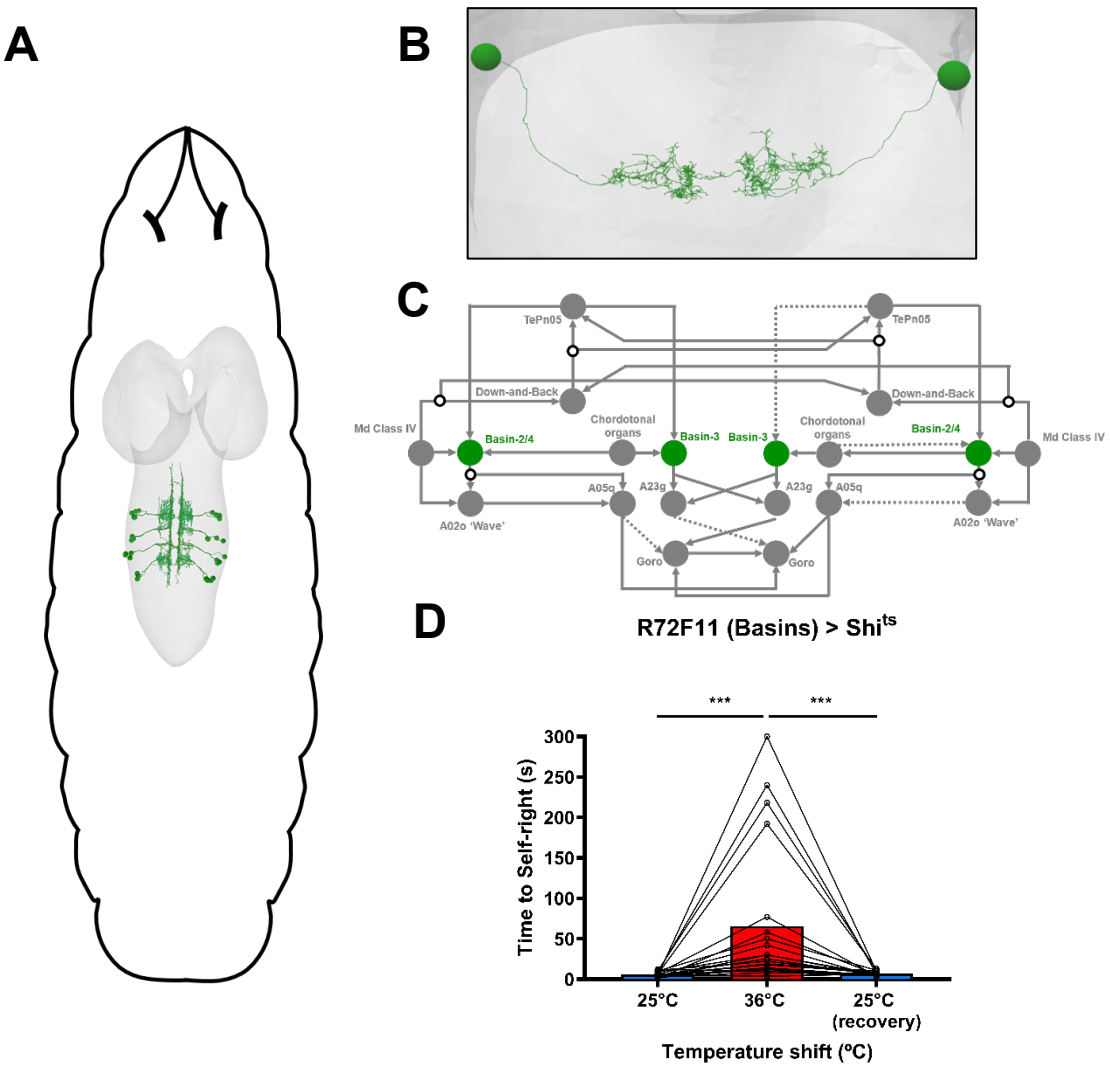

Figure 4.2.4 Thermogenetic inhibition of Basin neuronal activity results in delayed larval self-righting

(A) The Basin-2, Basin-3, and Basin-4 interneurons (green) are a group of ventromedially-projecting, first order interneurons that are hemisegmentally repeated along the length of the ventral nerve cord. **(B)** A transverse view of the Basin-2 interneurons in segment A1. All Basin interneurons project from dorsolateral regions of the ventral nerve cord into the ventromedial neuropil where they arborise forming synaptic connections with upstream and downstream neurons **(C)** In our neural wiring diagram, the Md Class IV sensory

neurons and chordotonal organs provide input to the first-order Basin-2/4 and Basin-3 interneurons, respectively. The Basin-2/4 interneurons then provide synaptic input to the A02o ‘Wave’ and A05q interneurons while the Basin-3 interneurons provide synaptic input to the A23g interneurons. **(D)** Thermogenetic inhibition of Basin neuronal activity results in significantly delayed self-righting at restrictive temperatures. Average self-righting times are raised from 6.1 seconds at 25˚C to 66 seconds at 36˚C. (n = 22. Average self-righting time is indicated by bar height and self-righting times of individuals are indicated by circles. Wilcoxon matched-pairs signed-rank test, *** $p < 0.001$). *Behavioural experiment performed by Dr. Joao Picao-Osorio.*

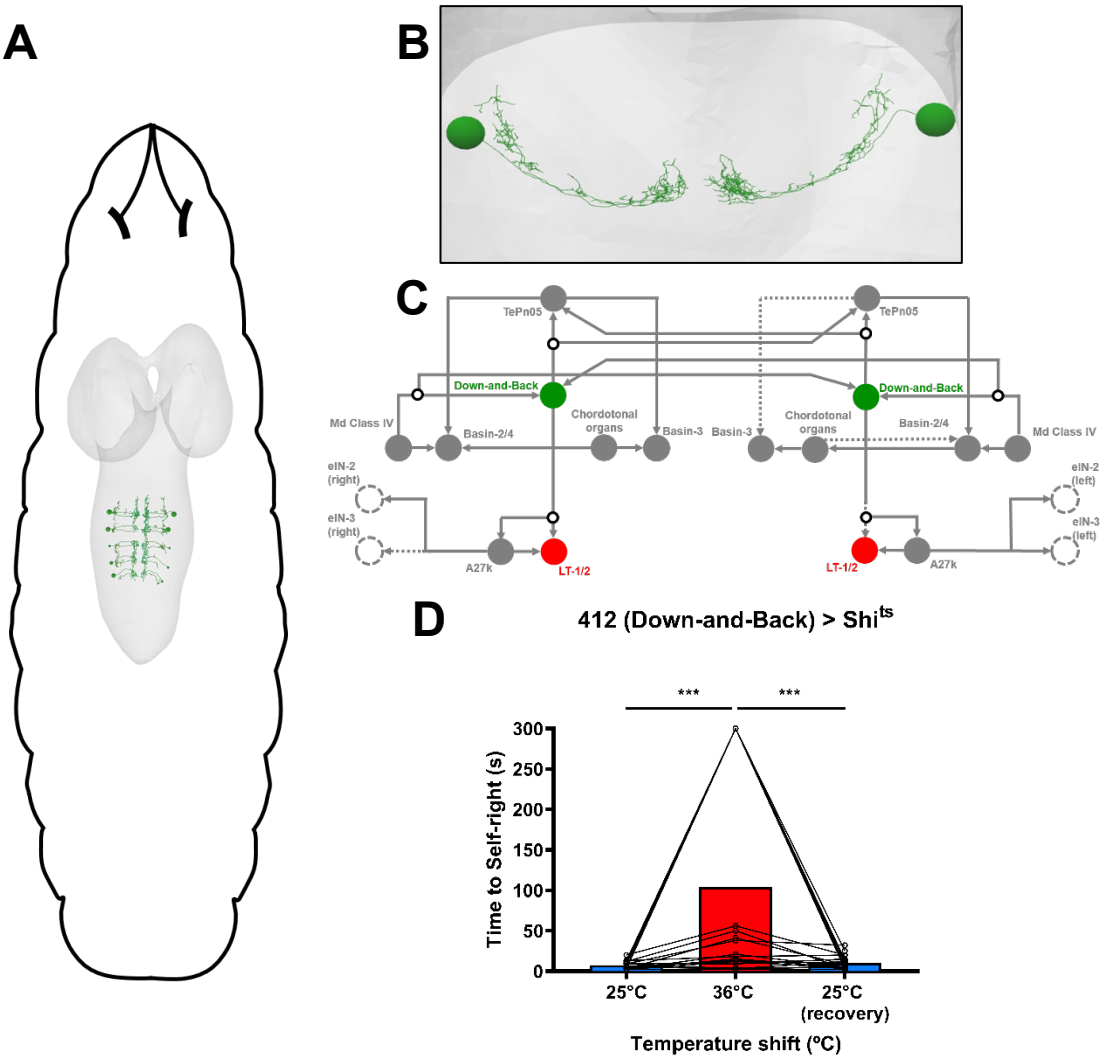

Figure 4.2.5 Thermogenetic inhibition of Down-and-Back neuronal activity results in delayed larval self-righting

(A) The Down-and-Back interneurons (green) are single, first order, interneurons that are hemisegmentally repeated along the length of the ventral nerve cord. **(B)** A transverse view of the Down-and-Back interneurons in segment A1. Each Down-and-Back interneuron has a long projection from the cell body towards the ventromedial neuropil where arborisation occurs, before a second large projection then extends dorsolaterally back towards the cell body. **(C)** In our neural wiring diagram, the Down-and-Back interneurons (green) receive input from the Md Class IV sensory neurons and provide ipsilateral and

contralateral output to the TePn05 interneurons. The Down-and Back interneurons also communicate both indirectly (via the A27k interneurons) and directly with the LT-1/2 motor neurons. **(D)** Thermogenetic inhibition of Down-and-Back neuronal activity results in significantly delayed self-righting at restrictive temperatures. Average self-righting times are raised from 7.7 seconds at 25˚C to 104.4 seconds at 36˚C. (n = 23. Average self-righting time is indicated by bar height and self-righting times of individuals are indicated by circles. Wilcoxon matched-pairs signed-rank test, *** $p < 0.001$).

4.2.4 The role of rolling circuit neurons in self-righting behaviour

4.2.4.1 The A05q interneurons

Our identification of the Basin interneurons' role in self-righting behaviour prompted us to also test the involvement of neurons downstream of the Basins that had previously been identified as part of the circuit underlying rolling behaviour (Ohyama *et al.,* 2015).

Our connectomics work confirms that the A05q neurons receive input from Basins 2 and 4 and provide input to the Goro interneurons as described by Ohyama and colleagues (Ohyama *et al.,* 2015) (Figure 4.2.6C). Currently, only four A05q interneurons have been identified within the larval VNC (one on each side of abdominal segments A1 and A2). Morphologically, A05q neurons consist of an extended projection towards the medial region of the neuropil where arborisation occurs (Figure 4.2.6B). In all neurons, a second projection is also extended into the three thoracic segments of the VNC (Figure 4.2.6A). Functionally, thermogenetic activation of A05q neurons using the R47D07-GAL4 line is sufficient to drive rolling behaviour (Ohyama *et al.,* 2015) and we express *shibire* using the same GAL4 line to test the involvement of A05q in self-righting behaviour.

4.2.4.2 The Goro interneurons

The Goro interneurons are a pair of interneurons with cell bodies and arbors located on either side of segment T2 (Figures 4.2.7A and 4.2.7B). The Goro interneurons are characterised by their long projections that extend into the dorsomedial regions of all abdominal and thoracic segments of the VNC. As

with the other neurons of the ‘rolling’ circuit described by Ohyama and colleagues, thermogenetic activation of the Goro neurons is able to stimulate rolling in larvae however unlike the Basin and A05q interneurons, “fast crawling” is not observed once rolling ends. The specificity of Goro’s involvement in rolling behaviour, therefore, has led to the Goro interneurons being termed as ‘command-like’ neurons for rolling behaviour.

The question of how Goro links to motor components to control rolling behaviour remains open and we examine this in Section 4.2.7. Here, we test Goro involvement in self-righting behaviour using the R16E11-GAL4 line identified by Ohyama and colleagues (Ohyama *et al.,* 2015) as it is more specific to the Goro neurons than the alternative R69F06-GAL4 line.

4.2.4.3 Thermogenetic inhibition of A05q and Goro neuronal activity delays self-righting

The results of our thermogenetic inhibition of neuronal components that make up the previously described ‘rolling circuit’ show that the normal activity of these neurons is necessary for normal self-righting behaviour (Figures 4.2.6D and 4.2.7D). Thermogenetic inhibition of the A05q and Goro interneurons both result in significant delays to self-righting behaviour that are ameliorated after a recovery period at 25˚C. As with the first-order interneurons, we suggest that this opens the question of overlap between the neural systems controlling functionally similar behaviours. While rolling is exhibited as a continuous rotation, self-righting is a singular sequence of shorter behaviours that occur in a stereotyped order with a beginning and end defined by body position.

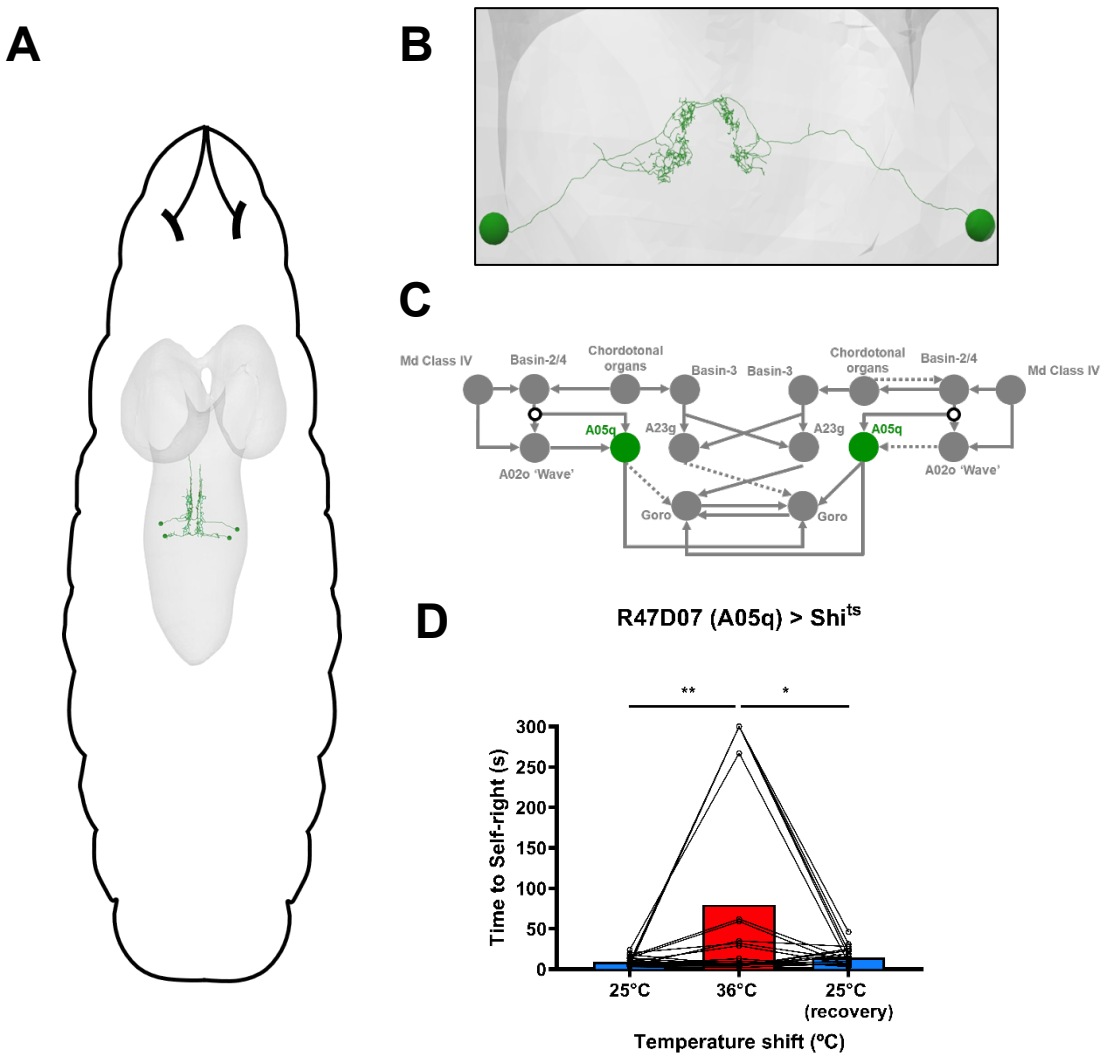

Figure 4.2.6 Thermogenetic inhibition of A05q neuronal activity results in delayed larval self-righting

(A) The A05q interneurons (green) are a pair of second order interneurons present in segments A1 and A2. **(B)** A transverse view of the A05q interneurons in segment A1. A05q interneurons project dorsomedially towards the midline of the VNC where they arborise. **(C)** The A05q interneurons (green) receive input from the first order Basin-2 and Basin-4 interneurons (as well as the nociceptive integrator A02o 'Wave' neurons). In our neural wiring diagram, the A05q interneurons then provide contralateral and ipsilateral output to the Goro

interneurons. **(D)** Thermogenetic inhibition of A05q neuronal activity results in significantly delayed self-righting at restrictive temperatures. Average self-righting times are raised from 9.4 seconds at 25˚C to 79.9 seconds at 36˚C. (n = 22. Average self-righting time is indicated by bar height and self-righting times of individuals are indicated by circles. Wilcoxon matched-pairs signed-rank test, * $p < 0.05$, ** $p < 0.01$)

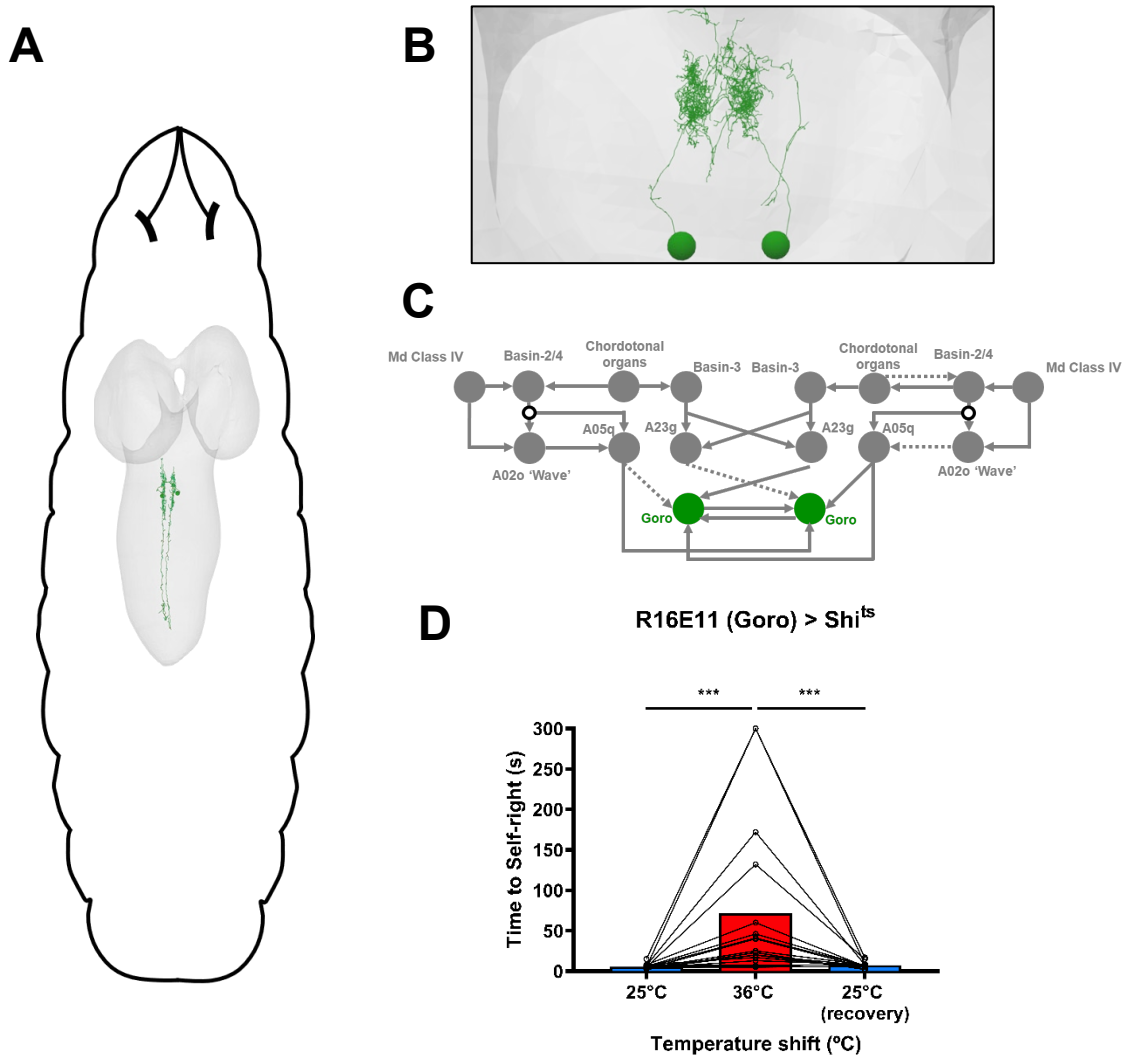

Figure 4.2.7 Thermogenetic inhibition of Goro neuronal activity results in delayed larval self-righting

(A) The Goro interneurons (green) are a pair of interneurons with cell bodies located in the thoracic segment T2 and long projections extending throughout the length of the VNC. **(B)** A transverse view of the two Goro interneurons. From the ventrally-located cell bodies, the two Goro interneurons have dorsal projections which then extend for long distances along both directions of the anteroposterior axis. **(C)** In our neural wiring diagram, the Goro interneurons (green) receive synaptic input from the A05q and A23g interneurons but the

routes by which Goro exerts motor influence remain unknown and are discussed further in Section 4.2.7. **(D)** Thermogenetic inhibition of the neuronal activity of Goro interneurons results in significantly delayed self-righting at restrictive temperatures. Average self-righting times are raised from 5.6 seconds at 25˚C to 72.2 seconds at 36˚C. (n = 22. Average self-righting time is indicated by bar height and self-righting times of individuals are indicated by circles. Wilcoxon matched-pairs signed-rank test, *** $p < 0.001$). *Behavioural experiment performed by Dr. Joao Picao-Osorio.*

The shared dorsoventral rotational aspect of the behaviours, however, may depend on the activity of common neuronal components which contribute to each behaviour.

4.2.5 The role of nociceptive integrator neurons in self-righting behaviour

4.2.5.1 The TePn05 interneurons

In our neural self-righting wiring diagram (Figure 3.2.9), the neurons termed 'nociceptive integrators' by Burgos and colleagues (Burgos *et al.,* 2018), link the neurons of the rolling circuit and the mini-circuit formed between the Down-and-Back interneurons and LT-1/2 motor neurons. Our connectomics work shows substantial connectivity between the A02o 'Wave' and TePn05 interneurons and other neurons in the neural wiring diagram but we observe no connectivity to A09e. Here, we functionally test the role of TePn05 interneurons in larval self-righting behaviour.

The TePn05 neurons are a pair of interneurons with cell bodies in segment A8 and long projections extending throughout the medial regions of all abdominal and thoracic segments of the VNC (Figures 4.2.8A and 4.2.8B). Related to the TePn04 interneurons, the functional roles of TePn05 interneurons have not been fully elucidated although they may play a role in decision-making when the larva is presented with a mechanosensory cue (Masson *et al.,* 2020). At the level of connectivity, reconstruction work by others has revealed connections between TePn05, multidendritic class IV neurons and interneuronal elements (Takagi *et al.,* 2017; Burgos *et al.,* 2018; Jovanic *et al.,* 2019) and we confirm this with our connectomics work (Figure 4.2.8C). To test the involvement of

TePn05 neurons in larval self-righting behaviour, we target *shibire* expression using the R61A01-GAL4 line. Although this is the most accurate GAL4 line that is reported to include the TePn05 neurons in its expression domain, we note that the R61A01-GAL4 line also targets three alternative neurons (A10j, A09o and TePn04) (Masson *et al.,* 2020).

4.2.5.2 Thermogenetic inhibition of TePn05 neuronal activity delays self-righting

The results of our behavioural tests show that thermogenetically inhibiting the activity of the TePn05 neurons using the R61A01 line results in a significant delay to self-righting in early L1 larvae (Figure 4.2.8D). We interpret this cautiously considering the targeting of three other neurons in the R61A01 domain however, we do note that the each of the other three neurons also interact with components of the self-righting circuit (Masson *et al.,* 2020).

We therefore suggest that, as with the first-order interneurons, this demonstrates the necessity of functional components within the system able to relay sensory information to other domains of the circuit. Without this, although a larva may be able to sense its position while inverted, the appropriate premotor and motor components may not receive the appropriate signals to initiate the self-righting program.

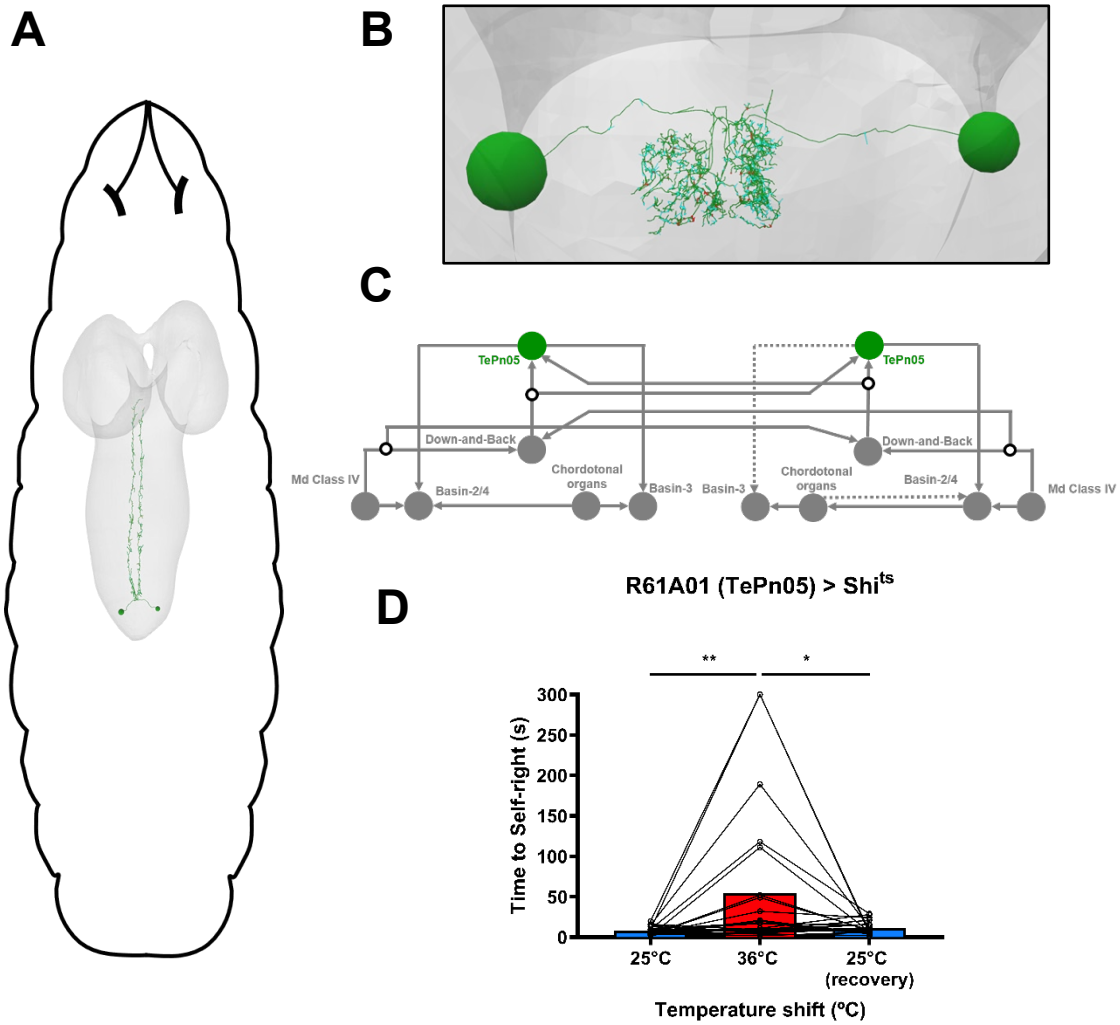

Figure 4.2.8 Thermogenetic inhibition of TePn05 neuronal activity results in delayed larval self-righting

A) The TePn05 interneurons (green) are a pair of interneurons with cell bodies located in the posterior abdominal segment A8 and long projections extending throughout all sections of the VNC (including the suboesophageal zone). **(B)** A transverse view of the two TePn05 interneurons. The TePn05 interneurons have cell bodies located in the mediolateral region of A8 that then extend for long distances along the VNC. As the TePn05 interneurons are based in the most posterior abdominal segment, these projections only extend in the anterior

direction. **(C)** In our neural wiring diagram, the TePn05 interneurons (green) receive synaptic contralateral and ipsilateral input from Down-and-Back interneurons (as well as input from the contralateral TePn05 interneuron). Our neural wiring diagram also identifies output to the ipsilateral Basin interneurons. **(D)** Thermogenetic inhibition of the neuronal activity of the TePn05 interneurons results in significantly delayed self-righting at restrictive temperatures. Average self-righting times are raised from 7.8 seconds at 25˚C to 54.7 seconds at 36˚C. (n = 24. Average self-righting time is indicated by bar height and self-righting times of individuals are indicated by circles. Wilcoxon matched-pairs signed-rank test, * $p < 0.05$, ** $p < 0.01$)

4.2.6 The role of pre-LT interneurons in self-righting behaviour

4.2.6.1 The eIN-1 and eIN-2 pre-LT interneurons

Finally, having functionally validated roles for the majority of neurons in the SR wiring diagram, we test the role of the premotor neurons directly upstream of the LT-1/2 motor neurons (themselves previously identified as key facilitators of self-righting behaviour) (Picao-Osorio *et al.,* 2015; Issa *et al.,* 2019) .

Three neurons have been characterised in literature that have been functionally shown to provide excitatory premotor input to the LT-1/2 motor neurons. The excitatory interneurons known as eIN-1, eIN-2 and eIN-3 exist as singular neurons within each hemisegment of the VNC. The neurons have extended projections across the midline of the VNC (Figures 4.2.9B and 4.2.10B) and provide contralateral input to the LT motor neurons (Figures 4.2.9C and 4.2.10C) as well as the transverse motor neuron DT1 (Zwart *et al.,* 2016). This input has been shown to be excitatory as the three neurons each co-stain for the neurotransmitter acetylcholine (Zwart *et al.,* 2016).

“eIN-1” has been identified as a neuron derived from the A18 neuronal lineage (NB 2-4) and is alternatively known as A18j while “eIN-2” and “eIN-3” have both been identified as neurons belonging to the A01 neuronal lineage (NB 1-2) (Lacin and Truman, 2016). While eIN-2 has been identified as the A01c neuron, “eIN-3” has only putatively been identified as the A01d neuron and we were unable to conclusively identify this neuron in our reconstruction work. Although the activities of eIN-1, eIN-2 and eIN-3 have been implicated in the generation of the premotor excitatory drive during locomotion, their roles in other behaviours have not been investigated. Here, we test the involvement of eIN-2

in self-righting behaviour using the conventional GAL4 line R75H04 and use a “split” GAL4 line (ss01970) based on the intersection of two conventional GAL4 lines (Dolan *et al.,* 2017) to target *shibire* expression to eIN-1.

4.2.6.2 The iIN-1 and iIN-3 pre-LT interneurons

Three inhibitory interneurons providing important input to the LT motor neurons have also been identified by Zwart and colleagues (Zwart *et al.,* 2016).

The iIN-1, iIN-2 and iIN-3 interneurons provide GABAergic input onto the LT motor neurons however only iIN-1 shows wave-like activity during locomotion and has therefore been characterised more fully than iIN-2 and iIN-3 (Zwart *et al.,* 2016). In a similar fashion to the excitatory interneurons, iIN-1 neurons have extended projections across the midline of the VNC (Figures 4.2.11A and 4.2.11B) and provide contralateral input to the LT-1/2 motor neurons (Figure 4.2.11C) as well as DT1. Derived from the A14 neuronal lineage (NB 4-1), the iIN-1 neurons delay the contraction of transverse muscle during larval locomotion (Zwart *et al.,* 2016).

Little is known about the iIN-2 interneurons and our reconstruction and connectomics analyses revealed no contralateral neurons similar to iIN-1 providing strong and consistent input to the LT-1/2 motor neurons along the length of the VNC. We do, however, identify the iIN-3 interneurons as neurons derived from the A19 neuronal lineage known as A19l interneurons. The A19l interneurons provide strong contralateral and ipsilateral input to the LT-1/2 motor neurons (Figure 4.2.12C) however they also have small medial projections along the anteroposterior axis of the VNC that extend into adjacent

segments (Figure 4.2.12A). Unusually, we were only able to identify A19l neurons in the first three abdominal segments of the VNC and in segment A3, were only able to identify one A19l neuron located on the right-hand side. We did, however, observe that the contralateral dendritic portions of all five A19l neurons extended into posterior abdominal segments facilitating input to LT-1/2 motor neurons as distant as segment A5. Here, we use the split GAL4 line ss01411 to test the involvement of iIN-1 in self-righting behaviour. We also note that the apparent lack of symmetry we observe in the iIN-3 interneurons of segment A3 is reflected in the expression pattern of the GAL4 line we use to functionally test iIN-3, R16E12 (Janelia FlyLight).

4.2.6.3 Thermogenetic inhibition of the neuronal activity of all pre-LT interneurons tested except iIN-3 delays self-righting

Our results show that thermogenetic inhibition of the excitatory interneurons eIN-1 (Figure 4.2.9D) and eIN-2 (Figure 4.2.10D) both result in significant delays to larval self-righting behaviour and conclude that the premotor excitatory drive specifically provided to the LT-1/2 motor neurons is fundamental for normal self-righting behaviour. We also propose that this confirms our previous assertations regarding the LT-1/2 motor neurons as key facilitators of self-righting (Picao-Osorio *et al.,* 2015; Issa *et al.,* 2019).

While we also observe that thermogenetic inhibition of the inhibitory interneuron iIN-1 results in a significant delay to self-righting behaviour (Figure 4.2.11D), we observe no significant difference in self-righting time when iIN-3 is inhibited (Figure 4.2.12D). Considering our results showing that suppression of inhibitory

premotor drive results in self-righting delays (as in the case of iIN-1), this result was unexpected. We hypothesise that this result could be explained by differences in the level of input provided to each LT-1/2 motor neuron by the inhibitory premotor interneurons. As previously discussed (see Section 3.2.4), we only identified a set of 5 iIN-3 neurons spread across the first three abdominal segments from our reconstruction work. In contrast, our reconstruction work shows that the iIN-1 neurons are segmentally repeated for at least the first six abdominal segments (and we would also predict their existence in segment A7). This disparity may result in *shibire*-mediated inhibition of neuronal activity having a stronger effect as the activity of more neurons (which are spread more evenly along the entire length of the VNC) is inhibited.

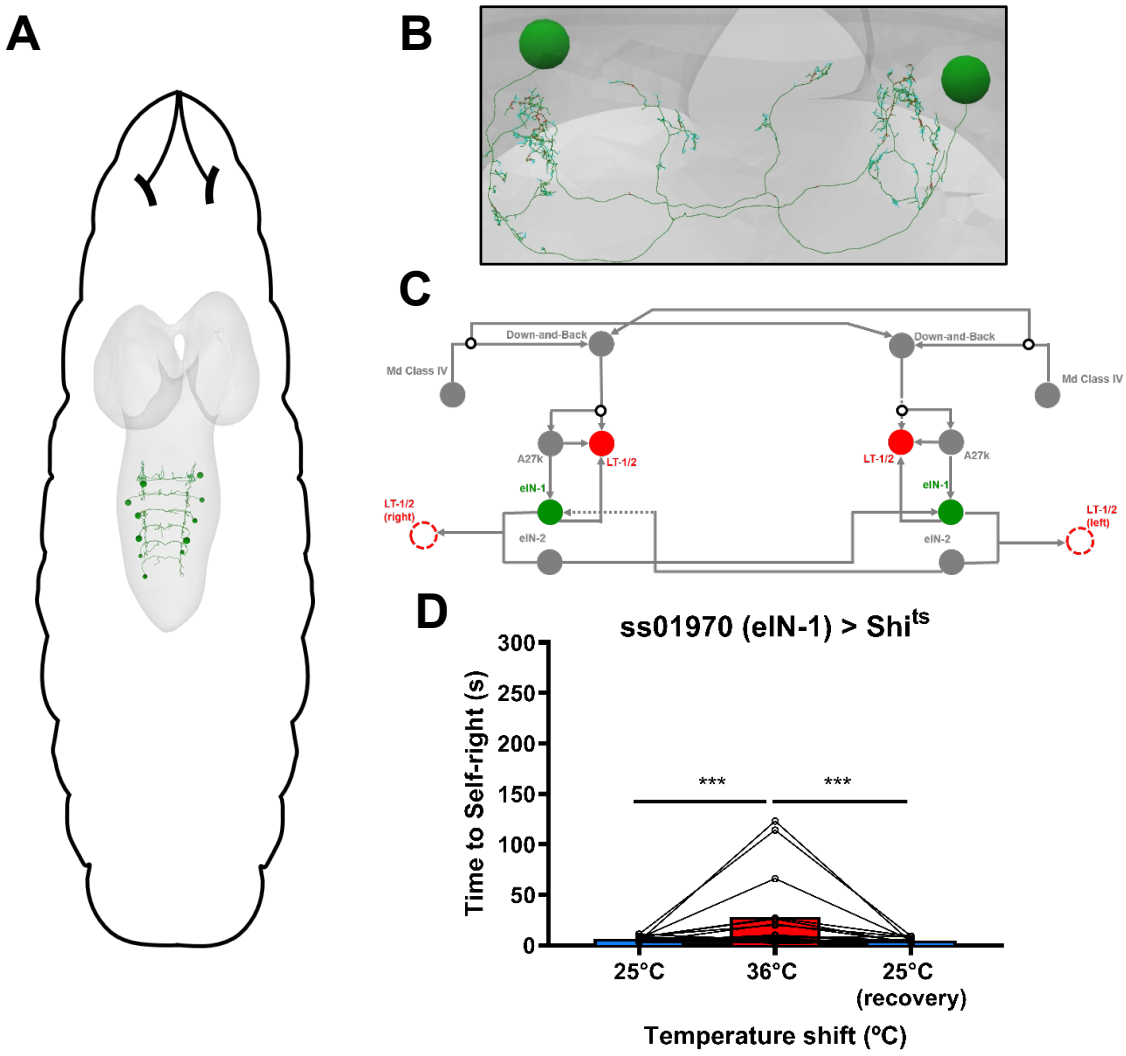

Figure 4.2.9 Thermogenetic inhibition of eIN-1 neuronal activity results in delayed larval self-righting

(A) The eIN-1 interneurons (green) are single interneurons that are hemisegmentally-repeated along the length of the VNC. **(B)** A transverse view of the eIN-1 interneurons in segment A1. The eIN-1 interneurons extend projections across the midline of the VNC and communicate contralaterally with upstream and downstream neurons. Ipsilateral pre- and post-synaptic interactions also take place with eIN-1 interneurons at secondary projections extending dorsally from the medial region of the neuron. **(C)** In our neural wiring

diagram, the eIN-1 interneurons (green) receive synaptic input from the A27k interneurons as well as the eIN-2 pre-LT interneurons. The eIN-1 interneurons then provide synaptic output both ipsilateral (filled red circles) and contralateral (dashed red circles) LT-1/2 MNs. (**D)** Thermogenetic inhibition of eIN-1 neuronal activity results in significantly delayed self-righting at restrictive temperatures. Average self-righting times are raised from 6.6 seconds at 25˚C to 28 seconds at 36˚C. (n = 22. Average self-righting time is indicated by bar height and self-righting times of individuals are indicated by circles. Wilcoxon matched-pairs signed-rank test, *** $p < 0.001$). *Behavioural experiment performed by Dr. Joao Picao-Osorio.*

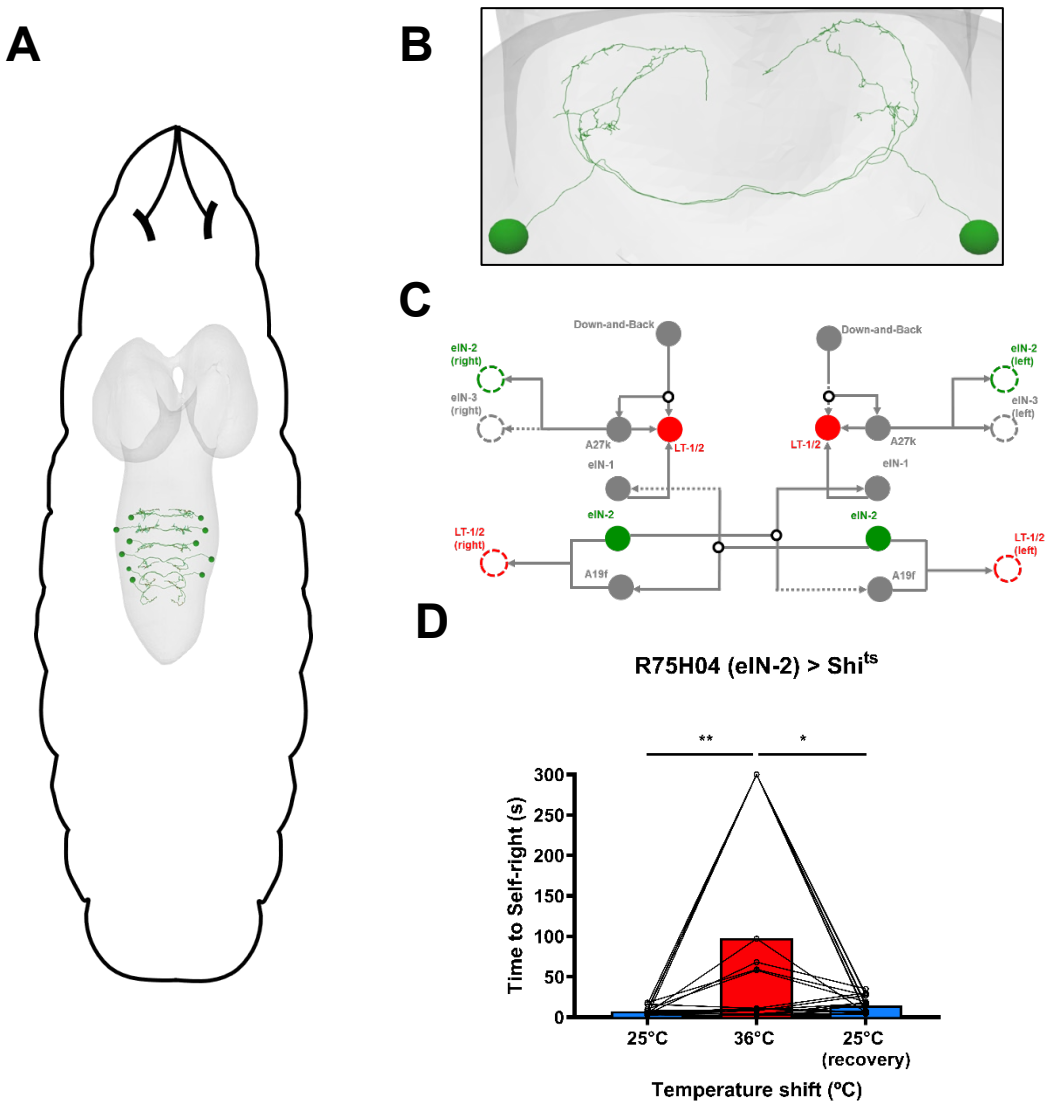

Figure 4.2.10 Thermogenetic inhibition of eIN-2 neuronal activity results in delayed larval self-righting

(A) The eIN-2 interneurons (green) are single interneurons that are hemisegmentally-repeated along the length of the VNC. **(B)** A transverse view of the eIN-2 interneurons in segment A1. Similar to the eIN-1 interneurons, the eIN-2 interneurons also extend projections across the midline of the VNC where they contralaterally communicate with upstream and downstream neurons. Ipsilateral connection, however, is rare in comparison to eIN-1. **(C)** In our neural wiring diagram, the eIN-2 interneurons (green, dashed and filled circles) receive

contralateral synaptic input from the A27k interneurons and provide synaptic output to the A19f premotor interneurons. **(D)** Thermogenetic inhibition of eIN-2 neuronal activity results in significantly delayed self-righting at restrictive temperatures. Average self-righting times are raised from 7.5 seconds at 25˚C to 98.2 seconds at 36˚C. (n = 22. Average self-righting time is indicated by bar height and self-righting times of individuals are indicated by circles. Wilcoxon matched-pairs signed-rank test, * $p < 0.05$, ** $p < 0.01$).

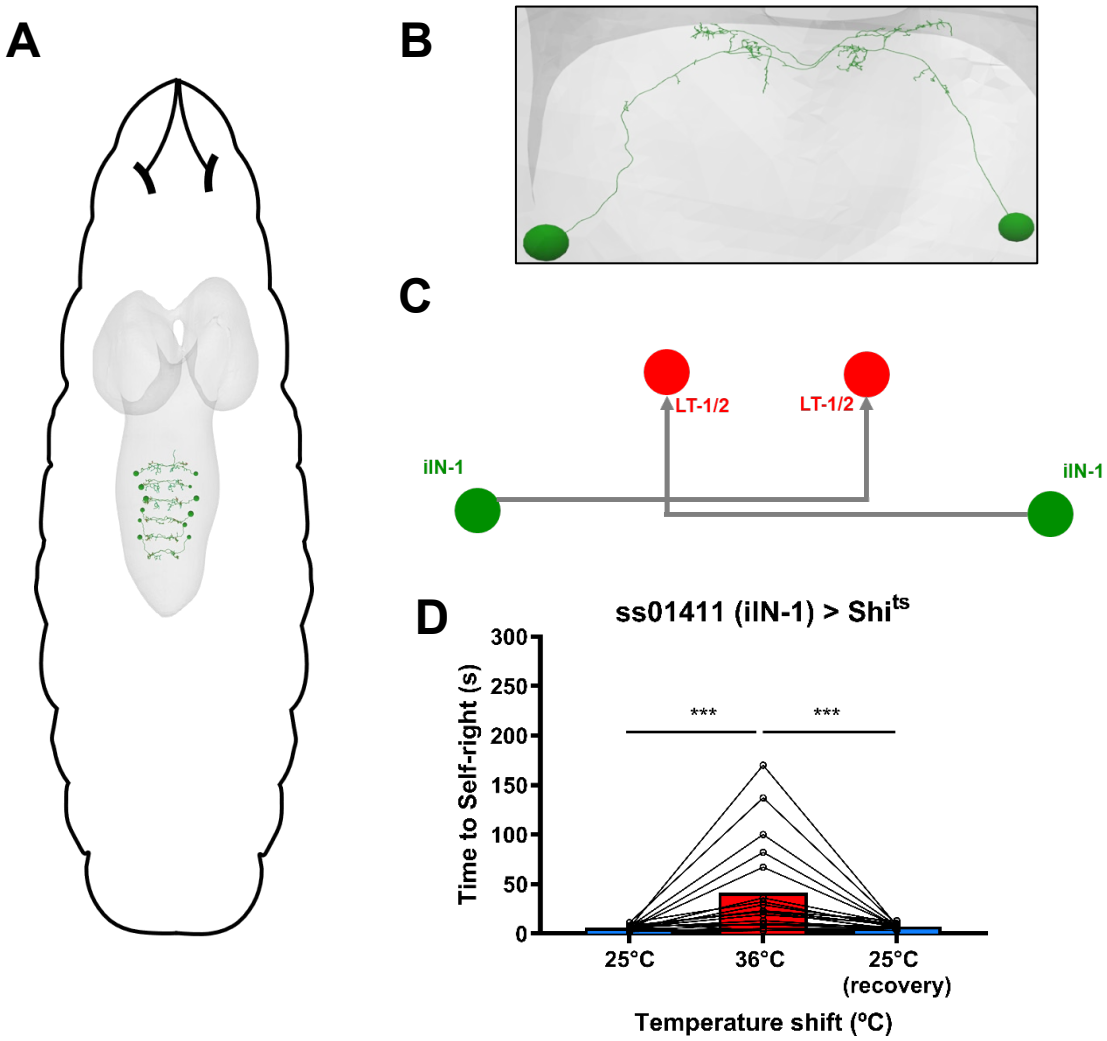

Figure 4.2.11 Thermogenetic inhibition of iIN-1 neuronal activity results in delayed larval self-righting

(A) The iIN-1 interneurons (green) are single interneurons that are hemisegmentally-repeated along the length of the VNC. **(B)** A transverse view of the iIN-1 interneurons in segment A1. From ventrally-located cell bodies, the iIN-1 neurons have dorsally-extending projections that cross the midline of the VNC and arborise contralaterally. **(C)** In our neural wiring diagram, the iIN-1 interneurons (green) receive no strong input from other self-righting circuit neurons but provide strong contralateral output to the LT-1/2 MNs (red). **(D)** Thermogenetic inhibition of iIN-1 neuronal activity results in significantly delayed self-righting at restrictive temperatures. Average self-righting times are raised

from 6.2 seconds at 25˚C to 41.5 seconds at 36˚C. (n = 22. Average self-righting time is indicated by bar height and self-righting times of individuals are indicated by circles. Wilcoxon matched-pairs signed-rank test, *** $p < 0.001$). *Behavioural experiment performed by Dr. Joao Picao-Osorio.*

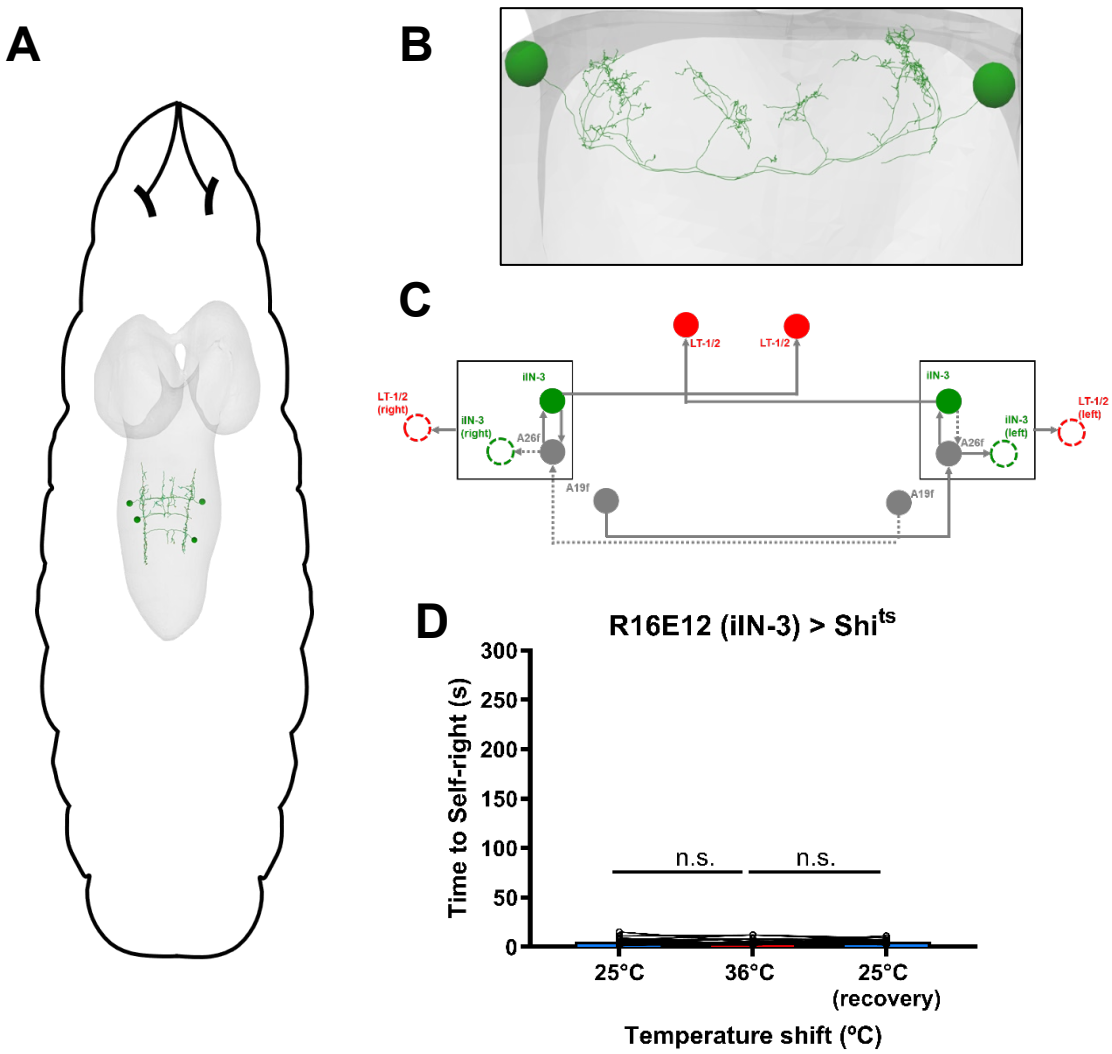

Figure 4.2.12 Thermogenetic inhibition of iIN-3 neuronal activity does not significantly affect larval self-righting time

(A) The iIN-3 interneurons (green) are comprised of a pair of interneurons that are present in segments A1 and A2 as well as a single interneuron in segment A3. **(B)** A transverse view of the iIN-3 interneurons in segment A1. The iIN-3 interneurons have contralaterally-extending projections similar to other pre-LT interneurons however, in the medial region, there are also long projections extending along the anteroposterior axis that contact neurons in anterior and posterior segments. **(C)** In our neural wiring diagram, the iIN-3 interneurons (green, filled and dashed circles) form contralateral and ipsilateral feedback

loops with the pre-LT A26f interneurons as well as communicating with contralateral and ipsilateral LT-1/2 MNs (red, filled and dashed circles). **(D)** Thermogenetic inhibition of iIN-3 neuronal activity does not significantly change larval self-righting time. Average self-righting times are raised from seconds at 25˚C to at 36˚C. (n = 22. Average self-righting time is indicated by bar height and self-righting times of individuals are indicated by circles. Wilcoxon matched-pairs signed-rank test, n.s. – non-significant). *Behavioural experiment performed by Dr. Joao Picao-Osorio.*

4.2.7 An investigation of potential motor neurons through which Goro could exert motor influence

As previously discussed, the Goro interneurons have been termed the ‘master’ neurons for rolling behaviour in *Drosophila* larvae due to the specificity of their role in controlling rolling behaviour (Ohyama *et al.,* 2015). Our identification of Goro as a neuron whose activity is necessary for normal self-righting behaviour (Figure 4.2.7) prompted the question of the motor elements that may facilitate Goro’s influence on self-righting behaviour. Through connectomics analysis, we identify direct and indirect synaptic connections between Goro and dorsal motor components through which motor influence could be exerted (Figure 4.2.13).

Here, we thermogenetically inhibit the activity of these identified dorsal motor components to analyse their roles in the normal exhibition of self-righting behaviour. We also thermogenetically inhibit the activity of motor neurons with ventral muscle targets to further our understanding of how motor activity is coordinated across the dorsoventral body axis during self-righting.

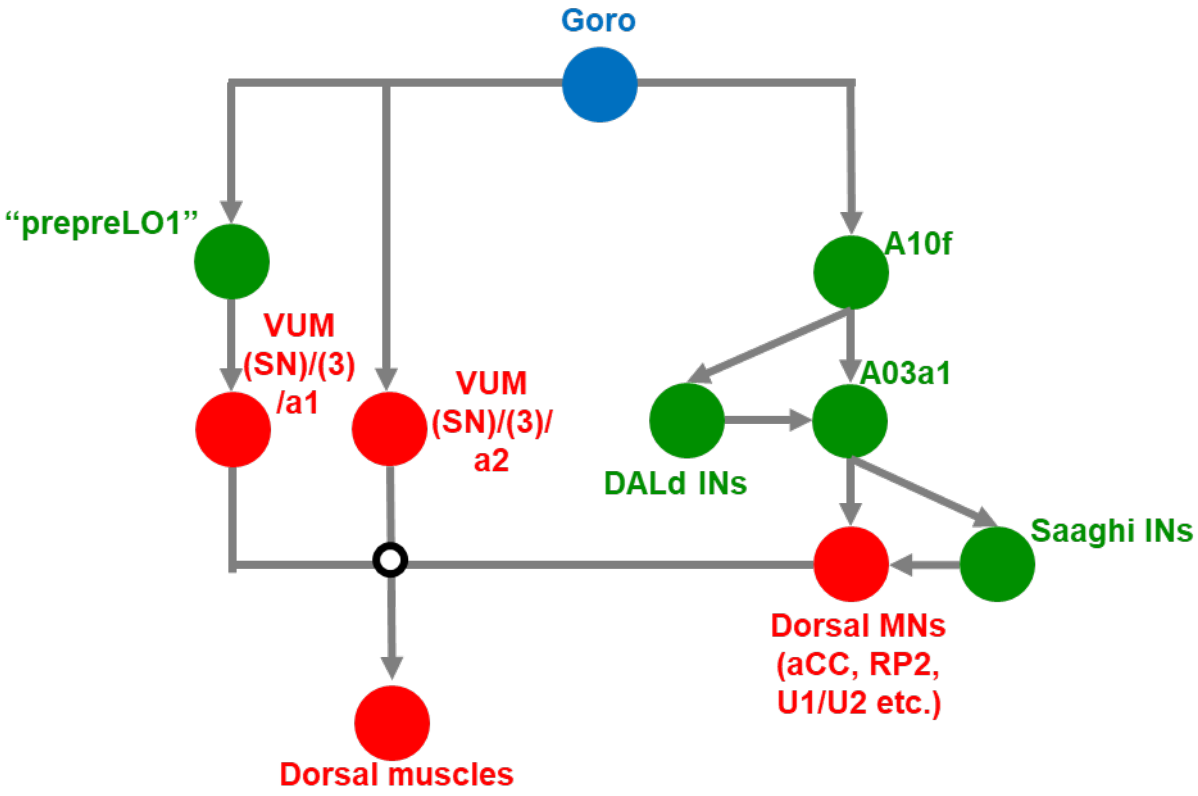

Figure 4.2.13 The Goro interneurons provide strong and consistent input to dorsal motor components

Our connectomics analysis reveals the presence of four neurons to which the Goro interneurons (blue) provide strong and consistent input. Identifying interneurons (green) and muscles downstream of these four neurons, we identified motor neurons targeting dorsal muscles (red) as potential effectors for the influence of the Goro interneuron on motor output.

4.2.8 An investigation of the role of alternative motor components in self-righting

4.2.8.1 The aCC, pCC and RP2 neurons

The aCC and RP2 motor neurons are dorsal motor neurons that exist one per hemisegment along the length of the VNC (Figure 4.2.14A). The aCC neuron innervates the dorsal muscle DA1 (Landgraf *et al.,* 1997; Choi *et al.,* 2004) while the RP2 neuron innervates the entire dorsal muscle field (Landgraf *et al.,* 2003). The aCC and RP2 neurons both express the homeobox-containing transcription factor *even-skipped* and belong to a group of *even-skipped* positive neurons that includes the interneuron, pCC (Broadus *et al.,* 1995). The pCC interneuron also exists one per hemisegment along the length of the VNC and is located adjacent to the aCC motor neuron (Doe *et al.,* 1988).

At the functional level, the roles of the aCC, pCC and RP2 neurons in larval locomotion have been investigated (and in the case of aCC and RP2 well-characterised) (Pulver *et al.,* 2015; Fushiki *et al.,* 2016; Karagyzov *et al.,* 2018) but their activities have never been linked to rolling or self-righting behaviours. Here, we target expression of *shibire* to all three neurons using the RN2-O-GAL4 line (Fujioka *et al.,* 2003; Baines, 2003).

4.2.8.2 The U motor neurons

The U motor neurons (alternatively known as the CQ neurons) exist in groups of five that are repeated in each hemisegment along the length of the VNC (Figure 4.2.15A). Although each U motor neuron develops from the same neuroblast (NB 7-1), the U1 and U2 motor neurons contralaterally target the dorsal DO1

and DO2 muscles, respectively. The U3 and U4 motor neurons target ipsilateral muscles, innervating the DA3 and LL1 muscles respectively (Landgraf *et al.,* 1997). Little is known about the behavioural functions of the U motor neurons but here we target expression of *shibire* to them using CQ-H GAL4 line (Landgraf *et al.,* 2003) to investigate their role in self-righting behaviour.

4.2.8.3 Motor neurons targeting ventral muscles

During embryonic development, the LIM transcription factors play a significant role in the differentiation of neural progenitors into motor neurons or interneurons (Thaler *et al.,* 2002). Specifically, the Lim3 transcription factors significantly influence the development of motor neurons targeting ventral muscles such as RP1, RP3, RP4 and RP5 (Thor *et al.,* 1999; Certel and Thor, 2004) (Figure 4.2.16A). Here we use the Lim3B GAL4 line (Thor *et al.,* 1999) to target expression of *shibire* to these ventral motor neurons and examine their role in self-righting behaviour.

4.2.8.4 Only thermogenetic inhibition of motor neurons targeting ventral muscles significantly delays self-righting

The results of our behavioural tests reveal a stark contrast between the roles of the tested dorsal and ventral neurons tested in larval self-righting behaviour. We find that the thermogenetic inhibition of neither the aCC/RP2/pCC neurons (Figure 4.2.14D) nor the U motor neurons (Figure 4.2.15D) significantly affects the larva's ability to self-right. In contrast, the thermogenetic inhibition of the activity of ventral motor neurons significantly delays self-righting in larvae

(Figure 4.2.16D) and we note that even after 5 minutes of recovery, average self-righting time in Lim3B > shi^{ts} larvae is still only significantly different to that observed at the restrictive temperature by a small degree.

The results of these behavioural analyses suggest that the influence of the Goro interneurons on self-righting behaviour (Figure 4.2.7) is mediated by, as of yet, unknown motor components of the central nervous system. While we identify the activity of motor neurons targeting the ventral muscles as necessary for self-righting behaviour, our connectomics analysis has revealed no paths through which Goro is connected to ventral motor neurons in a strong and consistent manner along the length of the VNC. In addition to this, the fact that we have observed no significant role for the aCC, pCC, RP2 or U motor neurons and yet observe a role for Goro in the control of self-righting prompts us to question whether Goro neurons may exert motor influence through other motor neurons that have yet to be reconstructed. Our connectomics analysis found no strong and consistent route by which Goro is connected the dorsal LT-1/2 motor neurons along the length of the VNC but the solving of the question of Goro's motor influence could have important implications for our understanding of related behaviours such as rolling or C-bending.

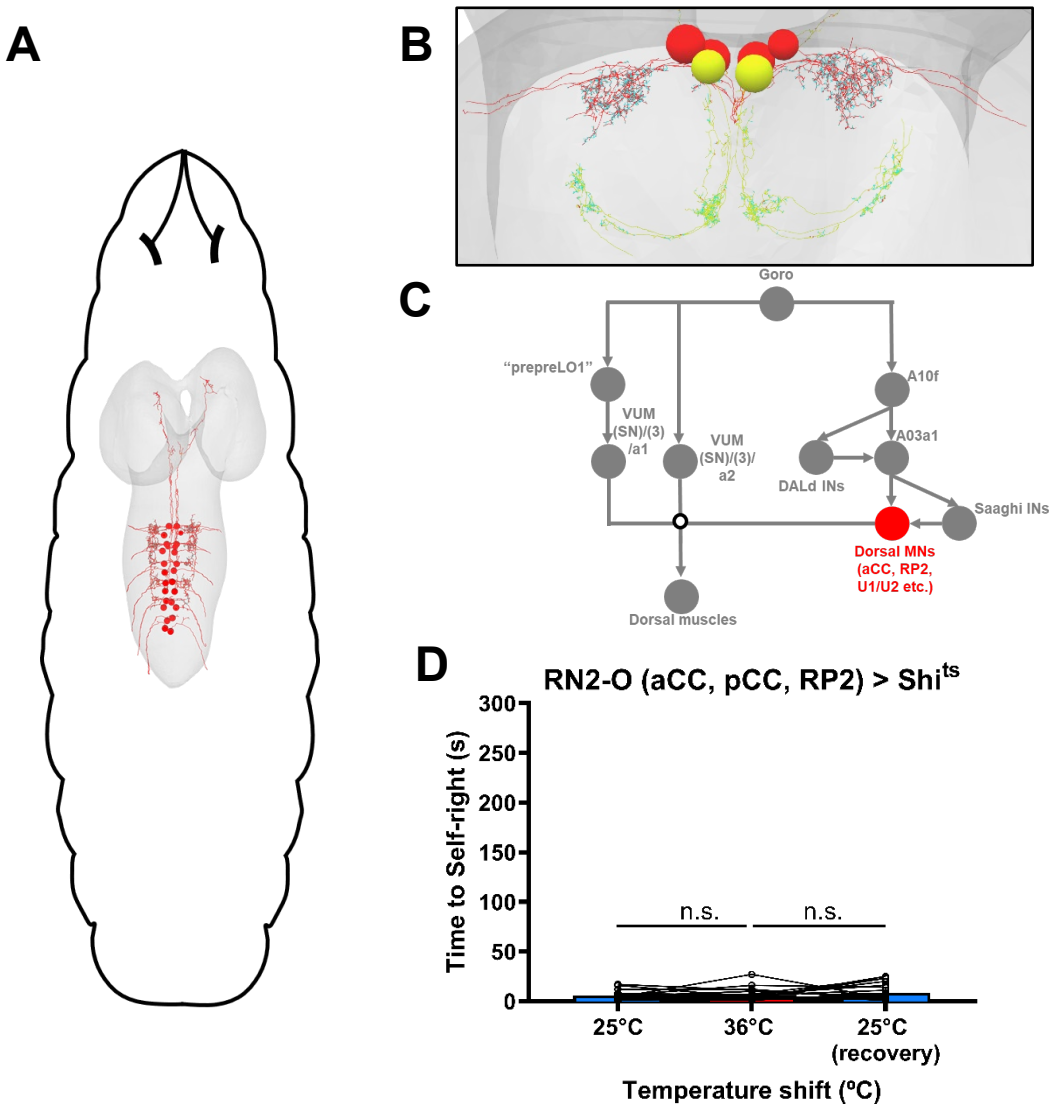

Figure 4.2.14 Thermogenetic inhibition of aCC, pCC and RP2 neuronal activity does not significantly affect larval self-righting time

(A) The aCC and RP2 neurons are dorsally located motor neurons that are interneurons that are hemisegmentally-repeated along the length of the VNC. The pCC interneurons are located in close proximity to the aCC and RP2 motor neurons and all three neurons (red) are positive for the transcription factor, *even-skipped.* **(B)** A transverse view of the aCC, pCC and RP2 interneurons in segment A1. The aCC and RP2 motor neurons (red) both have dorsally-located cell bodies with axonal projections extending into lateral regions where they arborise. The pCC interneurons (yellow) also have dorsally-located cell bodies,

however their axonal projections extend ventrally with arborisation and synaptic communication occurring in the ventrolateral region of the VNC. **(C)** Our connectomics analysis reveals that Goro is linked to the aCC, RP2 and pCC neurons via a chain of interneurons arranged in a way that provides redundancy in Goro-to-motor neuron communication. **(D)** Thermogenetic inhibition of aCC, pCC and RP2 neuronal activity does not significantly change larval self-righting time. Average self-righting times are raised from seconds at 25˚C to at 36˚C. (n = 24. Average self-righting time is indicated by bar height and self-righting times of individuals are indicated by circles. Wilcoxon matched-pairs signed-rank test, n.s. – non-significant).

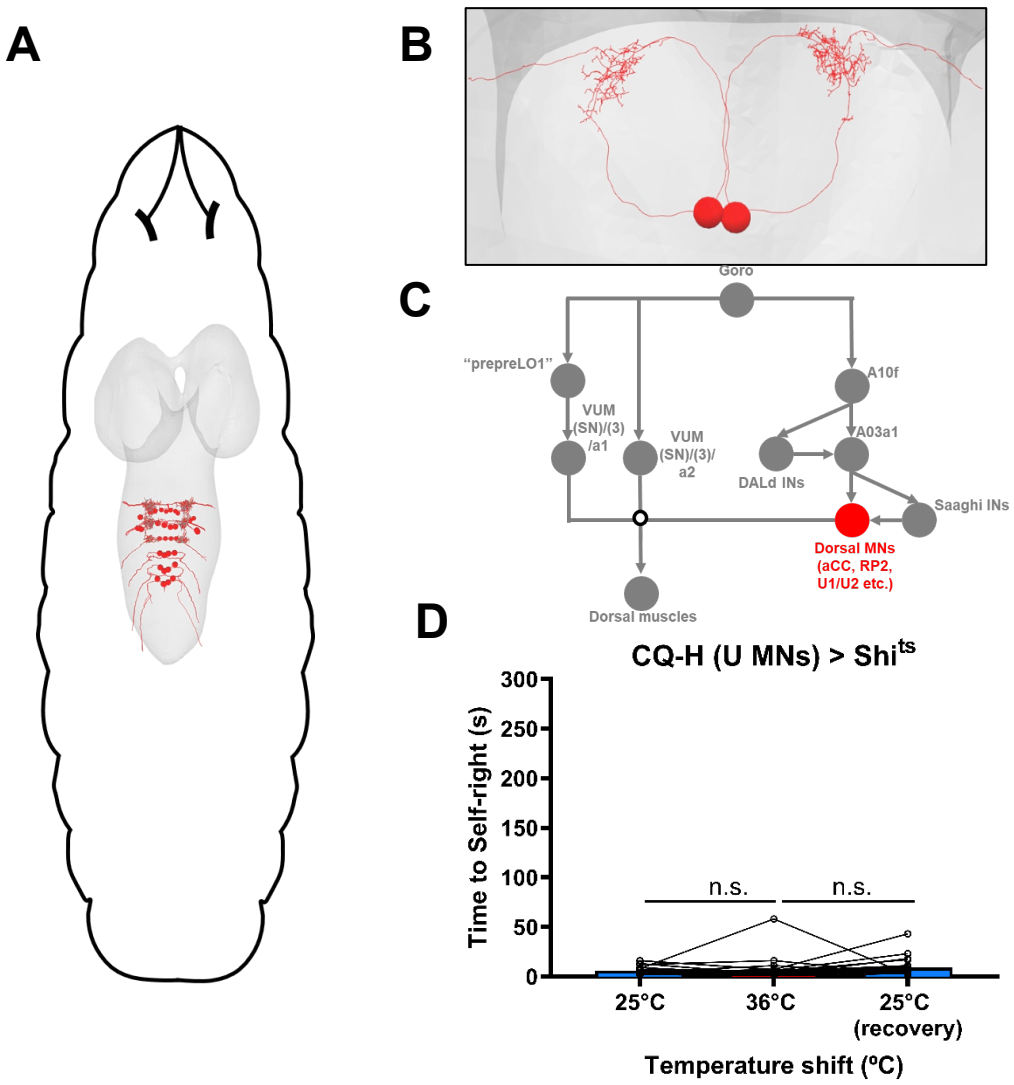

Figure 4.2.15 Thermogenetic inhibition of U motor neuron activity does not significantly affect larval self-righting time

(A) The U motor neurons (red) exist as groups of five hemisegmentally-repeated motor neurons that are present along the length of the VNC. **(B)** A transverse view of the U1 motor neurons in segment A1. The U1 and U2 motor neurons target the contralateral muscles DO1 and DO2 via the anterior root of the intersegmental nerve a (ISNa) while the U3 and U4 motor neurons target the ipsilateral DA3 and LL1 muscles via ISNa. **(C)** Our connectomics analysis reveals that Goro is also linked to the U motor neurons via the same, chain of

interneurons linking it to the aCC, pCC and RP2 neurons. **(D)** Thermogenetic inhibition of U motor neuron activity does not significantly change larval self-righting time. Average self-righting times are raised from seconds at 25˚C to at 36˚C. (n = 23. Average self-righting time is indicated by bar height and self-righting times of individuals are indicated by circles. Wilcoxon matched-pairs signed-rank test, n.s. – non-significant)

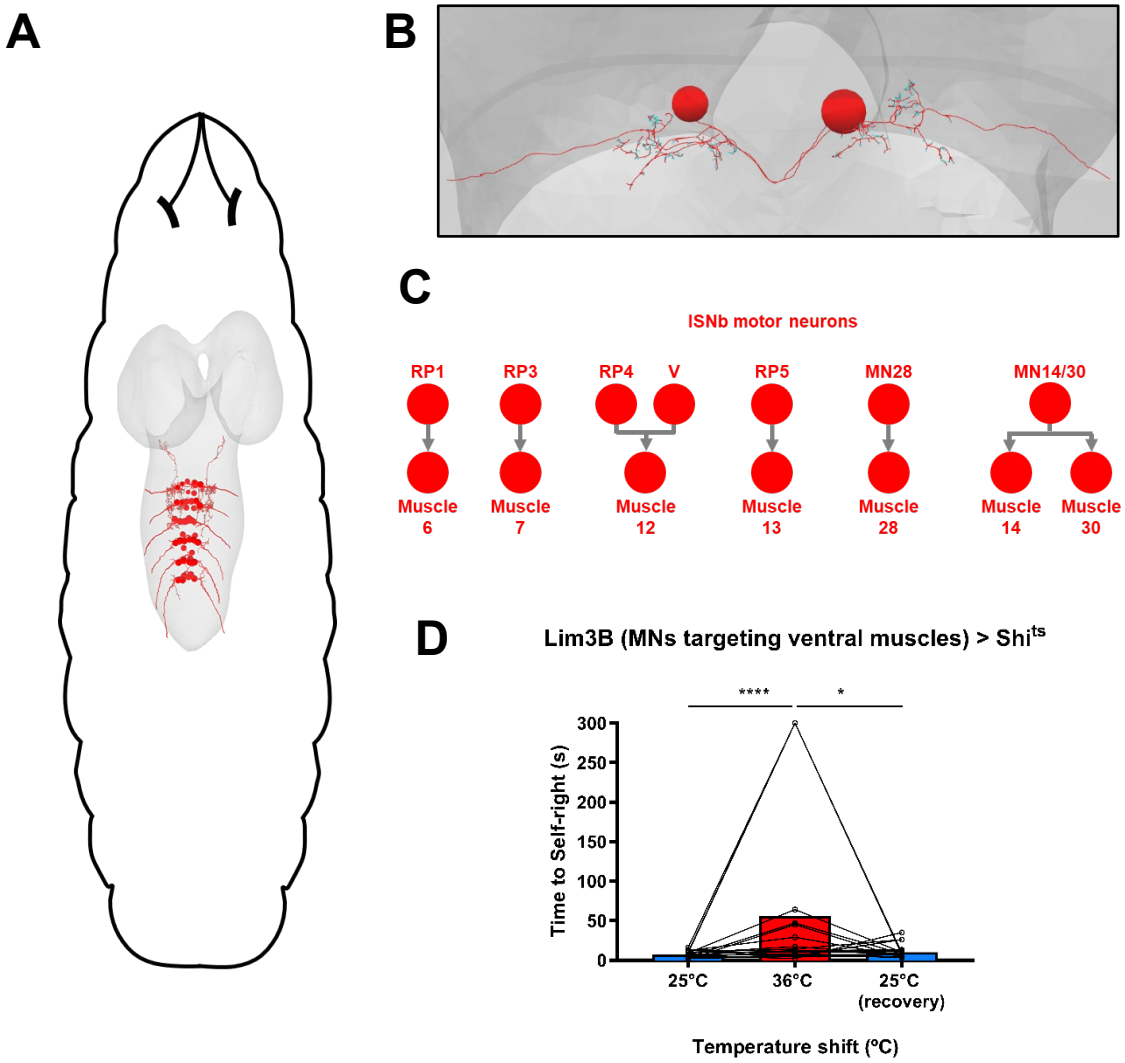

Figure 4.2.16 Thermogenetic inhibition of motor neurons targeting ventral muscles results in delayed larval self-righting

(A) The Lim3 transcription factors are expressed in the hemisegmentally-repeated ISNb motor neurons (red). **(B)** A transverse view of the RP1 interneurons in segment A1. The *Lim3B*-positive motor neurons mostly have dorsally-located cell bodies but target ventral muscles via the branch of the intersegmental nerve, ISNb **(C)** A schematic showing the ISNb motor neurons that are positive for *Lim3B* (as described by Thor and colleagues) (Thor *et al.,* 1999) **(D)** Thermogenetic inhibition of motor neurons targeting ventral muscles

results in significantly delayed self-righting at restrictive temperatures. Average self-righting times are raised from 7.2 seconds at 25˚C to 55.6 seconds at 36˚C. (n = 22. Average self-righting time is indicated by bar height and self-righting times of individuals are indicated by circles. Wilcoxon matched-pairs signed-rank test, * $p > 0.05$, **** $p < 0.0001$).

4.2.9 Summary of the effects of thermogenetic neuronal inhibition on larval self-righting

In this chapter, we examine the involvement of 12 of the 18 components of the self-righting wiring diagram (Figure 3.2.9) in larval self-righting *in vivo*.

Regarding the remaining six components, we note that the LT-1/2 motor neurons have already been shown to be necessary for self-righting (Picao-Osorio et al., 2015) and, while efforts were made to obtain GAL4 lines for the other five components (A02o 'Wave', A19f, A23g, A26f and A27k), these were severely hindered due to the global COVID-19 pandemic. We aim to complete thermogenetic inhibition testing of the remaining components in the near future to provide full coverage of the SRC neurons.

The results of our tests show that the normal activity of all neurons tested (except for iIN-3) is necessary for timely self-righting by the larva (Figure 4.2.17). Overall, we conclude that the neurons identified constitute a functional behavioural circuit that facilitates the behavioural sequence underlying self-righting behaviour *in vivo*.

In this chapter, we also build on connectomics work (Figure 4.2.13) to investigate the routes through which the Goro interneuron exerts an influence on the motor system during self-righting (Figure 4.2.7). Although we identify strong connections with the dorsal motor neurons, our thermogenetic inhibition testing shows that the activity of selected dorsal motor neurons is not necessary for timely self-righting but rather that self-righting is dependent on the ventral motor neurons.

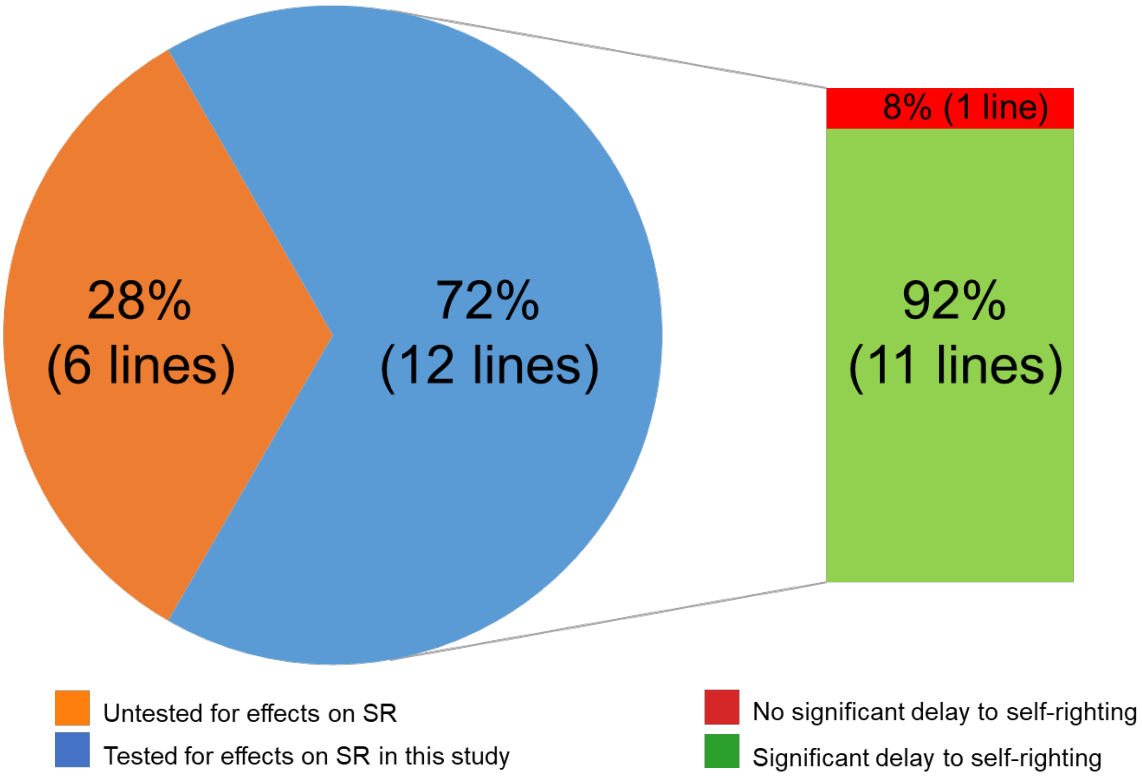

Figure 4.2.17 Thermogenetic inhibition of the majority of self-righting wiring diagram neurons leads to significantly delayed self-righting

In this study, we thermogenetically inhibit 12 of the 18 neurons of the self-righting wiring diagram to examine their roles in self-righting *in vivo.* Our results show that the normal activity of the vast majority of neurons tested is necessary for timely self-righting by the larva, validating the wiring diagram as a functional behavioural circuit.

4.3 Discussion

A notable observation made in this chapter is the lack of change to self-righting behaviour observed when iIN-3 interneurons are thermogenetically inhibited. The iIN-3 interneurons provide GABAergic inhibition to the LT-1/2 MNs (Zwart *et al.,* 2016) and although one could hypothesise that the release of this inhibition (via cessation of iIN-3 activity) may promote quicker self-righting, the fact that inhibition of the related iIN-1 interneurons leads to delayed self-righting only opens further questions.

Comparing the iIN-1 and iIN-3 interneurons, our reconstruction work shows that iIN-1 interneurons are present in a hemisegmentally-repeated fashion along (at least) the first six abdominal segments of the VNC, whereas the iIN-3 interneurons are only present in segments A1-A3. Our reconstruction work was also only able to identify an iIN-3 interneuron on the right of segment A3 however we note that this matches the publicly-available expression pattern of the GAL4 driver (R16E12-GAL4) used to manipulate the interneurons.

One hypothesis that could explain the lack of change to self-righting upon iIN-3 inhibition is that, although the iIN-3 interneurons contact LT-1/2 MNs in the first six abdominal segments, the strength of these connections dissipates towards the posterior segments and thus inhibition of iIN-3 activity does not affect LT-1/2 MN activity in a uniform manner along the length of VNC. This, in turn, may allow the larva to still self-right in a timely manner even when the iIN-3 neurons are inhibited. The downstream effects of iIN-1 thermogenetic inhibition, however, are consistent along the VNC and therefore result in a more severe cumulative change to LT-1/2 MN activity, distorting the larva's ability to co-

ordinate its body during the self-righting sequence. An experimental approach to test this model could be the expression of a genetically encoded calcium indicator (such as GCaMP) within the LT-1/2 MNs and the comparison of segment-specific LT-1/2 MN activity after stimulation of the iIN-1 and iIN-3 interneurons.

We also note that the iIN-1 interneurons receive no strong input from other neurons in the self-righting circuit whereas the iIN-3 interneurons form ipsilateral and contralateral feedback loops with the pre-LT interneuron, A26f. This difference in the input provided to the iIN-1 and iIN-3 interneurons and their subsequent functional relevance could also represent a interesting topic for research in future. For example, the examination of whether the A26f to iIN-3 connection comprises an excitatory or inhibitory connection and the implications of this for the behavioural results we present.

Although the involvement of the LT-1/2 MNs in self-righting behaviour has been well-characterised, our study also reveals that other motor neurons innervating dorsal muscles (aCC, pCC, RP2 and U motor neurons) play no role in facilitating the self-righting sequence. The identification of the need for the normal activity of motor neurons targeting ventral muscles for timely self-righting suggests that the LT-1/2 MNs may facilitate a specific part of the self-righting sequence that stands alone from the parts facilitated by ventral muscles.

One approach to probe this in future studies, could be the use (or development) of behavioural tracking software, able to automatically discern how specific parts of the self-righting sequence are changed in larvae when particular neurons are inhibited. An early version of this analysis was presented by Picao-

Osorio and colleagues (Picao-Osorio *et al.,* 2017) in the context of miRNA mutant self-righting, but with the identification of the cellular substrates of self-righting behaviour, this analysis could be expanded and increased in precision.

Finally, a new avenue for investigation opened by the results of this chapter could be the coherence between the neural circuit underlying self-righting behaviour in the L1 larva and the corresponding circuit in the third instar (or 'L3') larva. Work by our lab has shown that the expression of the miRNA *miR-iab-4* is also necessary for timely self-righting in the L3 larva (Issa *et al.,* 2019) however the cellular substrates of the behaviour at this stage remain uncharacterised.

The neuronal complement of the CNS is largely not added to (Truman and Bate, 1988) during larval development but rather, neuronal circuits become reinforced in strength due to an increase in the number of synapses between neurons (Zwart *et al.,* 2013, Gerhard *et al.,* 2017). The same serial reconstruction approach used in this study, therefore, could be applied to examine the cellular substrates of self-righting behaviour which are upstream of key L3 motor components and produce a neural wiring diagram that can be compared with that underlying self-righting behaviour in the L1 larva.

Overall, we conclude that the transformation of the wiring diagram underlying self-righting in the L1 larva into an *in vivo* behavioural circuit reveals new insights into the control of complex motor behaviours. Our findings support the view that thermogenetic inhibition is a powerful tool for circuit analysis and can reveal unexpected insights about the involvement (or lack thereof) of specific neurons in behaviours of interest.

Chapter 5

The role of microRNAs in *Drosophila* larval locomotion

5.1 Chapter overview

Post-transcriptional regulation of gene expression by microRNAs (miRNAs) is fundamental for a variety of processes across many organisms including neural development in mice and zebrafish (Zhao *et al.,* 2009; Mokabber *et al.,* 2019; Leucht *et al.,* 2008) , apoptosis and homeostasis in the fruit fly (Stark *et al.,* 2003; Çiçek *et al.,* 2016), and leaf and flower development in plants (reviewed in Kidner and Martienssen, 2005). The identification of gene regulation by miRNAs in the cells of the CNS has led to the identification of several behaviours that are regulated through miRNA expression (as discussed in Section 1.12). At the mechanistic level, however, very few complete pathways (which include the target genes regulated by miRNAs, the cellular processes that rely on this and the contribution of this process to behavioural output) have been identified. Although the overall molecular-cellular control of behaviour has been investigated at length, mechanistic studies provide us with an understanding of exactly how miRNA-based gene regulation fits into this framework and are, therefore, key.

Drosophila melanogaster, with a relatively small nervous system and full genetic availability, represents an excellent model system in which to investigate this and elucidate the roles of miRNAs in behaviour.

Multiple studies have demonstrated the involvement of miRNA-based regulation in the performance of various motor behaviours in the adult fly (Sokol *et al.,* 2008; Zhang *et al.,* 2016; Cusumano *et al.,* 2018). In larval *Drosophila* however, study of miRNAs in the context of their roles in controlling behaviour comprises few publications. For example, normal expression of *miR-1* is necessary for

larval locomotion (Sokol and Ambrose, 2005) while Donelson and colleagues have identified 44 miRNAs whose inhibition significantly affects one or more locomotor parameters (Donelson *et al.,* 2020).

One key example is a study produced by our lab demonstrating that expression of the miRNA, *miR-iab-4*, is necessary for the normal execution of a complex larval behaviour (self-righting) at the early first instar (L1) stage, even when the development of the neurons facilitating this behaviour appears unimpeded (Picao-Osorio *et al.,* 2015). A later study by our lab also showed that, in addition to *miR-iab-4*, self-righting is facilitated by the expression of 32 other miRNAs (Picao-Osorio *et al.,* 2017) prompting us to explore the generality of miRNA involvement in overall larval motor control.

To this end, we postulated three questions:

1) Is miRNA-based regulation necessary for normal larval locomotor behaviour in the early L1 larva?
2) If so, is the need for miRNA-based regulation as pervasive in general larval locomotor behaviour as in larval self-righting behaviour?
3) Does the necessity of miRNA-based regulation for normal locomotor behaviour change over the course of larval development?

To answer these questions, we combined genetic and quantitative behavioural approaches. In particular, we used an FTIR-based approach known as the FIMTable (Risse *et al.,* 2013; 2017) to produce behavioural videos of free crawling in a collection of miRNA mutant larvae representing over 95% of miRNAs expressed in late embryogenesis (Chen *et al.,* 2014b; Zhou et al., 2018). We then analysed larval locomotion using the associated FIMTrack

software in addition to a custom Microsoft Excel macro and Python 3 package to extract data on multiple behavioural parameters.

Firstly, we found that (at the early L1 stage) average larval crawling speed was significantly reduced in 79% of miRNA mutant lines tested. When analysing other aspects of locomotor behaviour, we also observed significant changes to both pausing and turning. We combined this data into a multidimensional dataset and analysed this with principal component analysis, the results of which revealed a disproportionate influence of pausing behaviour on the total variance in the multidimensional dataset.

In a subset of miRNA mutants with a wide variation of average crawling speeds at the L1 stage, we also analysed the effects of these mutations on the same behavioural parameters at the third instar (L3) larval stage. We find that, in many cases, the impact of miRNA mutation on the locomotion of L1 larvae is reduced over larval development while in other cases, abnormal locomotor phenotypes are still displayed at L3. Correlation analyses between the two larval stages also identified no significant relationship in any behavioural parameters.

The results of our unbiased genetic screens indicate that the expression of specific miRNAs is necessary for normal crawling, turning, and pausing behaviours at the L1 and L3 developmental stages. Our results also indicate that, over the course of larval development, the necessity of specific miRNAs for regulation of these behaviours changes suggesting that developmental stage has an impact on the roles played by specific miRNAs in motor behaviour control.

5.2 Results

5.2.1 A screen for locomotor defects in miRNA mutant *Drosophila* larvae at L1

5.2.1.1 Motivation for performing a locomotor screen in miRNA mutant larvae

Previous data from our lab has shown that post-transcriptional regulation by miRNAs plays an important role in the control of larval movement in *Drosophila* (Picao-Osorio *et al.,* 2015, 2017; Issa *et al.,* 2019) but much of this work has so far focused on miRNA impact on self-righting (a complex movement in which the larva performs a 180˚ rotation when turned upside-down). In Picao-Osorio *et al.,* 2017, early first instar (L1) larvae (less than 30 minutes post-hatching) from 83 miRNA mutant lines representing over 95% of the miRNAs expressed in late *Drosophila* embryogenesis (Zhou *et al.,* 2018) were tested for delayed SR behaviour. Testing was carried out at this early stage of life to avoid any previous exposure to odour stimuli that may impact subsequent behaviour as well as the development of memory. Significant SR delays were found in 33 lines encoding 48 miRNAs, which are henceforth termed “SR-miRNAs”.

Considering the pervasive roles of miRNAs in normal SR, the question arose as to the generality of miRNA involvement in overall motor control. One hypothesis is that significantly delayed SR in miRNA mutants could be the result of pleiotropic effects to the motor system caused by miRNA mutation. To investigate this, the possibility of a relationship between crawling speed of SR-miRNA mutants and time to SR was explored in Picao-Osorio *et al.,* 2017 (Figure 2F in Picao-Osorio *et al.,* 2017) and the results of this correlation

analysis showed no relationship between the two behavioural variables. In addition to this, the possibility of a relationship between scores on a “touch response” test designed to assess anterior mechanosensory function and time to SR was also examined in SR-miRNA mutants with the results also showing no significant correlation (Figure 2E in Picao-Osorio *et al.,* 2017). The results of these analyses indicated that the effect of miRNA mutations on SR behaviour was specific, however, the lab’s perspective remained that although other larval behaviours may not be as sensitive to miRNA mutation as SR, they may still be regulated by miRNAs.

5.2.1.2 Selection of miRNA mutants for analysis in the locomotor screen

We, therefore, carried out a screen for general locomotor defects in the early L1 larvae of 84 miRNA mutant lines, covering 117 individual miRNAs (Figure 5.2.1). These 84 mutant lines are part of the same collection of miRNA mutant lines used in the aforementioned study of self-righting behaviour (Picao-Osorio *et al.,* 2017) and originally produced by the lab of Steve Cohen (A*STAR Institute, Singapore) (Chen *et al.,* 2014b).

Briefly, current estimates indicate that 258 miRNA genes (which, in turn, give rise to 469 mature miRNA sequences) are present in the *Drosophila* genome (Kozomara & Griffiths-Jones, 2014). However, 99.97% of miRNA expression is accounted for by only 152 miRNA genes (Chung *et al.,* 2008; Chen *et al.,* 2014b) (of which, 22 are not conserved outside of the *Drosophila* subgroup (Granzotto *et al.,* 2009)).

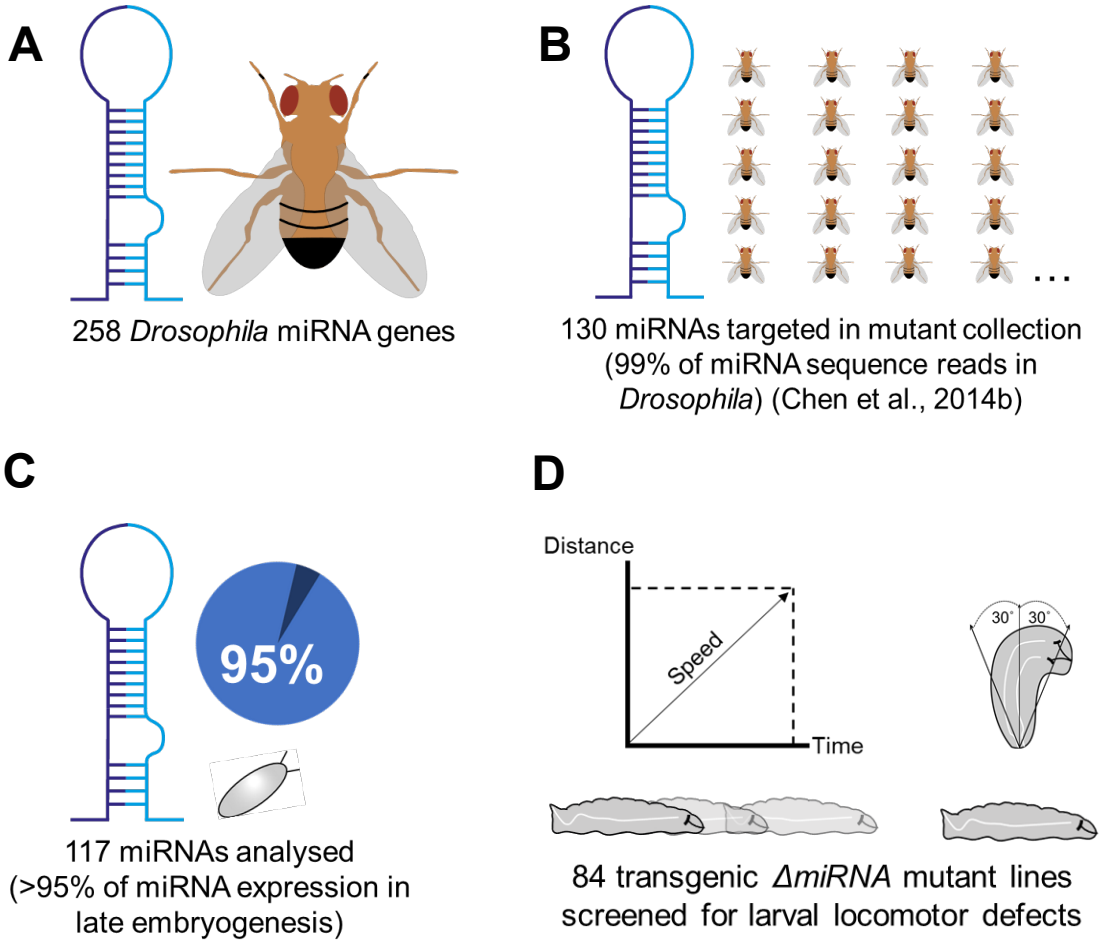

Figure 5.2.1 Design of the screen for locomotor defects in miRNA mutant larvae

(A) In the *Drosophila* genome, 258 miRNA genes encode 469 mature miRNA sequences. **(B)** The lab of Steve Cohen (A*STAR Institute, Singapore) produced a collection of 95 miRNA mutant (or '*ΔmiRNA'*) lines, deleting 130 conserved miRNAs that represent 99% of miRNA expression in *Drosophila* (Chen *et al.,* 2014b). **(C)** In our study, we screened 84 *ΔmiR* mutant lines for larval locomotor defects. These 84 lines cover 117 individual miRNAs that comprise over 95% of miRNA expression in the late *Drosophila* embryo (Zhou *et al.,* 2018).

Building on this, the Cohen lab produced a group of 95 transgenic miRNA mutant fly lines covering the remaining 130 miRNAs (Chen *et al.,* 2014b).

Of these 95 miRNA mutant lines, 6 mutants (*ΔmiR-1006, ΔmiR-1007, ΔmiR-1011, ΔmiR-1014, ΔmiR-12/284/304 and ΔmiR-7)* were found to affect the splicing of miRNA host genes (Chen *et al.,* 2014b) and so, were excluded from this study to avoid the identification of behavioural phenotypes caused by aberrant splicing as opposed to miRNA removal. We also excluded 5 miRNA mutants in which we found homozygous miRNA mutation to result in either survival issues during embryonic development (*ΔmiR-308, ΔmiR-9a and ΔmiR-963/964)* or, in which the effects of homozygous miRNA mutation on female survival/fertility prevented the obtaining of homozygous mutant larvae in sufficient numbers (*ΔmiR-279/996 and ΔmiR-994).* For clarity, *miR-303* was deleted in both the *ΔmiR-303* and *ΔmiR-982/303* mutants tested.

The 84 mutants screened in this study represent over 95% of total miRNA expression at the end of embryogenesis (based on reads from an miRNA sequencing experiment in *Drosophila* embryos 18 to 24h AEL (Zhou *et al.,* 2018).

5.2.1.3 Description of methodological approach used in the locomotor screen

We began by looking out for a high-throughput methodology that would allow us to extract information on multiple features of each larva's locomotion in parallel. After comparing different options (including JAABA (Kabra *et al.,* 2013) and wrMTrck (Brooks *et al.,* 2016)) we decided to implement the use of the

frustrated total internal reflection (FTIR) method, which produces high-resolution and high-contrast behavioural movies of *Drosophila* larvae. *Drosophila* larvae show an avoidance response to visible light, decelerating to a stop (if already crawling) and crawling in a different direction to escape the light source (Busto *et al.,* 1999; Gong *et al.,* 2019). FTIR relies upon the use of infrared light, which is invisible to *Drosophila* larvae, and therefore allows the examination of free crawling behaviour in the absence of any stimuli. In this study, we used the FTIR-based Imaging Method, (or "FIM") developed by Christian Klämbt and colleagues (University of Münster, Germany) (Risse *et al.,* 2013).

In brief, the FIM approach is based on the use of a "FIMTable", a 25x25cm acrylic glass plate resting on top of a 4-legged, table-like structure (Figure 5.2.2A). The acrylic glass plate is flooded with infrared light from bulbs surrounding its edges and distortions to the internal reflection of this light (caused by contact between an object and the surface of the acrylic glass plate) can be recognised by a camera with an infrared filter (Risse *et al.,* 2013) (Figure 5.2.2B). In our analysis, larvae are placed on a 1.5% agar plate on top of the FIMTable surface and allowed to freely crawl while images collected by a camera mounted below the FIMTable are then used to produce behavioural videos of larval crawling. These videos are then analysed with the FIMTable-associated software, FIMTrack (Risse *et al.,* 2017) (Figures 5.2.2C and 5.2.2D).

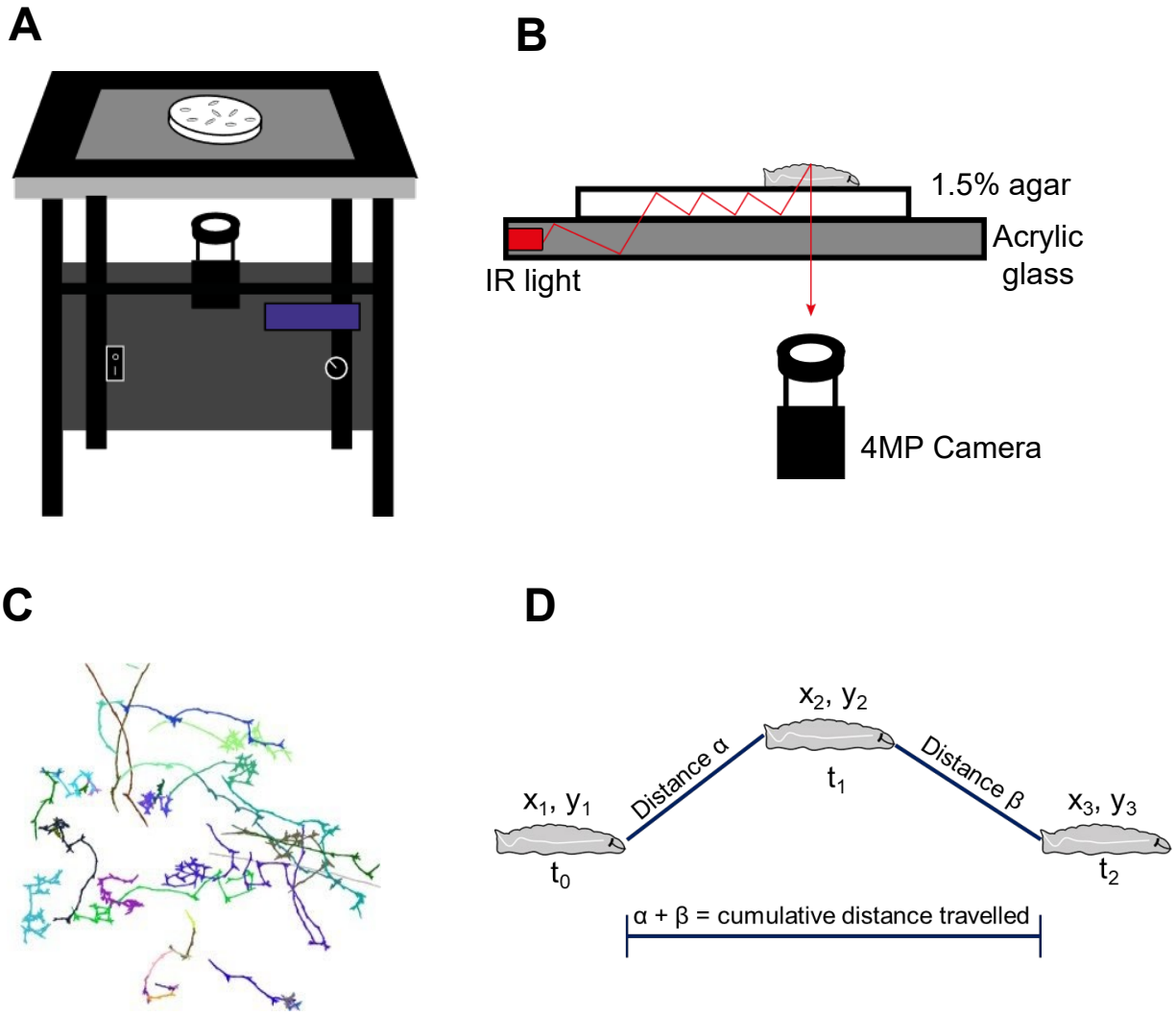

Figure 5.2.2 Using the FIMTable and associated software FIMTrack to analyse larval locomotion

(A) A schematic showing the FIMTable being used to record larval locomotion. Larvae are placed on a 1.5% agar plate and recorded crawling freely using a monochrome, 90fps 4MP Basler acA2040-90um camera mounted below. **(B)** Frustrated Total Internal Reflection (FTIR) of infrared (IR) light during recordings of larval locomotion. Differences in the refractive indices of an acrylic glass plate, an agar plate, and the larval body result in differences in the internal

reflection of IR light. These differences are recorded using a 4MP camera mounted below the FIMTable surface. **(C)** Example cumulative larval “tracks” produced by FIMTrack representing the total paths of larval movement over the course of a recording. **(D)** Average larval crawling speed is calculated by dividing the cumulative distance travelled by the larva over recording in μm, by the length of the recording in seconds.

5.2.2 Pervasive effects of miRNA regulation on larval crawling speed

Based on the importance of miRNA-based regulation to larval SR behaviour, we initially expected that a fraction of miRNAs would be essential for normal larval locomotion. Using the FIM approach, we calculated distance travelled by larvae over recording time as each larva's "average crawling speed", dividing cumulative distance travelled in μm by the length of the recording in seconds (Figure 5.2.2D).

Our results indicate that, of the 84 miRNA mutant lines analysed, 66 lines (representing 92 individual miRNAs and 79% of lines tested) crawl significantly more slowly than control larvae, and the remaining 12 lines show no significant difference (Figure 5.2.3). This suggests that the system is optimised for maximal speed, and absence of miRNAs can never lead to a significant increase in average crawling speed in L1 larvae, only a reduction.

Among these 66 significantly slower mutants, a range of average crawling speeds is exhibited. The majority of mutants exhibit a comparatively mild effect on average crawling speed; however, for the slowest 10 miRNA mutants, average crawling speed is reduced by 30μm/sec or more.

5.2.2.1 The relationship between miRNA-dependent larval speed control and self-righting

To explore the specificity of the miRNA-dependent effects on larval crawling speed, we examined the question of whether changes to self-righting behaviour in larvae were related to changes to crawling speed.

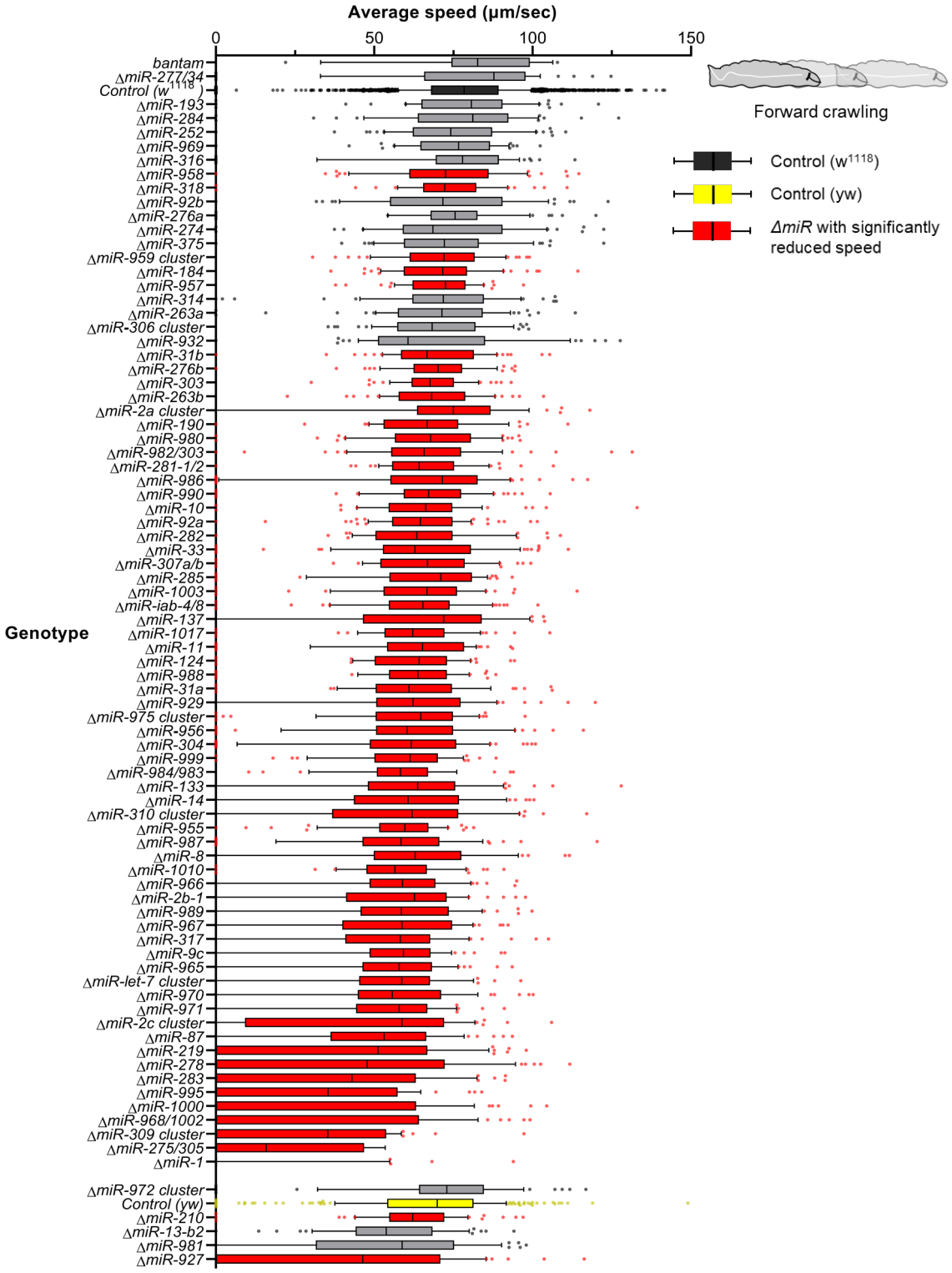

Figure 5.2.3 The widespread effect of miRNA regulation on crawling speed in first instar larvae

(Legend on the following page)

The results of our FIMTable analysis of 84 miRNA mutants show that miRNAs have a pervasive influence on larval locomotion. 66 miRNA mutant lines (red) tested at the first instar larval stage show a significant reduction in average crawling speed (Mann-Whitney U test with Bonferroni correction, $p \leq 0.0006$). 79 mutants were compared to w^{1118} larvae (black) as a control while the remaining 5 were compared to yw larvae (yellow) to correspond to their genetic background. Boxplots show the 25-75 percentile (box), median (line), 10-90 percentile (whiskers) and outliers (individual points). n = an average of 56 larvae per genotype.

Having now performed a large screen of miRNA mutant locomotion, we were in a position to perform a larger correlation analysis between the two behavioural variables than that performed in Picao-Osorio *et al.,* 2017. For this (and all correlation analyses moving forward), median values for each variable were used to minimise the impact of individual outliers from each genotype.

27 of the 33 SR-miRNA mutants identified in Picao-Osorio *et al.,* 2017 also crawl significantly more slowly in this study, however, the results of our correlation analysis (Figure 5.2.4) indicate that there is no statistically significant relationship between the effects of miRNA mutations on the two behaviours. This analysis further supports the notion that the effects of miRNA mutation on SR are not simply pleiotropic effects resulting from miRNA removal having an adverse effect on total motor system function but rather, that a complex network of context-dependent miRNA function is key for individual behaviours within the *Drosophila* larva.

5.2.3 Description of larval locomotion as a composite behaviour

The identification of such a pervasive role for miRNA-based regulation in control of larval crawling speed prompted us to consider how this may relate to the hierarchical organisation of exploratory behaviour in the L1 larva. Larval forward crawling is the behavioural output of peristaltic waves of muscle contraction passing along the larval body towards the head (Lahiri *et al.,* 2011). “Speed” as an aspect of larval locomotion however, describes the distance travelled by a larva over time and this travel is a combination of several, different, individual sub-behaviours.

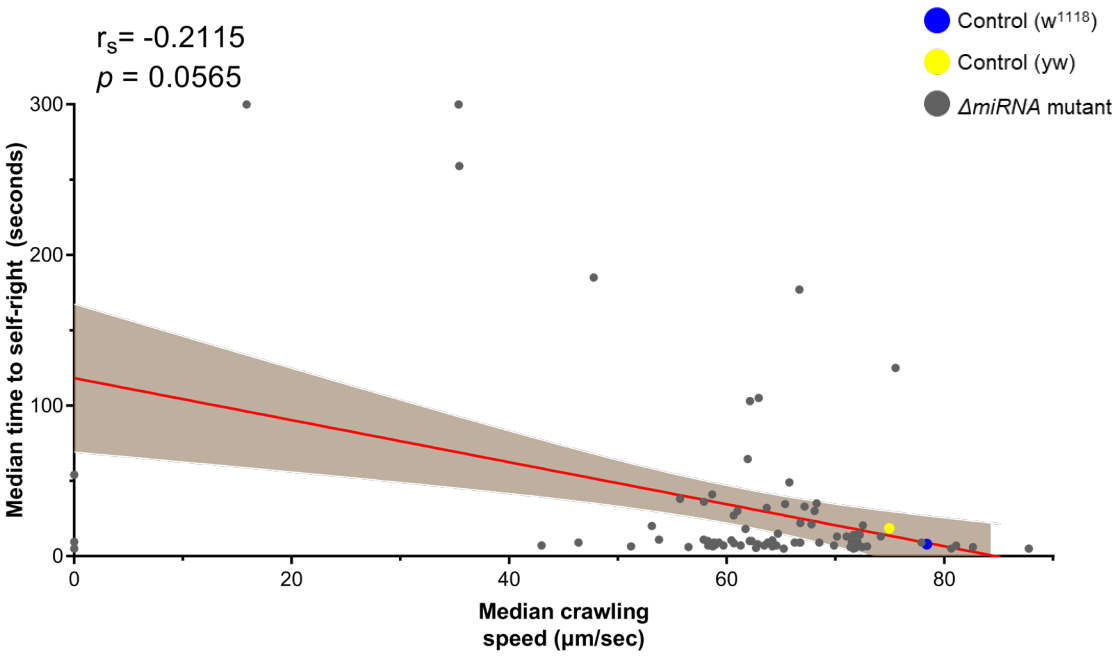

Figure 5.2.4 The crawling speed of miRNA mutant larvae is not significantly linked to time to self-right

No significant correlation is present between the crawling speed of miRNA mutant larvae and their time to self-right. On the x axis, the median crawling speed of miRNA mutant first instar larvae is plotted in µm/sec while on the y axis, their median time to self-right (Picao-Osorio *et al.,* 2017) is plotted. No significant correlation is observed between the two behavioural variables when statistically tested using the Spearman correlation test. The Spearman coefficient (r_s) and *p* value are shown while the 95% confidence interval for the linear regression (red line) is indicated by the red shaded area.

.

Specifically, larval locomotion is a combination of forward/backward “runs” (in which the larva travels in a straight line), pauses (in which the larva remains stationary) and turns (in which the larva, pauses, re-orients itself and begins another “run” (Berni *et al.,* 2012). The organisation of these behaviours can be visualised as a decision tree (Figure 5.2.5) that ultimately facilitates the coverage of a large area of substrate during the search for food.

Investigating the mechanistic basis of miRNA regulation of these behaviours is important to determine whether all aspects of locomotion are affected equally by miRNA removal or whether some aspects are particularly sensitive. We therefore sought to examine whether miRNA mutations also affect larval turning and pausing behaviour with a view to eventually analysing the importance of each component to overall locomotion.

To do this, we required a method to efficiently extract data on turning and pausing behaviours from the complex output files produced during analysis of behavioural videos in FIMTrack. We identified a custom Python 3 package developed by Philipp Schlegel and colleagues (University of Cambridge, UK) named PyFIM, which contains functions that allow the extraction of data on particular behavioural parameters from FIMTrack output files. In this study, we used PyFIM to analyse the frequencies of pauses longer than 0.75 seconds (5 frames) as well as their average duration. We chose 5 frames as a minimal pause threshold as anything lower resulted in short pauses between peristaltic waves being treated as significant by the software, skewing our results.

We also used PyFIM to analyse the frequencies of bends to the larval body greater than 30˚. Bending of the body greater than >30˚ was used as an

indicator for turning as, previous work (Almeida-Carvalho *et al.,* 2017) has demonstrated that a change in bearing to larval heading greater than 30˚ indicates a turn that can be separated from instances in which a larva is performing a “head-sweep” (Wystrach *et al.,* 2016, Gomez-Marin *et al.,* 2010).

Finally, we also analysed the cumulative time spent by larvae in a conformation bent greater than 30˚ by each larva as a measure of the “time spent turning” during recording. For this measurement, we designed a custom Microsoft Excel macro to analyse FIMTrack output files and produce the percentage of a recording that a larva’s body spent in this bent conformation.

5.2.4 Investigating turning behaviour in L1 miRNA mutant larvae

5.2.4.1 Specific miRNA mutations lead to significant changes in cumulative time spent turning by L1 larvae

Applying the aforementioned custom macro to FIMTrack output files, we find that, cumulative time spent turning by larvae is significantly affected by the removal of a number of miRNAs. Compared to control larvae, 23 of the 84 miRNA mutant lines tested spend a significantly changed time turning (Figure 5.2.6). Among these 23 mutants, the group is divided between 11 mutants showing a significant increase in cumulative time spent turning and 12 showing a significant decrease .

Comparing this to the effects of miRNA mutation on average crawling speed (Figure 5.2.3), the effect of miRNA mutation on the cumulative time spent turning by larvae is less pervasive, significantly affecting fewer miRNA mutant lines. In addition to this, the distribution of cumulative times spent turning by the

84 miRNA mutant lines is centred around the average value for control larvae suggesting that that unlike average crawling speed (which we suggest is optimised by the total complement of miRNAs), the amount of turning behaviour that occurs may be constantly positively and negatively regulated by miRNAs during locomotion.

Efficient substrate exploration by animals requires the energetic cost of exploring a large amount of substrate for food to be balanced with the probability of encountering food. In *C. elegans*, for example, this balance is facilitated by the adoption of a “biased random walk” strategy, with changes in direction increased as the concentration of appetitive odours decreases (Pierce-Shimomura *et al.,* 1999; Albrecht and Bargmann, 2011). More recently, it has been suggested that this biased random walk strategy is also combined with longer periods of straight travel to increase the efficiency of substrate exploration (Moy *et al.,* 2015). In the *Drosophila* larva, a specific balance between forward/backward “runs” is required and it has been hypothesised that larval locomotion can best be described as a Lévy Walk (Sims *et al.,* 2019), a random walk model in which search behaviour is optimised when the distribution of flight lengths (or in the case of the larva, run lengths) follows an inverse square power-law (Viswanathan *et al.,* 1999). The relevance of this to the results of our analysis is a potential role for miRNAs in the optimisation of the forward crawling-turning balance during locomotion.

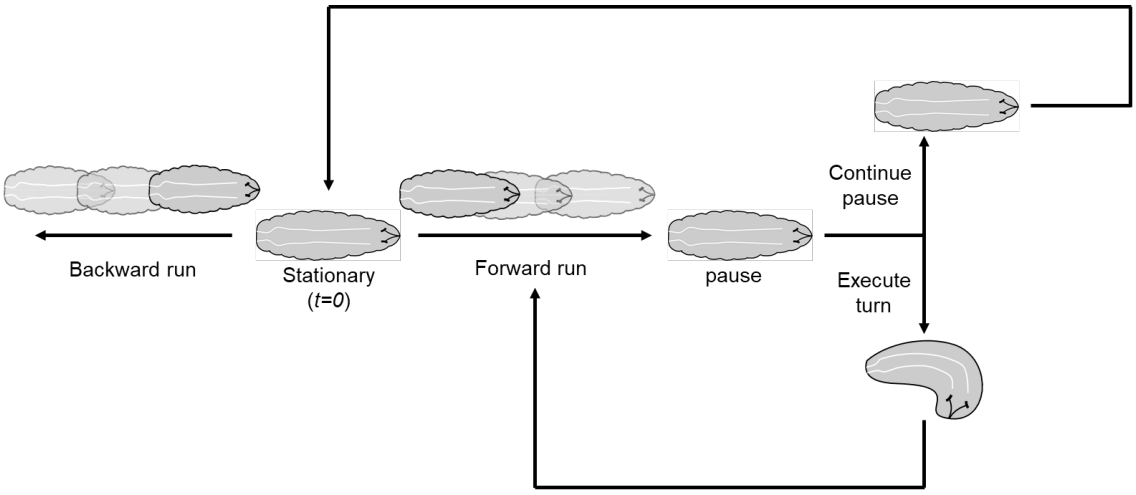

Figure 5.2.5 Larval locomotion consists of runs, pauses, and turns

A decision tree for larval locomotion. Larval locomotion consists of a series of forward/backward “runs” (in which the larva travels in a straight line), pauses and pause-turns (in which the larva bends and reorients itself). These behaviours are executed in a stereotyped order.

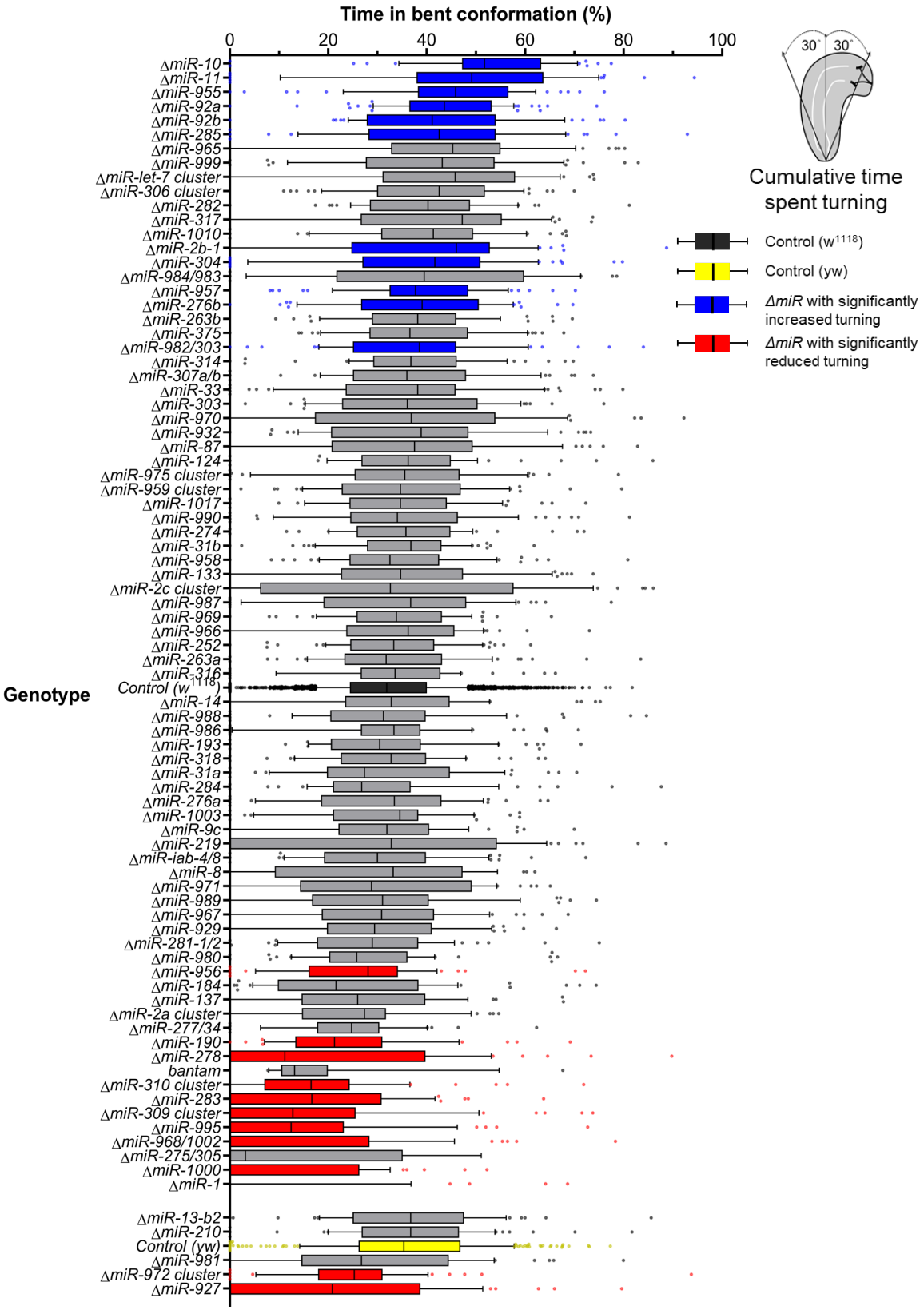

Figure 5.2.6 The effect of miRNA regulation on time spent turning by first instar larvae

(Legend on the following page)

The results of our FIMTable analysis show that specific miRNAs influence the time spent turning by first instar larvae. 23 miRNA mutant lines tested at the first instar larval stage show a significant change in the time spent turning during recording. 11 mutants (blue) show a significant increase in time spent turning and 12 mutants (red) show a significant reduction (Mann-Whitney U test with Bonferroni correction, $p \leq 0.0006$). 79 mutants were compared to w^{1118} larvae (black) as a control while the remaining 5 were compared to yw larvae (yellow) to correspond to their genetic background. Boxplots show the 25-75 percentile (box), median (line), 10-90 percentile (whiskers) and outliers (individual points). n = an average of 56 larvae per genotype.

5.2.4.2 Changes to cumulative time spent turning are not significantly correlated with changes to crawling speed in L1 miRNA mutant larvae

Further examining whether the optimisation of the forward crawling-turning relationship by miRNAs during locomotion underpins their regulation of crawling speed, we sought to analyse whether the previously observed changes to crawling speed in miRNA mutant larvae were directly related to changes in cumulative time spent turning. To address this, we performed a correlation analysis between the two variables expecting to see a significant correlation based on the aforementioned description of the relationship between turning and crawling runs as a key aspect of efficient larval locomotion. Unexpectedly, however, we observe no significant correlation (Figure 5.2.7) suggesting that although miRNA mutations may affect the ability of the larva to regulate the amount of turning produced during locomotion, this does not contribute significantly to our observed reductions in average crawling speed (Figure 5.2.3).

5.2.4.3 Specific miRNA mutations lead to significant changes in the turning frequency of L1 larvae

We also considered whether by using the cumulative time spent bent >30˚ (as discussed in Section 5.2.3) as a measure for turning, we were overlooking more subtle temporal dynamics in the forward crawling-turning relationship during larval locomotion. For example, if one larva performs many turns, constantly changing direction, and another simply bends its body but does not actually move for most of the recording, the two could be treated as turning the same amount, leading to an overestimation of the time spent turning.

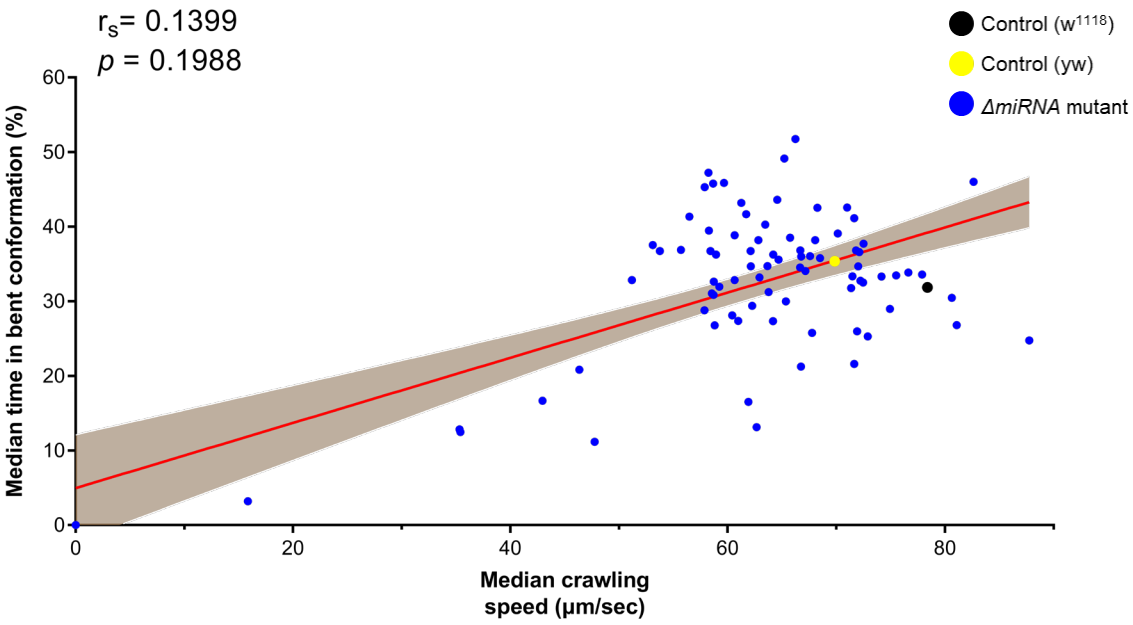

Figure 5.2.7 The crawling speed of miRNA mutant larvae is not significantly linked to the time spent turning

No significant correlation is present between the crawling speed of miRNA mutant larvae and the time spent turning during recording. On the x axis, the median crawling speed of miRNA mutant first instar larvae is plotted in µm/sec while on the y axis, the median time spent by miRNA mutant larvae bent >30˚ is plotted as a percentage of recording time. No significant correlation is observed between the two behavioural variables using the Spearman correlation test. The Spearman coefficient (r_s) and *p* value are shown while the 95% confidence interval for the linear regression (red) is indicated by the red shaded area.

To tease apart these distinct scenarios, we analysed the frequency of turning and find that of the 84 mutant lines tested, 19 turn at significantly different frequencies to control larvae with 13 mutants showing a significant increase and 6 mutants showing a significant decrease (Figure 5.2.8). The turning frequencies we observe among miRNA mutants differs by nearly three-fold from lowest to highest (4.8 – 13.7 turns per minute). This was expected, as based on the wide range of average crawling speeds observed (Figure 5.2.3) , we expected to also observe miRNA mutants with both mildly and severely changed turning. These results indicate that, in the wild-type larva, the normal expression of several miRNAs is essential for normal turning patterns at the L1 stage.

Similar to cumulative time spent turning (Figure 5.2.6), the distribution of results for turning frequency are also centred around the average value for control larvae however the distribution of significant effects differed. Although a near equal number of miRNA mutants show significant increases and decreases to cumulative time spent turning, the majority of significant changes to turning frequency are increases.

5.2.4.4 A significant correlation is observed between cumulative time spent turning and turning frequency in L1 miRNA mutant larvae

Given the fact that in both turning variables, we observe similar distributions of effects in miRNA mutants around the values for control larvae (as well as reductions in the pervasiveness of effects compared to average crawling speed), we sought to analyse whether a significant relationship exists between

cumulative time spent turning and turning frequency. Our aim was to understand whether the two turning variables are interdependent and the results of this analysis (Figure 5.2.9A) demonstrate a significant relationship. Along with demonstrating interdependency, this result also suggests that our measurement of cumulative time spent in a bent confirmation is a reliable proxy for turning behaviour as this positively increases with the number of turns identified during recording time.

5.2.4.5 Changes to turning frequency are not significantly correlated with the crawling speed of L1 miRNA mutant larvae

Having established that time spent turning and turning frequency are significantly correlated in L1 miRNA mutant larvae, we sought to validate this finding by analysing the relationship between changes to turning frequency and changes to crawling speed in mutant larvae.

As cumulative time spent turning and turning frequency are linked (Figure 5.2.9A) and cumulative time spent turning is not significantly correlated with crawling speed (Figure 5.2.7), we also expected to see no significant correlation between turning frequency and crawling speed. The results of the analysis (Figure 5.2.9B) met this expectation with no significant relationship demonstrated.

Overall, our analyses of turning behaviour in miRNA mutant larvae reveal that, although miRNAs play a role in regulating the choice to turn or not during locomotion, this is at a much more limited scale than the role played in establishing an optimal crawling speed.

Our analyses also reveal that neither time spent turning, nor turning frequency, are aspects of locomotion that (when changed through miRNA removal) account for the removal of miRNAs affecting average larval crawling speed in such a pervasive manner. We suggest that, although there must be a tightly regulated balance between forward crawling and turning for substrate exploration to be at its most efficient (Berni, 2015), changes to turning (imposed by miRNA mutation) do not directly impact crawling speed in a linked fashion.

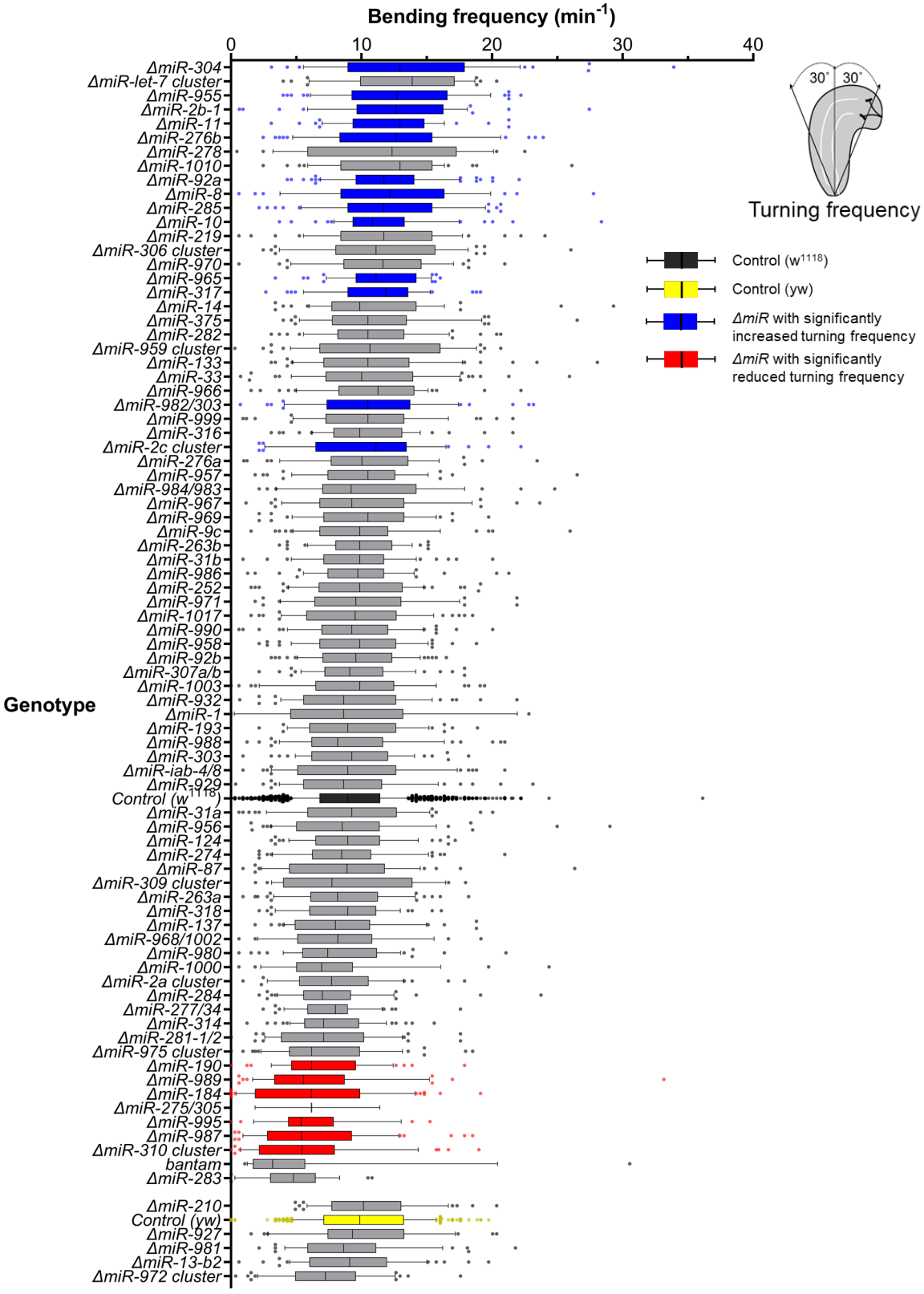

Figure 5.2.8 The effect of miRNA regulation on the frequency of turning in first instar larvae

(Legend on the following page)

The results of our FIMTable analysis show that specific miRNAs influence the frequency of turning by first instar larvae. 19 miRNA mutant lines tested at the first instar larval stage show a significant change in turning frequency during recording. 13 mutants (blue) show a significant increase in turning frequency and 6 mutants (red) show a significant reduction (Mann-Whitney U test with Bonferroni correction, $p \leq 0.0006$). 79 mutants were compared to w^{1118} larvae (black) as a control while the remaining 5 were compared to yw larvae (yellow) to correspond to their genetic background. Boxplots show the 25-75 percentile (box), median (line), 10-90 percentile (whiskers) and outliers (individual points). n = an average of 56 larvae per genotype.

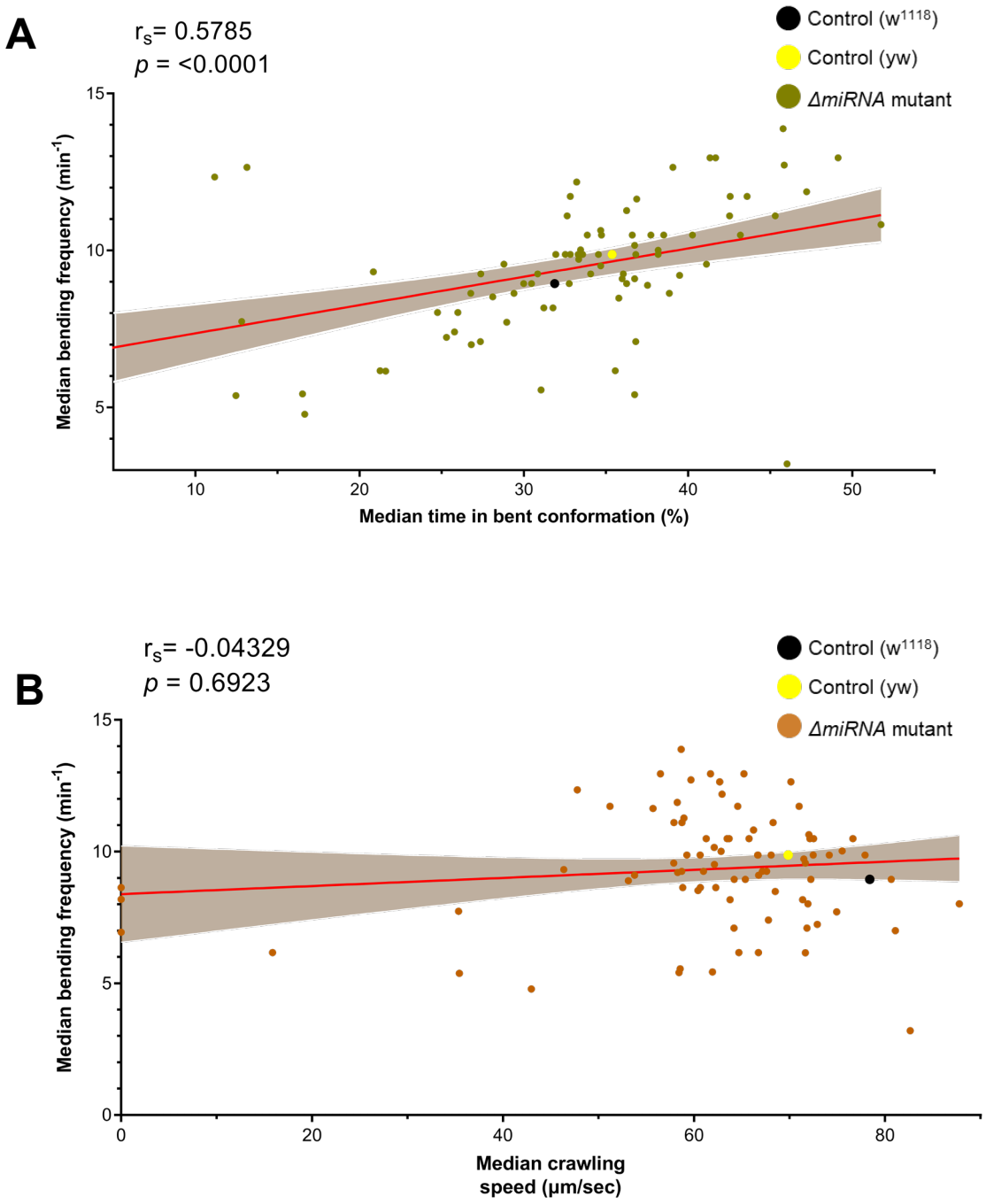

Figure 5.2.9 The frequency of turning in miRNA mutant larvae is significantly linked to the time spent turning but not to crawling speed

Our statistical analysis shows that the frequency of turning is significantly correlated with time spent turning but not crawling speed. (A and B) In both graphs, the median frequency of turning events per minute by miRNA mutant larvae is plotted on the y axis. These values are then compared to the

median time spent turning **(A)** or median crawling speed **(B)** of mutants. Using the Spearman correlation test, a significant correlation is observed between median turning frequency and median time spent turning ($p \leq 0.0001$) but not between median turning frequency and median crawling speed. The Spearman coefficients (r_s) and *p* values are shown and the 95% confidence intervals for the linear regressions (red) are indicated by the red shaded areas.

5.2.5 Investigating pausing behaviour in L1 miRNA mutant larvae

5.2.5.1 Specific miRNA mutations lead to significant changes in the frequency of pausing by L1 larvae

To analyse the effects of miRNA mutation on pausing behaviour in L1 larvae, we used the custom Python 3 package PyFIM. We firstly studied how the frequency of pauses longer than 0.75 seconds (5 frames) was affected by the removal of miRNA expression and found that 29 out of 84 mutant lines pause at a significantly different frequency during locomotion to control larvae (Figure 5.2.10). 10 mutants pause significantly more frequently while 19 mutants pause significantly less frequently and, similar to effects on turning behaviour, the distribution of effects is centred around the average control value suggesting that, in addition to regulating turning, miRNAs also regulate the balance between increased and decreased pausing during locomotion.

Also, similar to changes to turning frequency (Figure 5.2.8), the range of pausing frequencies observed among the miRNA mutants differs by three-fold from lowest to highest (3.41 –10.25 pauses per minute). We suggest that the variability of turning and pausing frequencies that we observe in miRNA mutants indicates that the contribution of miRNA regulation to these behaviours exists on a spectrum. In other words, we propose that a network of miRNAs continuously fine-tunes gene expression to ensure that pausing/turning does not occur too little or too much during locomotion, and that the effects of removing these miRNAs can be subtle as well as severe.

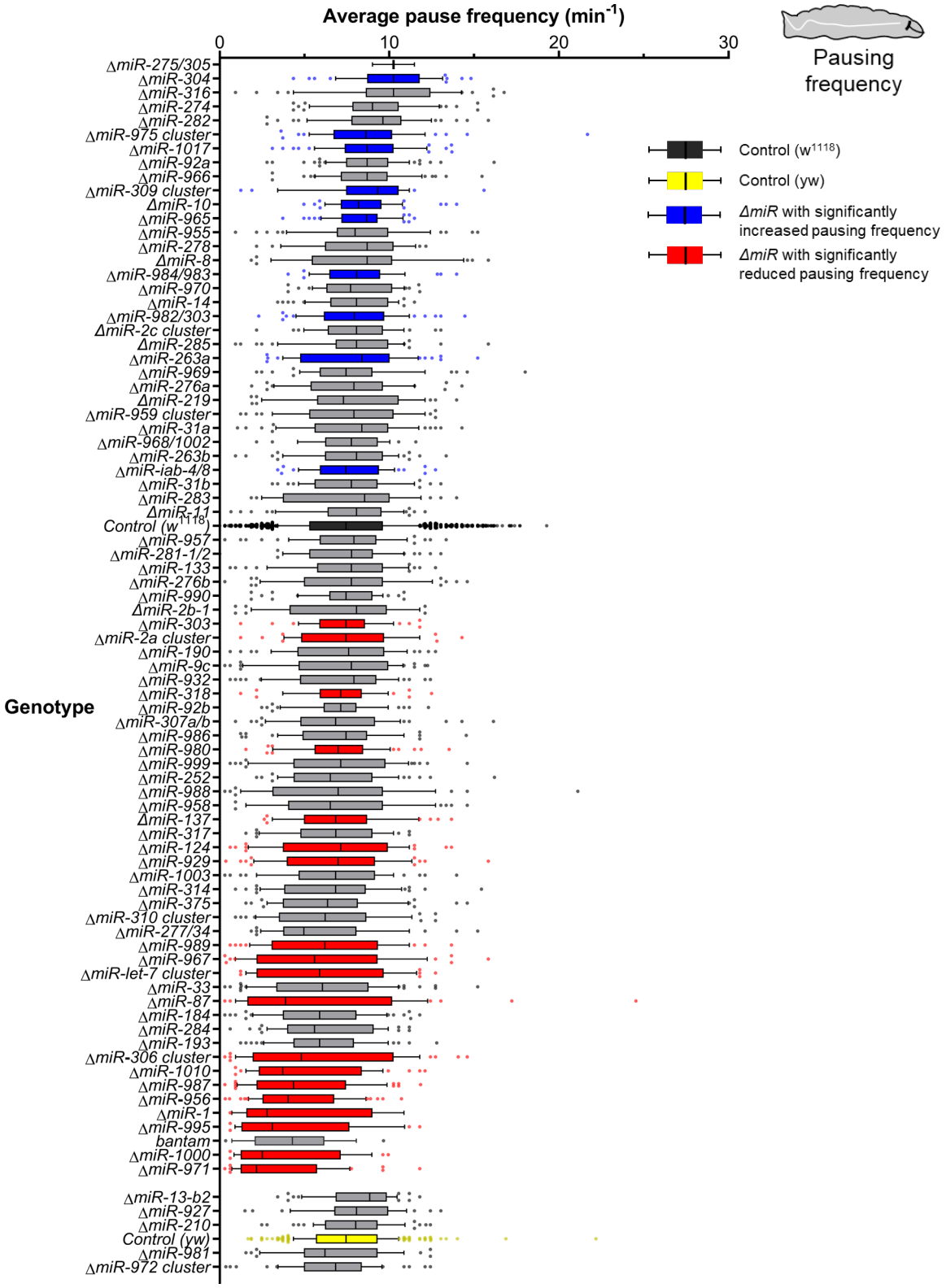

Figure 5.2.10 The effect of miRNA regulation on the frequency of pausing in first instar larvae

(Legend on the following page)

The results of our FIMTable analysis show that specific miRNAs influence the frequency of pausing by first instar larvae. 29 miRNA mutant lines tested at the first instar larval stage show a significant change to the frequency of pauses longer than 0.75 seconds during recording. 10 mutants (blue) show a significant increase in time spent turning and 19 mutants (red) show a significant reduction (Mann-Whitney U test with Bonferroni correction, $p \leq 0.0006$). 79 mutants were compared to w^{1118} larvae (black) as a control while the remaining 5 were compared to yw larvae (yellow) to correspond to their genetic background. Boxplots show the 25-75 percentile (box), median (line), 10-90 percentile (whiskers) and outliers (individual points). n = an average of 56 larvae per genotype.

5.2.5.2 Changes to pause frequency are not significantly correlated with changes to crawling speed in L1 miRNA mutant larvae

In our aim to establish the behavioural variable with the most impact on average larval crawling speed, we also performed a correlation analysis between the frequency of pausing behaviour in miRNA mutants and their crawling speed (Figure 5.2.11). We observe no significant correlation between pause frequency and crawling speed suggesting that pause frequency, although affected in 35% of miRNA mutant lines tested, is not a highly significant factor in the previously observed reductions in crawling speed (Figure 5.2.3).

5.2.5.3 The average pause duration of L1 larvae is strongly affected by miRNA mutation

Finally, we used PyFIM to analyse changes to the average pause duration of miRNA mutant larvae during recording. Compared to significant changes to cumulative time spent turning (seen in 27% of lines), turning frequency (seen in 23% of lines) and pause frequency (seen in 35% of lines), we observe an increased proportion of miRNA mutants with significantly increased average pause duration. 46 mutants pause for significantly longer on average, while 6 mutants pause for significantly shorter amounts of time leading to a final proportion of 62% of miRNA mutant lines with significantly changed average pause duration (Figure 5.2.12).

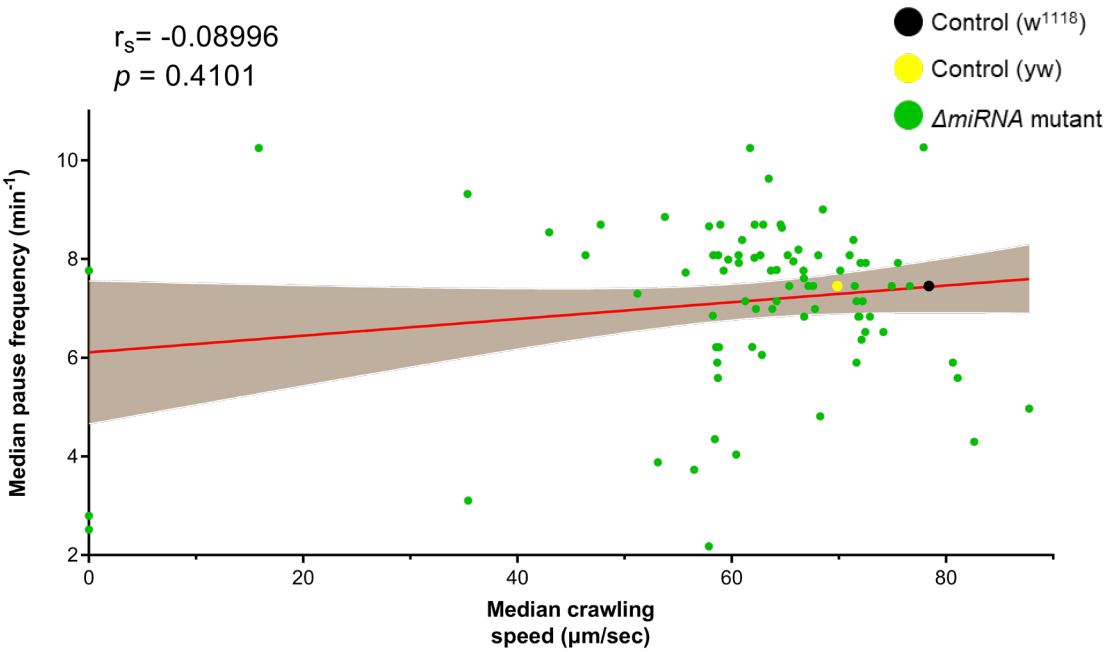

Figure 5.2.11 The crawling speed of miRNA mutant larvae is not significantly linked to the frequency of pausing

No significant correlation is present between the crawling speed of miRNA mutant larvae and the frequency of pauses during crawling. On the x axis, the median crawling speed of miRNA mutant first instar larvae is plotted in µm/sec while on the y axis, the median frequency of pauses per minute by miRNA mutant larvae is plotted. No significant correlation is observed between the two behavioural variables using the Spearman correlation test. The Spearman coefficient (r_s) and *p* value are shown while the 95% confidence interval for the linear regression (red) is indicated by the red shaded area.

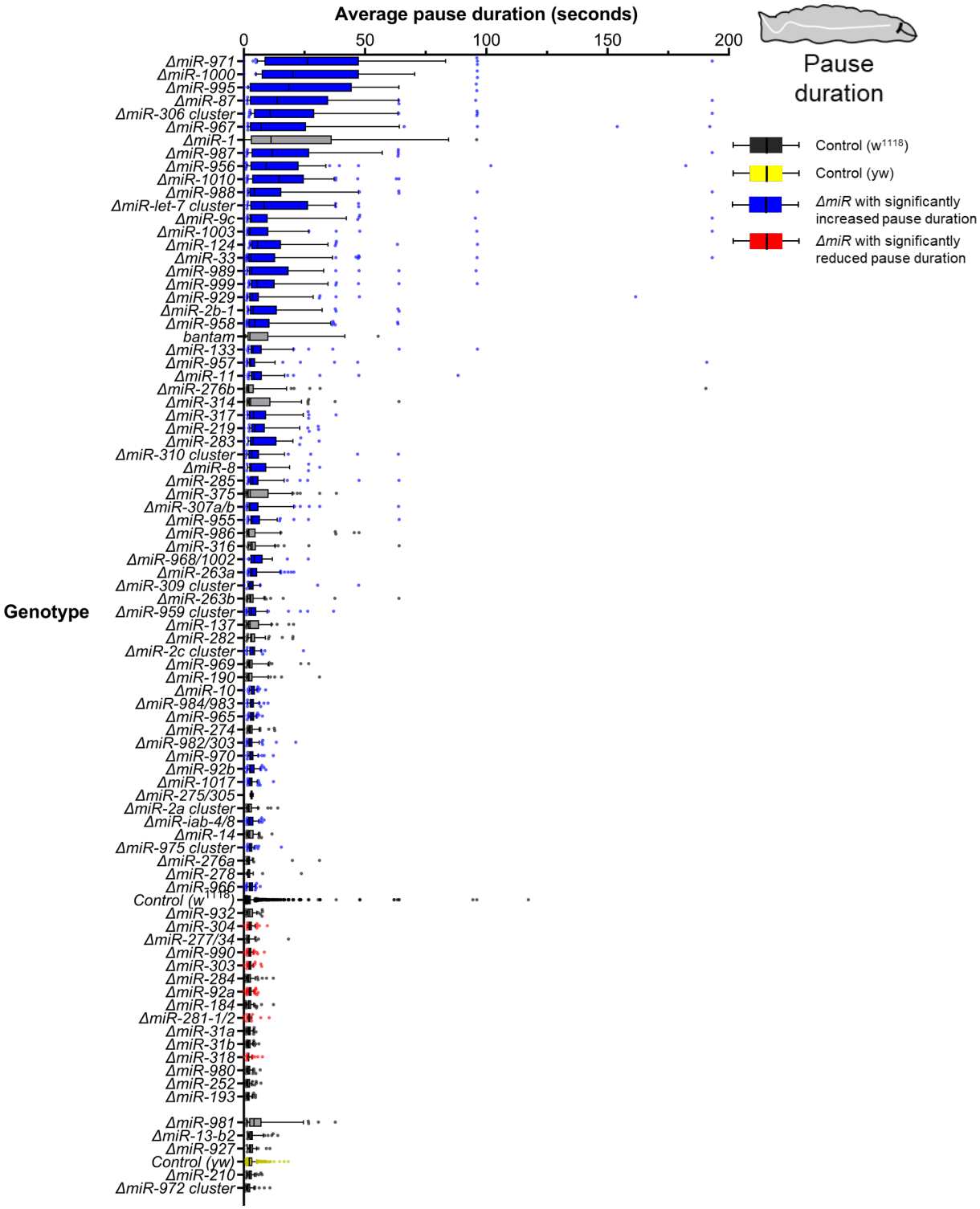

Figure 5.2.12 The effect of miRNA regulation on the duration of pauses in first instar larvae

(Legend on the following page)

The results of our FIMTable analysis show that specific miRNAs influence the average duration of pauses by first instar larvae. 52 miRNA mutant lines tested at the first instar larval stage show a significant change to the average duration of pauses while recording. 46 mutants (blue) show a significant increase in time spent turning and 6 mutants (red) show a significant reduction (Mann-Whitney U test with Bonferroni correction, $p \leq 0.0006$). 79 mutants were compared to w^{1118} larvae (black) as a control while the remaining 5 were compared to yw larvae (yellow) to correspond to their genetic background. Boxplots show the 25-75 percentile (box), median (line), 10-90 percentile (whiskers) and outliers (individual points). n = an average of 56 larvae per genotype.

While the effects of miRNA mutation on time spent turning (Figure 5.2.6), turning frequency (Figure 5.2.8) and pause frequency (Figure 5.2.10) are more centred around the average control value, the effects of miRNA mutations on average pause duration (Figure 5.2.12) are mostly significant increases (seen in 46/52 lines) leading us to consider whether a potentially reciprocal relationship between this and crawling speed existed.

5.2.5.4 Discovery of a link between impact on pause duration and crawling speed of L1 miRNA mutant larvae

To confirm this hypothesis, we carried out a correlation analysis between the crawling speed of miRNA mutant larvae and their pause duration and found a significant inverse correlation between the two behavioural variables (Figure 5.2.13).

The fact that an inverse correlation is observed between pause duration and crawling speed and yet, no significant correlation is observed between pause frequency and crawling speed raises the question of whether there is any relationship between pause frequency and pause duration.

5.2.5.5 Discovery of a link between pausing frequency and pause duration in L1 miRNA mutant larvae

We would expect that even if one pausing variable was more influential on crawling speed, there would still be an inverse relationship between the pause duration of larvae and the frequency of these pauses.

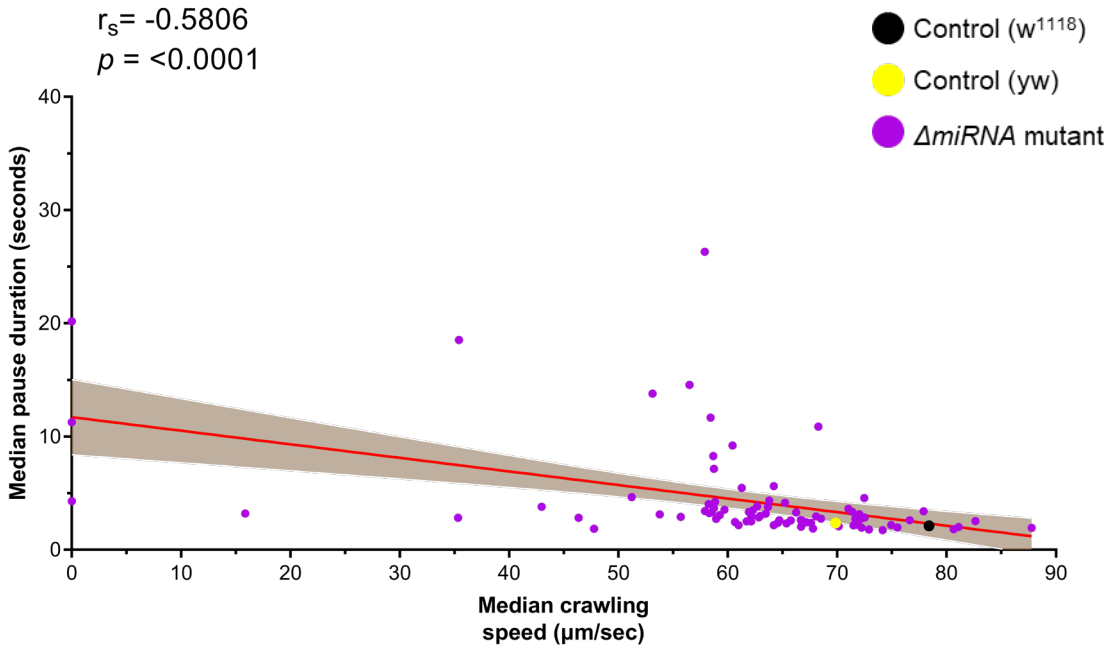

Figure 5.2.13. Changes to the crawling speed of miRNA mutant larvae are significantly linked to changes in pause duration

Our statistical analysis shows that the crawling speed of miRNA mutant larvae and the duration of pauses longer than 0.75 seconds are significantly negatively correlated. On the x axis, the median crawling speed of miRNA mutant first instar larvae is plotted in µm/sec while on the y axis, the median duration of pauses by miRNA mutant larvae is plotted in seconds. A significant correlation is observed between the two behavioural variables using the Spearman correlation test (p = <0.0001). The Spearman coefficient (r_s) is shown while the 95% confidence interval for the linear regression (red) is indicated by the red shaded area.

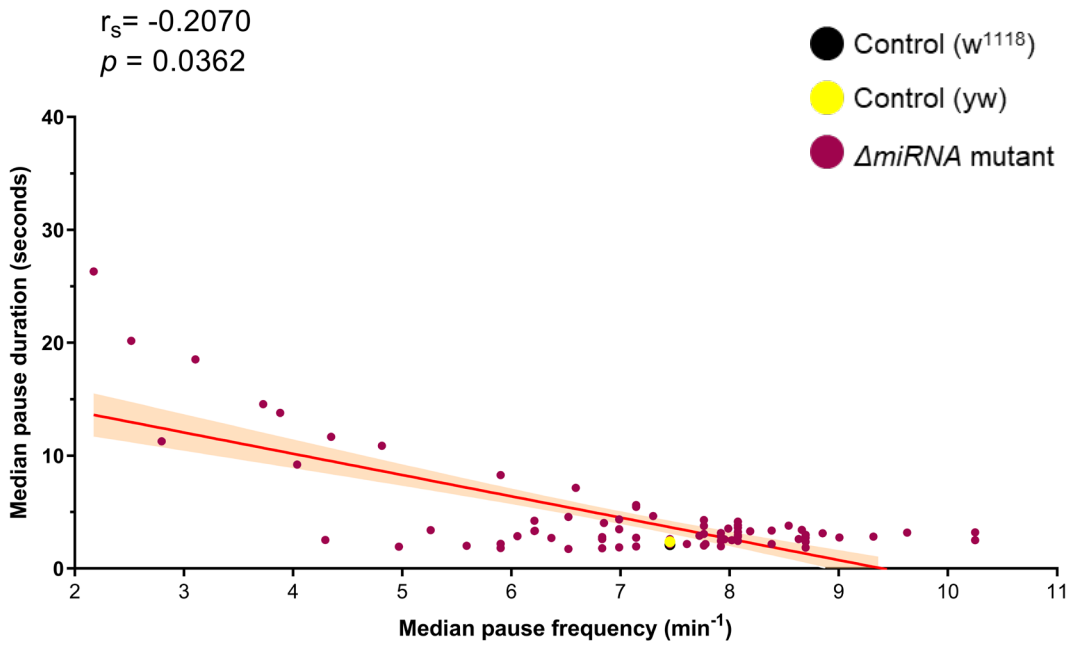

Figure 5.2.14 Changes to pause duration in miRNA mutant larvae are significantly linked to changes in pause frequency

Our statistical analysis shows that the duration of pauses by miRNA mutant larvae and the frequency of these pauses are significantly correlated. On the x axis, the median frequency of pauses per minute by miRNA mutant first instar larvae is plotted while on the y axis, the median duration of pauses by miRNA mutant larvae is plotted in seconds. A significant correlation is observed between the two behavioural variables using the Spearman correlation test (p = 0.0362). The Spearman coefficient (r_s) is shown while the 95% confidence interval for the linear regression (red) is indicated by the red shaded area.

We therefore performed a correlation analysis between these two variables and observe a significant inverse correlation between them (Figure 5.2.14). This suggests that the expected interdependency is present, pausing data extracted from FIMTrack was reliable and pausing duration could indeed be confirmed as a highly influential factor on crawling speed as distance travelled over time.

5.2.6 Principal component analysis of locomotor variables

5.2.6.1 Construction of a multidimensional dataset from analysis of locomotor variables of miRNA mutant larvae

Our results show that miRNAs are essential for various aspects of larval locomotion (Figure 5.2.15). Building on this conclusion, we sought to investigate whether any of the behavioural variables analysed had a disproportionate influence on locomotion as whole. Should this be the case, any further mechanistic study of miRNAs' roles in larval locomotion could then be more precise - focusing on the role of miRNAs in this variable.

The previously-generated data on average crawling speed, cumulative time spent turning, average turning frequency, average pause frequency and average pause duration was combined into a multidimensional dataset. Our initial expectation was that changes to average pause duration would explain much of the overall variance in the multidimensional dataset.

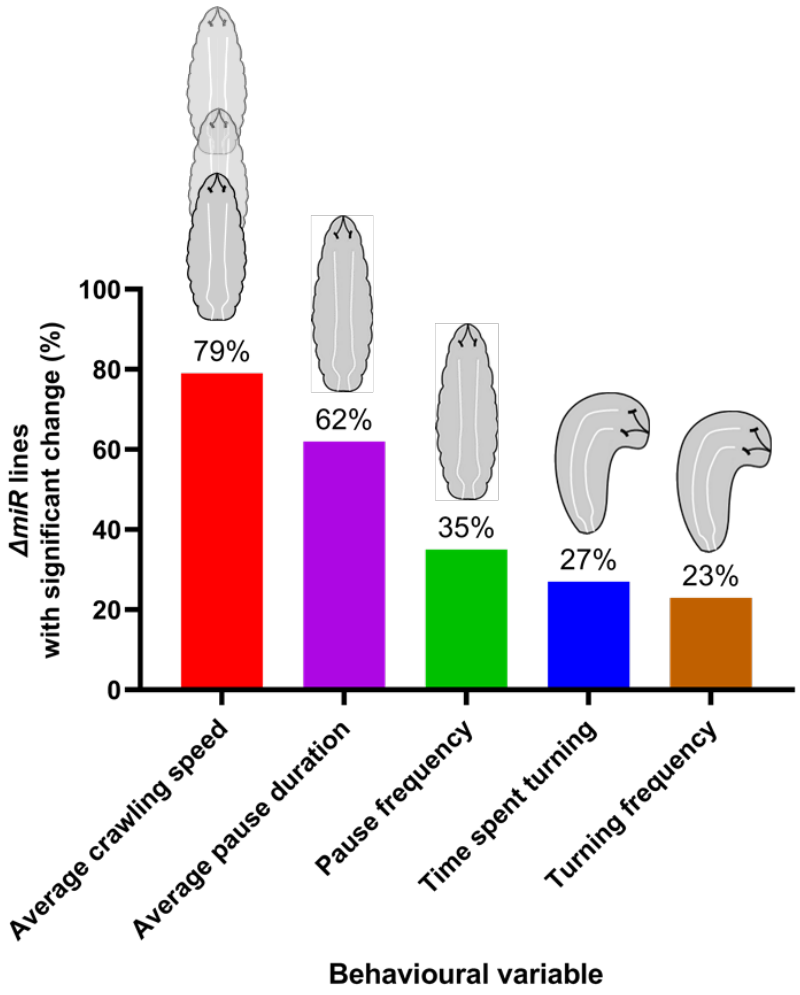

Figure 5.2.15 The overall results of the screen for locomotor defects in miRNA mutant first instar larvae

Removal of miRNA expression had significant effects on the five behavioural variables tested in first instar larvae. Compared to control larvae, 79% of mutant lines showed a significant reduction in average crawling speed. Pausing behaviour was the next most significantly affected variable with 62% and 35% of lines showing significantly changed average pause duration and average pause frequency, respectively. The cumulative time spent turning by larvae was significantly changed in 27% of miRNA mutant lines while the frequency of these turns was significantly changed in 23% of lines.

Pause duration was the only behavioural variable significantly correlated with crawling speed as well as the behavioural variable in which the most miRNA mutants showed significant differences to control larvae (excluding average crawling speed).

5.2.6.2 Changes to pausing behaviour correlate with principal components representing most of the variance in the multidimensional dataset

We tested this hypothesis by performing a principal component analysis (or PCA) on our multidimensional data set. Principal component analysis aims to reduce the dimensionality of multidimensional datasets, improving their interpretability and potentially revealing individual variables which account for disproportionate amounts of the total variance.

PCA decomposed our multidimensional dataset into five principal components, with the first three principal components explaining 92.8% of the variance in the multidimensional dataset (Figure 5.2.16A).

When the first two principal components (explaining 73% of the variance in the dataset) are plotted on a biplot (Figure 5.2.16B), the eigenvectors representing average pause duration and pause frequency show mild, positive correlations with PC1 and PC2, respectively. In other words, a positive relationship between pausing behaviour as a whole and the two principal components representing the largest amounts of variance in the dataset is identified. All other eigenvectors (representing the three remaining behavioural variables – cumulative time spent turning, turning frequency and average crawling speed; not shown) show mild, negative correlations with both PC1 and PC2.

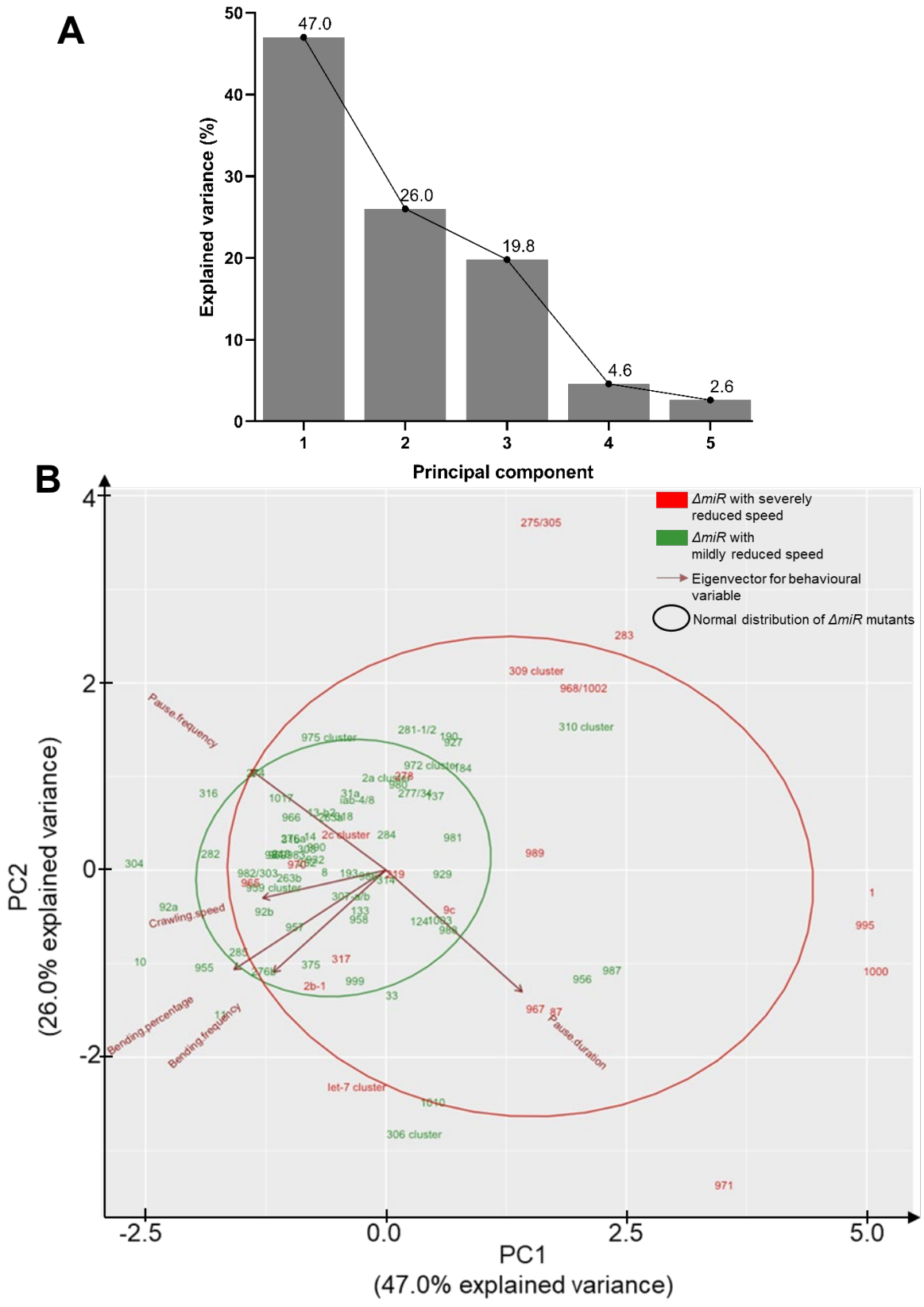

Figure 5.2.16 PCA of behavioural variables in miRNA mutant larvae reveals a strong influence of pausing behaviour on overall variance

(Legend on the following page)

(A) Eigenvalues for each of the five principal components derived from larval locomotion data. Principal components (PCs) 1-3 capture 93% of the total variance across the dataset. **(B) A biplot representation of the PCA performed on the locomotor dataset.** The eigenvectors (brown arrows) for the variables “pause duration” and “pause frequency” show strong, positive correlations with PCs 1 and 2 respectively (explaining a total of 73% of variance in the dataset). The eigenvector for the “crawling speed” variable shows a strong, positive correlation with PC3 (not shown) which explains 19.8% of variance within the dataset. Ellipses represent normal distribution of mutants with “mild” (green) and “severe” (red) defects to average crawling speed.

The eigenvector representing average crawling speed however, is the only eigenvector strongly and positively correlated with PC3 (not shown, representing 19.8% of variance in the dataset) suggesting that, although not as influential as pausing behaviours, differences in average distance travelled over time still contribute substantially to overall variance.

The normal distributions of miRNA mutants with severely reduced average crawling speed (Figure 5.2.16B, red) and those with more mildly affected average crawling speed (Figure 5.2.16B, green) overlap substantially along the first two principal components. This suggests that variables positively correlated with PC1 do not influence the variance observed in the “severe” group to a substantially different degree than they influence the variance observed in the “mild” group.

5.2.6.3 miRNA mutants cannot be separated into discrete clusters based on similar behavioural phenotypes

Considering most (92.8%) of the overall variance in the multidimensional dataset for locomotion is positively correlated with just three eigenvectors (average pause duration, pause frequency and average crawling speed), we then asked whether the genotypes screened could be divided into discrete groups that may share common behavioural features.

To do this, we applied a k-means clustering algorithm to the multidimensional dataset (selecting 3 as the optimal number of clusters based on the “Elbow method” (Thorndike, 1953)) (Figure 5.2.17). We also tested 10 initial centres for stability in all analyses to ensure that the most optimal centres were used to

partition the mutants into clusters. We observe that 59 miRNA mutants fall into cluster 1, 16 fall into cluster 2 and the remaining 8 fall into cluster 3. These clusters all overlap with one another, suggesting that (at least along 2 dimensions), the collection of miRNA mutants screened could not be separated into distinct clusters with similar behavioural features.

5.2.7 Summary of the locomotor screen in L1 miRNA mutant larvae

At the L1 developmental stage, we observed a significant impact of miRNA mutation on average crawling speed. 79% of lines tested crawled significantly more slowly than control larvae (Figure 5.2.3). This led us to propose a model in which miRNAs act to optimise average distance crawled over time. We have also attempted to decompose “speed” by examining sub-behaviours of general locomotion, namely turning and pausing (Figure 5.2.15).

We performed multiple correlation analyses, comparing crawling speed with cumulative time spent turning, turning frequency, pause duration and pause frequency in an attempt to identify behavioural variables with the most significant relationship with overall speed. We found that, of these, only pause duration is significantly correlated with crawling speed (Figure 5.2.13) (with further testing demonstrating its importance for total variance in a multidimensional locomotor dataset (Figure 5.2.16)).

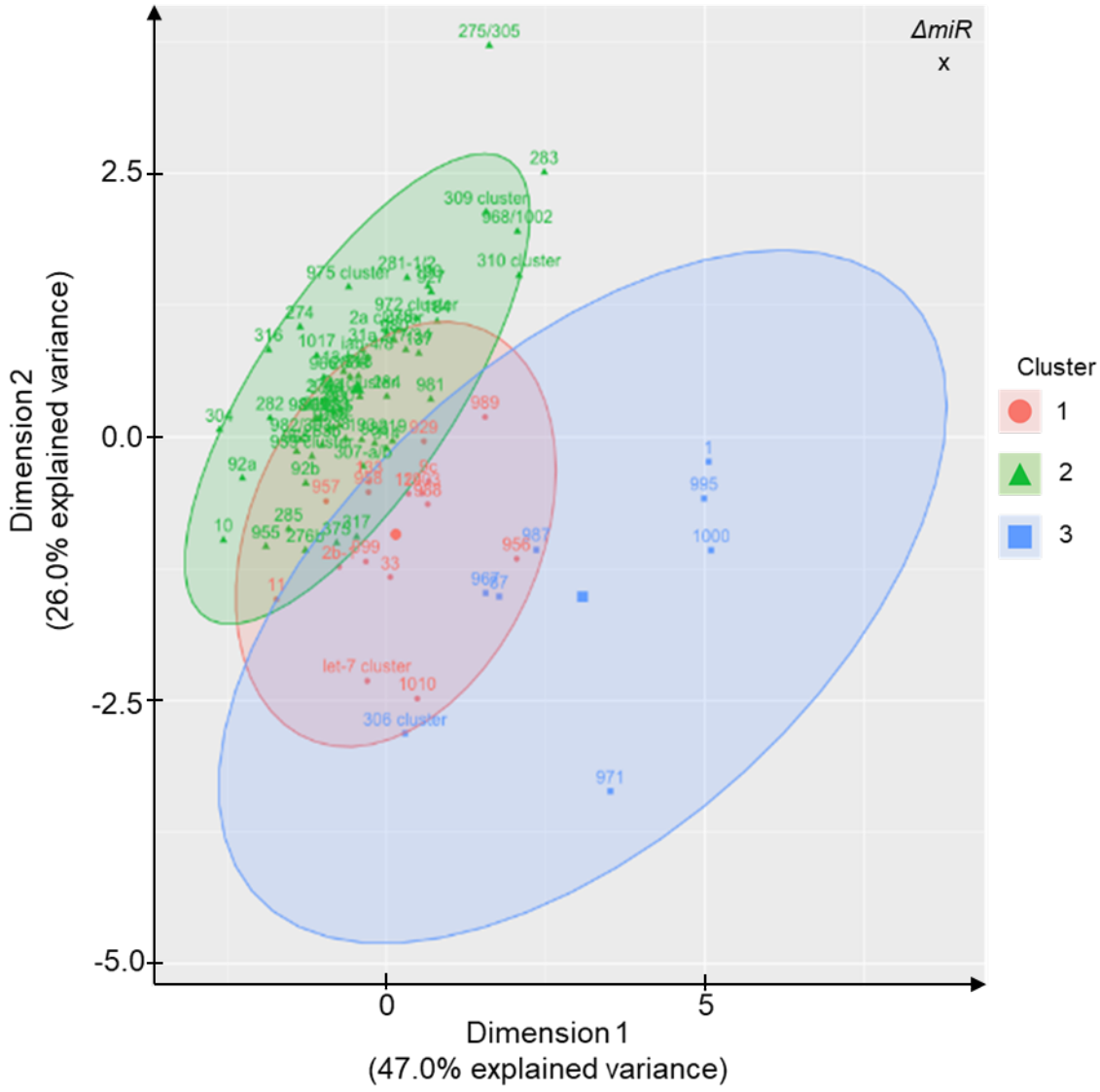

Figure 5.2.17 miRNA mutants cannot be separated into discrete clusters based on similar behavioural phenotypes

A k-means clustering analysis (3 centres) of miRNA mutants produces three overlapping clusters along dimensions corresponding to the first two principal components. 16 miRNA mutants fall into cluster 1 (red), 60 fall into cluster 2 (green) and the remaining 8 fall into cluster 3 (blue).

5.2.8 A pilot study of the effects of miRNA mutations on locomotion in third instar (L3) *Drosophila* larvae

5.2.8.1 Motivation and selection of miRNA mutants for locomotor analysis at the L3 stage

Over the course of larval development, *Drosophila* undergo drastic morphological changes (Keshishian *et al.,* 1993). However, for the most part, new functional neurons are not added to the larval CNS (Truman and Bate, 1988) but rather, neurons become larger and circuits become reinforced in strength due to an increase in the number of synapses between neurons (Zwart *et al.,* 2013, Gerhard *et al.,* 2017). At the behavioural level, one of the few major studies comparing a large range of behaviours in the L1 and L3 larva (Almeida-Carvalho *et al.,* 2017) has also shown that locomotor behaviour is largely similar between L1 and L3 wild type larvae although specific differences are observed in bending/turning behaviour.

We wanted to determine whether the observed effects of miRNA mutation on larval locomotion were mostly related to the maturity of the larval motor system and, if so, disappeared at later stages.

We considered two models: one, in which, changes to larval locomotion seen at the L1 stage due to miRNA mutation would not be present at the L3 stage and one, in which, the effects of miRNA mutation are permanent and continuously hamper the animal's ability to perform normal locomotion. The change in a miRNA target's expression would either result in an acute effect with long-lasting consequences (e.g., failure to develop specific body wall muscles during larval development) or a chronic effect that continuously impairs locomotion

(e.g., failure to produce enough glutamate at neuromuscular junctions). The effects of a miRNA's removal on locomotion in either example would therefore be evident in both L1 and L3 larvae of the same genotype.

In order to test these models, we selected a subset of the 84 miRNA mutant lines tested at the L1 larval stage to also search for locomotor defects at the L3 larval stage. We used the graph of average crawling speeds to select a group of 17 miRNA mutants representing a vast range of speed phenotypes and with different genetic backgrounds (Figure 5.2.18A). Some mutants showed no significant difference in average crawling speed to control larvae at L1, some exhibited a mild speed defect while others exhibited severe speed defects.

We applied the same FTIR-based approach previously discussed (Figure 5.2.2) to obtain behavioural videos of L3 larvae with the FIMTable but, considering their increased size and speed, provided a larger arena for locomotion (25 x 25cm) and filmed at higher frame rate (10 fps). A consequence of these changes is shorter behavioural movies (2 minutes) than those made of L1 larvae (3 minutes) (Risse *et al.,* 2013). We then used an adapted version of the custom Microsoft Excel macro previously described to extract information on cumulative time spent turning as well as the PyFIM package previously discussed to extract information on bending frequencies, pause frequencies and average pause durations.

5.2.9 The impact of miRNA mutation on average crawling speed of L3 larvae

Examining changes to average crawling speed in L3 larvae, we observe significant changes in 9 of the 17 miRNA mutants tested (Figure 5.2.18B). Of these 9 mutants, *ΔmiR-193* mutants display a significant increase to average crawling speed while the other 8 genotypes crawl significantly more slowly than control larvae.

Based on the aforementioned findings that, for the most part, new functional neurons are not added to the larval CNS during larval development (Truman and Bate, 1988), and that L1 and L3 locomotor behaviours are similar (Almeida-Carvalho *et al.,* 2017), we expected to observe that miRNA mutation would not lead to increases to average crawling speed in L3 larvae in a similar fashion to L1 larvae.

The identification of increased average crawling speed in *ΔmiR-193* larvae at the L3 stage was, therefore, unexpected. We note that the average crawling speed of *ΔmiR-193* mutants at the L1 stage is not significantly different from that of wild-type larvae (Figure 5.2.3) and, in fact, there is only a 0.98 μm/sec difference in average speed between the two (Figure 5.2.3). This suggests that *miR-193* may not be necessary for regulation of average crawling speed at L1 stage but, during the transition between the L1 and L3 stages, acquires a role in suppressing crawling speed.

Although a relatively small subset of the miRNA mutants tested at L1 are included in testing at L3, we selected mutants with a vast range of average crawling speeds at L1 (41.26 – 76.88 μm/sec) and so postulate that testing our

aforementioned models on the effect of larval development on average crawling speed of miRNA mutants against this dataset is valid (even if this dataset only acts the precursor to an eventual screen of all miRNA mutant lines at L3).

5.2.10 The developmental progression of the effects on average crawling speed of miRNA mutations

Comparing the graph of average crawling speeds at L3 (Figure 5.2.18B) to that of L1 (Figure 5.2.3) therefore, we observe a difference in the distribution of average crawling speeds. At L1, the vast majority of lines (79%) show significant reductions in speed from the control values. At L3 however, roughly half of the lines tested also show a significant reduction in speed from control values, an equal number show no significant difference to control larvae and, unlike at L1, a significant increase in average crawling speed was identified in a miRNA mutant (*ΔmiR-193*).

ΔmiR-193 belongs to a group of three miRNA mutants tested at both the L1 and L3 stages that show no significant difference in average crawling speed to control larvae at L1. While the results show that the average crawling speed of *ΔmiR-193* mutant larvae becomes significantly faster than control larvae over the course of development, results show that the other two miRNA mutants (*ΔmiR-276a* and *ΔmiR-13-b2*) become significantly slower than control larvae over the course of development.

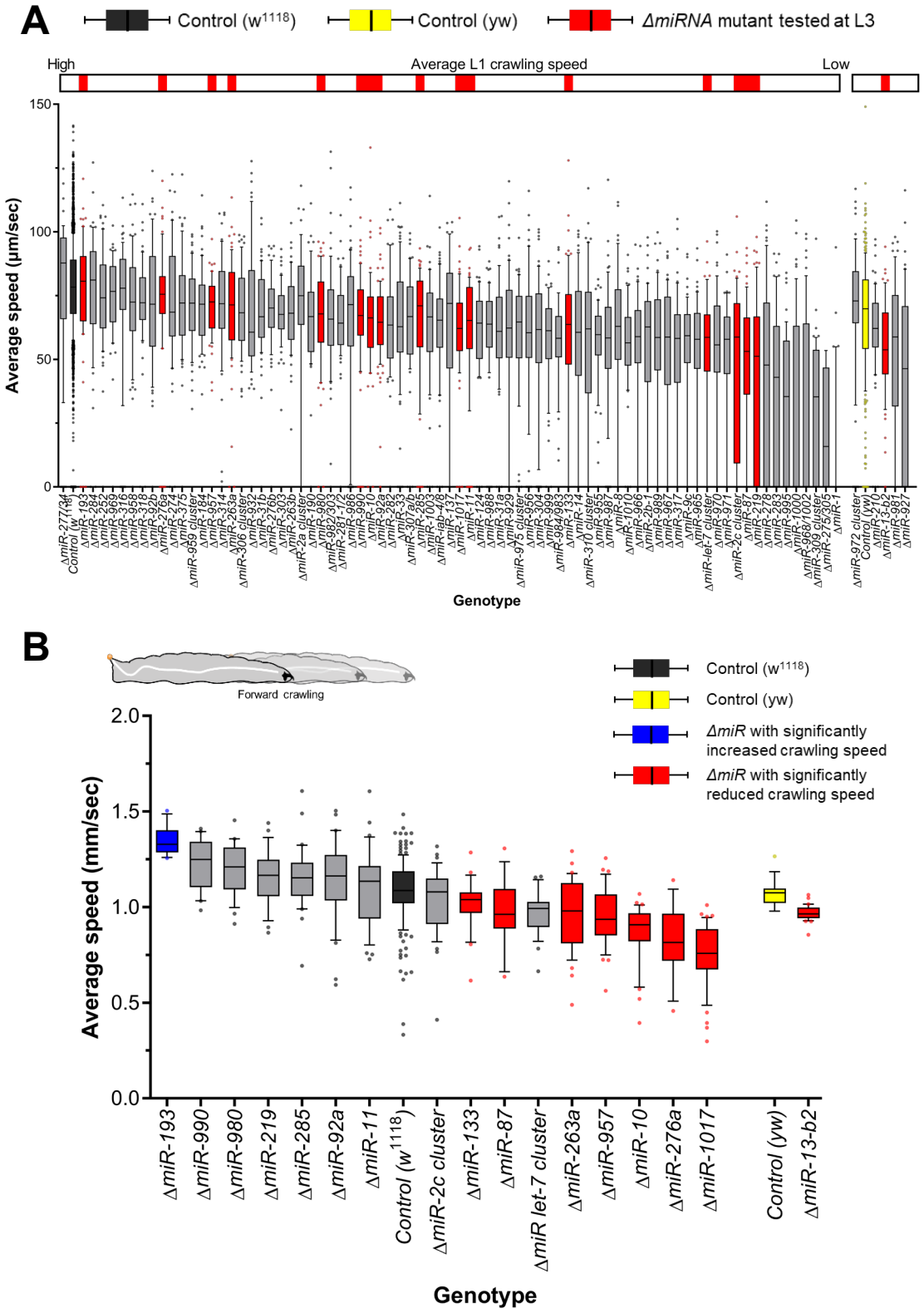

Figure 5.2.18 The effect of miRNA mutation on third instar larval crawling speed

(Legend on the following page)

(A) miRNA mutants displaying a range of average crawling speeds at the first instar stage were selected for locomotor testing at the third instar stage. For this pilot study, 17 miRNA mutant lines (red) were selected for locomotor testing at the third instar stage. 16 of these lines were compared to w^{1118} larvae (black) as a control while the remaining 5 were compared to yw larvae (yellow) to correspond to their genetic background. **(B) Our FIMTable analysis shows that miRNA mutation can both increase and decrease average crawling speed in third instar larvae.** 9 miRNA mutant lines tested at the third instar larval stage showed a significant change to average crawling speed. *ΔmiR-193* mutant larvae (blue) showed a significant increase in average crawling speed and 8 mutants (red) showed a significant reduction (Mann-Whitney U test with Bonferroni correction, $p \leq 0.0029$). 16 mutants were compared to w^{1118} larvae (black) as a control while *ΔmiR-13-b2* larvae were compared to yw larvae (yellow) to correspond to their genetic background. Boxplots show the 25-75 percentile (box), median (line), 10-90 percentile (whiskers) and outliers (individual points). n = an average of 35 larvae per genotype.

For the other 14 miRNA mutants tested at both stages that crawled significantly more slowly than control larvae at L1, we observe that the effects of miRNA mutation on average crawling speed are either reduced or maintained over larval development. 8 of these “slow” mutants at L1 do not crawl at speeds significantly different to control larvae at L3, while the remaining 6 “slow” L1 mutants remain unable to match or exceed the average crawling speeds of control larvae at L3.

We interpret these results as evidence for an effect of developmental stage on the regulation of motor control by *Drosophila* miRNAs.

Within the group of miRNA mutants tested, we observe examples of both of our initial hypotheses about the impact of development on the role of miRNAs in larval locomotion. Our evidence suggests that the effects of specific miRNA mutations on locomotion can be reduced over the course of larval development, with average crawling speed unhampered by the time the animal reaches the L3 stage. Our evidence also suggests the existence of a group of miRNAs, for whom removal has either acute or chronic repercussions that lead to a permanent inability to crawl at the same average speed as control larvae with full miRNA complements.

The increase in average crawling speed seen in *ΔmiR-193* mutant larvae over development also leads us to tentatively suggest that, with the large number of *Drosophila* miRNAs expressed with different temporal dynamics over the *Drosophila* lifespan (Zhou *et al.,* 2018), there may be other miRNAs eventually revealed in a full coverage L3 screen that also play a role in restricting average crawling speed at the L3 developmental stage.

5.2.11 Investigating turning behaviour in selected L3 miRNA mutant larvae

5.2.11.1 Increases to cumulative time spent turning are observed in L3 miRNA mutant larvae

Building on the observations that miRNAs are key for facilitating normal average crawling speed at both the L1 and L3 stages, we sought to decompose L3 average crawling speed in a similar manner to L1 crawling speed by analysing the turning and pausing components of larval locomotion in miRNA mutants. Applying the custom Microsoft Excel macro used to analyse cumulative time spent turning in L1 larvae, we analysed this behavioural variable in the 17 lines re-tested at the L3 developmental stage. For clarity, the macro was adjusted to take into account the shorter behavioural videos produced of L3 larvae (as discussed in Section 5.2.8.1).

We postulated that, similar to the L1 larva, the balance between turning and forward crawling is also key for normal locomotion in the L3 larva. Considering the fact that groups of miRNAs were shown to be important for the ability to increase and reduce the amount of turning behaviour in L1 larvae (Figure 5.2.6), we also predicted that we would also observe examples of miRNAs key for positively and negatively regulating turning behaviour at L3, even though only a subset of miRNAs were tested.

Our analysis showed that of the 17 mutants analysed, 6 show significant changes to cumulative time spent turning, all of them significant increases compared to control larvae. In the case of *ΔmiR-1017* mutants, this increase is particularly pronounced with time spent turning increasing by three-fold (Figure 5.2.19A).

5.2.11.2 The developmental progression of effects on cumulative time spent turning of miRNA mutations

Examining the possible impact of larval development on miRNA-based regulation of time spent turning, we divided the group of 17 mutants tested at L3 into those with and without significant changes to turning at L1.

In the 12 mutants tested at L3 with no significant change to cumulative time spent turning at L1, we observe that turning values either remain similar to control larvae at L3 (7 mutants) or become significantly increased (5 mutants). In the 5 mutants tested at L3 with significant changes to cumulative time spent turning at L1 however, we observe that over development, the effect of miRNA mutation on cumulative time spent turning is only maintained in one mutant genotype (*ΔmiR-957*) while the abnormal phenotype is ameliorated in the remaining four.

From these results, we conclude that (in a similar fashion to average crawling speed) normal turning behaviour is dependent upon the expression of specific miRNAs at the L3 stage and provide evidence that the dependency of turning behaviour on specific miRNAs can change over the course of larval development.

5.2.11.3 No significant relationship is found between cumulative time spent turning and the crawling speed of L3 miRNA mutant larvae

Finally, we endeavoured to understand whether the relationship between cumulative time spent turning by miRNA mutant larvae at L3 and their crawling speed remains the same as previously observed in L1 (Figure 5.2.7).

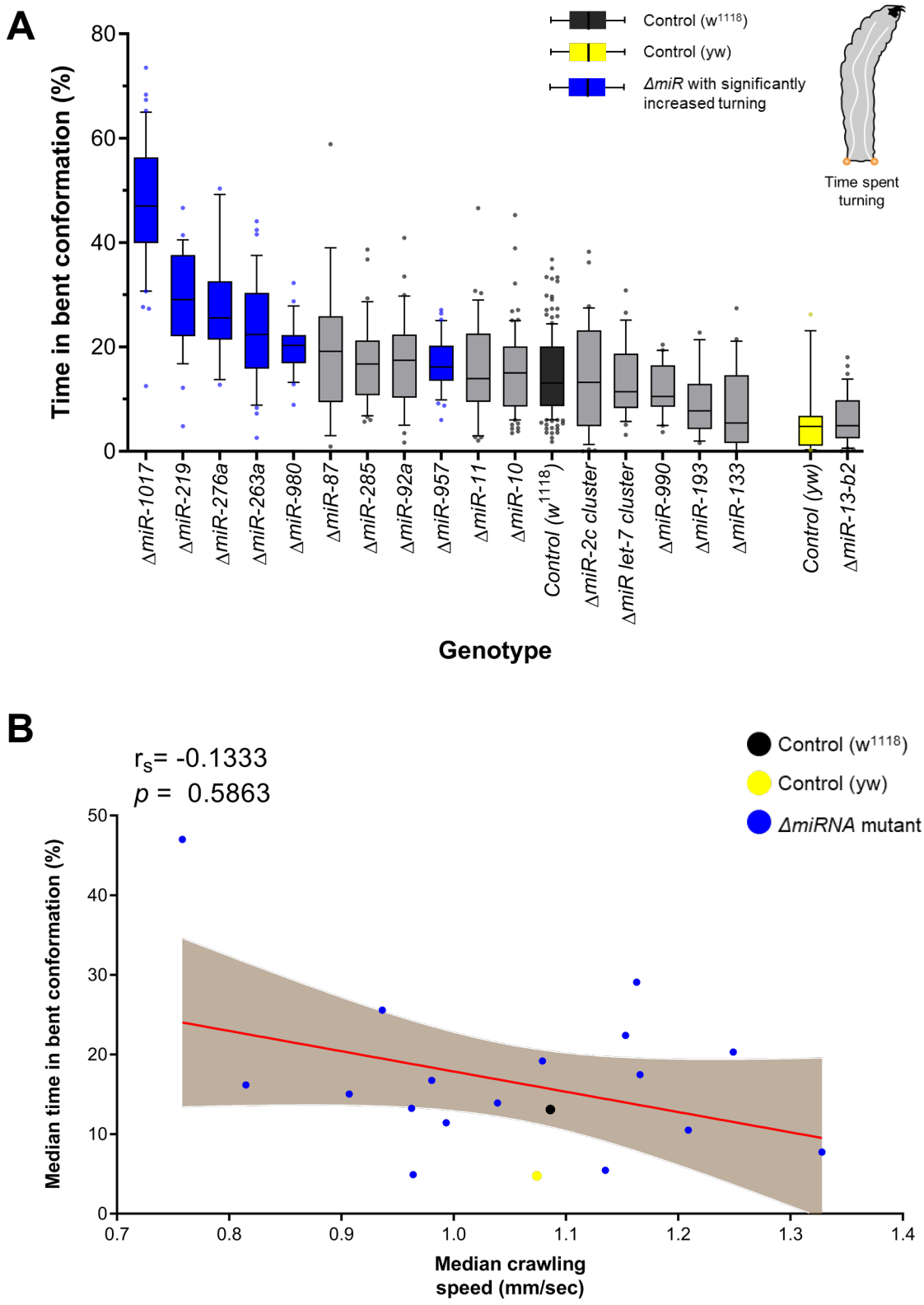

Figure 5.2.19 The effect of miRNA regulation on time spent turning by third instar larvae and its relationship to crawling speed

(Legend on the following page)

(A) Our FIMTable analysis shows that that time spent turning is significantly increased in 6 miRNA mutants at the third instar larval stage. 6 miRNA mutant lines (blue) tested at the third instar larval stage show a significant increase in time spent turning (Mann-Whitney U test with Bonferroni correction, $p \leq 0.0029$). 16 mutants were compared to w^{1118} larvae (black) as a control while *ΔmiR-13-b2* larvae were compared to yw larvae (yellow) to correspond to their genetic background. Boxplots show the 25-75 percentile (box), median (line), 10-90 percentile (whiskers) and outliers (individual points). n = an average of 35 larvae per genotype. **(B) No significant correlation is present between the crawling speed of third instar miRNA mutant larvae tested and the time spent turning.** On the x axis, the median crawling speed of miRNA mutant third instar larvae is plotted in µm/sec while on the y axis, the median time spent turning is plotted as a percentage of recording time. No significant correlation is observed between the two behavioural variables using the Spearman correlation test. The Spearman coefficient (r_s) and *p* value are shown while the 95% confidence interval for the linear regression (red) is indicated by the red shaded area.

Based on our previous analysis showing that there is no significant correlation between cumulative time spent turning by miRNA mutants and their crawling speed at L1 (Figure 5.2.7), we expected a similar result when this analysis was performed at L3. Comparison of L1 and L3 behaviour has also shown that while the absolute speed of larvae increases during development, the amount of turning they perform significantly decreases (Almeida-Carvalho *et al.,* 2017) and based on this, we also predicted that turning would not have a significant impact on crawling speed in older miRNA mutant larvae.

The results of our correlation analysis validate this prediction, demonstrating that, for the miRNA mutants tested at the L3 stage, there is no significant correlation between their crawling speed and cumulative time spent turning (Figure 5.2.19B). This suggests that changes to cumulative time spent turning do not significantly contribute to changes to larval crawling speed in L3 miRNA mutant larvae but, we note that this result is only from a subset of miRNA mutants and remain cautious about deriving overarching conclusions.

5.2.11.4 miRNA mutation leads to increases in the frequency of turning behaviour in L3 larvae

Similar to cumulative time spent turning, we predicted that examples of miRNAs would be revealed with the ability to both promote and suppress turning behaviour as was observed when the frequency of turning was investigated in L1 miRNA mutant larvae (Figure 5.2.8).

Analysing the effect of miRNA mutations on the frequency of turning behaviour in L3 miRNA mutants with the custom Python package PyFIM reveals that of

the 17 mutants analysed, 8 show significant changes to turn frequency (Figure 5.2.20A). In all 8 mutants, we note that these changes comprise significant increases in turn frequency (similar to the changes previously observed in cumulative time spent turning (Figure 5.2.19A)) suggesting that at the L3 stage, a subset of miRNAs is responsible for suppressing turning behaviour.

5.2.11.5 The developmental progression of effects on the frequency of turning of miRNA mutations

To analyse the progression of abnormal turn frequency phenotypes over developmental time, we divided the group of 17 mutants tested at L3 into those with (12 mutants) and without significant changes (5 mutants) to turning frequency at L1.

The group of 12 mutants tested at L3 with no significant change to turning frequency at L1 is itself evenly divided at L3 with 6 mutants showing significant increases to turn frequency and 6 showing no significant change compared to wild type larvae. In the 5 mutants tested at L3 with significant changes to cumulative time spent turning at L1 however, we observe that the effects of miRNA mutation on turning frequency are only maintained in 2 mutants (*ΔmiR-92a* and *ΔmiR-285*) while turning frequency is restored to values similar to control larvae in the remaining 3. We, therefore, conclude from this that the frequency of turning is also regulated by a group of specific miRNAs and that this process can be affected by developmental stage.

5.2.11.6 No significant relationship is found between the frequency of turning and the crawling speed of L3 miRNA mutant larvae

As in L1, we also sought to understand the impact of miRNA regulation on sub-behaviours that may account for changes to crawling speed. Here, we also performed a correlation analysis, examining the relationship between the frequency of turning behaviour in miRNA mutant larvae at L3 and their crawling speed.

Based on our previous analysis of the turning frequency-crawling speed relationship in L1 (Figure 5.2.9), as well as reported insights into changes in turning behaviour between L1 and L3 (Almeida-Carvalho *et al.,* 2017), we predicted that the frequency of turning behaviour would not have a significant impact on crawling speed in older miRNA mutant larvae. The results of our correlation analysis (Figure 5.2.20B) validate this prediction, demonstrating that, for the miRNA mutants tested at the L3 larval stage, there is no significant correlation between their crawling speed and the frequency of turning behaviour.

From this pilot experiment in L3 larvae, we conclude that, like crawling speed, these results are evidence that the reliance of normal turning behaviour on the expression of specific miRNAs is not necessarily constant between larval stages. We remain cautious about drawing conclusions as to whether these results discount our initial predictions about the existence of miRNA groups serving to both promote and suppress different aspects of turning behaviour however due to the limited subset of miRNA mutants tested.

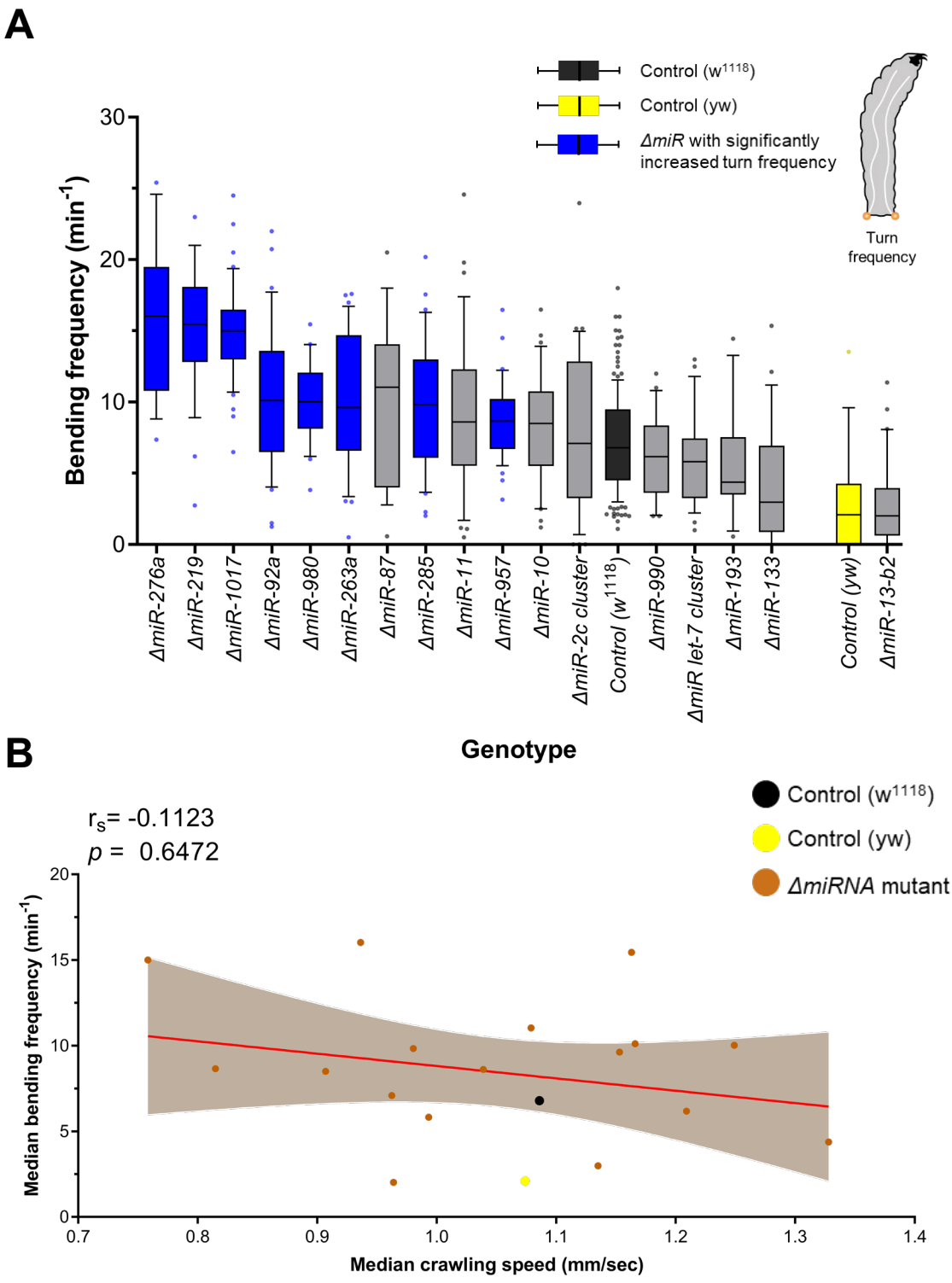

Figure 5.2.20 The effect of miRNA regulation on the frequency of turning by third instar larvae and its relationship to crawling speed

(Legend on the following page)

(A) Our FIMTable analysis shows that that turning frequency is significantly increased in 8 miRNA mutants at the third instar larval stage. 8 miRNA mutant lines (blue) tested at the third instar larval stage showed a significant increase in time spent turning (Mann-Whitney U test with Bonferroni correction, $p \leq 0.0029$). 16 mutants were compared to w^{1118} larvae (black) as a control while *ΔmiR-13-b2* larvae were compared to yw larvae (yellow) to correspond to their genetic background. Boxplots show the 25-75 percentile (box), median (line), 10-90 percentile (whiskers) and outliers (individual points). n = an average of 35 larvae per genotype. **(B) No significant correlation was found between the frequency of turning in third instar miRNA mutant larvae tested and their crawling speed.** On the x axis, the median crawling speed of miRNA mutant third instar larvae is plotted in μm/sec while on the y axis, the median frequency of turning events per minute is plotted. No significant correlation was observed between the two behavioural variables using the Spearman correlation test. The Spearman coefficient (r_s) and *p* value are shown while the 95% confidence interval for the linear regression (red) is indicated by the red shaded area.

Having observed the removal of a miRNA (*miR-1017*) leading to a three-fold increase in cumulative time spent turning (Figure 5.2.19) for example, the possibility remains that the removal of other miRNAs not covered in this screen may have inverse effects on turning behaviour, drastically (and significantly) reducing both amount of time spent turning by larvae at L3 and the frequency of these turns.

5.2.12 Investigating pausing behaviour in selected L3 miRNA mutant larvae

Previous data showed that, apart from average crawling speed, the average duration of pausing behaviour in L1 larvae is the metric most pervasively affected by miRNA mutation. We observe that 62% and 35% of miRNA mutant lines exhibit significant difference to control larvae in average pause duration and pause frequency respectively (Figure 5.2.15). In addition to this, once combined into a multidimensional dataset and analysed via principal component analysis (Figure 5.2.16), the average duration of pauses is the only behavioural metric shown to be positively correlated with the principal component explaining the largest proportion of total variance. For these reasons (in addition to our overall aim of analysing the relationship between development and its impact on miRNA-based regulation of motor control), we decided to also analyse the frequency and duration of pauses in miRNA mutant L3 larvae. The following data was all analysed using the same PyFIM-based approach as that used for analysis of L1 miRNA mutant data.

5.2.13 The effect of miRNA regulation on average pause duration

5.2.13.1 The average pause duration of L3 larvae is both increased and decreased as a result of miRNA mutation

Based on the pervasiveness of the effects of miRNA mutation on average pause duration in L1 miRNA mutant larvae (in addition to its disproportionate impact on the total variance in the combined dataset), we predicted that average pause duration would also be significantly affected by specific miRNA mutations at the L3 stage. Although a limited subset of mutants tested at L1 were re-tested at L3, we predicted that the importance of miRNAs for regulating average pause duration at L1 would also be shown at L3 with significant changes in a large proportion of mutants tested.

While the results of our analysis are able to disprove a null hypothesis (i.e., that miRNA mutation would have no effect on average pause duration at L3), we observe that miRNA mutation only affects pause duration in 5 of the 17 miRNA mutant lines tested at L3 (Figure 5.2.21A). Of these 5 lines, 3 (*ΔmiR-1017*, *ΔmiR-let-7/100/125* and *ΔmiR-263a* mutants) pause for significantly longer on average than control larvae while *ΔmiR-11* and *ΔmiR-92a* mutants pause for significantly shorter periods of time on average.

5.2.13.2 The developmental progression of effects on average pause duration of miRNA mutations

When we compare these results to the results of testing on the same 17 miRNA mutants at the L1 stage (Figure 5.2.12) we observe that 5 of the 17 mutants tested show no significant difference in average pause duration to control larvae

at either developmental stage. Of the remaining 12 that do show a significant change in average pause duration at the L1 stage, this phenotype is ameliorated in 7 over the course of larval development (Figure 5.2.21A)

5.2.13.3 The duration of pauses by miRNA mutant larvae at L3 is not significantly correlated with their crawling speed

Finally, we also analysed the impact of pause duration on the crawling speed of larvae at the L3 stage and, unlike L1 data, find no significant relationship between the two behavioural variables (Figure 5.2.21B). Considering the opposite finding in L1 larvae, this may suggest that the impact of pause duration on crawling speed is reduced over the course of larval development in general or, that as the complement of miRNAs expressed changes over time, the mechanisms regulating pause duration become altered.

Overall, we hesitate to suggest that, from these results, we can establish a rule whereby the general pervasive effect of miRNA mutation on average pause duration is mostly ameliorated over larval development. Without a full-coverage screen, we may be observing a limited portion of the possibilities. We do, however, conclude that our data suggests that miRNA regulation of pausing behaviour may vary over developmental time.

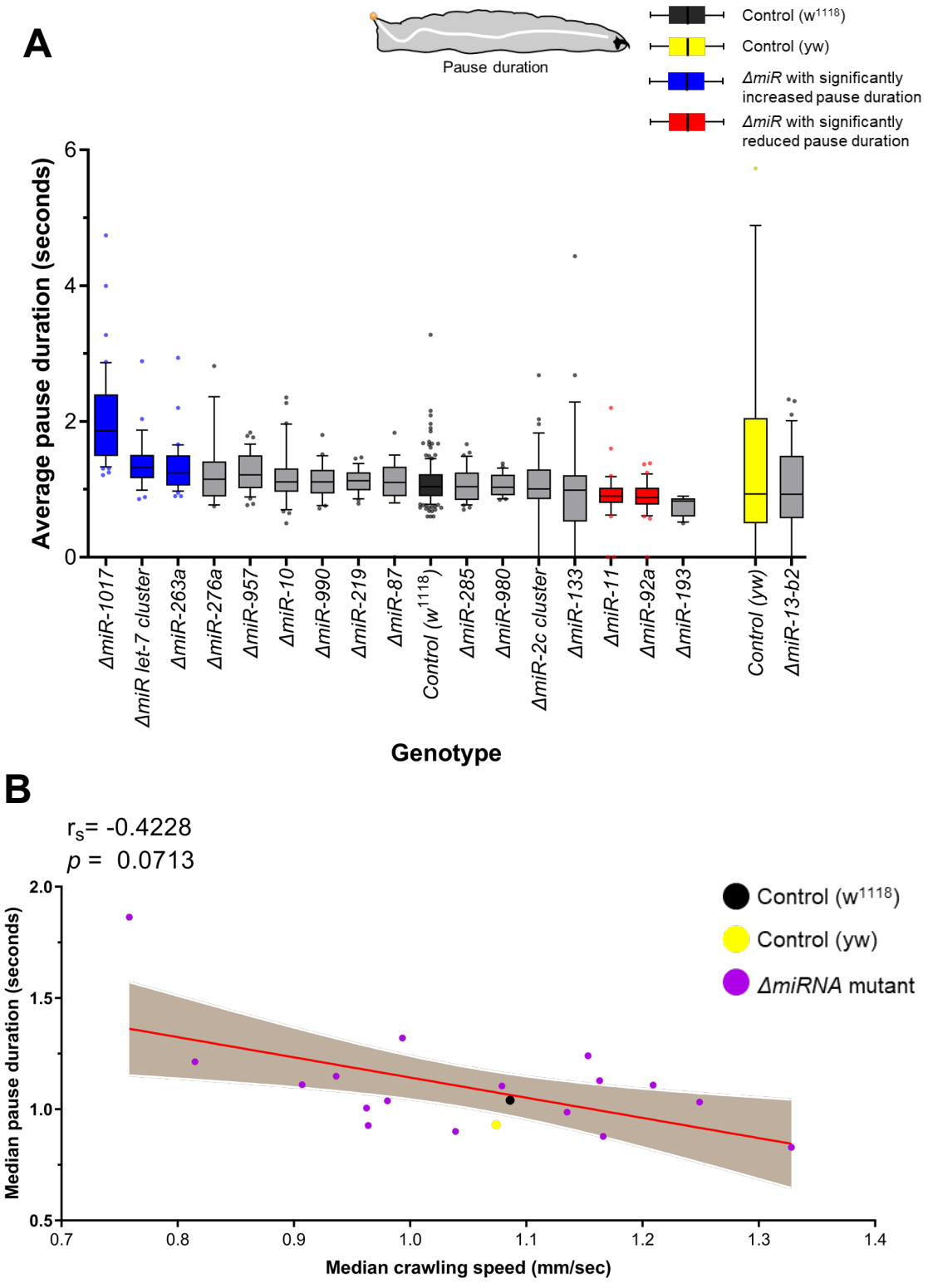

Figure 5.2.21 The effect of miRNA mutation on the duration of pauses by third instar larvae and its impact on crawling speed

(Legend on the following page)

(A) Our FIMTable analysis shows that miRNA mutation can lead to both increases and decreases to pause duration in third instar larvae. 5 miRNA mutant lines tested at the third instar larval stage show a significant change to pause duration. 3 mutant lines (blue) show a significant increase in pause duration and 2 mutant lines (red) show a significant reduction (Mann-Whitney U test with Bonferroni correction, $p \leq 0.0029$). 16 mutants were compared to w^{1118} larvae (black) as a control while *ΔmiR-13-b2* larvae were compared to yw larvae (yellow) to correspond to their genetic background. Boxplots show the 25-75 percentile (box), median (line), 10-90 percentile (whiskers) and outliers (individual points). n = an average of 35 larvae per genotype. **(B) The crawling speed of miRNA mutant third instar larvae is not significantly correlated with the duration of pauses during crawling.** On the x axis, the median crawling speed of miRNA mutant third instar larvae is plotted in μm/sec while on the y axis, the median duration of pauses is plotted in seconds. No significant correlation is observed between the two behavioural variables using the Spearman correlation test. The Spearman coefficient (r_s) is shown while the 95% confidence interval for the linear regression (red) is indicated by the red shaded area.

5.2.14 The effect of miRNA regulation on pause frequency

5.2.14.1 The frequency of pauses is significantly increased in specific miRNA mutant larvae tested at L3

Continuing our analysis of the impact of miRNA mutation on pausing behaviour, we finally explored the effects of miRNA mutation the frequency of pausing behaviour in L3 larvae. We previously observed that, compared to control larvae, 11 out of the 84 mutant lines tested at L1 pause significantly more frequently while 20 pause significantly less frequently (Figure 5.2.10). We therefore considered whether we would also identify examples of miRNAs involved in the promotion and suppression of pausing instances at L3.

Having only performed a partial screen of miRNA mutants at L3, we had no clear expectations on whether or not we would observe an impact of miRNA mutation on pause frequency at this stage. The results of our analysis show that, of the 17 miRNA mutants whose locomotion was tested at L3, 5 miRNA mutants pause significantly more frequently than controls while the remaining 12 pause at frequencies statistically similar to control larvae (Figure 5.2.22A).

We remain hesitant about drawing firm conclusions on the nature of miRNA-based control of pausing behaviour from this dataset, as a full screen of miRNA mutants at L3 could yet reveal miRNA mutations that also lead to reductions in pause frequency. We do, however, suggest that (similar to L1 larvae), the frequency of pausing behaviour by L3 larvae is also regulated by specific miRNAs.

5.2.14.2 The developmental progression of effects on the frequency of pauses in miRNA mutants

Subsequently, we compared the effects of miRNA mutation on the frequency of pausing behaviour in mutants tested at L1 and L3. Our results indicate that, when compared to control larvae, 8 out of the 10 mutants with no significant change to pause frequency at L1 also show no abnormal phenotype at the L3 stage. Of the remaining 7 mutants tested that do show abnormal pausing frequency at the L1 stage, pausing frequencies are not significantly different to control L3 larvae in 4 lines.

As with the pause duration metric, we also analysed the impact of the frequency of pausing on the crawling speed of larvae at the L3 stage via a correlation analysis with results showing no significant relationship between the two behavioural variables (Figure 5.2.22B).

5.2.15 Summary of all correlation analyses between crawling speed of miRNA mutants at L3 and other behavioural variables

Overall, the results of our correlation analyses between crawling speed and other behavioural variables were mostly similar to those identified in L1. Comparing crawling speed of L3 miRNA mutant larvae with time spent turning (Figure 5.2.19B), turning frequency (Figure 5.2.20B), pause duration (Figure 5.2.21B) and pause frequency (Figure 5.2.22B), we found that none were significantly correlated with crawling speed.

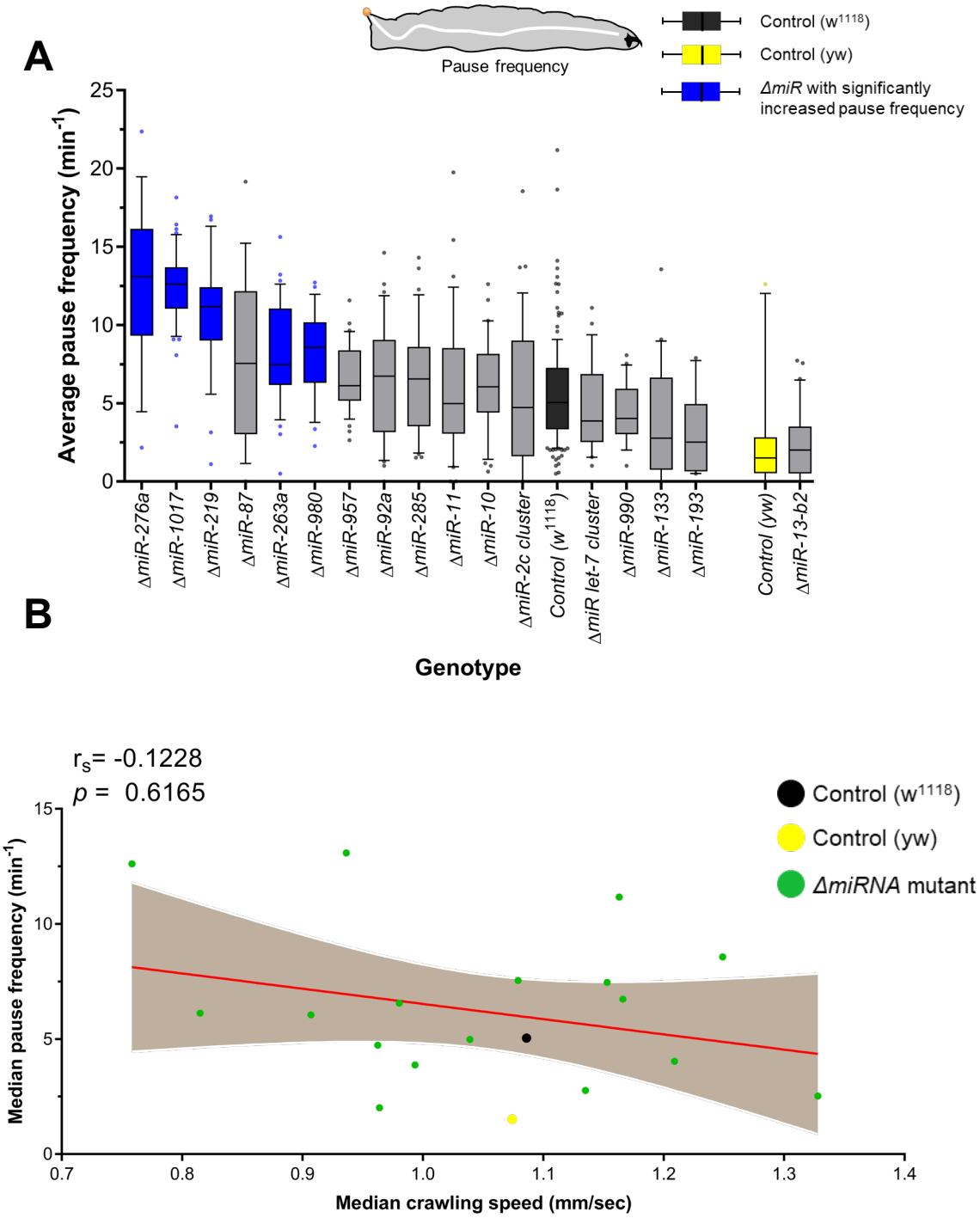

Figure 5.2.22 The effect of miRNA regulation on the frequency of pauses by third instar larvae and its relationship to crawling speed

(Legend on the following page)

(A) Our FIMTable analysis shows that that pause frequency is significantly increased in 5 miRNA mutants at the third instar larval stage. 5 miRNA mutant lines (blue) tested at the third instar larval stage show a significant increase in time spent turning (Mann-Whitney U test with Bonferroni correction, $p \leq 0.0029$). 16 mutants were compared to w^{1118} larvae (black) as a control while *ΔmiR-13-b2* larvae were compared to yw larvae (yellow) to correspond to their genetic background. Boxplots show the 25-75 percentile (box), median (line), 10-90 percentile (whiskers) and outliers (individual points). n = an average of 35 larvae per genotype. **(B) No significant correlation is present between the frequency of pauses by third instar miRNA mutant larvae tested and their crawling speed.** On the x axis, the median crawling speed of miRNA mutant third instar larvae is plotted in μm/sec while on the y axis, the median frequency of pauses per minute is plotted. No significant correlation is observed between the two behavioural variables using the Spearman correlation test. The Spearman coefficient (r_s) and *p* value are shown while the 95% confidence interval for the linear regression (red) is indicated by the red shaded area.

This suggest that after the larval body has significantly changed through maturation, the importance of the duration of pauses to overall locomotion changes and represents an interesting possibility for further investigation.

5.2.16 No significant correlation was found between behavioural variables tested in miRNA mutants at the L1 and L3 stages

We also compared the consistency of effects on behavioural variables of miRNA mutations in an attempt to understand how the severity of impacts of miRNA mutations may change over developmental time. We took the 17 miRNA mutants tested at both stages and analysed the relationships between their measurements for each of the five behavioural variables at the L1 and L3 stages. Our analyses showed that no significant correlation exists between L1 and L3 mutant larvae in any behavioural variable (Figures 5.2.23A-E) suggesting a wide variation in the importance of miRNAs according to different stages of larval development. In other words, miRNAs that regulate a specific behaviour at one development stage do not necessarily regulate the same behaviour at another developmental stage.

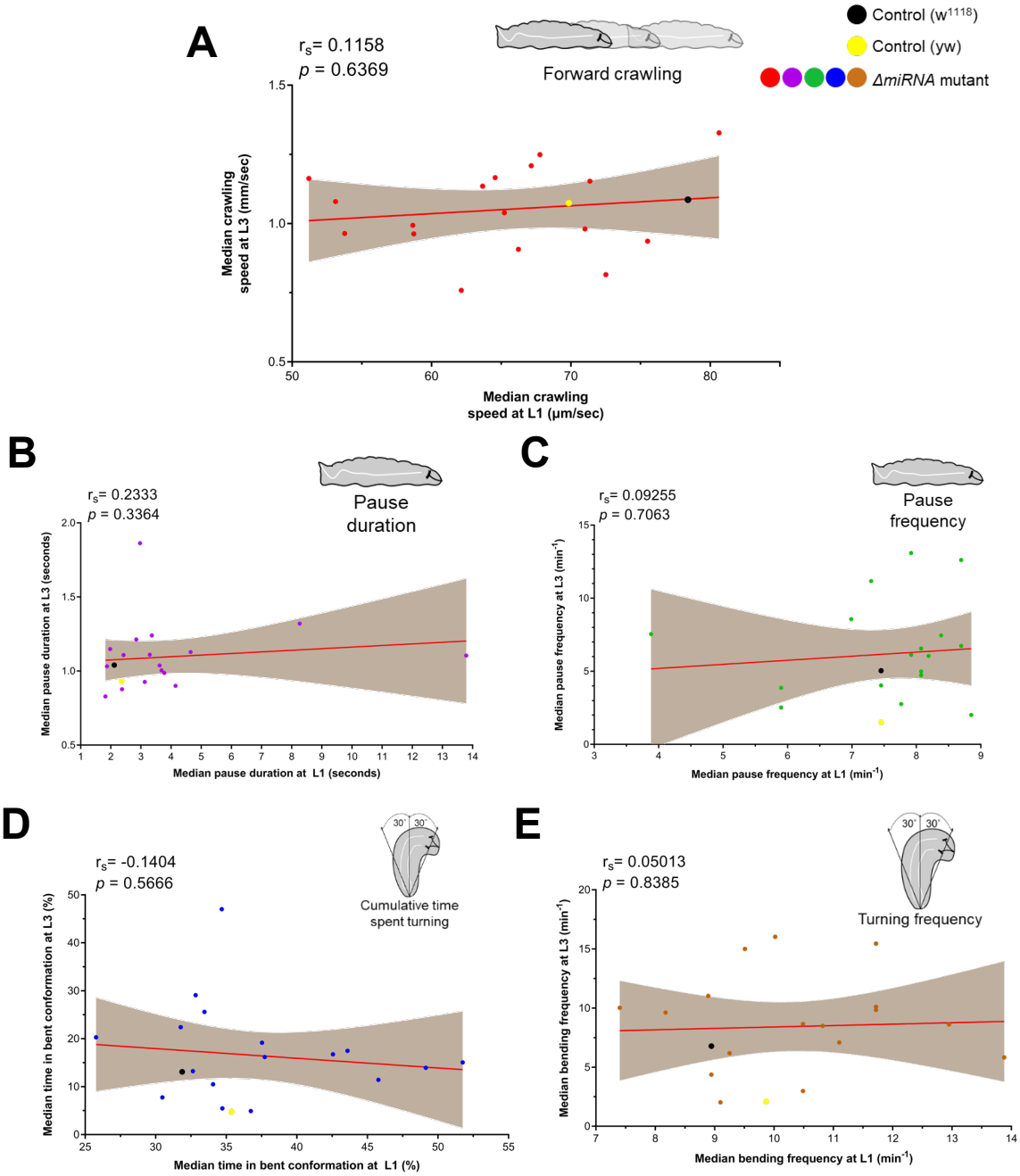

Figure 5.2.23 The relationships between behavioural variables tested in miRNA mutants at the first instar and third instar larval stages

(A-E) In all graphs, median values for behavioural variables in the 17 mutant lines tested at both larval stages are compared. L1 values are plotted on the x axis and L3 values are plotted on the y axis. No significant correlation is observed between L1 and L3 values for **(A)** median crawling speed, **(B)** median

pause duration, **(C)** median pause frequency, **(D)** median cumulative time spent turning or **(E)** median frequency of turning behaviour. All tests were done using the Spearman correlation test and the Spearman coefficient (r_s) and *p* value are shown in each graph. The 95% confidence intervals for each linear regression (red) are indicated by the red shaded area.

5.3 Discussion

In this chapter, we examine the generality of miRNA-based regulation's involvement in motor control in *Drosophila* larvae. It had already been shown that normal expression of a group of miRNAs were key for facilitating the complex self-righting response (Picao-Osorio *et al.,* 2017) and we questioned whether miRNA expression was also necessary for other behaviours, such as locomotion. In the first instar (L1) larva, we find that the vast majority of miRNA mutants tested are unable to crawl at speeds similar to control larvae (Figure 5.2.3) with average crawling speed reduced by more than 30μm/second in some cases.

During the production of this thesis, a related study by the lab of Leslie Griffith (Department of Biology, Brandeis University, USA) also examined the roles of miRNAs in *Drosophila* larval locomotion (Donelson *et al.,* 2020). The authors of this study expressed 128 specific miRNA "sponges" (small RNA sequences designed to sequester individual miRNAs from mRNA targets through complementary base-pairing (Ebert *et al.,* 2007)) pan-neuronally to artificially modulate miRNA expression throughout the central nervous system and examined the effects of this on locomotion in the second instar (L2) larva. The results of their screen indicated that 20 of the "miR-SP" lines tested showed significant changes to average crawling speed. This is substantially different to the results of the locomotor screen presented in this study, in which 66 mutants (covering 92 miRNAs) show significant reductions in average crawling speed.

One reason for this difference may be that our genetic approach was unbiased, screening for locomotor defects in a collection of null miRNA mutants (Chen *et*

al., 2014b), and the approach used by Donelson and colleagues relied upon pan-neuronal expression of miRNA sponges. Changes to behaviour which occur as a result of targeted miRNA sponge expression are difficult to interpret due to the subtlety of sponge impact on miRNA activity (when compared to a null mutation). In addition to this, a small number of miRNA molecules may fail to be sequestered from their mRNA targets by sponge constructs, resulting in a small amount of negative gene regulation by miRNAs still occurring. Our screen was designed in an unbiased fashion, ensuring that the expression of each miRNA was uniformly modulated in all larval tissues (preventing the issue of some miRNA molecules still negatively regulating gene expression).

Another reason for the difference between the results of this study and those reported by Donelson and colleagues could be that we screened for locomotor defects in the early L1 larva (less than 30 minutes post-hatching) while Donelson and colleagues used the L2 larva. As our data shows, the developmental stage of the larva has an impact on the regulation of motor behaviours by miRNAs and we suggest that the results presented by Donelson and colleagues may only be applicable to the L2 developmental stage.

Having identified a subset of mutants with severe defects in average crawling speed at L1, we moved on to address our questions about the potential pleiotropic effects of miRNA mutation on motor control. The lack of significant correlation identified between crawling speed and time to self-right subsequently identified in our study (Figure 5.2.4) suggests that the expression of specific miRNAs during movement may be context-dependent. For example, neurological processes driving the decision to perform certain behaviours may also lead to changes in miRNA expression that serve to reinforce that decision

by repressing expression of neuromodulators in key central pattern generators (CPGs). An alternative hypothesis is that the expression levels of specific miRNAs are maintained at different “base levels” and external triggers such as stress or aversive stimuli cause changes to miRNA expression levels that then lead to changes in external locomotor behaviour.

Larval locomotion itself has been described as fitting a Lévy Walk model in which periods of movement containing smaller “steps” are occasionally interspersed with periods containing longer “steps” during which the animal travels to a new area (Viswanathan *et al.,* 1999, 2001; Berni, 2015; Sims *et al.,* 2019). The balance between forward crawling and other ‘sub-behaviours’ (such as bending or pausing) is therefore key for efficient locomotion and our study opens the question of potential roles for miRNAs in these processes. The results of our analyses identify specific miRNAs necessary for normal time spent turning, turning frequency, average pause duration and pause frequency suggesting that miRNA regulation is key for maintaining a balance between all of these factors which, in turn, facilitates efficient locomotion.

One hypothesis that could be investigated in future study is that general locomotion and its sub-behaviours fit a hierarchical organisation model in which neuronal dynamics are nested with each sub-level of activity related to the exhibition of a specific sub-behaviour (Tinbergen, 1951, 1996; Kaplan *et al.,* 2020). At the level of the CPGs underlying locomotion, miRNAs may regulate the production of neuromodulators such as dopamine or serotonin (as discussed in Section 1.4) or the expression of ion channels sensitive to particular neurotransmitters. In this way, miRNA regulation may determine the dynamics of neuron activity within CPGs and, therefore, regulate the coupling of

smaller behaviours, such as turning or pausing, during locomotion. Examining the roles of miRNAs in this behavioural coupling process may represent an interesting topic of research in the future with the results having implications for how we view the organisation of motor control.

When examining these sub-behaviours in detail, we identify that changes to pausing behaviour (pause frequency and average pause duration) represent a disproportionate amount of variance when data on all locomotor variables were combined into a multidimensional dataset and analysed with principal component analysis.

The control of pausing (or “stopping”) behaviour in the *Drosophila* larva has only been characterised at the mechanistic level in a few studies (Schulze *et al.,* 2015; Gepner *et al.,* 2015; Hernandez-Nunez *et al.,* 2015; Tastekin *et al.,* 2018) with most studies characterising pausing as related to reorientation of larval crawling upon stimulation of sensory pathways. In other words, larval pausing has mainly been investigated as part of reorientation during odour-taxis and mechanisms for pausing have mostly linked olfactory and gustatory components to the execution of pauses with little interneuronal circuitry identified. The work of Tastekin and colleagues, however, identified the sensorimotor pathway between these olfactory components and specific premotor neurons in 2018. Our finding that changes to pausing behaviour represent a substantial contribution of the effects of miRNA mutation to overall locomotion, therefore, presents an opportunity to examine miRNA-target interactions within the neurons of this pathway in future study and produce a detailed mechanism by which specific miRNAs regulate larval pausing behaviour.

Finally, we addressed our initial question of whether the necessity of miRNA-based regulation for normal locomotion changes over the course of larval development by performing a screen for locomotor defects in a selection of miRNA mutant third instar (L3) larvae. Within this subset of mutants, we find a variety of effects including examples of changes to behaviours not observed at L1 (e.g., an average increase to crawling speed of *ΔmiR-193* mutant larvae) and examples of significant behavioural phenotypes observed in L1 mutants not present in the same genotypes at L3. In addition to this, we find that, in genotypes tested at L1 and L3, no significant correlation exists between the severity of any behavioural phenotype. During our pilot study of miRNA mutants at the L3 stage, therefore, we observe that miRNA-based regulation of motor behaviour can change according to the developmental stage of the larva.

This opens several questions on the mechanisms through which miRNA regulation of behaviour changes during larval development. For example, is there a gradual change in target expression that changes the likelihood of a miRNA binding to one target over another? Is there a gradual change in the expression domains of miRNAs themselves? Does the significance of a specific miRNA-target interaction to overall locomotion change between larval stages?

The results of investigations addressing these questions may have implications for, not only our understanding of larval motor behaviour regulation in general but also, the processes that facilitate differences in motor behaviour between the freshly-hatched L1 larva and the larger L3 larva preparing for pupariation.

Chapter 6

The role of *miR-133* in *Drosophila* larval head-rearing behaviour

6.1 Chapter overview

In order to understand the exact roles played by miRNAs in regulation of *Drosophila melanogaster* motor behaviour, it is necessary to have a comprehensive grasp of the mechanisms through which they act. Larval self-righting behaviour depends on both, the regulation of Ultrabithorax expression in LT-1/2 motor neurons by *miR-iab-4* (Picao-Osorio *et al.,* 2015; Issa *et al.,* 2019) and regulation of *atonal* expression in the sensory neurons by *miR-263b* (Klann *et al.,* 2020). miRNAs, therefore, have been demonstrated to regulate complex behaviour by regulating neural activity in both the sensory and motor components of the *Drosophila* nervous system.

To date, general screens for locomotor defects in transgenic fly lines with artificially reduced miRNA expression have been used to investigate the regulation of general locomotor behaviour by miRNAs. Donelson and colleagues (Donelson *et al.,* 2020) have shown that larval locomotion relies on normal expression of miRNAs within the central nervous system (CNS). Neither the exact miRNA-target relationships that facilitate larval locomotion, however, nor the exact cellular locations in which these interactions occur have ever been elucidated. Knowledge of these factors is essential for the determination of the mechanisms through which miRNAs regulate larval locomotion and here, we present a mechanistic investigation in which these factors are analysed.

In the previous chapter, we identified a pervasive role for miRNA regulation in the control of larval crawling with the vast majority of miRNA mutant stocks tested showing a reduction in average crawling speed. We also identified roles for miRNA regulation in control of various other aspects of larval locomotion

such as pausing and turning at the first (L1) and third (L3) instar developmental stages. This suggests that miRNAs not only serve to optimise average crawling speed but also to maintain a balance between the exhibition of different behaviours during larval locomotion. Finally, we identified that in the L1 larva, changes to pausing behaviour explain the majority of variance in a combined locomotor dataset and that the mutants tested could not be separated into clusters based on the distinct permutations of behavioural phenotypes that formed their behavioural profiles.

Considering the widespread modulation of pausing behaviour in miRNA mutant larvae and our aim of investigating the mechanisms through which miRNAs regulate decision making during locomotion, we examined the mechanisms by which miRNAs regulate the decision to remain stationary during a pause in crawling. After consideration of the miRNA mutants showing increased average pause duration at L1, the Δ*miR-133* mutant presented as a good candidate for mechanistic analysis due to its lack of abnormal phenotype in other behaviours (except a reduction in crawling speed) and the predominant expression of this miRNA in the CNS of the early L1 larva (as revealed in an RNA-seq experiment conducted by members of the Alonso lab (Picao-Osorio *et al.,* unpublished data)).

During behavioural analysis of Δ*miR-133* null mutant larvae, we observed an unusual “head-rearing” phenotype in which Δ*miR-133* mutant larvae would raise their anterior segments from the substrate and hold them aloft briefly before returning to normal crawling. Although identified as a *Drosophila* larval behaviour in the 1980s (Green *et al.,* 1983), the mechanisms underlying head-rearing behaviour have only been investigated in a single study (Okusawa *et al.,*

2014). Okusawa and colleagues have shown that the normal activity of the serotonergic system (and in particular, the serotonin-sensitive ABLK leucokinergic neurons) is key for control of head-rearing but nothing is known about the behaviour's genetic basis, prompting us to investigate the mechanism by which *miR-133* may regulate rearing during locomotion.

Using an intersectional *in silico* miRNA target prediction approach, we identified the biosynthetic enzyme tryptophan hydroxylase (or 'Trh') as a potential target for *miR-133* regulation and showed via RT-PCR that *miR-133* mutation leads to a significant increase in tryptophan hydroxylase expression. Tryptophan hydroxylase acts as the rate-limiting enzyme in the production of the biogenic amine serotonin (Lundell and Hirsh, 1994) and in the CNS of L1 Δ*miR-133* mutant larvae, we used immunohistochemistry to identify an increase in serotonin levels compared to controls. Finally, we were able to phenocopy the increased rearing phenotype seen in Δ*miR-133* mutant larvae by overexpressing the *Trh* gene in larval serotonergic neurons, confirming the sufficiency of increased serotonin production to cause increased rearing behaviour.

Altogether, we have identified *miR-133* as a regulator of head-rearing behaviour in *Drosophila* larvae and present evidence to suggest that *miR-133* inhibits serotonin production by inhibiting the expression of *Trh*. The results of this study represent a novel addition to the little that is currently known about rearing behaviour as well as the identification of a previously unknown mechanism through which a miRNA regulates pausing behaviour in larvae.

6.2 Results

6.2.1 A null mutation in the *miR-133* gene leads to a significant increase in larval head-rearing

6.2.1.1 *miR-133* is a putative regulator of pause duration in *Drosophila* larvae

Building on the observation that changes in average pause duration in early first instar (L1) miRNA mutant larvae are correlated with principal components representing the majority of variance in a multidimensional locomotor dataset (Section 5.2.6.2), we planned further investigations into the mechanisms by which miRNAs regulate average pause duration.

The results of our screen for behavioural defects in miRNA mutant larvae at the L1 stage indicate that the removal of miRNA expression leads to significant changes in average crawling speed, cumulative time spent turning, turning frequency, average pause duration and pause frequency (Figure 5.2.15). In order to select a miRNA mutant for the mechanistic study of miRNA-based regulation of average pause duration, we identified a group of 46 mutants with significantly increased average pause duration. Many of these 46 mutants also display abnormal phenotypes in other behavioural variables and, to avoid the possibility of investigating changes to pause duration that were purely pleiotropic, we identified a group of 13 mutants (from the original 46) with no significant differences to control stocks in pause frequency, time spent turning, or turning frequency. Our aim was to elucidate the mechanisms through which miRNAs regulated the neural control of decision-making behaviour during locomotion and, in this vein, we cross-referenced these 13 mutants with data

from an RNA-seq transcriptomics experiment in the early L1 CNS and other tissues performed by former members of the Alonso lab (Picao-Osorio *et al.,* unpublished data) to identify 3 miRNAs (*miR-219*, *miR-133* and *miR-970*), predominantly expressed in the early L1 CNS. Of these 3, Δ*miR-133* mutant larvae show the strongest delays to average pause duration at the early L1 stage and we, therefore, planned an investigation into the role of *miR-133* in the neural regulation of average pause duration.

6.2.1.2 Description of the methodological approach used to study pausing behaviours

Our initial recordings of miRNA mutant larval behaviour were performed using the FIMTable (as discussed in Section 5.2.1.3). A disadvantage of this is that, although experiments are high-throughput and easily analysed, behavioural videos are filmed from below using infrared light (Figure 5.2.2B). This means that larvae appear as silhouettes in videos and behaviours in 3-dimensions are not captured. In addition to this, the small size of the early L1 larva (at approximately 0.5mm) (Schuman and Triphan, 2020) presents challenges when attempting to resolve more subtle behavioural phenotypes using the FIMTable setup. For example, changes to peristaltic wave propagation can only be resolved in larger larvae (Risse *et al.,* 2017) meaning that, if changes to pause behaviour were a result of changes to this, we would be unable to identify this relationship with our previous methodology.

To address these issues and characterise changes to pausing behaviours in a more detailed fashion, we produced a new set of behavioural videos in early

Δ*miR-133* mutant larvae by filming their locomotion for 3 minutes from above and under constant visible light (Figure 6.2.1A). These films were produced using a Leica DFC 340 FX camera mounted on a Leica M165 FC microscope and Leica Application Suite software.

6.2.1.3 Δ*miR-133* mutant larvae rear significantly more than wild type larvae during locomotion

While filming Δ*miR-133* mutant larvae under these conditions, we observed that occasionally, larvae would stop crawling, contract their anterior segments, and raise them from the substrate (Figure 6.2.1B). This “rearing” behaviour would typically last for around 2 seconds before the larva would return its anterior segments to the substrate and continue front crawling (Figure 6.2.1C). Occasionally, larvae would perform several rears in succession before beginning to front crawl again. Comparing the films of Δ*miR-133* mutant larvae to control larvae (w^{1118}) filmed under identical conditions, we observe that rearing behaviour occurred significantly more frequently during the three minutes of locomotion recorded (Figures 6.2.1D and 6.2.1E).

Head-rearing in *Drosophila* larvae has been briefly characterised (Benz, 1956; Green *et al.,* 1983) but the neural basis of larval head-rearing has rarely been studied (Okusawa *et al.,* 2014) and its genetic basis remains unknown. In the larvae of other insects, head-rearing is also performed as an aggressive behaviour to ward off potential predators (Gross, 1993) and is conserved in animals with similar body plans such as the nematode, *Neoplectana carpocapsae* (Gaugler *et al.,* 1980).

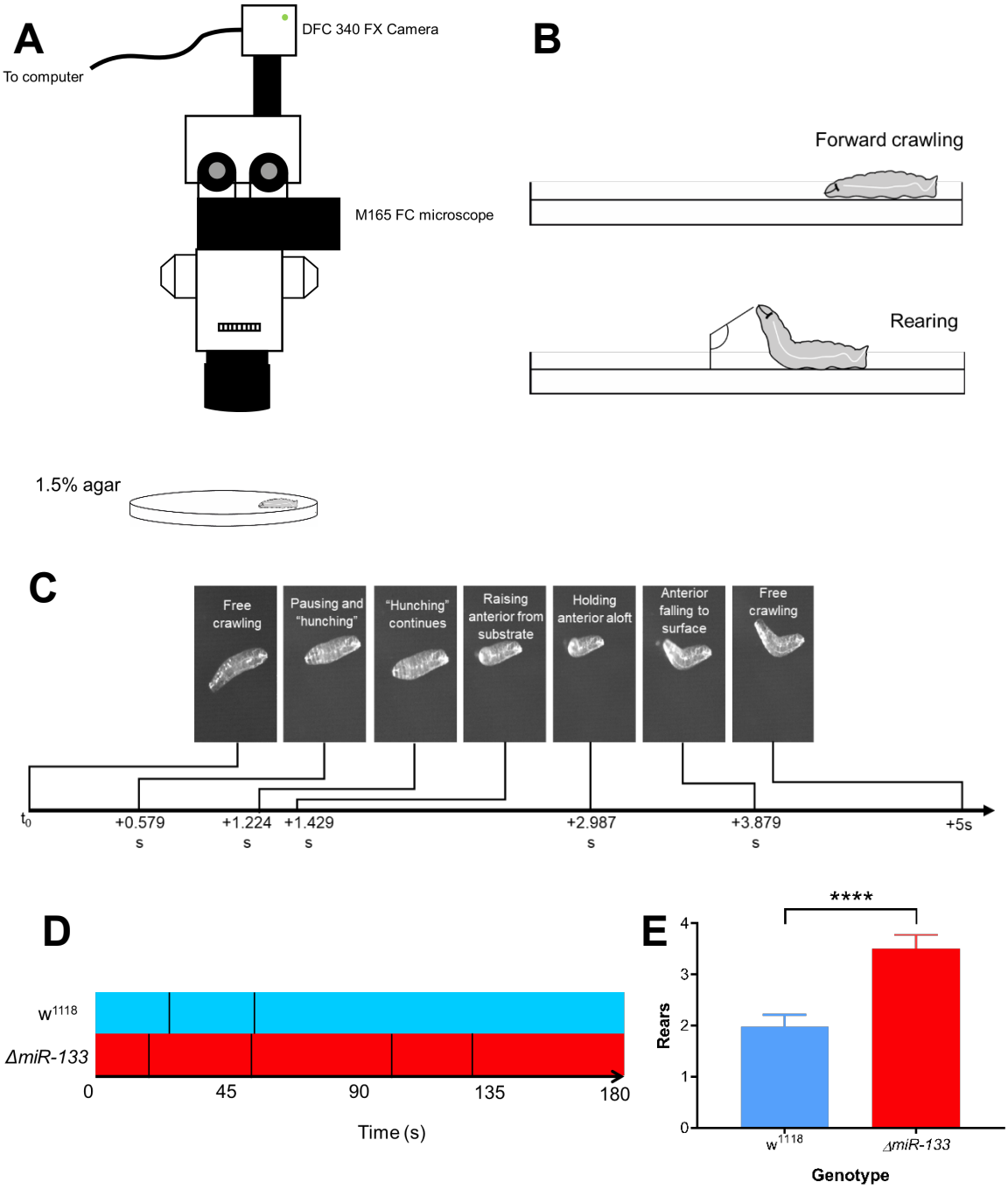

Figure 6.2.1 First instar Δ*miR-133* larvae show a significant increase in rearing behaviour

(A) A schematic of the recording setup for filming larval pausing behaviour. A larva crawling on a 1.5% agar plate was filmed using a Leica M165 microscope and Leica Application Suite 4.5 software for 3 minutes. **(B)** (Top) Larvae typically crawl with their bodies flat against the crawling surface whereas in

rearing (Bottom) the anterior segments of the larval body are raised and held aloft. **(C)** A time series showing the typical sequence of larval head-rearing behaviour. Typically, a freely crawling larva will pause and “hunch”, contracting the anterior segments of the body. The anterior segments are then raised from the substrate and held aloft briefly before they fall back to the substrate and the larva resumes free crawling. **(D)** A schematic of the frequency of rearing events in representative w1118 and Δ*miR-133* mutant larvae. Rearing events during filming are represented by black vertical lines. **(E)** Δ*miR-133* mutant larvae rear significantly more than control larvae (w^{1118}) over the course of filming (Mann-Whitney U test, mean ± SEM; n = 45).

Therefore, the description in this chapter of the potential involvement of *miR-133* in control of rearing, represents a new contribution to our understanding of the mechanisms by which miRNAs facilitate evolutionarily-conserved motor behaviours which have functional relevance to the survival of organisms.

6.2.2 Confirmation of removal of *miR-133* expression in the Δ*miR-133* mutant

6.2.2.1 The structure of the *miR-133* gene

In order to confirm that *miR-133* was involved in the control of head-rearing, our first step was to confirm the lack of *miR-133* expression in mutant larvae. The primary *miR-133* sequence (6.2.2A) is expressed in the wild-type L1 larva as part of *CR44909*, a long non-coding RNA (lncRNA) found in the second chromosome. The uncharacterised genes *CG31677*, *CG15475* and the lncRNA *CR43608* are also present in *CR44909* as well as the miRNA *miR-288* (Figure 6.2.2B). The reported results of miRNA-sequencing experiments show that *miR-288* is not expressed at any stage during embryogenesis (Zhou *et al.,* 2018) making it unlikely to contribute to early larval behavioural control.

6.2.2.2 *miR-133* is not expressed in Δ*miR-133* mutant flies

In the Δ*miR-133* mutant line developed as part of a collection of miRNA mutants by the lab of Stephen Cohen, the gene encoding the miRNA sequence has been excised and replaced with a *mini-white* gene (Chen *et al.,* 2014b). To confirm removal of the *miR-133* sequence from Δ*miR-133* mutant DNA, we

designed primers complementary to sequences flanking the normal miRNA sequence (Figure 6.2.2A, black arrows). We then carried out PCR with these primers using wild type, Δ*miR-133* heterozygote mutant and Δ*miR-133* homozygote mutant larval DNA. These PCR primers were designed to amplify a 152bp PCR amplicon (containing the 98bp primary miRNA sequence) in wild-type DNA and we observe the presence of this amplicon after agarose gel electrophoresis of the PCR product (Figure 6.2.2B, w^{1118} lane). Using heterozygote Δ*miR-133* mutant DNA, we also observe a band just below 100bp in size (Figure 6.2.2B, Δ/+ lane) but using homozygote Δ*miR-133* mutant DNA (Figure 6.2.2B, Δ/Δ lane), we observe no band confirming the removal of primary *miR-133* sequence from the mutant genome.

The confirmation of a lack of *miR-133* expression in Δ*miR-133* mutants allowed us to consider a model in which removal of *miR-133* expression resulted in the increases in larval head-rearing behaviour previously described (Section 6.2.1.3). miRNAs are negative regulators of gene expression (Lai, 2002; Ameres & Zamore, 2013) and by binding to complementary sequences in the 3'-UTR of target mRNA transcripts, they prevent protein translation by promoting mRNA degradation (Bartel, 2004). miRNAs regulate the expression levels of several genes simultaneously, for example, Lim and colleagues have reported that in HeLa cells, *miR-124* and *miR-1* both regulate around 100 genes (Lim *et al.,* 2005) and in the zebrafish, Giraldez and colleagues report that *miR-430* regulates several hundred target genes during development (Giraldez *et al.,* 2006). In the case of *miR-133*, we, therefore, considered how increases in the expression of genes usually inhibited by the action of *miR-133* may then lead to behavioural change (Figure 6.2.2C).

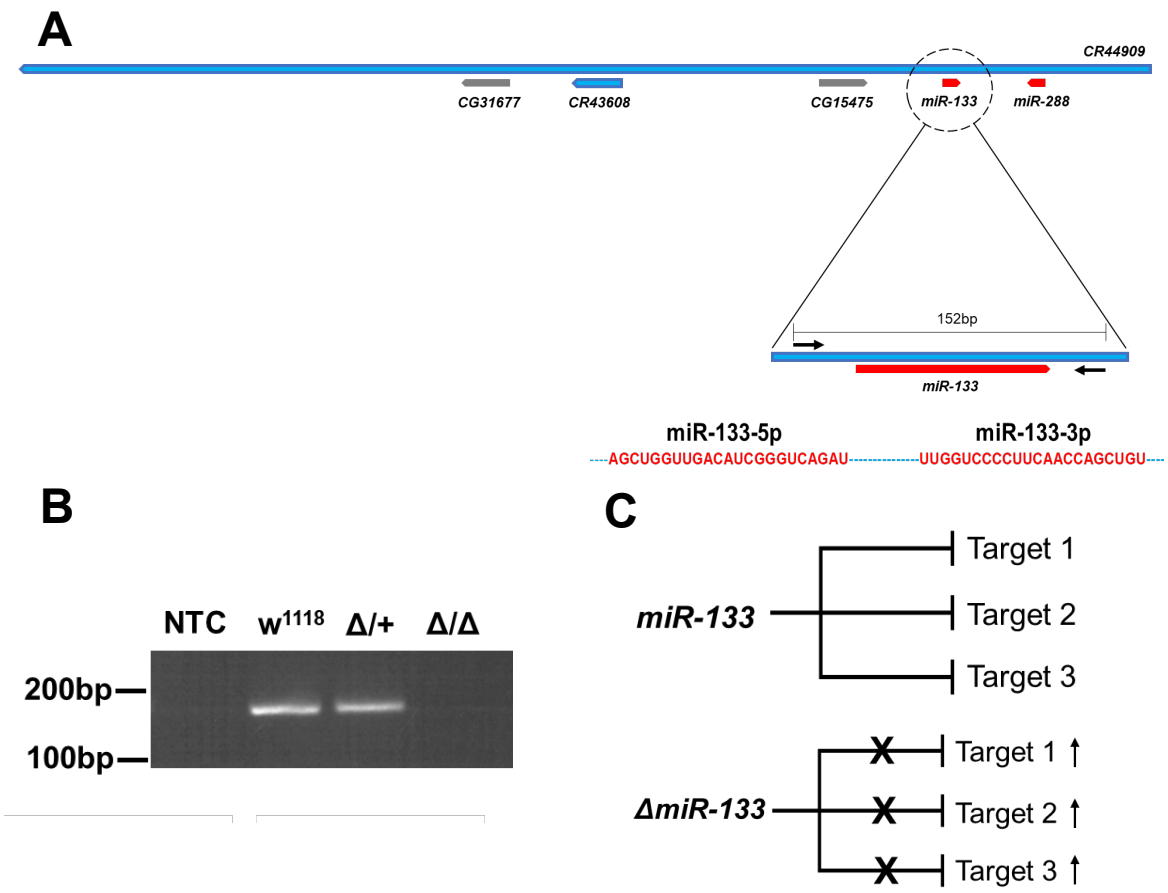

Figure 6.2.2 Genomic confirmation of lack of *miR-133* expression in Δ*miR-133* mutants

(A) The *miR-133* primary miRNA sequence is transcribed as part of the long non-coding RNA (lncRNA) *CR44909*. Two uncharacterised genes (*CG31677* and *CG15475*, grey) and another lncRNA (*CR43608*, blue) are also located within *CR44909*. To confirm lack of *miR-133* expression in Δ*miR-133* mutant flies, DNA primers (black arrows) were designed flanking the mature *miR-133* sequence to produce an amplicon of 152bp. The sequences of the -3p and -5p forms of the mature *miR-133* miRNA are shown below in red. (**B)** A representative agarose gel showing a lack of *miR-133* expression in homozygous (Δ/Δ) Δ*miR-133* mutant files. NTC = non-template control. **(C)** A

schematic demonstrating a model in which removal of *miR-133* expression by mutation results in the expression of *miR-133* target genes being upregulated.

6.2.3 Development of an intersectional *in silico* target prediction approach

To investigate the mechanism through which *miR-133* may regulate larval head-rearing, we applied *in silico* miRNA target prediction methods to search for mRNA transcripts whose translation or stability would normally be inhibited by *miR-133* binding. *In silico* approaches using algorithms for predicting miRNA-mRNA interactions (as well as characteristics such as the free energy of binding, the number of binding sites and binding site conservation) have become a powerful tool for researchers searching for mechanistic details about the roles of miRNAs (Witkos *et al.,* 2011).

One of the earliest target prediction methods developed was the miRanda algorithm, which primarily considers the level of complementarity (between an mRNA seed sequence and a mature miRNA sequence) and the conservation of these sequences into account when considering whether a miRNA-mRNA interaction is likely to occur *in vivo* (Enright *et al.,* 2003).

The TargetScan approach (developed in the same year as miRanda) applies an alternative strategy (Lewis *et al.,* 2003). Prioritizing the avoidance of false positives, predicted interactions are firstly filtered to remove those with less than perfect complementarity between the mRNA seed sequence and the mature miRNA sequence. The predicted interactions that remain, are then analysed for conservation through comparison with 3’ UTRs in organisms other than the organism queried by the user.

While these approaches both primarily use sequence complementarity as the initial basis upon which the likelihood of *in vivo* miRNA-mRNA binding is predicted, other approaches such as RNAHybrid (Rehmsmeier *et al.,* 2004)

primarily consider the favourability of interactions at the thermodynamic level as a basis upon which to initially filter potential *in vivo* interactions.

Of these thermodynamics-based target approaches, the first to consider the accessibility of the seed sequence in a 3' UTR was the PITA approach (Kertesz *et al.,* 2007). PITA works through the application of a model which firstly weighs the energy gained through miRNA-mRNA interaction against the energy needed to make the mRNA seed sequence accessible for miRNA binding. PITA, therefore, does not require perfect complementarity between miRNA and mRNA (unlike TargetScan) and Kertesz and colleagues report that this approach more accurately predicts miRNA-mRNA interactions *in vivo* (Kertesz *et al.,* 2007).

In this study, we sought to combine these analytic methods to provide the best balance between miRNA-mRNA interactions that were predicted to occur based on sequence complementarity and those that were predicted to occur based in favourable thermodynamics.

Our model was one in which the removal of the *miR-133* would lead to an increase in gene expression that would then lead to behavioural change (Figure 6.2.2C). To provide a starting point for the investigation of this model's accuracy, we used an intersectional *in silico* target prediction approach (seeking targets predicted in common by the three methods described above). Our aim was to identify genes that would, not only be likely to be regulated by *miR-133 in vivo* but also linked to behaviour and amenable to further mechanistic study.

6.2.4 Six genes are predicted to be *miR-133* targets by PITA, TargetScan, and miRanda

Firstly, we used the PITA prediction software (Kertesz *et al.,* 2007) to identify highly-conserved transcripts with 3'UTRs containing a 7 or 8 bp sequence complementary to the *miR-133* seed sequence, identifying 11 potential targets. These 11 targets were then cross-referenced with the 78 *miR-133* targets predicted using TargetScan software (Release 7.2) (Agarwal *et al.,* 2015) and the 134 *miR-133* targets predicted using miRanda software (Betel *et al.,* 2008) (Figure 6.2.3A).

This approach reveals 6 commonly predicted target transcripts: *aop* (or '*yan'*), *CG30158, CG17193, GalNac-T1* (or '*Pgant1'*), *Pde1c* and *Trh* (tryptophan hydroxylase) (Figure 6.2.3B).

CG30158 and *CG17193* are uncharacterised genes, while the glycosyltransferase *GalNac-T1* has not been previously linked to behaviour control. Of the remaining three genes, changes to the expression of the cyclic nucleotide phosphodiesterase *Pde1c* have only been linked to adult male mating behaviour (Morton *et al.,* 2010) and the transcription factor *aop* has been well-characterised as a developmental gene, regulating the differentiation of the photoreceptors (Lai and Rubin, 1992; Li and Carthew, 2005) as well as promoting dorsal closure during embryonic development (Harden, 2002). The remaining gene, *Trh*, encodes tryptophan hydroxylase - the rate-limiting enzyme catalysing the production of the neuromodulator serotonin (Lundell and Hirsh, 1994). As discussed in Section 1.4, serotonergic neuromodulation has been shown to be key for locomotor behaviour in a variety of organisms and the

identification of the *Trh* transcript as a potential *miR-133* target prompted us to investigate whether *miR-133* regulates head-rearing through regulation of the serotonergic system.

6.2.5 *miR-133* is predicted to bind to one site in the 3' UTR of the transcript encoding tryptophan hydroxylase

As in mammals, the production of the biogenic amine serotonin in *Drosophila* relies upon the hydroxylation of the amino acid tryptophan by tryptophan hydroxylase. 5-Hydroxy-tryptophan is then decarboxylated by the enzyme DOPA decarboxylase (or DDC) to produce serotonin (Figure 6.2.3C) (Lundell and Hirsh, 1994).

Predicted binding between *miR-133* and *Trh* transcripts is predicted by all three target prediction softwares to occur at one site in the 3'UTR (Figure 6.2.3D) and, according to the more detailed results given by miRanda, this site is 7bp long (base pairs 45-51 of the 3'UTR) and fully complementary to the seed sequence of *miR-133*.

The fact that tryptophan hydroxylase is a key component of the serotonergic system led us to hypothesise that the influence of *miR-133* on rearing behaviour may be mediated via the neuromodulatory system of the larval CNS. Another piece of evidence, independent from our miRNA target analysis, provided further support to this model. A study by Okusawa and colleagues showed that changes to the function of the larval serotonergic system promoted changes to rearing behaviour in larvae (Okusawa *et al.,* 2014), providing further support to

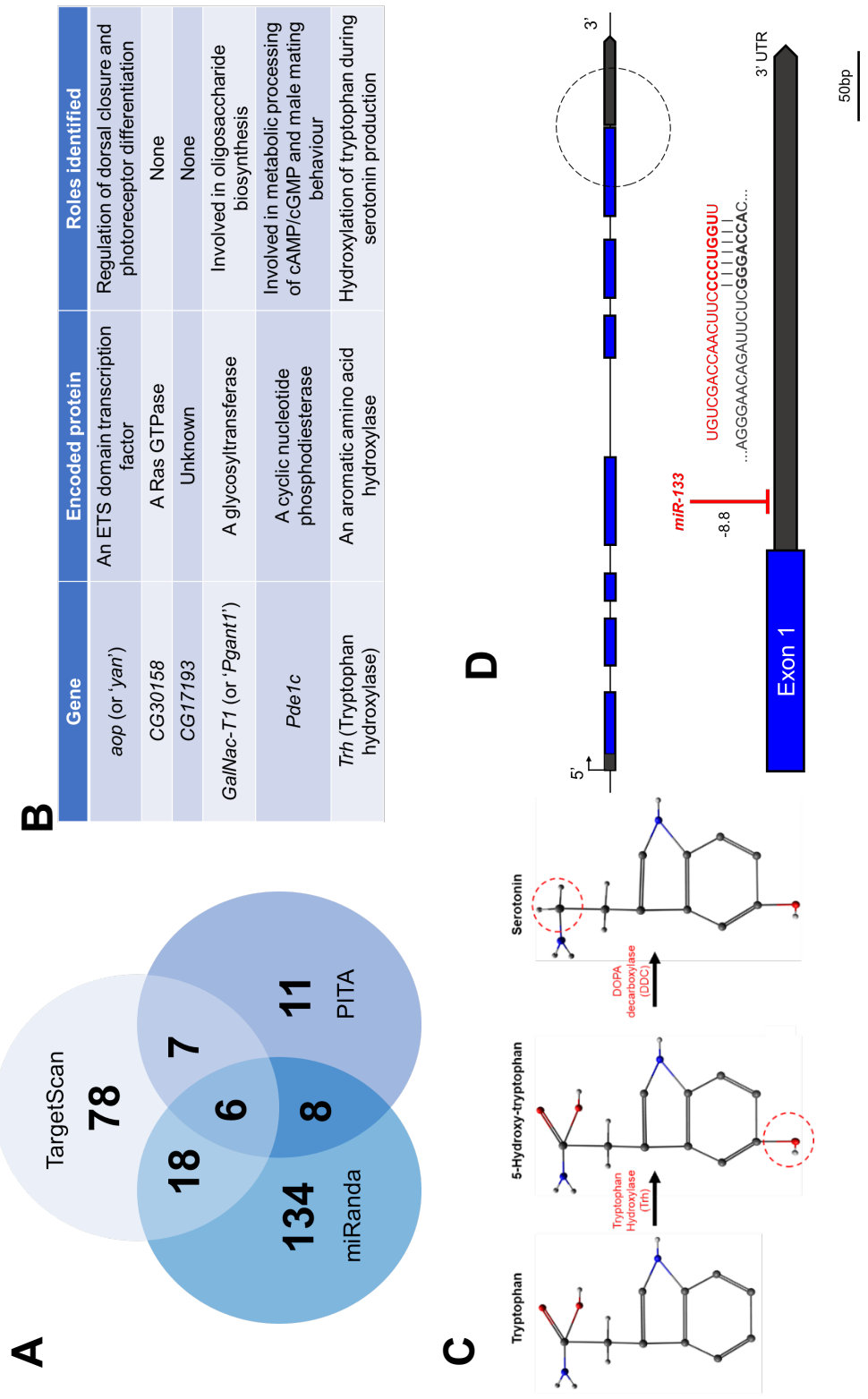

Figure 6.2.3 An *in silico* target prediction approach identifies the transcript encoding tryptophan hydroxylase as a likely *miR-133* target

(Legend on the following page)

(A) *miR-133* was predicted to interact with sequences in the 3’ UTR of six mRNA transcripts by all three target prediction softwares used (miRanda, PITA & TargetScan). **(B)** A summary of the six genes predicted in (A) as likely targets for *miR-133* binding. **(C)** The biosynthesis pathway of serotonin. Tryptophan hydroxylase catalyses the addition of a hydroxyl group to tryptophan to form 5-hydroxy-tryptophan (hydroxyl group circled in red). **(D)** A schematic showing the location of the predicted *miR-133* binding site in the 3’UTR of *Trh* mRNA transcripts. A 6bp sequence of the mature *miR-133* miRNA (red, bold letters) binds to a complementary sequence in the *Trh* 3’UTR (grey, bold letters). The PITA prediction score is also indicated.

the idea that *miR-133* may regulate the same behaviour through the same system.

6.2.6 Expression of *Trh* is significantly upregulated in *ΔmiR-133* mutant late-stage embryos

The hypothesis that *Trh* is a target of miR-133 leads to the prediction that removal of miR-133 expression will lead to an increase in *Trh* expression. To test this hypothesis, we examined whether there was a change to *Trh* expression in Δ*miR-133* mutants using RT-PCR.

We performed RT-PCR experiments using RNA from Δ*miR-133* mutant stage 16 embryos as this is the earliest point when serotonin is produced (Lundell and Hirsh, 1994) and is close to the early L1 larval stage in which we observe behavioural effects.

We designed a pair of DNA primers, of which one was complementary to a sequence within exon 7 of the *Trh* transcript, and one was complementary to a sequence base flanking the end of exon 6 and beginning of exon 7 to produce an amplicon of 495bp (Figure 6.2.4A, black arrows). The purpose of this design was to ensure that only cDNA reverse transcribed from the *Trh* mRNA transcript (as opposed to any potential contaminating genomic DNA) would be amplified in the subsequent PCR giving us the most accurate representation of *Trh* mRNA levels. We analysed these RT-PCR products using a combination of agarose gel electrophoresis and image processing software, normalising *Trh* expression to that of the housekeeping gene *actin*.

The results of our analysis show a significant increase in the expression of *Trh* in Δ*miR-133* mutant embryos when compared to controls (Figures 6.2.4B and 6.2.4C). We conclude therefore that, in the wild-type embryo, *miR-133* does negatively regulate the expression of *Trh* as predicted by *in silico* target prediction softwares. This result suggests that neuromodulatory processes are refined through post-transcriptional regulation and that this occurs during embryogenesis, potentially refining motor output as preparation for hatching..

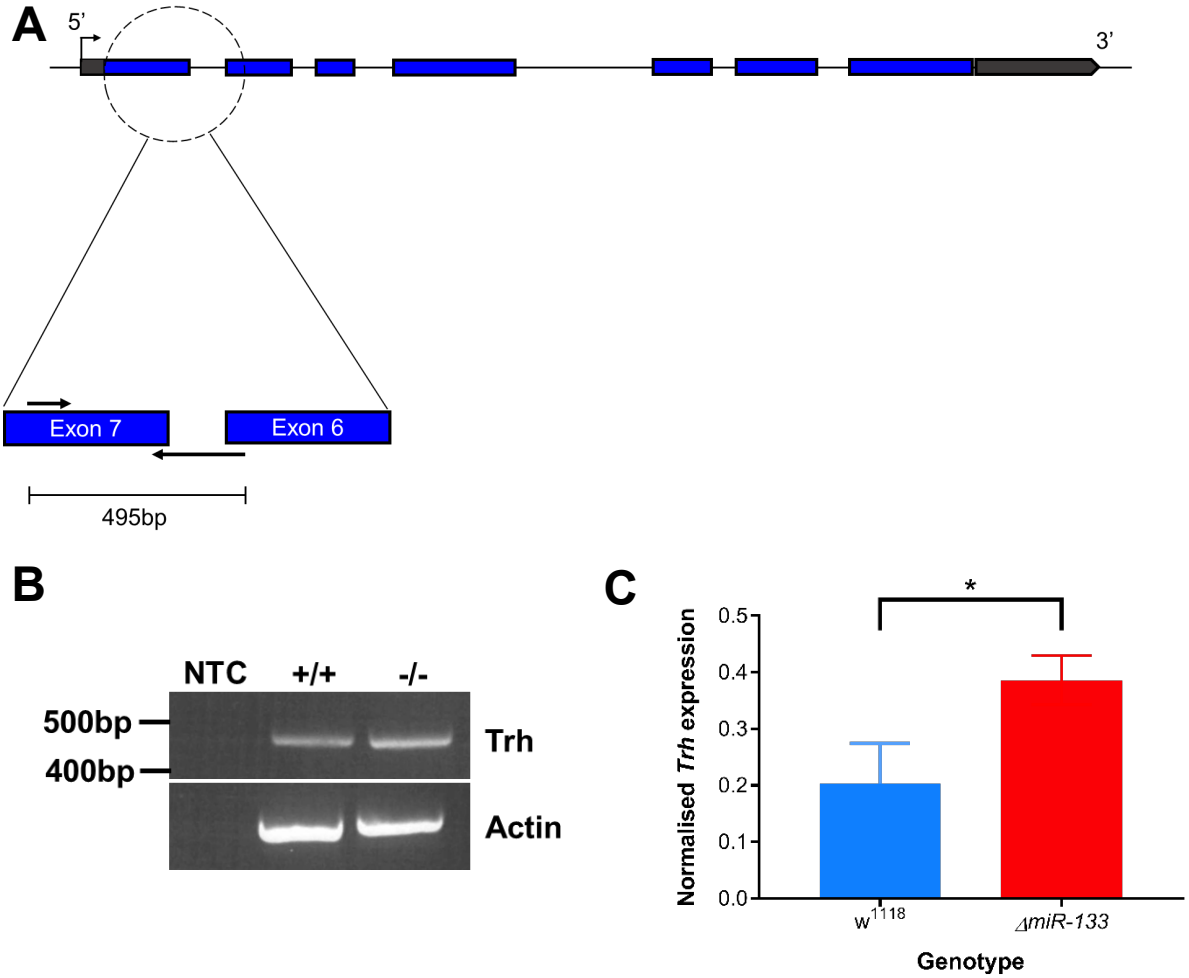

Figure 6.2.4 Elevated levels of *Trh* mRNA are present in *ΔmiR-133* mutants

(A) A schematic showing the structure of the *Trh* gene (exons are in blue, introns are represented by black lines between exons and UTRs are highlighted in dark grey). A pair of primers (black arrows) was designed with one primer flanking the exon 6-exon 7 junction in the *Trh* mRNA transcript to give an amplicon of 495bp using Reverse Transcriptase PCR (RT-PCR). **(B)** An example agarose gel showing an increase in *Trh* levels in Δ*miR-133* mutant cDNA (-/- lane) compared to wild type cDNA (+/+). NTC = non-template control. **(C)** Quantification of RT-PCR results demonstrates a significant increase in *Trh* expression in Δ*miR-133* mutant cDNA. (Mann-Whitney U test, mean ± SEM; n =

approximately 100 embryos per biological repeat; biological repeats and technical repeats were performed in triplicate and band intensities were normalised to the reference gene, *actin*).

6.2.7 Serotonin production is increased in the CNS of *ΔmiR-133* mutant larvae

6.2.7.1 The structure of the larval CNS serotonergic system

As previously discussed, tryptophan hydroxylase acts as the rate-limiting enzyme in the production of serotonin (Monastirioti, 1999) and is therefore used as a marker for serotonergic neurons in *Drosophila* (Huser *et al.,* 2012).

The CNS serotonergic system of the *Drosophila* first instar (L1) larva consists of a pair of serotonergic neurons in each abdominal hemisegment of the ventral nerve cord (except in the most posterior abdominal hemisegments which contain one serotonergic neuron each) (Lundell and Hirsh, 1994) (Figure 6.2.5A). In the third instar (L3) larva, serotonergic expression has also been mapped to small, specific clusters of neurons within the brain lobes (Vallés and White, 1988; Huser *et al.,* 2012). Lundell and Hirsh (Lundell and Hirsh, 1994; Lundell *et al.,* 1996) have confirmed that serotonergic expression is also present in the brain lobes of L1 larvae but no full characterisation of the structure of these neuronal clusters at this stage has been performed.

6.2.7.2 Investigating serotonin levels in the CNS of *ΔmiR-133* mutant larvae

As previously shown, the removal of *miR-133* expression in mutant *Drosophila* leads to a significant increase in *Trh* expression (Figure 6.2.4C). As the rate-limiting enzyme catalysing the production of serotonin, we hypothesised that an increase in *Trh* expression would lead to an increase in serotonin production by serotonergic neurons of the early L1 CNS. Therefore, if *Trh* expression was

increased as a result of the removal of miR-133 expression, we expected serotonin production to be increased in the Δ*miR-133* mutant CNS.

To test this, we performed an immunohistochemistry experiment, staining central nervous systems from early L1 Δ*miR-133* mutant larvae with an antibody against serotonin (Sigma-Aldrich, S5545) (Figure 6.2.5B). We imaged these stained CNS' using a confocal microscope to produce Z-stacks and subsequently used image processing software to quantify the level of fluorescence produced by antibody-target binding as a measure of serotonin levels (the "gray value"). These measures were normalised by the gray values of non-fluorescent regions of the CNS, and the maximum expression was then plotted as a percentage of the maximum control value.

The results of this analysis show a general increase in serotonin production by serotonergic neurons of the Δ*miR-133* mutant CNS (Figure 6.2.5C). Comparing the ventral nerve cords (VNCs) of Δ*miR-133* mutants to those of the wild type, we identify higher average serotonin production in the serotonergic neurons of all three thoracic segments and all eight abdominal segments except A4. While the ranges of fluorescence fluctuate along the length of the VNC, in segments T1, A2, A5 and A6 we observe a strong increase in serotonin expression in the Δ*miR-133* mutant compared to w^{1118}. From the result of this experiment, we therefore conclude that (in accordance with previous experiments showing a significant increase in *Trh* expression in Δ*miR-133* mutants) the removal of *miR-133* results in increased serotonin production in the early L1 CNS.

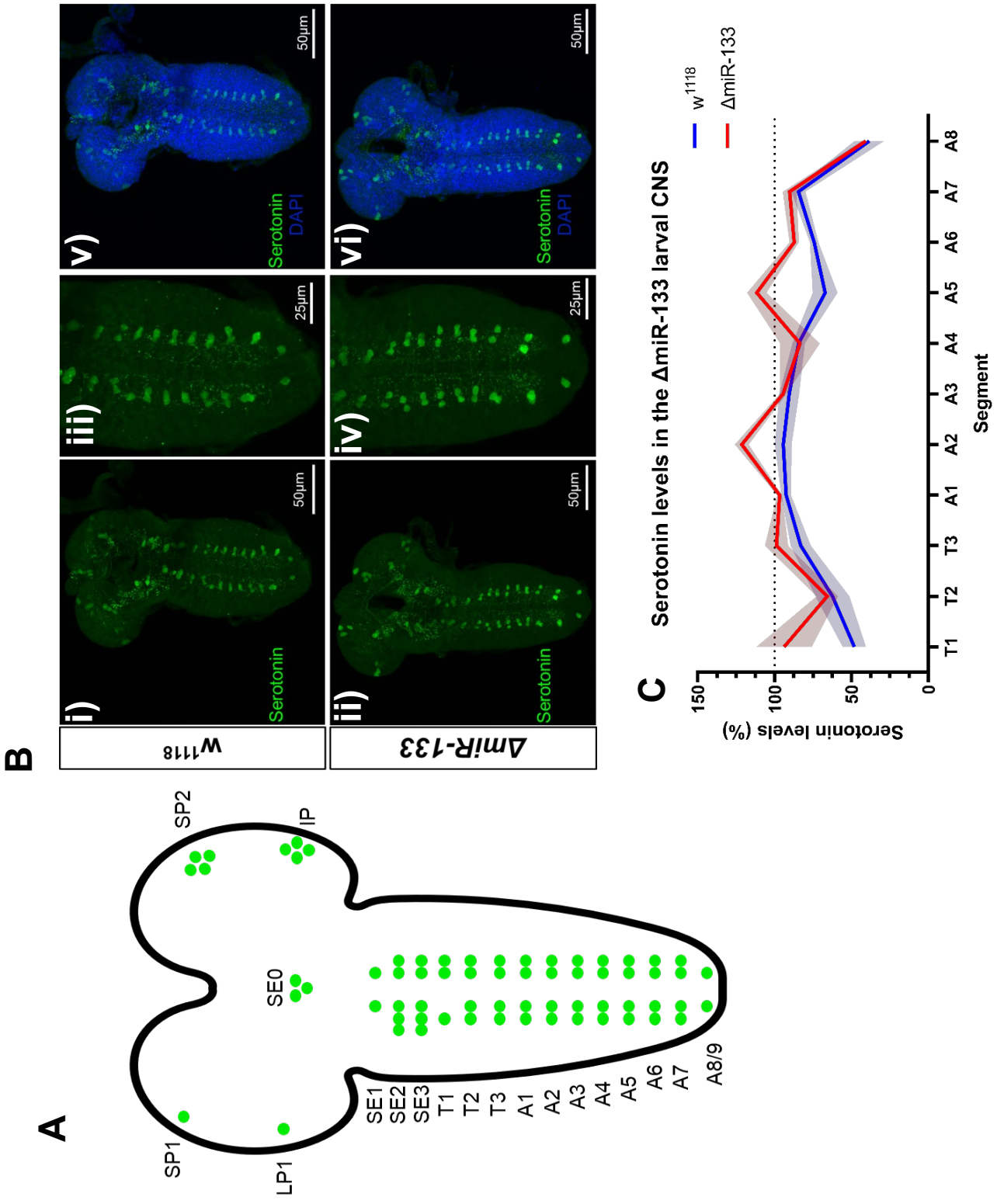

Figure 6.2.5 Elevated levels of serotonin protein are present in *ΔmiR-133* mutants

(Legend on the following page)

(A) A schematic showing the position of the serotonergic neurons (green) within the larval central nervous system. **(B) (i and ii)** Immunohistochemistry was used to reveal serotonin protein expression (green) in central nervous systems of w^{1118} and Δ*miR-133* first instar larvae. **(iii and iv)** Magnified images of the serotonergic neurons of the ventral nerve cord in images i) and ii) respectively. **(v and vi)** Central nervous systems were also counterstained with DAPI (blue). **(C)** Quantification of serotonin protein expression in w^{1118} and Δ*miR-133* first instar larval central nervous systems. Along the ventral nerve cord, levels of serotonin protein in most pairs of serotonergic neurons were elevated in Δ*miR-133* larval central nervous systems compared to w^{1118} larval central nervous systems (n = 21, SEM is indicated by the shaded areas).

6.2.8 The expression of *miR-133* is detectable in larval serotonergic neurons

To confirm the expression of *miR-133* within the serotonergic neurons of the larva, we considered many approaches including *in situ* hybridisations with probes designed against *miR-133* and the creation of a new transgenic fly line in which a sequence encoding GAL4 replaced the *miR-133* locus. *In situ* hybridisation of miRNAs presents a technical challenge due to their small size and although the creation of a new line with a GAL4 sequence replacing *miR-133* locus is feasible, it is also a lengthy process. To localise miRNA expression in the most efficient manner possible, therefore, we applied an approach comprising fluorescent-activated cell sorting (FACS) to isolate serotonergic cells and real-time quantitative PCR (qPCR) for transcriptional analysis (Klann *et al.,* 2020).

Briefly, we used the GAL4-UAS binary expression system (Brand and Perrimon, 1993) to produce a line of flies expressing myristolated GFP (mGFP) in neurons expressing tryptophan hydroxylase. These flies are referred to as "*Trh*>GFP" flies. We then used a combination of papain and collagenase (Harzer *et al.,* 2013) to chemically dissociate early L1 larvae from a GFP-negative control line and the *Trh*>GFP line separately, producing cell suspensions (Figure 6.2.6A) from which populations of GFP-negative (control) and GFP-positive (serotonergic) cells could be selectively isolated using FACS (Figures 6.2.6A' and 6.2.6B). Finally, we extracted RNA from sorted serotonergic cell enriched and control cell populations and synthesised cDNA that was used in qRT-PCR to examine the expression levels of *miR-133* in early larvae. In all qRT-PCR

experiments, expression data was normalised to the expression of the housekeeping gene, *actin*.

The results of our analysis (Figure 6.2.6C) show that, compared to the control sample (in which a random selection of GFP-negative cell types was sorted), expression of GFP and *Trh* is increased in the serotonergic cell enriched population (as expected). As expected, we also observed a large decrease in expression of the motor neuron marker VGlut (Mahr & Aberle, 2006) in the serotonergic cell enriched population compared to the control population of random cells (data not shown). The expression of *miR-133* was detected in serotonergic-cell enriched populations and mildly upregulated (a 0.34-fold increase) compared to control populations (n = 150 larvae per population). We, therefore, suggest that the although the expression of *miR-133* is detected in serotonergic cells, it occurs at low levels.

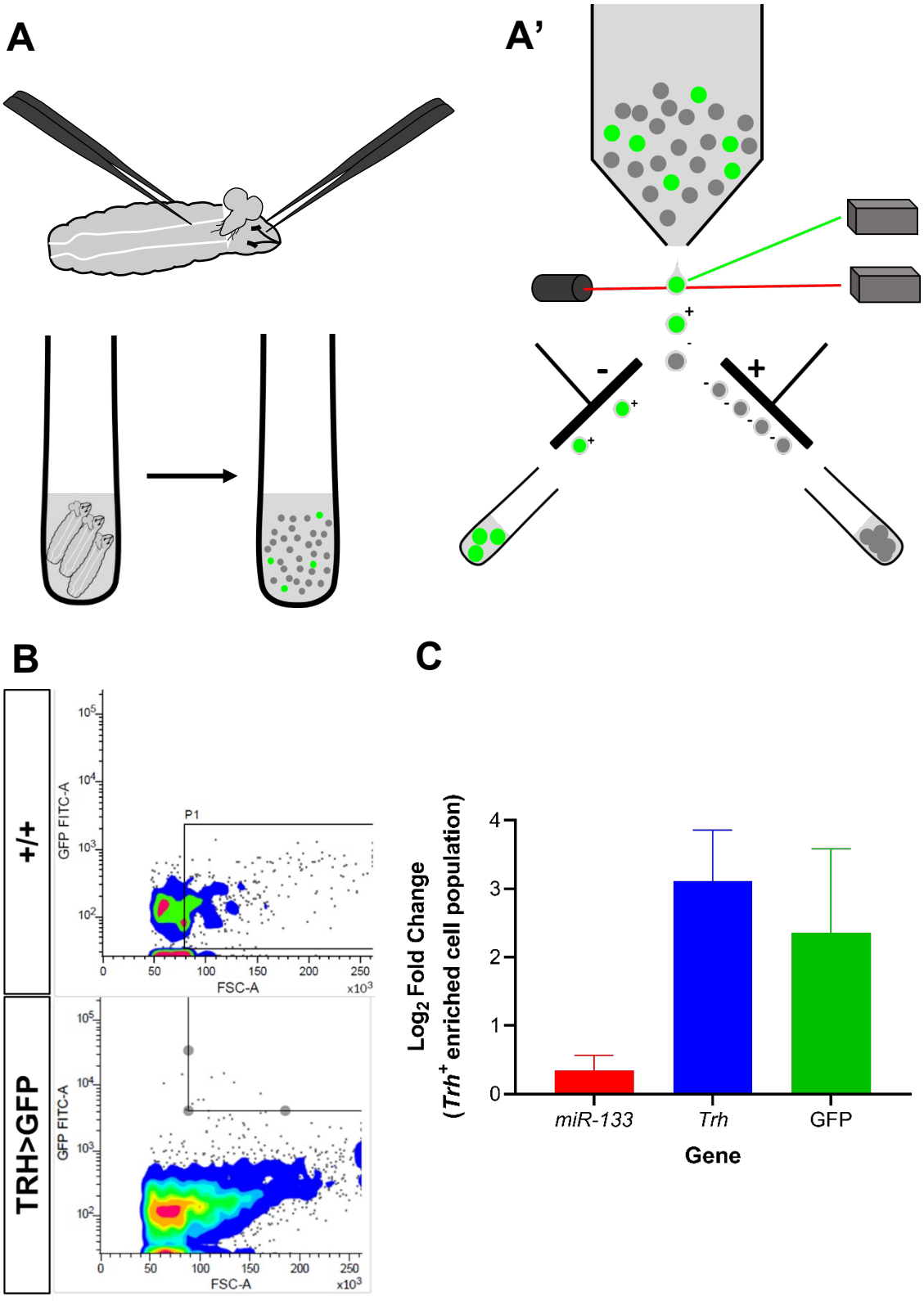

Figure 6.2.6 *miR-133* is expressed in the serotonergic neurons of the first-instar larva

(Legend on the following page)

(A and A') A schematic demonstrating the FACS protocol used to study miRNA expression in serotonergic cells. **(A)** Larvae were dissected to expose the CNS and chemically dissociated using collagenase and papain to create a cell suspension. **(A')** FACS was then used to isolate GFP-labelled serotonergic neurons from the central nervous systems of *Trh*>GFP larvae. RNA was then extracted from this serotonergic cell enriched cell population, converted to cDNA, and profiled using quantitative PCR (qRT-PCR). **(B)** Examples of equivalent gates (black rectangles) used during FACS to isolate GFP-negative control (+/+) and GFP-positive serotonergic (*Trh*>GFP) cells by size and fluorescence. **(C)** qPCR results show that the expression of *miR-133* is detectable and mildly increased in RNA from a serotonergic cell enriched cell population (n = 50 larvae per genotype per biological repeat, biological and technical repeats were performed in triplicate).

6.2.9 Artificially upregulating serotonin production in larvae is sufficient to phenocopy increased rearing behaviour

Having identified a significant increase in the expression of *Trh* in Δ*miR-133* mutants (Figure 6.2.4C) as well as increased serotonin production by serotonergic neurons (Figure 6.2.5C), we sought to confirm a link between increased serotonin production and increased larval head-rearing behaviour.

To do this, our approach consisted of artificially increasing (or "overexpressing") *Trh* expression in the early L1 larva. We used the GAL4-UAS binary expression system (Brand and Perrimon, 1993) previously used to produce *Trh*>GFP flies (Section 6.2.8) to produce a line of "*Trh*>*Trh*" flies overexpressing *Trh* in serotonergic neurons (Figure 6.2.7A). Our hypothesis was that in larvae overexpressing *Trh*, serotonin production would be increased and as a consequence would lead to a significant increase in rearing behaviour.

We analysed rearing behaviour in early L1 *Trh*>*Trh* larvae as well as in two other control genotypes, larvae with one copy of the *Trh*-GAL4 gene and larvae with one copy of the UAS-*Trh* gene. The results of our analysis show that artificially increasing serotonin production in larvae by overexpressing *Trh* results in a significant increase to rearing behaviour (Figures 6.2.7B and 6.2.7C). In addition to this, larvae from the two control genotypes do not rear significantly more or less than each other indicating that the singular expression of either *Trh*-GAL4 or UAS-*Trh* has no significant effect on behaviour.

We interpret the phenocopying of the rearing phenotype observed in Δ*miR-133* mutants as support for a model in which increased serotonin production leads to specific behavioural change in the form of significantly increased rearing.

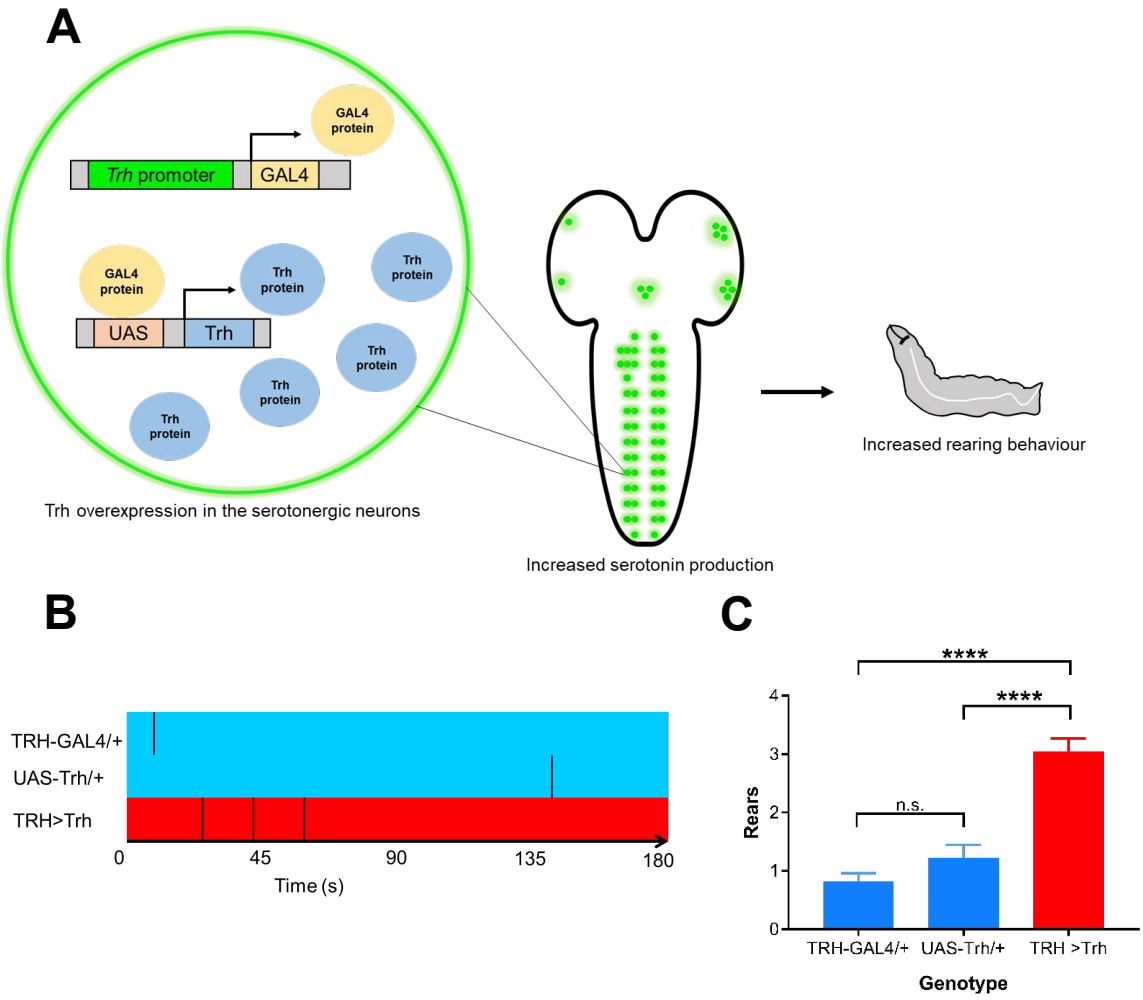

Figure 6.2.7 Increased rearing behaviour in *ΔmiR-133* larvae can be phenocopied by artificially increasing serotonin production within the *Trh* domain

(A) A schematic showing the strategy for the *Trh* overexpression experiment. The larval progeny of a cross between *Trh*-GAL4 and UAS-*Trh* flies express the GAL4 transcription factor in the *Trh*-positive serotonergic cells where it promotes transcription of *Trh* by binding to the upstream UAS. The increased production of *Trh* is expected to increase serotonin production by the serotonergic neurons and we hypothesise that this will increase rearing

behaviour by the larva. **(B)** A schematic of the frequency of rearing events in representative control (TRH-GAL4/+ and UAS-Trh/+) and *Trh* overexpressing larvae. Rearing events during filming are represented by black vertical lines. **(C)** Quantification of rearing behaviour in larvae overexpressing the *Trh* gene. Larvae overexpressing the *Trh* gene (TRH > Trh, red) rear significantly more than control larvae from parental strains (TRH-GAL4/+ and UAS-Trh/+, blue) (Kruskal-Wallis ANOVA test, n.s. = non-significant, mean ± SEM; n = 45).

We also suggest that these results, in combination with previous data, provide support to the idea that the upregulation of *Trh* expression caused by *miR-133* mutation causes an increase in serotonin production which is then the cause of the changes to rearing behaviour observed in Δ*miR-133* mutant larvae.

6.2.10 A model for *miR-133* based regulation of rearing behaviour in *Drosophila* larvae

Although rearing behaviour in *Drosophila* larvae was described in the 1980s (Green *et al.,* 1983), very little is known about the neural substrates underlying this behaviour. In 2014, Okusawa and colleagues investigated rearing behaviour as a component of turning in L3 larvae, and identified a role for leucokinergic interneurons in rearing control (Okusawa *et al.,* 2014). These leucokinergic neurons (the “abdominal LK neurons” or ABLKs) were also found to express the serotonin receptor 5-HT1B and the authors demonstrated that the addition of a chemical agonist to serotonin production is sufficient to reduce rearing behaviour (Discussed in more detail in Section 6.3).

In order to develop a comprehensive mechanistic understanding of the role of the serotonergic system in the control of rearing behaviour, however, it is necessary to identify the neuromuscular systems that are subject to serotonergic neuromodulation during rearing. Currently, the motor neurons and muscles responsible for rearing control remain unidentified, however, our behavioural observations (Figure 6.2.1) lead us to postulate that the dorsal motor neurons (such as aCC, RP2, RP5 etc.) and potentially longitudinal motor

neurons (such as LO1) may be involved in the raising of the body's anterior from the substrate.

From the results of the study performed, however, we conclude that we have demonstrated the involvement of serotonergic neurons in the control of rearing and that the amount of serotonin they produce is dependent upon *miR-133* control of *Trh* expression.

We also conclude that miRNA-based regulation of motor control does not only act in an on-off fashion (i.e., ensuring that crawling occurs at the "correct" speed or not) but also acts to regulate more subtle aspects of locomotion. Our initial identification of *miR-133* as a miRNA involved in the regulation of average pause duration during locomotion led us to the identification of its role in rearing, a behaviour that we could not observe in our initial FIMTable recordings. We suggest therefore that the involvement of miRNAs in larval motor control may be even more pervasive than originally imagined, regulating a wide variety of unexplored behavioural sequences at both the larval and adult stages.

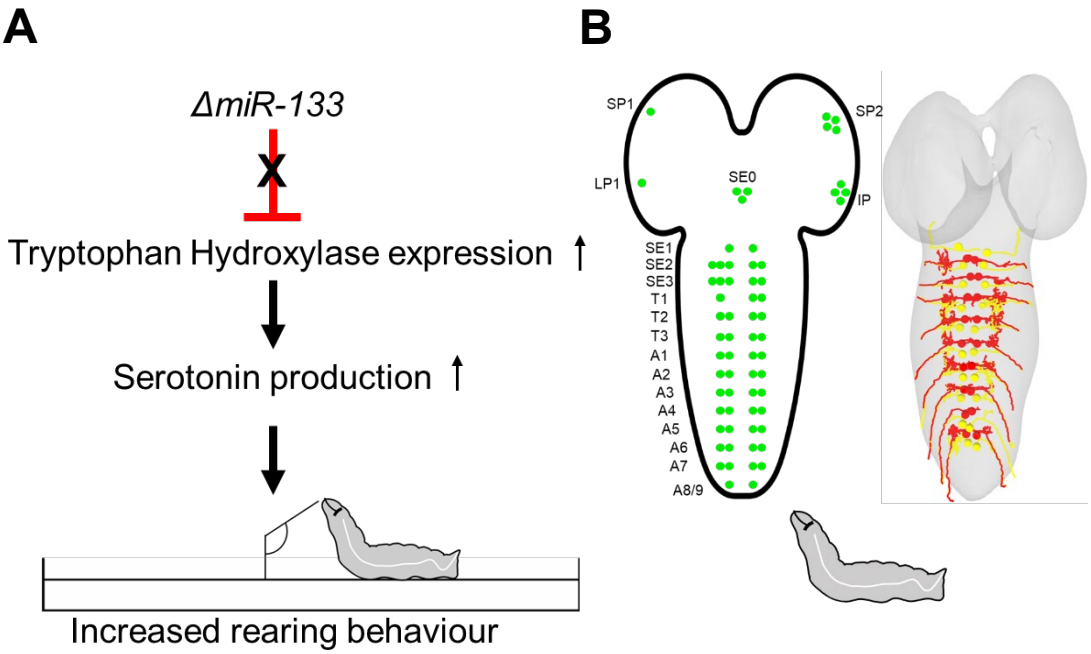

Figure 6.2.8 A model for *miR-133* regulation of pause behaviour in first instar larvae

(A) A schematic showing a model for *miR-133* control of larval head-rearing behaviour. Removal of *miR-133* expression leads to an increase in the expression of *Trh*, which, in turn, leads to an increase in serotonin production. This increase in serotonin production leads to a significant increase in rearing during locomotion. **(B)** We suggest that as well as serotonergic neurons (green), neuromuscular control of rearing in larvae might also involve the activity of dorsal motor neurons such as aCC (red) and RP2 (yellow).

6.3 Discussion

In this chapter, we identify a novel role for *miR-133* in larval head-rearing behaviour. We present a model in which, in the wild type larva, *miR-133* negatively regulates the expression of the biosynthetic enzyme, tryptophan hydroxylase. The negative regulation of *Trh* expression results in a decrease in serotonin production by the serotonergic neurons of the larval central nervous system (CNS) which, in turn, leads to a suppression of rearing during locomotion.

As previously mentioned, little is known about the neuromuscular basis of rearing behaviour and, to date, only one study has examined the neural basis of the behaviour (Okusawa *et al.,* 2014). In this study, Okusawa and colleagues examined rearing behaviour as a component of larval turning in third instar (L3) larvae, identifying a role for leucokinin-producing neurons (the 'ABLKs') expressing 5-HT1B serotonin receptors in rearing control (Okusawa *et al.,* 2014). Our identification of tryptophan hydroxylase (the main rate-limiting enzyme in serotonin production) as a target for negative regulation by *miR-133*, therefore, presents a strong argument for *miR-133* effects on rearing being mediated via the larval serotonergic system.

The conclusions of this study, however, stand in contrast to the results of Okusawa *et al.,* 2014. Okusawa and colleagues demonstrated that thermogenetic inhibition of serotonergic neuron activity led to a significant increase in rearing. They also demonstrated that addition of a serotonin agonist (8-OH-DPAT) resulted in a corresponding suppression of rearing. Both of these results contrast with what we would expect from the model developed in this

chapter. We do, however, note important differences between the studies of Okusawa and colleagues and the one presented in this chapter.

Firstly, we observe significant changes to rearing behaviour in early first instar (L1) larvae whereas Okusawa and colleagues performed their study in L3 larvae. As indicated by earlier analyses (Section 5.2.8), regulation of motor behaviours by miRNAs varies over larval development and we previously observed an amelioration of the increased average pause duration phenotype in Δ*miR-133* mutants at the L3 stage (Figure 5.2.21). This raises the question of whether importance of serotonergic signalling to average pause duration changes over development and whether the relationship presented by Okusawa and colleagues is specific to the L3 larva.

We also note that Okusawa and colleagues remarked upon the temperature-dependence of the effects they observed. After thermogenetically inhibiting the activities of serotonergic neurons and the 5-HT1B receptors, they also tested a non-temperature dependent method of neuronal inhibition (UAS-Kir) and observed a degree of temperature-dependence to their results. All behavioural studies in this chapter were performed in an environment consistently maintained at 25˚C, a temperature in which Okusawa and colleagues identified no significant relationship between manipulation of serotonergic activity and incidences of rearing. We therefore suggest that the presence of thermal stimuli may also influence the behavioural results presented by Okusawa and colleagues after serotonergic manipulation and that the results of this study may characterise rearing behaviour with more consistency.

We hypothesise that the results presented by Okusawa and colleagues and those presented in our study could be reconciled by the consideration of a model in which the constant overproduction of serotonin (as a result of de-repression of *Trh* expression) saturates serotonergic receptors in the Δ*miR-133* mutant CNS. This would, in turn, lead to serotonergic receptors losing the ability to respond to further serotonergic signalling and we would expect the behavioural consequence of this to mimic that of no serotonin production at all.

A study by Moncalvo and Campos provides further context to our work (Moncalvo and Campos, 2009). Here, the authors examine the relationship between serotonin signalling and larval response to light exposure during locomotion. Moncalvo and Campos show that, in L3 larvae, artificially reducing the activity of serotonergic neurons increases the average duration of light-induced pauses during locomotion. While we conclude the inverse (that increases in serotonin production increases the average duration of pauses), a factor differentiating our study from that conducted by Moncalvo and Campos is the presence of constant light (infrared and visible wavelengths) exposure during locomotion.

We observe significant increases in average pause duration of L1 Δ*miR-133* mutant larvae during recording with the FIMTable (Figure 5.2.12) under infrared light as well as significant increases in rearing in L1 Δ*miR-133* mutant larvae under constant visible light. Therefore, the relationship between serotonin signalling and pausing response to light exposure is difficult to compare to the relationship between serotonin signalling and pausing behaviours generated spontaneously during locomotion. Indeed, Huser and colleagues (Huser *et al.,* 2012) have since presented results of refined phototaxis assays in *Drosophila*

larvae that stand in contrast to those of Moncalvo and Campos; leaving the role of serotonin in light-induced larval pausing open for debate.

The results presented in this chapter open many questions for future study. A more detailed characterisation of rearing would be a novel addition to what is already known about larval motor behaviour, especially as the behaviour is part of a select group of three-dimensional larval behaviours and has been relatively rarely investigated. A more in-depth analysis of metrics such as the duration of each rearing event and the angle formed between the anterior larval segments and the substrate could provide clues about the neuromuscular basis of rearing control. This, in turn, could enable a better understanding of exactly how serotonergic neuromodulation affects motor behaviour by regulating motor neuron output.

We also note that in this study, we chose to study *miR-133* as it was the miRNA whose mutation led to the most severe increase in average pause duration of a group of 3 miRNA mutants. Two other miRNA mutants (Δ*miR-219* and *ΔmiR-970*), represented miRNAs that were also predominantly expressed in the CNS and shared similar behavioural profiles with *miR-133*, leaving the question open of whether they too regulate pause duration by regulating head-rearing behaviour. Indeed, there may be a degree of hierarchy to the importance of each miRNA's influence on rearing behaviour due to compensatory effects (i.e., the removal of *miR-970* may have a less severe effect on rearing than *miR-219* as upregulation of *miR-219* targets compensates for upregulation of *miR-970* targets).

Finally, it is important to note that we observe a reduction in average pause duration of Δ*miR-133* mutant larvae at the L3 stage to the point that it is not significantly different to control larvae (Figure 5.2.21). This raises the question of whether mechanisms develop during development to offset upregulation of *Trh*, whether the different size and physical properties of larvae at L1 and L3 significantly affect rearing behaviour, or whether the significance of the relationship between *miR-133* and *Trh* changes over development due to a change in miRNA expression levels in the serotonergic neurons. Confirmation of these hypotheses could have important implications for our view of neuromodulation and its relationship to behaviour over the course of larval development.

Chapter 7

General Discussion

7.1 General discussion

In this thesis, we explore the molecular-cellular basis of behaviour. In the first part, we determine the cellular basis for control of a complex motor behaviour in the *Drosophila* larva using connectomics and functional perturbations. In the second part, we examine the extent to which miRNAs affect larval locomotion, identifying pervasive changes to crawling speed, turning, and pausing. Finally, we demonstrate a previously-unknown mechanistic link between *miR-133* and control of larval pausing behaviour through the serotonergic system.

miRNAs are key for nervous system development and functional behavioural output throughout the animal kingdom (reviewed in Meza-Sosa *et al*., 2011 and Sun and Lai, 2013). Since the mid-20th Century, the genetically amenable fruit fly *D. melanogaster* has been widely used as a model organism for the study of behavioural genetics (Benzer, 1967; Hotta and Benzer, 1972; 1976) and has emerged as a particularly useful model organism for the study of miRNA-based regulation of behaviour.

The miRNA *miR-iab-4* is essential for self-righting in the *D. melanogaster* larva and negatively regulates *Ultrabithorax* (*Ubx*) expression in the LT-1/2 motor neurons (Picao-Osorio *et al*., 2015; Issa *et al*., 2019). In addition, the results of a genetic screen conducted by our lab have also demonstrated that the normal expression of at least 47 other miRNAs are necessary for normal larval self-righting (Picao-Osorio *et al*., 2017).

Determining whether these miRNAs are exerting an influence throughout a behavioural circuit or in specific elements is important to facilitate an understanding of how they regulate self-righting behaviour. To investigate this,

we firstly mapped the structure of the minimal neuronal circuit underlying larval self-righting behaviour, utilising an approach based on *in silico* neuronal reconstruction and connectomic analysis (Saalfeld *et al*., 2009; Schneider-Mizell *et al*., 2016). From this approach, we successfully produced a wiring diagram for information flow between larval sensory components and the LT-1/2 motor neurons which, in turn, enabled us to investigate whether the neurons of the self-righting wiring diagram function as a circuit to control self-righting *in vivo.*

We examined this by thermogenetically inhibiting the neurons of the wiring diagram to establish the necessity of their activity during self-righting and validated the role of most wiring diagram neurons. The establishment of a cellular “map” (upon which the expression of miRNAs known to regulate self-righting behaviour could be plotted in future) prompted us to question the generality of miRNA effects on larval motor behaviour and we investigated whether larval locomotion is also dependent on miRNA-based regulation of gene expression.

We addressed this question with a screen for locomotor defects in miRNA mutant larvae, the results of which revealed pervasive changes to crawling, pausing, and turning behaviours at different developmental stages. The identification of pausing as a behaviour particularly sensitive to miRNA mutation led us to examine the mechanisms through which miRNAs regulate larval pausing behaviour and, after selecting *miR-133* for in-depth analysis, we identified a mechanism involving the larval serotonergic system and the control of head-rearing behaviour.

7.2 The neural circuit underlying self-righting behaviour in *Drosophila* larvae

In the first part of this thesis, we identify a substantial segment-specific component to the morphology and connectivity of the LT-1/2 motor neurons (themselves, previously identified as key cellular substrates for self-righting behaviour by Picao-Osorio and colleagues (Picao-Osorio *et al*., 2015). We reconstruct the neurons in the posterior segments and identify fluctuations in morphology and connectivity as well as an increase in the rarity of input synapses towards the posterior of the VNC (Figure 3.2.2).

Considering the genetic mechanisms which could influence this arrangement, the Hox genes are well-known to be key drivers of segmental identity in the *Drosophila* larva (reviewed in Technau *et al*., 2014) and prior to the discovery of a role for *Ubx* in the functional activity of the LT-1/2 motor neurons (Picao-Osorio *et al.,* 2015), were primarily considered to be “developmental” genes. It has been previously hypothesised that the organisation of the circuits underlying the peristaltic waves of contraction that facilitate locomotion may be reliant upon the co-ordinated expression of Hox genes (reviewed in Jung and Dasen, 2015) and we propose that the case of the LT-1/2 motor neurons may represent just a single example of simultaneous developmental and functional roles for the Hox genes in the *Drosophila* CNS.

The structure of the wiring diagram we elucidated for self-righting is complex, including input from two sets of sensory components and information processing between 15 sets of interneurons (Figure 3.2.9). We began the construction of the wiring diagram by identifying neurons providing substantial

input to the LT-1/2 motor neurons and, not only confirmed input from five, previously-identified premotor interneurons (Zwart *et al*., 2016), but also a completely uncharacterised neuron named A26f. The identification of A26f as a contributor to the premotor input provided to the LT-1/2 motor neurons indicates that, even with the amount of collaborative reconstruction performed using CATMAID (including a previous study of LT-1/2 premotor input (Zwart *et al*., 2016)), much remains unknown about the structure of the neuronal networks comprising the CNS. This is attested to by the constant stream of new CATMAID-based insights being reported and even as recently as March 2021, new neurons were still being discovered and characterised (Hiramoto *et al*., 2021).

At the behavioural level, the self-righting sequence (that the neurons of the wiring diagram facilitate) begins with attempts by the larva to gain purchase on the substrate with its mouth hooks by bending its body and ends with a dorsoventral 180˚ rotation (Picao-Osorio *et al*., 2017; Loveless *et al*., 2020). The neural circuits underlying individual behaviours that comprise parts of this modular sequence (e.g., C-bending and rolling) have already been elucidated (Ohyama *et al*., 2015; Burgos *et al*., 2018) and it was expected that these cellular substrates would be present as part of the cellular network that facilitates the self-righting sequence.

Burgos and colleagues have reported that the Down-and-Back interneurons (which facilitate C-bending behaviour) show “modest” connections to the LT1 motor neuron in their own reconstruction work (Burgos *et al*., 2018) and suggest a potential relationship with self-righting behaviour based on the work carried out by Picao-Osorio and colleagues (Picao-Osorio *et al*., 2015). We confirm

these Down-and-Back to LT1 connections with our reconstruction/connectomics work as well as confirming the connections between this Down-and-Back-to-LT1 circuit and the circuit controlling rolling behaviour previously identified by Ohyama and colleagues (Ohyama *et al*., 2015).

We also note that the structure of the wiring diagram underlying self-righting behaviour includes various sensorimotor pathways (Figure 3.2.9) however, our connectomics analysis indicates that these pathways are not conserved in each abdominal segment (Figure 3.2.10 to 3.2.12) suggesting that there may be a degree of segment-specificity to the control of the LT-1/2 motor neurons during self-righting. Segment-specific influence on behavioural output has been demonstrated before in the case of the nociceptive integrator A02o 'Wave' interneurons (Takagi *et al*., 2017) however, it has never been demonstrated in the control of complex, modular motor behaviour such as self-righting. Future study could ablate the activity of the LT-1/2 motor neurons (or other upstream components in these sensorimotor pathways) in a segment-specific manner, observing how behavioural output changes as a result.

The deduction of the overall structure of the "average" self-righting circuit (Figure 3.2.9) and subsequent connectomic analysis also reveals substantial differences between the strength of synaptic connections on the left and right of the VNC. As discussed in Section 3.3, we hypothesise that these asymmetries may be underlying factors in the decision to make initial attempts to self-right towards the larva's left and right-hand sides. We note that the CATMAID volume used to serially reconstruct the neurons of the self-righting wiring diagram comprised of one larva (Saalfeld *et al*., 2009) and it would be informative to reconstruct the same set of neurons in a different CATMAID

volume to examine similarities and differences in neuronal architecture. From experiments performed in our lab on a limited number of larvae, we have observed that the decision to self-right towards the left or right-hand side appears unrelated to the direction in which inversion is performed suggesting that, if synaptic asymmetries do indeed underlie the directionality of self-righting, this may be an intrinsic “handedness” determined during the course of embryonic development. This mechanism may also be conserved as, for example, studies of self-righting in the cockroach have shown that asymmetrical wing-opening more successfully facilitates the completion of the self-righting sequence (Li *et al*., 2017). Although morphologically distinct from the *Drosophila larva* there is, therefore, potential for the neural basis for the decision to open the left or right wings to be based on similar synaptic asymmetries.

The results of our overall connectomic analysis also reveal a strikingly tight balance between the number of intrasegmental and intersegmental connections between the neurons of the self-righting wiring diagram (Section 3.2.12.4). This was expected as, although self-righting requires general co-ordination between the segments of the body in order to gain purchase on the substrate and fully rotate, the fact that the activity of a single pair of segmentally-repeated motor neurons is necessary for self-righting suggests that the intrasegmentally co-ordinated activity of motor neurons is also fundamental. We identify hemisegmentally-repeated neurons such as A27k and A020 ‘Wave’ interneurons as key facilitators of intersegmental co-ordination during self-righting and suggest that these neurons (which can be considered ‘second-order’ interneurons) primarily relay information (provided intrasegmentally to the

first-order Basin and Down-and-Back interneurons) throughout the rest of the larval body.

In addition to this, we hypothesise that the nature of information flow to and from the neurons of the self-righting wiring diagram may be reflective of their functional roles. For example, the Down-and-Back interneurons primarily receive information from sensory components in the same segment. They then relay this information to downstream interneurons which are also primarily in the same segment and we hypothesise that this may relate to their ability to promote C-bending, ensuring that neuronal connectivity is consistent along the larval body during behavioural exhibition. In contrast, the A02o 'Wave' interneurons play a role in the initiation of peristaltic wave propagation during locomotion (Takagi *et al*., 2017) and our analysis reveals that they primarily receive and provide input to wiring diagram neurons in adjacent segments in the context of the self-righting wiring diagram. Peristaltic waves are propagated as part of the self-righting behavioural sequence (Picao-Osorio *et al*., 2017) and we suggest, therefore, that A02o 'Wave' activity may occur in this context based on its synaptic profile.

Overall, the findings of this chapter demonstrate that the LT-1/2 motor neurons are connected to a complex network of upstream sensory components and interneurons. We facilitate the identification of multiple routes for information transfer between these neurons and characterise the flow of information along the anteroposterior and mediolateral axes of the larval CNS. This chapter also demonstrates that the serial reconstruction and connectomics-based approach used in other studies can also be used to decipher network architectures, as well as provide insights into information flow between neurons prior to any *in*

vivo testing. The connectomics analyses carried out in this chapter provide a foundation for comparative analyses between the neuronal network underlying motor behaviours in different stages of *Drosophila* larval life, and even between the systems underlying complex motor behaviours in different organisms.

Building on our connectomics work, we then present a functional validation of the roles of wiring diagram neurons in *in vivo* larval self-righting. To do this, we thermogenetically inhibit individual neuronal components of the wiring diagram through targeted expression of the temperature-sensitive allele of the gene *shibire* (shi^{ts}) (Kitamoto *et al*., 2001). The results of our behavioural analysis indicate that thermogenetic inhibition of all of the wiring diagram components tested (with the exception of the iIN-3 pre-LT interneurons), results in significantly delayed self-righting – validating the wiring diagram as a functional circuit for self-righting behaviour. We also show that inhibition of other dorsal neurons (including the well-characterised aCC, RP2 and U motor neurons as well as the pCC interneurons) has no significant effect on self-righting behaviour but that the unimpeded activity of motor neurons targeting ventral muscles is a necessity.

Sequential thermogenetic inhibition has been applied as a strategy to determine the neuronal components underlying larval locomotion (Kitamoto *et al*., 2001; Yoshikawa *et al*., 2016) but has not been applied to the determination of the neuronal substrates of complex, modular motor behaviours. The results of this study, therefore, further validate the dissection of neuronal circuits through sequential thermogenetic inhibition as a viable strategy for behavioural investigation in *Drosophila* larvae.

A notable result from this chapter was the identification of iIN-3 as a neuron whose activity is not necessary for normal self-righting behaviour. This was unexpected as our connectomics analysis identified iIN-3 as a premotor interneuron strongly connected to LT-1/2 motor neurons. Although only identified and reconstructed in the first three abdominal segments, the iIN-3 interneurons provide strong input to the LT-1/2 motor neurons in more posterior segments, but we do note that when first identified by others using CATMAID, their functional role was not investigated further as they were found not to show wave-like activity during fictive locomotion (Zwart *et al*., 2016). Unlike iIN-1, therefore (which was shown to facilitate a phase delay between longitudinal and transverse muscle contraction), the behavioural contribution of the iIN-3-to-LT-1/2 connection remains unclear. In future studies, investigations of this could include the characterisation of iIN-3 activity during LT-1/2 activity via simultaneous expression of calcium reporters or even the total ablation of iIN-3 activity through targeted expression of tetanus toxin (Sweeney *et al*., 1995) and the investigation of the behavioural consequence.

In this study, we used the LT-1/2 motor neurons as a starting point in the construction of the wiring diagram underlying self-righting due to their previous characterisation as key facilitators of self-righting behaviour (Picao-Osorio *et al*., 2015). With 30 muscles in most larval abdominal hemisegments (Bate, 1990, Bate and Martinez Arias, 1993) however, it is unlikely that the LT-1/2 motor neurons are the sole facilitators of larval self-righting, and our identification of a dependency on motor neurons targeting ventral muscles for normal self-righting (Figure 4.2.16) suggests that there may yet be unidentified circuitry supporting the behaviour.

The larger aim of the elucidation of this circuit was to provide a map of cellular substrates, upon which the expression of miRNAs shown to regulate self-righting (or 'SR-miRNAs') could be charted. Having identified the SR-miRNAs though previous study (Picao-Osorio *et al*., 2017) (and their potential cellular expression domains in this study), the aim is to perform mechanistic investigations, identifying how miRNA-based regulation of target genes regulates the ability to self-right. We propose that the future mapping of sensorimotor pathways to the ventral motor neurons previously discussed could, not only reveal how alternative neuronal circuitry contributes to self-righting in parallel with the circuit elucidated here, but also provide further targets for SR-miRNA mapping (Picao-Osorio *et al*., 2017).

The work of Issa and colleagues has demonstrated a requirement for the normal expression of the miRNA *miR-iab-4* for normal self-righting behaviour in L2 and L3 larvae (Issa *et al*., 2019) and, as discussed previously, neuronal circuitry remains relatively consistent during larval development (Zwart *et al*., 2013; Gerhard *et al*. 2017). We propose, therefore, that the establishment of the circuit for self-righting in the L1 larva which we present may also provide a starting point for the establishment of a similar circuit in the L3 larva (along with associated investigations of SR-miRNA expression). While correlations have been previously drawn between L1 and L3 behavioural exhibition (Almeida-Carvalho *et al*., 2017), the neural control of self-righting in L1 and L3 larvae remains uncharacterised and considering the findings of Section 5.2.8 (in which we show that miRNA regulation of locomotor behaviour changes over development), we predict that that miRNA influence on self-righting also changes.

Finally, we note that our establishment of the behavioural circuit underlying self-righting relies upon the determination of whether the inhibition of each neuron significantly delays the behavioural output. In future, we suggest that the contribution of each neuron to self-righting could be elucidated even more fully through detailed analysis of behavioural videos. Indeed, this is a strategy that has been applied by Loveless and colleagues to produce a physical description of self-righting behaviour (Loveless *et al*., 2020) and we propose that the use of behavioural annotation softwares such as ViTBAT (Biresaw *et al*., 2016) and DeepLabCut (Mathis *et al*., 2018) could provide further information on exactly which part of the self-righting sequence is affected by neuronal inhibition. In addition to this, the use of the photoconvertible fluorescent probe CAMPARI for the permanent labelling of active neural circuits (Fosque *et al*., 2015) may represent an efficient way to relate neural activity in the circuit to self-righting (as opposed to use of calcium reporters which, in this context, would prove technically challenging).

Overall, however, the validation of the behavioural circuit underlying self-righting behaviour *in vivo* represents an addition to our knowledge on the neural control of complex motor behaviours in the *Drosophila* larva and provides the foundation for future studies of their genetic basis.

7.3 The pervasive role of miRNA regulation in larval locomotion

In this thesis, we also investigate miRNA-based regulation of locomotor behaviour in *Drosophila* larvae by using a high-throughput, computer-based tracking approach (Risse *et al*., 2013; 2017) to screen a collection of miRNA mutants (Chen *et al*., 2014b). The first key finding of this investigation is that miRNAs pervasively regulate the average crawling speed of L1 larvae. We find that the removal of miRNAs significantly reduces average crawling speed (compared to control) in almost all stocks tested and that miRNA removal does not promote significant increases in average crawling speed. We, therefore, suggest that *Drosophila* miRNAs form an interdependent gene regulatory network which acts to optimise average crawling speed in L1 larvae.

As discussed in Section 1.6, normal forward/backward crawling behaviour requires the co-ordination of a large group of neurons that serve to regulate muscular contraction both intra- and intersegmentally (reviewed in Kohsaka *et al*., 2017 and Clark *et al*., 2018). Several studies have also shown that perturbing the activity of individual neurons in this group is sufficient to inhibit normal larval locomotion (Kohsaka *et al*., 2014, 2019; Yoshikawa *et al*., 2016). With the necessity of such complex and intertwined regulation at the cellular level, therefore, the processes regulating the activity of each neuron are even more important to promote overall co-ordination. When considering this, therefore, it becomes feasible that the removal of any miRNA which then affects the activity of any of these cellular substrates will reduce overall locomotor efficiency. The mapping of miRNA expression to the cellular substrates controlling locomotion, therefore, may not only reveal more detail about the mechanisms underlying crawling speed optimisation but could also lead to the

identification of uncharacterised cellular substrates that can then be functionally tested.

Potential approaches for the investigation of the mechanisms underlying crawling speed regulation in larvae include the use of softwares such as DeepLabCut (Mathis *et al*., 2018) to provide insights about more subtle changes to body posture during locomotion or targeted expression of GCaMP to identify how miRNA removal affects neural activity dynamics (Pulver *et al*., 2015; Karagyozov *et al*., 2018). We note, from our own RNA-seq experiments (Picao-Osorio et al., unpublished data) that the expression of miRNAs in the early L1 larva varies (with some predominantly expressed in tissues other than the central nervous system) and although our predominant aim is to elucidate neural mechanisms of locomotor control, miRNA expression in the muscles or cuticle may also represent viable mechanisms for regulation of motor control.

Donelson and colleagues have also examined miRNA-based regulation of locomotor control (Donelson *et al*., 2020) however, the method used to impose reductions in miRNA expression onto larvae (as well as the results obtained) differ substantially from those in this study. Donelson and colleagues spatially and temporally regulate miRNA expression through the pan-neuronal expression of “miRNA sponges”, small RNA molecules designed to sequester miRNAs from mRNA targets through complementary base-pairing (Ebert *et al*., 2007; Fulga *et al*., 2015). In contrast, our approach takes advantage of a collection of miRNA mutant stocks in which the miRNA sequence has been removed from the genome and replaced with alternative genetic elements (including loxP sites, *mini-white* genes and GAL4 coding sequences). A disadvantage of the sponge technique used by Donelson and colleagues is the

uncertainty as to whether all miRNA molecules will be sequestered from the target mRNA as intended. In cases where the affinity for binding between a miRNA and mRNA is higher than that between the miRNA and the sponge, negative gene regulation may still occur. As shown from our own results, the miRNA network responsible for regulating locomotion is extremely sensitive to alteration and it follows that partial removal of miRNA expression through sponges may result in behavioural effects different to those observed as a result of total miRNA removal. In addition to this, the pan-neuronal expression of miRNA sponges may also lead to off-target effects as has been observed in the similar RNAi technique which also relies on complementary base pairing with target mRNA to prevent translation (Ma et al., 2006; Perrimon and Mathey-Prevot, 2007). Should this be the case and miRNA sponges do interact with host transcripts unintentionally, the source of changes to behaviour in the larva would be unclear.

Donelson and colleagues screen 128 “miR-SP” lines (each pan-neuronally expressing a sponge targeting a single miRNA) for changes to locomotor behaviour, finding that 20 lines show a significant change to average speed (which stands in contrast to our results). We propose though that, as well as the differing mechanisms through which we impose miRNA mutations, the different developmental stages used in our respective experiments may also account for this disparity as miRNA- based regulation of locomotion also appears to be sensitive to developmental stage (discussed further below).

In this study, we also identified roles for miRNAs in the control of bending and pausing behaviours during locomotion. The results of our analysis show that removal of miRNA expression significantly affects cumulative time spent in a

bent conformation (used to represent turning) as well as the frequency of bending and pausing behaviour in mutant larvae. By far, however, apart from average crawling speed, the behavioural variable most significantly changed by removal of miRNA expression is the average duration of pauses by larvae (Figure 5.2.14).

The relationship between turning, pausing, and crawling during locomotion is one that we discuss in Section 5.2.3 and this balance is regulated through a variety of neural and physical mechanisms (Berni, 2015; Otto *et al*., 2018; Loveless *et al*., 2019). The results of our analysis, however, prompt questions about the specific mechanisms by which miRNAs regulate aspects of pausing and bending control. Building on work exploring the hierarchical organisation of motor behaviour in *C. elegans* (Kaplan *et al*., 2020), one hypothesis is that is the neural control of locomotion is hierarchically nested, and that negative regulation by miRNAs may be fundamental for differential behavioural output through the control of neural activity at different temporal scales.

At the level of combinatorial regulation by miRNAs, although it has been demonstrated that related miRNAs can (for example) separately regulate individual aspects of neural development (Stark *et al*., 2005; Smibert and Lai, 2010), the results of our cluster analysis (Figure 5.2.17) show that miRNA mutants cannot be separated into discrete clusters based on similar behavioural phenotypes. Building on this, we propose that, if mechanistic study is a key goal, further investigation is needed to elucidate the degree to which miRNAs regulate similar functional aspects of behavioural control. For example, this could comprise several miRNAs regulating the activity of a particular motor neuron or the contraction dynamics of longitudinal/transverse muscle and

examining how these mechanisms link with the overall distributions of the datasets we have obtained may provide insight into the dynamics of miRNA-regulation during behavioural output.

Overall, we suggest that the dependency of particular behaviours on particular miRNAs as revealed by our analysis also opens more questions. For example, while it is known that *miR-iab-4* is expressed in the LT-1/2 motor neurons (Picao-Osorio et al., 2015) and *miR-263b* is expressed in the sensory organs (Klann et al., 2020), the exact expression domains of many miRNAs remain unknown and this represents a key missing piece in any attempts to understand the mechanisms by which miRNAs regulate behaviour. The lab's RNA-seq data (Picao-Osorio et al., unpublished data) has provided us with the ability to narrow down miRNA expression locations to the CNS or other tissues but in future, investigation of how this relates to individual neurons, muscles or other tissues is essential for comprehensive understanding of mechanism.

In addition to this, miRNAs have the capacity to regulate the expression of large numbers of genes (Lim et al., 2005; Giraldez et al., 2006; Selbach et al., 2008) which, in turn, means that miRNAs form part of a large gene regulatory network. With 469 mature miRNA sequences in the *Drosophila* genome (and the organisation of some miRNAs into 'families' that all target the same seed sequence (Lai et al., 2005)), it is feasible that some miRNAs may function in a redundant manner, still facilitating target repression in the absence of an individual miRNA.

Building on the identification of pervasive locomotor defects in miRNA mutant larvae at the L1 stage, in Chapter 5 we also examine the same locomotor

behaviours in a selection of miRNA mutants at the L3 larval stage. The results of our analysis indicate that the developmental stage of the larva has implications for the regulation of locomotor behaviour by miRNAs. We observe cases in which abnormal locomotor phenotypes are separately maintained and ameliorated during development – also finding that the near-ubiquitous reduction in L1 average crawling speed is not reflected in the set of miRNA mutants also tested at the L3 stage. We remain cautious about deriving overarching insights from the screen of miRNA mutants at L3 as it is only partial, however, at the level of the individual mutant we provide proof-of-concept for the impact of development on post-transcriptional regulation of behaviour.

One hypothesis to explain this is that spatiotemporal miRNA expression profiles may shift as a result of changes to the expression of gene regulatory components (which are upstream of miRNAs) during development. Indeed, temporal miRNA expression profiling has shown that even over the 21 hours of embryonic development, miRNA expression is dynamic (Zhou *et al*., 2018) and this, in combination with the lethality of certain homozygous miRNA mutations during larval development (Chen *et al*., 2014b), suggests that the functional importance of individual miRNAs during development is in constant flux.

At the level of the neural control of locomotion, the results of the L3 screen also raise questions regarding how the relationship between miRNA expression and neural function changes during development. In the zebrafish, the functional consequence of altered miRNA expression during development has been examined by Tal and colleagues who found that the ethanol-induced misexpression of the miRNAs miR-9/9∗ and miR-153c in larval and juvenile

zebrafish leads to several abnormal behavioural phenotypes (Tal *et al*., 2012). In the *Drosophila* larva, although it has been shown that behavioural circuit structure remains relatively consistent between the L1 and L3 stages (Zwart *et al*., 2013; Gerhard *et al*., 2017), the question of what happens when neurally-expressed miRNAs are removed remains.

Does the process of neural development go awry between the L1 and L3 stages? Is development maintained as normal but neural functionality impacted? To address these questions, expression mapping of miRNAs to determine how their expression changes in the cellular substrates underlying behaviour at L1 and L3 would provide further insight about the mechanisms underlying the behavioural differences we observe.

Overall, the results presented in this chapter provide a useful starting point from which to examine the mechanistic details of miRNA-based locomotor regulation in *Drosophila* larvae. In addition to this, the results also provide insight into the constantly changing nature of miRNA-based regulation and hint that the developmental stage of larvae used to examine larval locomotion may be more crucial than previously thought due to changes to gene expression.

We do note that there is a need to validate the results of this screen in future to ensure that the behavioural changes we observe are not the result of influence from genetic background as opposed to miRNA mutation specifically. We suggest that this validation could take the form of a variety of further testing including complementation tests with “deficiency” lines to uncover the miRNA mutation and see if the behavioural phenotype is still present or not (Chen et al., 2014b), producing backcrossed versions of the *ΔmiR* stocks for behavioural

testing or even producing miRNA mutants using alternative means such as CRISPR-Cas9 (Doudna and Charpentier, 2014)

7.4 *miR-133* regulates larval pausing behaviour through control of head-rearing

In the final experimental chapter of this thesis, we identify a mechanism through which *miR-133* regulates larval pausing via control of head-rearing behaviour (Figure 6.2.8). We demonstrate that removal of *miR-133* expression through mutation leads to upregulated expression of the biosynthetic enzyme tryptophan hydroxylase and that this leads to an increase in serotonin production by the serotonergic neurons of the *ΔmiR-133* ventral nerve cord. Through a combination of FACS and qPCR, we then verify *miR-133* expression in the serotonergic neurons and validate the role of serotonin in head-rearing by using the GAL4-UAS system to overexpress *Trh*.

Building on the identification of average pause duration as a significant contributor to overall variance in the locomotion of miRNA mutant larvae (see Section 5.2.6.2), we initially selected miRNAs for in-depth mechanistic study based on the behavioural effects identified in mutants and their previously determined spatial expression domains (Picao-Osorio et al., unpublished data). Although we investigated *miR-133*, we do note that *miR-219* and *miR-970* share similar expression profiles and effects upon mutation to *miR-133*. Over 90% of *miR-219* and *miR-970* reads were also found in the CNS and mutants for these miRNAs also exhibit significantly increased average pause duration while other variables (apart from average crawling speed) were not statistically different

from control values. Both miRNAs are conserved (miRbase Release 22.1, 2018) (Kozomara and Griffiths-Jones, 2014) however only *miR-219* has been shown to play a role in locomotion (in the context of behavioural response to pharmaceutical compounds) (Kocerha *et al*., 2009; Ling *et al*., 2020).

In *Drosophila*, dysregulation of *miR-219* has been heavily linked to neurodegenerative disease (Santa-Maria *et al*., 2015; Murai *et al*., 2016; Wang *et al*., 2019a) while *miR-970* remains mostly uncharacterised. Considering the previously-identified pervasive roles of miRNAs in control of both larval self-righting (Picao-Osorio *et al*., 2017) and general larval locomotion (This study; Donelson *et al*., 2020), we propose that it is unlikely that the regulation of head-rearing behaviour by *miR-133* is the sole way in which miRNAs regulate average pause duration in larvae and further investigation of *ΔmiR-219* and *ΔmiR-970* mutants may reveal alternate mechanisms.

The identification of head-rearing as an aspect of pausing behaviour in *Drosophila* larvae, is itself, a valuable finding from this thesis. Head-rearing behaviour in *Drosophila* larvae has only been characterised in a few studies (Green *et al*., 1983; Okusawa *et al*., 2014) and, in the study led by Okusawa and colleagues, head-rearing is characterised as a sub-component of turning behaviour in the L3 larva. We observe no significant change to either the time spent in a bent conformation (which we use as a proxy for turning) or the frequency of these bends in *miR-133* mutant larvae at the L1 stage (Figures 5.2.6 and 5.2.8, respectively). We, therefore, suggest that the increases in rearing behaviour we observe are not functionally coupled to turning in *miR-133* mutant larvae at this stage. We note that at the L3 stage, pausing and turning behaviours in *miR-133* mutant larvae are also not significantly different to

control larvae. Therefore, if rearing and turning are functionally coupled at the L3 stage as Okusawa and colleagues suggest, we hypothesise that they are either not coupled at the L1 stage or the neural systems controlling head-rearing and turning behaviour become somehow uncoupled with the removal of *miR-133* expression.

To test these hypotheses, it will be essential to probe the neuromuscular basis of turning and rearing behaviours. To date, the work of Heckscher and colleagues has provided a mechanism for the neural control of left-right symmetry during locomotion (Heckscher *et al*., 2015) but other neural substrates facilitating turning have yet to be identified. In addition to this, Okusawa and colleagues demonstrate the role of the leucokinin-expressing ABLK neurons in control of rearing behaviour (Okusawa *et al*., 2014) but the neuromuscular control of rearing remains uncharacterised. Through observation, we propose that it would be logical for the activity of dorsal motor neurons to facilitate the raising of the head from the substrate however, more in-depth studies (potentially using live calcium imaging (Karagyozov *et al*., 2018)) could further our understanding of exactly how head-rearing is controlled.

In this chapter, we also use a combination of techniques to identify the gene encoding Tryptophan hydroxylase as a regulatory target of *miR-133*, show that serotonin production is increased in the serotonergic neurons of the *miR-133* mutant larva and demonstrate a causal link between this and increased head-rearing behaviour. Serotonin is a key neuromodulator of the CNS and (as discussed in Section 1.4) has been shown to regulate locomotor behaviour in both adult (Howard *et al*., 2019) and larval (Huser *et al*., 2012) *Drosophila*. The

results of this study, therefore, are of particular interest when compared to other studies that demonstrate links between the serotonergic system and the control of pausing/head-rearing behaviour.

As discussed in Section 6.3, Okusawa and colleagues and Moncalvo and Campos have reported that reductions in serotonin levels are associated with decreases in larval head-rearing (Okusawa *et al*., 2014) and the duration of light-induced pauses (Moncalvo and Campos, 2009), respectively. In our study, we observe results that would appear to contradict this common theme of serotonin production resulting in less pausing/rearing as we demonstrate that artificially increasing serotonin production through tryptophan hydroxylase overexpression is sufficient to significantly increase head-rearing (Figure 6.2.7). While we note differences between this study and those carried out by Okusawa and colleagues and Moncalvo and Campos, we propose that further experimentation could resolve these differences into a coherent framework for neuromodulatory control of pausing/head-rearing.

In terms of pausing behaviour, while we show that the removal of *miR-133* expression leads to both a significant increase in larval head-rearing and the average duration of pauses, the relationship between the duration of these rears and the significantly increased average pause duration we observe remains uncharacterised. In other words, although we observe increased rearing behaviour, if the average duration of each rearing event does not account for the increased pause durations previously observed, then increases in serotonin production may yet reduce pause duration through other mechanisms as suggested by Moncalvo and Campos.

In terms of head-rearing, decreases in serotonergic neuron activity have been shown to significantly increase head-rearing in the L3 larva (Okusawa *et al*., 2014). While it has been demonstrated that the neural circuits controlling behaviour remain structurally consistent during larval development (Zwart *et al*., 2013; Gerhard *et al*., 2017), we propose that our data (in which we show that average pause duration in *ΔmiR-133* larvae at the L3 stage is not significantly different that of control larvae) raises the question of whether the importance of serotonergic signalling to average pause duration changes over development and, therefore, whether the relationship presented by Okusawa and colleagues is specific to the L3 larva.

Finally, we demonstrate that although *miR-133* expression is upregulated in serotonergic neurons (compared a random body-wide selection of cells), this upregulation is mild. We observe a 0.34-fold upregulation of *miR-133* in a serotonergic neuron-enriched cell population but note that *miR-133* has also been predicted by target prediction algorithms to regulate alternative targets within the CNS (Figure 6.2.3). Building on this, we therefore suggest that expression of *miR-133* may be more prevalent in other neurons where these targets are expressed at higher levels.

miR-133 is conserved in zebrafish and mice and although other roles of the miRNA have not been demonstrated in *Drosophila melanogaster*, it has been shown to have cardiac-related functions in both (Yin *et al*., 2012; Muraoka *et al*., 2014). The findings of this chapter, therefore, represent a novel addition to our knowledge of miRNA-based regulation of behaviour and provide a precedent upon which studies of mechanistic control of other behaviours exhibited during locomotion can be based.

7.5 Concluding remarks

In this thesis, we use *Drosophila melanogaster* as a model organism to both investigate the cellular basis of a miRNA-dependent motor behaviour (larval self-righting) and how miRNA regulation of gene expression facilitates larval locomotion. We find that, not only is self-righting enabled by a complex network of neurons but that miRNAs also pervasively regulate a variety of locomotor behaviours. From these findings, we propose that miRNAs provide an important contribution to overall behaviour and that miRNA-dependent gene regulatory networks in the *Drosophila* larva are key for motor control.

References

Adler, J. (1969) 'Chemoreceptors in bacteria', *Science,* 166: 1588-97.

Agarwal, V., Bell, G. W., Nam, J. W. and Bartel, D. P. (2015) 'Predicting effective microRNA target sites in mammalian mRNAs', *Elife*, 4: e05005

Ainsley, J. A., Pettus, J. M., Bosenko, D., Gerstein, C. E., Zinkevich, N., Anderson, M. G., Adams, C. M., Welsh, M. J. and Johnson, W. A. (2003) 'Enhanced locomotion caused by loss of the Drosophila DEG/ENaC protein Pickpocket1', *Current Biology*, 13: 1557-63.

Akerboom, J., Chen, T. W., Wardill, T. J., Tian, L., Marvin, J. S., Mutlu, S., Calderón, N. C., Esposti, F., Borghuis, B. G., Sun, X. R., Gordus, A., Orger, M. B., Portugues, R., Engert, F., Macklin, J. J., Filosa, A., Aggarwal, A., Kerr, R. A., Takagi, R., Kracun, S., Shigetomi, E., Khakh, B. S., Baier, H., Lagnado, L., Wang, S. S., Bargmann, C. I., Kimmel, B. E., Jayaraman, V., Svoboda, K., Kim, D. S., Schreiter, E. R. and Looger, L. L. (2012) 'Optimization of a GCaMP calcium indicator for neural activity imaging', *Journal of Neuroscience*, 32: 13819-40.

Albrecht, D. R. and Bargmann, C. I. (2011) 'High-content behavioral analysis of Caenorhabditis elegans in precise spatiotemporal chemical environments', *Nature Methods*, 8: 599-605.

Almeida-Carvalho, M. J., Berh, D., Braun, A., Chen, Y.-c., Eichler, K., Eschbach, C., Fritsch, P. M. J., Gerber, B., Hoyer, N., Jiang, X., Kleber, J., Klämbt, C., König, C., Louis, M., Michels, B., Miroschnikow, A., Mirth, C., Miura, D., Niewalda, T., Otto, N., Paisios, E., Pankratz, M. J., Petersen, M., Ramsperger, N., Randel, N., Risse, B., Saumweber, T., Schlegel, P., Schleyer, M., Soba, P., Sprecher, S. G., Tanimura, T., Thum, A. S., Toshima, N., Truman, J. W., Yarali, A. and Zlatic, M. (2017) 'The Ol1mpiad: concordance of behavioural faculties of stage 1 and stage 3 Drosophila larvae', *The Journal of Experimental Biology*, 220: 2452-2475.

Ambros, V. (1989) 'A hierarchy of regulatory genes controls a larva-to-adult developmental switch in C. elegans', *Cell*, 57: 49-57.

Ambros, V. and Horvitz, H. R. (1987) 'The lin-14 locus of Caenorhabditis elegans controls the time of expression of specific postembryonic developmental events', *Genes & Development*, 1: 398-414.

Ameres, S. L., Martinez, J. and Schroeder, R. (2007) 'Molecular basis for target RNA recognition and cleavage by human RISC', *Cell*, 130: 101-12.

Ameres, S. L. and Zamore, P. D. (2013) 'Diversifying microRNA sequence and function', *Nature Reviews Molecular Cell Biology*, 14: 475-88.

Andres, A. J., Fletcher, J. C., Karim, F. D. and Thummel, C. S. (1993) 'Molecular analysis of the initiation of insect metamorphosis: a comparative study of Drosophila ecdysteroid-regulated transcription', *Developmental Biology*, 160: 388-404.

Baines, R. A. (2003) 'Postsynaptic protein kinase A reduces neuronal excitability in response to increased synaptic excitation in the Drosophila CNS', *Journal of Neuroscience*, 23: 8664-72.

Baltimore, D. (1970) 'RNA-dependent DNA polymerase in virions of RNA tumour viruses', *Nature,* 226: 1209-11.

Bartel, D. P. (2004) 'MicroRNAs: genomics, biogenesis, mechanism, and function', *Cell*, 116: 281-97.

Bate, M. (1990) 'The embryonic development of larval muscles in Drosophila', *Development*, 110: 791-804.

Bate, M. and Arias, A. M. (1993) *The development of Drosophila melanogaster*. Volume 2. Cold Spring Harbor Laboratory Press, USA.

Baudet, M. L., Zivraj, K. H., Abreu-Goodger, C., Muldal, A., Armisen, J., Blenkiron, C., Goldstein, L. D., Miska, E. A. and Holt, C. E. (2011) 'miR-124 acts through CoREST to control onset of Sema3A sensitivity in navigating retinal growth cones', *Nature Neuroscience*, 15: 29-38.

Bazzini, A. A., Lee, M. T. and Giraldez, A. J. (2012) 'Ribosome profiling shows that miR-430 reduces translation before causing mRNA decay in zebrafish', *Science,* 336: 233-7.

Bender, W. (2008) 'MicroRNAs in the Drosophila bithorax complex', *Genes & Development*, 22: 14-19.

Benz, G. (1956) 'Der trockenheitssinn bei larven von Drosophila melanogaster', *Experientia*, 12: 297-298.

Benzer, S. (1967) 'BEHAVIORAL MUTANTS OF Drosophila ISOLATED BY COUNTERCURRENT DISTRIBUTION', *Proceedings of the National Academy of Sciences of the United States of America*, 58: 1112-9.

Berni, J., Muldal, A. M. and Pulver, S. R. (2010) 'Using Neurogenetics and the Warmth-Gated Ion Channel TRPA1 to Study the Neural Basis of Behavior in Drosophila', *Journal of Undergraduate Neuroscience Education*, 9: A5-A14.

Berni, J., Pulver, S. R., Griffith, L. C. and Bate, M. (2012) 'Autonomous circuitry for substrate exploration in freely moving Drosophila larvae', *Current Biology*, 22: 1861-1870.

Berni, J. (2015) 'Genetic Dissection of a Regionally Differentiated Network for Exploratory Behavior in *Drosophila* larvae', *Current Biology*, 25: 1319-1326.

Bernstein, J. G., Garrity, P. A. and Boyden, E. S. (2012) 'Optogenetics and thermogenetics: technologies for controlling the activity of targeted cells within intact neural circuits', *Current Opinion in Neurobiology*, 22: 61-71.

Bertolazzi, G., Benos, P. V., Tumminello, M. and Coronnello, C. (2020) 'An improvement of ComiR algorithm for microRNA target prediction by exploiting coding region sequences of mRNAs', *BMC Bioinformatics*, 21: 201.

Betel, D., Wilson, M., Gabow, A., Marks, D. S. and Sander, C. (2008) 'The microRNA.org resource: targets and expression', *Nucleic Acids Research*, 36: D149-53.

Biresaw, T. A., Nawaz, T., Ferryman, J. and Dell, A. I. 'Vitbat: Video tracking and behavior annotation tool'. *2016 13th IEEE International Conference on Advanced Video and Signal Based Surveillance (AVSS)*: 295-301.

Bonev, B., Pisco, A. and Papalopulu, N. (2011) 'MicroRNA-9 reveals regional diversity of neural progenitors along the anterior-posterior axis', *Developmental Cell*, 20: 19-32.

Bovetti, S., Moretti, C., Zucca, S., Dal Maschio, M., Bonifazi, P. and Fellin, T. (2017) 'Simultaneous high-speed imaging and optogenetic inhibition in the intact mouse brain', *Scientific Reports,* 7: 40041.

Brand, A. H. and Perrimon, N. (1993) 'Targeted gene expression as a means of altering cell fates and generating dominant phenotypes', *Development*, 118: 401-415.

Brenner, S. (1974) 'The genetics of Caenorhabditis elegans', *Genetics*, 77: 71-94.

Broadus, J., Skeath, J. B., Spana, E. P., Bossing, T., Technau, G. and Doe, C. Q. (1995) 'New neuroblast markers and the origin of the aCC/pCC neurons in the Drosophila central nervous system', *Mechanisms of Development*, 53: 393-402.

Brooks, D. S., Vishal, K., Kawakami, J., Bouyain, S. and Geisbrecht, E. R. (2016) 'Optimization of wrMTrck to monitor Drosophila larval locomotor activity', *Journal of Insect Physiology*, 93-94: 11-17.

Brown, T. G. (1911) 'The intrinsic factors in the act of progression in the mammal', *Proceedings of the Royal Society B: Biological Sciences*, 84: 308-319.

Brustein, E., Chong, M., Holmqvist, B. and Drapeau, P. (2003) 'Serotonin patterns locomotor network activity in the developing zebrafish by modulating quiescent periods', *Journal of Neurobiology*, 57: 303-22.

Burgos, A., Honjo, K., Ohyama, T., Qian, C. S., Shin, G. J.-E., Gohl, D. M., Silies, M., Tracey, W. D., Zlatic, M., Cardona, A. and Grueber, W. B. (2018) 'Nociceptive interneurons control modular motor pathways to promote escape behavior in Drosophila', *Elife*, 7: 1557.

Bushati, N. and Cohen, S. M. (2008) 'MicroRNAs in neurodegeneration', *Current Opinion in Neurobiology*, 18: 292-6.

Busto, M., Iyengar, B. and Campos, A. R. (1999) 'Genetic dissection of behavior: modulation of locomotion by light in the Drosophila melanogaster larva requires genetically distinct visual system functions', *Journal of Neuroscience*, 19: 3337-44.

Calancie, B., Needham-Shropshire, B., Jacobs, P., Willer, K., Zych, G. and Green, B. A. (1994) 'Involuntary stepping after chronic spinal cord injury. Evidence for a central rhythm generator for locomotion in man', *Brain : a journal of neurology*, 117: 1143-1159.

Candiani, S., Moronti, L., De Pietri Tonelli, D., Garbarino, G. and Pestarino, M. (2011) 'A study of neural-related microRNAs in the developing amphioxus', *EvoDevo*, 2: 15.

Carthew, R. W., Agbu, P. and Giri, R. (2017) 'MicroRNA function in Drosophila melanogaster', *Seminars in Cell & Developmental Biology*, 65: 29-37.

Caygill, E. E. and Brand, A. H. (2017) 'miR-7 Buffers Differentiation in the Developing Drosophila Visual System', *Cell Reports*, 20: 1255-1261.

Celesia, G. G. (2012) 'Alcmaeon of Croton's observations on health, brain, mind, and soul', *Journal of the History of the Neurosciences*, 21: 409-26.

Certel, S. J. and Thor, S. (2004) 'Specification of Drosophila motoneuron identity by the combinatorial action of POU and LIM-HD factors', *Development*, 131: 5429-39.

Çiçek, I., Karaca, S., Brankatschk, M., Eaton, S., Urlaub, H. and Shcherbata, H. R. (2016) 'Hedgehog Signaling Strength Is Orchestrated by the mir-310 Cluster of MicroRNAs in Response to Diet', *Genetics*, 202: 1167-83.

Chen, W., Liu, Z., Li, T., Zhang, R., Xue, Y., Zhong, Y., Bai, W., Zhou, D. and Zhao, Z. (2014a) 'Regulation of Drosophila circadian rhythms by miRNA let-7 is mediated by a regulatory cycle', *Nature Communications*, 5: 5549.

Chen, X. and Rosbash, M. (2017) 'MicroRNA-92a is a circadian modulator of neuronal excitability in Drosophila', *Nature Communications*, 8: 14707.

Chen, Y.-W., Song, S., Weng, R., Verma, P., Kugler, J.-M., Buescher, M., Rouam, S. and Cohen, S. M. (2014b) 'Systematic Study of Drosophila MicroRNA Functions Using a Collection of Targeted Knockout Mutations', *Developmental Cell*, 31: 784-800.

Chiu, H., Alqadah, A., Chuang, C. F. and Chang, C. (2011) 'C. elegans as a genetic model to identify novel cellular and molecular mechanisms underlying nervous system regeneration', *Cell Adhesion & Migration*, 5: 387-94.

Choi, J. C., Park, D. and Griffith, L. C. (2004) 'Electrophysiological and morphological characterization of identified motor neurons in the Drosophila third instar larva central nervous system', *Journal of Neurophysiology*, 91: 2353-65.

Chong, J., Amourda, C. and Saunders, T. E. (2018) 'Temporal development of Drosophila embryos is highly robust across a wide temperature range', *Journal of the Royal Society Interface*, 15: 20180304.

Christodoulou, F., Raible, F., Tomer, R., Simakov, O., Trachana, K., Klaus, S., Snyman, H., Hannon, G. J., Bork, P. and Arendt, D. (2010) 'Ancient animal microRNAs and the evolution of tissue identity', *Nature,* 463: 1084-8.

Chung, W. J., Okamura, K., Martin, R. and Lai, E. C. (2008) 'Endogenous RNA interference provides a somatic defense against Drosophila transposons', *Current Biology*, 18: 795-802.

Clark, M. Q., Zarin, A. A., Carreira-Rosario, A. and Doe, C. (2018) 'Neural circuits driving larval locomotion in Drosophila', *Neural Development*, 13: 6.

Cobb, M. (2017) '60 years ago, Francis Crick changed the logic of biology', *PLoS Biology*, 15: e2003243.

Coolen, M., Katz, S. and Bally-Cuif, L. (2013) 'miR-9: a versatile regulator of neurogenesis', *Frontiers in Cellular Neuroscience*, 7: 220.

Cusumano, P., Biscontin, A., Sandrelli, F., Mazzotta, G. M., Tregnago, C., De Pittà, C. and Costa, R. (2018) 'Modulation of miR-210 alters phasing of circadian locomotor activity and impairs projections of PDF clock neurons in Drosophila melanogaster', *PLoS Genetics*, 14: e1007500.

Davis, I., Girdham, C. H. and O'Farrell, P. H. (1995) 'A nuclear GFP that marks nuclei in living Drosophila embryos; maternal supply overcomes a delay in the appearance of zygotic fluorescence', *Developmental Biology*, 170: 726-9.

DeFelipe, J. (2015) 'The dendritic spine story: an intriguing process of discovery', *Frontiers in Neuroanatomy*, 9: 14.

Doe, C. Q., Smouse, D. and Goodman, C. S. (1988) 'Control of neuronal fate by the Drosophila segmentation gene even-skipped', *Nature,* 333: 376-8.

Donelson, N. C., Dixit, R., Pichardo-Casas, I., Chiu, E. Y., Ohman, R. T., Slawson, J. B., Klein, M., Fulga, T. A., Van Vactor, D. and Griffith, L. C. (2020) 'MicroRNAs Regulate Multiple Aspects of Locomotor Behavior in', *G3: Genes, Genomes, Genetics*, 10: 43-55.

Doudna, J. A. and Charpentier, E. (2014) 'Genome editing. The new frontier of genome engineering with CRISPR-Cas9', *Science,* 346: 1258096.

Dulcis, D., Lippi, G., Stark, C. J., Do, L. H., Berg, D. K. and Spitzer, N. C. (2017) 'Neurotransmitter Switching Regulated by miRNAs Controls Changes in Social Preference', *Neuron,* 95: 1319-1333

Ebert, M. S., Neilson, J. R. and Sharp, P. A. (2007) 'MicroRNA sponges: competitive inhibitors of small RNAs in mammalian cells', *Nature Methods*, 4: 721-6.

Eichler, K., Li, F., Litwin-Kumar, A., Park, Y., Andrade, I., Schneider-Mizell, C. M., Saumweber, T., Huser, A., Eschbach, C., Gerber, B., Fetter, R. D., Truman, J. W., Priebe, C. E., Abbott, L. F., Thum, A. S., Zlatic, M. and Cardona, A. (2017) 'The complete connectome of a learning and memory centre in an insect brain', *Nature,* 548: 175-182.

Enright, A. J., John, B., Gaul, U., Tuschl, T., Sander, C. and Marks, D. S. (2003) 'MicroRNA targets in Drosophila', *Genome Biology*, 5: R1.

Eschbach, C., Fushiki, A., Winding, M., Schneider-Mizell, C. M., Shao, M., Arruda, R., Eichler, K., Valdes-Aleman, J., Ohyama, T., Thum, A. S., Gerber, B., Fetter, R. D., Truman, J. W., Litwin-Kumar, A., Cardona, A. and Zlatic, M. (2020) 'Recurrent architecture for adaptive regulation of learning in the insect brain', *Nature Neuroscience*, 23: 544-555.

Feinberg, E. H., Vanhoven, M. K., Bendesky, A., Wang, G., Fetter, R. D., Shen, K. and Bargmann, C. I. (2008) 'GFP Reconstitution Across Synaptic Partners (GRASP) defines cell contacts and synapses in living nervous systems', *Neuron,* 57: 353-63.

Field, L. H. and Matheson, T. (1998) 'Chordotonal organs of insects', *Advances in insect physiology*, 27: 1-228.

Fink, R. P. and Heimer, L. (1967) 'Two methods for selective silver impregnation of degenerating axons and their synaptic endings in the central nervous system', *Brain Research*, 4: 369-74.

Flourens, M.-J.-P. (1824) 'Recherches experimentales sur les propietes et fonctions due systeme nerveus dans les animaus vertebres. Paris', Polster, MR, Nadel, L, and Schacter, DL (1991) Cognitive neuroscience analysis of memory: A historical perspective. *Journal of Cognitive Neuroscience*, 3: 95-116.

Flourens, P. (1825) Expériences sur le système nerveux: faisant suite aux Recherches expérimentales sur les propriétés et les fonctions du système nerveux dans les animaux vertébrés.

Fosque, B. F., Sun, Y., Dana, H., Yang, C. T., Ohyama, T., Tadross, M. R., Patel, R., Zlatic, M., Kim, D. S., Ahrens, M. B., Jayaraman, V., Looger, L. L. and Schreiter, E. R. (2015) 'Neural circuits. Labeling of active neural circuits in vivo with designed calcium integrators', *Science,* 347: 755-60.

Friedman, R. C., Farh, K. K., Burge, C. B. and Bartel, D. P. (2009) 'Most mammalian mRNAs are conserved targets of microRNAs', *Genome Research*, 19: 92-105.

Fujioka, M., Lear, B. C., Landgraf, M., Yusibova, G. L., Zhou, J., Riley, K. M., Patel, N. H. and Jaynes, J. B. (2003) 'Even-skipped, acting as a repressor, regulates axonal projections in Drosophila', *Development*, 130: 5385-400.

Fulga, T. A., McNeill, E. M., Binari, R., Yelick, J., Blanche, A., Booker, M., Steinkraus, B. R., Schnall-Levin, M., Zhao, Y., DeLuca, T., Bejarano, F., Han, Z., Lai, E. C., Wall, D. P., Perrimon, N. and Van Vactor, D. (2015) 'A transgenic resource for conditional competitive inhibition of conserved Drosophila microRNAs', *Nature Communications*, 6: 7279.

Fushiki, A., Zwart, M. F., Kohsaka, H., Fetter, R. D., Cardona, A. and Nose, A. (2016) 'A circuit mechanism for the propagation of waves of muscle contraction in Drosophila', *Elife*, 5: e13253.

Gaugler, R., Lebeck, L., Nakagaki, B. and Boush, G. M. (1980) 'Orientation of the entomogenous nematode Neoaplectana carpocapsae to carbon dioxide', *Environmental Entomology*, 9: 649-652.

Gepner, R., Mihovilovic Skanata, M., Bernat, N. M., Kaplow, M. and Gershow, M. (2015) 'Computations underlying Drosophila photo-taxis, odor-taxis, and multi-sensory integration', *Elife*, 4: e06229.

Gerhard, S., Andrade, I., Fetter, R. D., Cardona, A. and Schneider-Mizell, C. M. (2017) 'Conserved neural circuit structure across Drosophila larva development revealed by comparative connectomics', *Elife*, 6: e29089.

Giraldez, A. J., Mishima, Y., Rihel, J., Grocock, R. J., Van Dongen, S., Inoue, K., Enright, A. J. and Schier, A. F. (2006) 'Zebrafish MiR-430 promotes deadenylation and clearance of maternal mRNAs', *Science,* 312: 75-9.

Glisovic, T., Bachorik, J. L., Yong, J. and Dreyfuss, G. (2008) 'RNA-binding proteins and post-transcriptional gene regulation', *FEBS Letters*, 582: 1977-86.

Gomez-Marin, A., Duistermars, B. J., Frye, M. A. and Louis, M. (2010) 'Mechanisms of odor-tracking: multiple sensors for enhanced perception and behavior', *Frontiers in Cellular Neuroscience*, 4: 6.

Gott, J. M. and Emeson, R. B. (2000) 'Functions and mechanisms of RNA editing', *Annu Review of Genetics*, 34: 499-531.

Granzotto, A., Lopes, F. R., Lerat, E., Vieira, C. and Carareto, C. M. (2009) 'The evolutionary dynamics of the Helena retrotransposon revealed by sequenced Drosophila genomes', *BMC Evolutionary Biology*, 9: 174.

Gray, E. G. (1963) 'Electron microscopy of presynaptic organelles of the spinal cord', *Journal of Anatomy*, 97: 101-6.

Green, C., Burnet, B. and Connolly, K. (1983) 'Organization and patterns of inter-and intraspecific variation in the behaviour of Drosophila larvae', *Animal Behaviour*, 31: 282-291.

Green, J., Adachi, A., Shah, K. K., Hirokawa, J. D., Magani, P. S. and Maimon, G. (2017) 'A neural circuit architecture for angular integration in Drosophila', *Nature,* 546: 101-106.

Gross, P. (1993) 'Insect behavioral and morphological defenses against parasitoids', *Annual review of entomology*, 38: 251-273.

Grueber, W. B., Jan, L. Y. and Jan, Y. N. (2002) 'Tiling of the Drosophila epidermis by multidendritic sensory neurons', *Development*, 129: 2867-78.

Grueber, W. B., Ye, B., Yang, C. H., Younger, S., Borden, K., Jan, L. Y. and Jan, Y. N. (2007) 'Projections of Drosophila multidendritic neurons in the central nervous system: links with peripheral dendrite morphology', *Development*, 134: 55-64.

Günther, M. N., Nettesheim, G. and Shubeita, G. T. (2016) 'Quantifying and predicting Drosophila larvae crawling phenotypes', *Scientific Reports*, 6: 27972.

Hall, D. H. and Russell, R. L. (1991) 'The posterior nervous system of the nematode Caenorhabditis elegans: serial reconstruction of identified neurons and complete pattern of synaptic interactions', *Journal of Neuroscience*, 11: 1-22.

Hamada, F. N., Rosenzweig, M., Kang, K., Pulver, S. R., Ghezzi, A., Jegla, T. J. and Garrity, P. A. (2008) 'An internal thermal sensor controlling temperature preference in Drosophila', *Nature,* 454: 217-20.

Harden, N. (2002) 'Signaling pathways directing the movement and fusion of epithelial sheets: lessons from dorsal closure in Drosophila', *Differentiation*, 70: 181-203.

Harris-Warrick, R. M. and Marder, E. (1991) 'Modulation of neural networks for behavior', *Annual Review of Neuroscience*, 14: 39-57.

Harzer, H., Berger, C., Conder, R., Schmauss, G. and Knoblich, J. A. (2013) 'FACS purification of Drosophila larval neuroblasts for next-generation sequencing', *Nature Protocols*, 8: 1088-1099.

Hasegawa, E., Truman, J. W. and Nose, A. (2016) 'Identification of excitatory premotor interneurons which regulate local muscle contraction during Drosophila larval locomotion', *Scientific Reports*, 6: 30806.

Heckscher, E. S., Zarin, A. A., Faumont, S., Clark, M. Q., Manning, L., Fushiki, A., Schneider-Mizell, C. M., Fetter, R. D., Truman, J. W., Zwart, M. F., Landgraf, M., Cardona, A., Lockery, S. R. and Doe, C. Q. (2015) 'Even-Skipped(+) Interneurons Are Core Components of a Sensorimotor Circuit that Maintains Left-Right Symmetric Muscle Contraction Amplitude', *Neuron,* 88: 314-29.

Helmstaedter, M., Briggman, K. L., Turaga, S. C., Jain, V., Seung, H. S. and Denk, W. (2013) 'Connectomic reconstruction of the inner plexiform layer in the mouse retina', *Nature,* 500: 168-74.

Herculano-Houzel, S. (2012) 'The remarkable, yet not extraordinary, human brain as a scaled-up primate brain and its associated cost', *Proceedings of the National Academy of Sciences of the United States of America*, 109: 10661-8.

Herculano-Houzel, S., Mota, B. and Lent, R. (2006) 'Cellular scaling rules for rodent brains', *Proceedings of the National Academy of Sciences of the United States of America*, 103: 12138-43.

Hernandez-Nunez, L., Belina, J., Klein, M., Si, G., Claus, L., Carlson, J. R. and Samuel, A. D. (2015) 'Reverse-correlation analysis of navigation dynamics in Drosophila larva using optogenetics', *Elife*, 4: e06225.

Hildebrand, D. G. C., Cicconet, M., Torres, R. M., Choi, W., Quan, T. M., Moon, J., Wetzel, A. W., Scott Champion, A., Graham, B. J., Randlett, O., Plummer, G. S., Portugues, R., Bianco, I. H., Saalfeld, S., Baden, A. D., Lillaney, K., Burns, R., Vogelstein, J. T., Schier, A. F., Lee, W. A., Jeong, W. K., Lichtman, J. W. and Engert, F. (2017) 'Whole-brain serial-section electron microscopy in larval zebrafish', *Nature,* 545: 345-349.

Hiramoto, A., Jonaitis, J., Niko, S., Kohsaka, H., Fetter, R. D., Cardona, A., Pulver, S. R. and Nose, A. (2021) 'Regulation of coordinated muscular relaxation by a pattern-generating intersegmental circuit', *bioRxiv preprint*, doi: 10.1101/2021.03.08.434356.

His, W. (1880) *Anatomie menschlicher embryonen*. 5th edition. Leipzig.

Hodgkin, A. L. and Huxley, A. F. (1952) 'A quantitative description of membrane current and its application to conduction and excitation in nerve', *Journal of Physiology*, 117: 500-44.

Hoff, E. (1932) 'Central nerve terminals in the mammalian spinal cord and their examination by experimental degeneration', *Proceedings of the Royal Society of London. Series B, Containing Papers of a Biological Character*, 111: 175-188.

Hotta, Y. and Benzer, S. (1970) 'Genetic dissection of the Drosophila nervous system by means of mosaics', *Proceedings of the National Academy of Sciences of the United States of America*, 67: 1156-63.

Hotta, Y. and Benzer, S. (1972) ‘Mapping of behaviour in Drosophila mosaics’, *Nature*, 240: 527-35.

Hotta, Y. and Benzer, S. (1976) 'Courtship in Drosophila mosaics: sex-specific foci for sequential action patterns', *Proceedings of the National Academy of Sciences of the United States of America*, 73: 4154-8.

Howard, C. E., Chen, C. L., Tabachnik, T., Hormigo, R., Ramdya, P. and Mann, R. S. (2019) 'Serotonergic Modulation of Walking in Drosophila', *Current Biology*, 29: 4218-4230.

Hughes, C. L. and Thomas, J. B. (2007) 'A sensory feedback circuit coordinates muscle activity in Drosophila', *Molecular and Cellular Neuroscience*, 35: 383-96.

Huser, A., Rohwedder, A., Apostolopoulou, A. A., Widmann, A., Pfitzenmaier, J. E., Maiolo, E. M., Selcho, M., Pauls, D., von Essen, A., Gupta, T., Sprecher, S. G., Birman, S., Riemensperger, T., Stocker, R. F. and Thum, A. S. (2012) 'The serotonergic central nervous system of the Drosophila larva: anatomy and behavioral function', *PLoS One*, 7: e47518.

Hwang, R. Y., Zhong, L., Xu, Y., Johnson, T., Zhang, F., Deisseroth, K. and Tracey, W. D. (2007) 'Nociceptive neurons protect Drosophila larvae from parasitoid wasps', *Current Biology*, 17: 2105-2116.

Ibáñez-Ventoso, C., Vora, M. and Driscoll, M. (2008) 'Sequence relationships among C. elegans, D. melanogaster and human microRNAs highlight the extensive conservation of microRNAs in biology', *PLoS One*, 3: e2818.

Issa, R., Picao-Osorio, J., Rito, N., Chiappe, M. E. and Alonso, C. R. (2019) 'A single MicroRNA-Hox gene module controls complex movement in biomechanically distinct developmental forms of Drosophila', *Current Biology,* 29: 2665-2675.

Issler, O. and Chen, A. (2015) 'Determining the role of microRNAs in psychiatric disorders', *Nature Reviews Neuroscience*, 16: 201-12.

Issler, O., Haramati, S., Paul, E. D., Maeno, H., Navon, I., Zwang, R., Gil, S., Mayberg, H. S., Dunlop, B. W., Menke, A., Awatramani, R., Binder, E. B., Deneris, E. S., Lowry, C. A. and Chen, A. (2014) 'MicroRNA 135 Is Essential for Chronic Stress Resiliency, Antidepressant Efficacy, and Intact Serotonergic Activity', *Neuron,* 83: 344-360.

Itakura, Y., Kohsaka, H., Ohyama, T., Zlatic, M., Pulver, S. R. and Nose, A. (2015) 'Identification of Inhibitory Premotor Interneurons Activated at a Late Phase in a Motor Cycle during Drosophila Larval Locomotion', *PLoS One*, 10: e0136660-24.

Jarman, A. P., Sun, Y., Jan, L. Y. and Jan, Y. N. (1995) 'Role of the proneural gene, atonal, in formation of Drosophila chordotonal organs and photoreceptors', *Development*, 121: 2019-30.

Jay, M., De Faveri, F. and McDearmid, J. R. (2015) 'Firing dynamics and modulatory actions of supraspinal dopaminergic neurons during zebrafish locomotor behavior', *Current Biology*, 25: 435-44.

Jensen, K. P., Covault, J., Conner, T. S., Tennen, H., Kranzler, H. R. and Furneaux, H. M. (2008) 'A common polymorphism in serotonin receptor 1B mRNA moderates regulation by miR-96 and associates with aggressive human behaviors', *Molecular Psychiatry*, 14: 381-389.

Jolliffe, I. T. and Cadima, J. (2016) 'Principal component analysis: a review and recent developments', *Philosophical Transactions of the Royal Society A: Mathematical, Physical and Engineering Sciences*, 374: 20150202.

Jones, C. I. and Newbury, S. F. (2010) 'Functions of microRNAs in Drosophila development', *Biochemical Society Transactions*, 38: 1137-43.

Jovanic, T., Winding, M., Cardona, A., Truman, J. W., Gershow, M. and Zlatic, M. (2019) 'Neural Substrates of Drosophila Larval Anemotaxis', *Current Biology*, 29: 554-566.

Jung, H. and Dasen, J. S. (2015) 'Evolution of patterning systems and circuit elements for locomotion', *Developmental Cell*, 32: 408-22.

Kabekkodu, S. P., Shukla, V., Varghese, V. K., D' Souza, J., Chakrabarty, S. and Satyamoorthy, K. (2018) 'Clustered miRNAs and their role in biological functions and diseases', *Biological Reviews of the Cambridge Philosophical Society*, 93: 1955-1986.

Kabra, M., Robie, A. A., Rivera-Alba, M., Branson, S. and Branson, K. (2013) 'JAABA: interactive machine learning for automatic annotation of animal behavior', *Nature Methods*, 10: 64-7.

Kamikouchi, A., Inagaki, H. K., Effertz, T., Hendrich, O., Fiala, A., Göpfert, M. C. and Ito, K. (2009) 'The neural basis of Drosophila gravity-sensing and hearing', *Nature,* 458: 165-71.

Kaplan, H. S., Salazar Thula, O., Khoss, N. and Zimmer, M. (2020) 'Nested Neuronal Dynamics Orchestrate a Behavioral Hierarchy across Timescales', *Neuron,* 105: 562-576.

Karagyozov, D., Skanata, M. M., Lesar, A. and Gershow, M. (2018) 'Recording Neural Activity in Unrestrained Animals with Three-Dimensional Tracking Two-Photon Microscopy', *Cell Reports*, 25: 1371-1383.

Kawamata, T. and Tomari, Y. (2010) 'Making RISC', *Trends in Biochemical Sciences*, 35: 368-76.

Kelly, M. A., Rubinstein, M., Phillips, T. J., Lessov, C. N., Burkhart-Kasch, S., Zhang, G., Bunzow, J. R., Fang, Y., Gerhardt, G. A., Grandy, D. K. and Low, M. J. (1998) 'Locomotor activity in D2 dopamine receptor-deficient mice is determined by gene dosage, genetic background, and developmental adaptations', *Journal of Neuroscience*, 18: 3470-9.

Kertesz, M., Iovino, N., Unnerstall, U., Gaul, U. and Segal, E. (2007) 'The role of site accessibility in microRNA target recognition', *Nature Genetics*, 39: 1278-84.

Keshishian, H., Chiba, A., Chang, T. N., Halfon, M. S., Harkins, E. W., Jarecki, J., Wang, L., Anderson, M., Cash, S. and Halpern, M. E. (1993) 'Cellular mechanisms governing synaptic development in Drosophila melanogaster', *Journal of Neurobiology*, 24: 757-87.

Kidner, C. A. and Martienssen, R. A. (2005) 'The developmental role of microRNA in plants', *Current Opinion in Plant Biology*, 8: 38-44.

Kim, E., Goren, A. and Ast, G. (2008) 'Alternative splicing: current perspectives', *Bioessays*, 30: 38-47.

Kim, H., Kirkhart, C. and Scott, K. (2017) 'Long-range projection neurons in the taste circuit of Drosophila', *Elife*, 6: e23386.

Kitamoto, T. (2001) 'Conditional modification of behavior in Drosophila by targeted expression of a temperature-sensitive shibire allele in defined neurons', *Journal of Neurobiology*, 47: 81-92.

Klann, M., Issa, A. R. and Alonso, C. R. (2020) 'microRNA-dependent control of sensory neuron function regulates posture behaviour in Drosophila', *bioRxiv preprint,* doi: 10.1101/2020.08.24.262626.

Klapoetke, N. C., Murata, Y., Kim, S. S., Pulver, S. R., Birdsey-Benson, A., Cho, Y. K., Morimoto, T. K., Chuong, A. S., Carpenter, E. J., Tian, Z., Wang, J., Xie, Y., Yan, Z., Zhang, Y., Chow, B. Y., Surek, B., Melkonian, M., Jayaraman, V., Constantine-Paton, M., Wong, G. K. and Boyden, E. S. (2014) 'Independent optical excitation of distinct neural populations', *Nature Methods*, 11: 338-46.

Kocerha, J., Faghihi, M. A., Lopez-Toledano, M. A., Huang, J., Ramsey, A. J., Caron, M. G., Sales, N., Willoughby, D., Elmen, J., Hansen, H. F., Orum, H., Kauppinen, S., Kenny, P. J. and Wahlestedt, C. (2009) 'MicroRNA-219 modulates NMDA receptor-mediated neurobehavioral dysfunction', *Proceedings of the National Academy of Sciences of the United States of America*, 106: 3507-12.

Kohsaka, H., Guertin, P. and Nose, A. (2017) ‘Neural Circuits Underlying Fly Larval Locomotion’, *Current Pharmaceutical Design,* 23: 1722-1733.

Kohsaka, H., Takasu, E., Morimoto, T. and Nose, A. (2014) 'A Group of Segmental Premotor Interneurons Regulates the Speed of Axial Locomotion in Drosophila Larvae', *Current Biology*, 24: 2632-2642.

Kohsaka, H., Zwart, M. F., Fushiki, A., Fetter, R. D., Truman, J. W., Cardona, A. and Nose, A. (2019) 'Regulation of forward and backward locomotion through intersegmental feedback circuits in Drosophila larvae', *Nature Communications*, 10: 2654.

Kozomara, A. and Griffiths-Jones, S. (2014) 'miRBase: annotating high confidence microRNAs using deep sequencing data', *Nucleic Acids Research*, 42: D68-73.

Krezel, W., Ghyselinck, N., Samad, T. A., Dupé, V., Kastner, P., Borrelli, E. and Chambon, P. (1998) 'Impaired locomotion and dopamine signaling in retinoid receptor mutant mice', *Science,* 279: 863-7.

Kung, C. (1971) 'Genic mutants with altered system of excitation in Paramecium aurelia. II. Mutagenesis, screening and genetic analysis of the mutants', *Genetics*, 69: 29-45.

Kwon, Y., Shen, W. L., Shim, H. S. and Montell, C. (2010) 'Fine thermotactic discrimination between the optimal and slightly cooler temperatures via a TRPV channel in chordotonal neurons', *Journal of Neuroscience*, 30: 10465-71.

Köbbert, C., Apps, R., Bechmann, I., Lanciego, J. L., Mey, J. and Thanos, S. (2000) 'Current concepts in neuroanatomical tracing', *Progress in Neurobiology*, 62: 327-51.

Lacin, H. and Truman, J. W. (2016) 'Lineage mapping identifies molecular and architectural similarities between the larval and adult Drosophila central nervous system', *Elife*, 5: e13399.

Lagos-Quintana, M., Rauhut, R., Lendeckel, W. and Tuschl, T. (2001) 'Identification of novel genes coding for small expressed RNAs', *Science,* 294: 853-8.

Lagos-Quintana, M., Rauhut, R., Yalcin, A., Meyer, J., Lendeckel, W. and Tuschl, T. (2002) 'Identification of tissue-specific microRNAs from mouse', *Current Biology*, 12: 735-9.

Lai, E. C. (2002) 'Micro RNAs are complementary to 3' UTR sequence motifs that mediate negative post-transcriptional regulation', *Nature Genetics*, 30: 363-4.

Lai, E. C., Tam, B. and Rubin, G. M. (2005) 'Pervasive regulation of Drosophila Notch target genes by GY-box-, Brd-box-, and K-box-class microRNAs', *Genes & Development*, 19: 1067-80.

Lai, E. C., Tomancak, P., Williams, R. W. and Rubin, G. M. (2003) 'Computational identification of Drosophila microRNA genes', *Genome Biology*, 4: R42.

Lai, S.-L. and Lee, T. (2006) 'Genetic mosaic with dual binary transcriptional systems in Drosophila', *Nature Neuroscience*, 9: 703-709.

Lai, Z. C. and Rubin, G. M. (1992) 'Negative control of photoreceptor development in Drosophila by the product of the yan gene, an ETS domain protein', *Cell*, 70: 609-20.

Landgraf, M., Bossing, T., Technau, G. M. and Bate, M. (1997) 'The Origin, Location, and Projections of the Embryonic Abdominal Motorneurons of Drosophila', *Journal of Neuroscience*, 17: 9642-55.

Landgraf, M., Jeffrey, V., Fujioka, M., Jaynes, J. B. and Bate, M. (2003) 'Embryonic Origins of a Motor System: Motor Dendrites Form a Myotopic Map in Drosophila', *PLoS Biology*, 1: E41.

Landthaler, M., Yalcin, A. and Tuschl, T. (2004) 'The human DiGeorge syndrome critical region gene 8 and Its D. melanogaster homolog are required for miRNA biogenesis', *Current Biology*, 14: 2162-7.

Larson, T. A., Lent, K. L., Bammler, T. K., MacDonald, J. W., Wood, W. E., Caras, M. L., Thatra, N. M., Budzillo, A., Perkel, D. J. and Brenowitz, E. A. (2015) 'Network analysis of microRNA and mRNA seasonal dynamics in a highly plastic sensorimotor neural circuit', *BMC Genomics,* 16: 905.

Lau, N. C., Lim, L. P., Weinstein, E. G. and Bartel, D. P. (2001) 'An abundant class of tiny RNAs with probable regulatory roles in Caenorhabditis elegans', *Science,* 294: 858-62.

Lee, R. C. and Ambros, V. (2001) 'An extensive class of small RNAs in Caenorhabditis elegans', *Science,* 294: 862-4.

Lee, R. C., Feinbaum, R. L. and Ambros, V. (1993) 'The C. elegans heterochronic gene lin-4 encodes small RNAs with antisense complementarity to lin-14', *Cell*, 75: 843-54.

Lee, T. and Luo, L. (1999) 'Mosaic analysis with a repressible cell marker for studies of gene function in neuronal morphogenesis', *Neuron,* 22: 451-61.

Leucht, C., Stigloher, C., Wizenmann, A., Klafke, R., Folchert, A. and Bally-Cuif, L. (2008) 'MicroRNA-9 directs late organizer activity of the midbrain-hindbrain boundary', *Nature Neuroscience*, 11: 641-8.

Lewis, B. P., Shih, I. H., Jones-Rhoades, M. W., Bartel, D. P. and Burge, C. B. (2003) 'Prediction of mammalian microRNA targets', *Cell*, 115: 787-98.

Li, C., Kessens, C. C., Fearing, R. S. and Full, R. J. (2017) 'Mechanical principles of dynamic terrestrial self-righting using wings', *Advanced Robotics*, 31: 881-900.

Li, X. and Carthew, R. W. (2005) 'A microRNA mediates EGF receptor signaling and promotes photoreceptor differentiation in the Drosophila eye', *Cell*, 123: 1267-77.

Li, X., Cassidy, J. J., Reinke, C. A., Fischboeck, S. and Carthew, R. W. (2009) 'A microRNA imparts robustness against environmental fluctuation during development', *Cell*, 137: 273-82.

Li, Y., Wang, F., Lee, J. A. and Gao, F. B. (2006) 'MicroRNA-9a ensures the precise specification of sensory organ precursors in Drosophila', *Genes & Development*, 20: 2793-805.

Li, Z., Liu, J., Zheng, M. and Xu, X. Z. (2014) 'Encoding of both analog- and digital-like behavioral outputs by one C. elegans interneuron', *Cell*, 159: 751-65.

Lim, L. P., Glasner, M. E., Yekta, S., Burge, C. B. and Bartel, D. P. (2003a) 'Vertebrate microRNA genes', *Science,* 299: 1540.

Lim, L. P., Lau, N. C., Garrett-Engele, P., Grimson, A., Schelter, J. M., Castle, J., Bartel, D. P., Linsley, P. S. and Johnson, J. M. (2005) 'Microarray analysis shows that some microRNAs downregulate large numbers of target mRNAs', *Nature,* 433: 769-73.

Lim, L. P., Lau, N. C., Weinstein, E. G., Abdelhakim, A., Yekta, S., Rhoades, M. W., Burge, C. B. and Bartel, D. P. (2003b) 'The microRNAs of Caenorhabditis elegans', *Genes & Development*, 17: 991-1008.

Ling, Y., Sun, L., Wang, D., Jiang, J., Sun, W., Ai, W., Wang, X. and Wang, H. (2020) 'Triclosan induces zebrafish neurotoxicity by abnormal expression of miR-219 targeting oligodendrocyte differentiation of central nervous system', *Archives of Toxicology*, 94: 857-871.

Longrigg, J. (1993) *'Philosophy and medicine in the fifth century I: Alcmaeon and the pre-Socratic philosophers'*, 1st edition. Routledge. London, UK & New York, USA.

Loveless, J., Garner, A., Issa, A. R., Roberts, R. J., Webb, B., Prieto-Godino, L. L., Ohyama, T. and Alonso, C. R. (2021) 'A physical theory of movement in small animals', *bioRxiv preprint*, doi: 10.1101/2020.08.25.266163.

Loveless, J., Lagogiannis, K. and Webb, B. (2019) 'Modelling the mechanics of exploration in larval Drosophila', *PLoS Computational Biololgy*, 15: e1006635.

Loya, C. M., Lu, C. S., Van Vactor, D. and Fulga, T. A. (2009) 'Transgenic microRNA inhibition with spatiotemporal specificity in intact organisms', *Nature Methods*, 6: 897-903.

Loya, C. M., McNeill, E. M., Bao, H., Zhang, B. and Van Vactor, D. (2014) 'miR-8 controls synapse structure by repression of the actin regulator enabled', *Development*, 141: 1864-74.

Luan, H., Peabody, N. C., Vinson, C. R. and White, B. H. (2006) 'Refined spatial manipulation of neuronal function by combinatorial restriction of transgene expression', *Neuron,* 52: 425-36.

Lund, E., Güttinger, S., Calado, A., Dahlberg, J. E. and Kutay, U. (2004) 'Nuclear export of microRNA precursors', *Science,* 303: 95-8.

Lundell, M. J., Chu-LaGraff, Q., Doe, C. Q. and Hirsh, J. (1996) 'The engrailed and huckebein genes are essential for development of serotonin neurons in the Drosophila CNS', *Molecular and Cellular Neuroscience*, 7: 46-61.

Lundell, M. J. and Hirsh, J. (1994) 'Temporal and spatial development of serotonin and dopamine neurons in the Drosophila CNS', *Developmental Biology*, 165: 385-96.

Ma, Y., Creanga, A., Lum, L. and Beachy, P. A. (2006) 'Prevalence of off-target effects in Drosophila RNA interference screens', *Nature,* 443: 359-63.

Mahr, A. and Aberle, H. (2006) 'The expression pattern of the Drosophila vesicular glutamate transporter: a marker protein for motoneurons and glutamatergic centers in the brain', *Gene Expression Patterns*, 6: 299-309.

Marder, E. (2012) 'Neuromodulation of neuronal circuits: back to the future', *Neuron,* 76: 1-11.

Marder, E. and Bucher, D. (2007) 'Understanding circuit dynamics using the stomatogastric nervous system of lobsters and crabs', *Annual Review of Physiology*, 69: 291-316.

Masson, J. B., Laurent, F., Cardona, A., Barré, C., Skatchkovsky, N., Zlatic, M. and Jovanic, T. (2020) 'Identifying neural substrates of competitive interactions and sequence transitions during mechanosensory responses in Drosophila', *PLoS Genetics*, 16: e1008589.

Mathis, A., Mamidanna, P., Cury, K. M., Abe, T., Murthy, V. N., Mathis, M. W. and Bethge, M. (2018) 'DeepLabCut: markerless pose estimation of user-defined body parts with deep learning', *Nature Neuroscience*, 21: 1281-1289.

Matsui, H., Namikawa, K., Babaryka, A. and Köster, R. W. (2014) 'Functional regionalization of the teleost cerebellum analyzed in vivo', *Proceedings of the National Academy of Sciences of the United States of America*, 32: 11846-11851.

Mazière, P. and Enright, A. J. (2007) 'Prediction of microRNA targets', *Drug Discovery Today*, 12: 452-8.

Medvedev, I. O., Ramsey, A. J., Masoud, S. T., Bermejo, M. K., Urs, N., Sotnikova, T. D., Beaulieu, J. M., Gainetdinov, R. R. and Salahpour, A. (2013) 'D1 dopamine receptor coupling to PLCβ regulates forward locomotion in mice', *Journal of Neuroscience*, 33: 18125-33.

Meitzen, J., Perkel, D. J. and Brenowitz, E. A. (2007) 'Seasonal changes in intrinsic electrophysiological activity of song control neurons in wild song sparrows', *Journal of Comparative Physiology A*, 193: 677-683.

Meza-Sosa, K. F., Valle-García, D., Pedraza-Alva, G. and Pérez-Martínez, L. (2011) 'Role of microRNAs in central nervous system development and pathology', *Journal of Neuroscience Research*, 90: 1-12.

Mirth, C., Truman, J. W. and Riddiford, L. M. (2005) 'The role of the prothoracic gland in determining critical weight for metamorphosis in Drosophila melanogaster', *Current Biology*, 15: 1796-807.

Mohammad, F., Stewart, J. C., Ott, S., Chlebikova, K., Chua, J. Y., Koh, T. W., Ho, J. and Claridge-Chang, A. (2017) 'Optogenetic inhibition of behavior with anion channelrhodopsins', *Nature Methods*, 14: 271-274.

Mohebbi, M., Ding, L., Malmberg, R. L. and Cai, L. (2021) 'Human MicroRNA Target Prediction via Multi-Hypotheses Learning', *Journal of Computational Biology*, 28: 117-132.

Mokabber, H., Najafzadeh, N. and Mohammadzadeh Vardin, M. (2019) 'miR-124 promotes neural differentiation in mouse bulge stem cells by repressing Ptbp1 and Sox9', *Journal of Cellular Physiology*, 234: 8941-8950.

Monastirioti, M. (1999) 'Biogenic amine systems in the fruit fly Drosophila melanogaster', *Microscopy Research and Technique*, 45: 106-21.

Moncalvo, V. G. R. and Campos, A. R. (2009) 'Role of serotonergic neurons in the Drosophila larval response to light', *BMC Neuroscience*, 10: 66.

Morgan, T. H. (1910) 'Sex limited inheritance in Drosophila', *Science,* 32: 120-2.

Morton, D. B., Clemens-Grisham, R., Hazelett, D. J. and Vermehren-Schmaedick, A. (2010) 'Infertility and male mating behavior deficits associated with Pde1c in Drosophila melanogaster', *Genetics*, 186: 159-65.

Motta, A., Berning, M., Boergens, K. M., Staffler, B., Beining, M., Loomba, S., Hennig, P., Wissler, H. and Helmstaedter, M. (2019) 'Dense connectomic reconstruction in layer 4 of the somatosensory cortex', *Science,* 366: eaay3134.

Moy, K., Li, W., Tran, H. P., Simonis, V., Story, E., Brandon, C., Furst, J., Raicu, D. and Kim, H. (2015) 'Computational Methods for Tracking, Quantitative Assessment, and Visualization of C. elegans Locomotory Behavior', *PLoS One*, 10: e0145870.

Mulvey, T. (1962) 'Origins and historical development of the electron microscope', *British journal of applied physics*, 13: 197.

Murai, K., Sun, G., Ye, P., Tian, E., Yang, S., Cui, Q., Trinh, D., Sun, O., Hong, T., Wen, Z., Kalkum, M., Riggs, A. D., Song, H., Ming, G. L. and Shi, Y. (2016) 'The TLX-miR-219 cascade regulates neural stem cell proliferation in neurodevelopment and schizophrenia iPSC model', *Nature Communications*, 7: 10965.

Muraoka, N., Yamakawa, H., Miyamoto, K., Sadahiro, T., Umei, T., Isomi, M., Nakashima, H., Akiyama, M., Wada, R., Inagawa, K., Nishiyama, T., Kaneda, R., Fukuda, T., Takeda, S., Tohyama, S., Hashimoto, H., Kawamura, Y., Goshima, N., Aeba, R., Yamagishi, H., Fukuda, K. and Ieda, M. (2014) 'MiR-133 promotes cardiac reprogramming by directly repressing Snai1 and silencing fibroblast signatures', *The EMBO Journal*, 33: 1565-81.

Nagel, G., Szellas, T., Huhn, W., Kateriya, S., Adeishvili, N., Berthold, P., Ollig, D., Hegemann, P. and Bamberg, E. (2003) 'Channelrhodopsin-2, a directly light-gated cation-selective membrane channel', *Proceedings of the National Academy of Sciences of the United States of America*, 100: 13940-5.

Nauta, W. J. (1952) 'Selective silver impregnation of degenerating axons in the central nervous system', *Stain Technology*, 27: 175-9.

Nian, X., Chen, W., Bai, W. and Zhao, Z. (2020) 'Regulation of circadian locomotor rhythm by miR-263a', *Biological Rhythm Research*, doi: 10.1080/09291016.2020.1726049

Niu, Y., Liu, Z., Nian, X., Xu, X. and Zhang, Y. (2019) 'miR-210 controls the evening phase of circadian locomotor rhythms through repression of Fasciclin 2', *PLoS Genetics*, 15: e1007655.

Ohyama, T., Jovanic, T., Denisov, G., Dang, T. C., Hoffmann, D., Kerr, R. A. and Zlatic, M. (2013) 'High-throughput analysis of stimulus-evoked behaviors in Drosophila larva reveals multiple modality-specific escape strategies', *PLoS One*, 8: e71706.

Ohyama, T., Schneider-Mizell, C. M., Fetter, R. D., Aleman, J. V., Franconville, R., Rivera-Alba, M., Mensh, B. D., Branson, K. M., Simpson, J. H., Truman,

J. W., Cardona, A. and Zlatic, M. (2015) 'A multilevel multimodal circuit enhances action selection in Drosophila', *Nature,* 520: 633-639.

Okamura, K., Hagen, J. W., Duan, H., Tyler, D. M. and Lai, E. C. (2007) 'The mirtron pathway generates microRNA-class regulatory RNAs in Drosophila', *Cell*, 130: 89-100.

Okusawa, S., Kohsaka, H. and Nose, A. (2014) 'Serotonin and Downstream Leucokinin Neurons Modulate Larval Turning Behavior in Drosophila', *Journal of Neuroscience*, 34: 2544-2558.

Otto, N., Marelja, Z., Schoofs, A., Kranenburg, H., Bittern, J., Yildirim, K., Berh, D., Bethke, M., Thomas, S., Rode, S., Risse, B., Jiang, X., Pankratz, M., Leimkühler, S. and Klämbt, C. (2018) 'The sulfite oxidase Shopper controls neuronal activity by regulating glutamate homeostasis in Drosophila ensheathing glia', *Nature Communications*, 9: 3514.

Parrish, J. Z., Xu, P., Kim, C. C., Jan, L. Y. and Jan, Y. N. (2009) 'The microRNA bantam functions in epithelial cells to regulate scaling growth of dendrite arbors in drosophila sensory neurons', *Neuron,* 63: 788-802.

Pasquinelli, A. E., Reinhart, B. J., Slack, F., Martindale, M. Q., Kuroda, M. I., Maller, B., Hayward, D. C., Ball, E. E., Degnan, B., Müller, P., Spring, J., Srinivasan, A., Fishman, M., Finnerty, J., Corbo, J., Levine, M., Leahy, P., Davidson, E. and Ruvkun, G. (2000) 'Conservation of the sequence and temporal expression of let-7 heterochronic regulatory RNA', *Nature,* 408: 86-9.

Perrimon, N. and Mathey-Prevot, B. (2007) 'Matter arising: off-targets and genome-scale RNAi screens in Drosophila', *Fly*, 1: 1-5.

Pfaffl, M. W. (2001) 'A new mathematical model for relative quantification in real-time RT-PCR', *Nucleic Acids Research*, 29: e45.

Pfeiffer, B. D., Ngo, T. T., Hibbard, K. L., Murphy, C., Jenett, A., Truman, J. W. and Rubin, G. M. (2010) 'Refinement of tools for targeted gene expression in Drosophila', *Genetics*, 186: 735-55.

Picao-Osorio, J., Johnston, J., Landgraf, M., Berni, J. and Alonso, C. R. (2015) 'MicroRNA-encoded behavior in Drosophila', *Science*, 350: 815-820.

Picao-Osorio, J., Lago-Baldaia, I., Patraquim, P. and Alonso, C. R. (2017) 'Pervasive Behavioural Effects of microRNA Regulation in Drosophila', *Genetics*, 206: 195776-14.

Picao-Osorio, J., Lago-Baldaia, I., Klann M., Pinho S. and Alonso C. R. The microRNA transcriptome of the early *Drosophila* larva. *Unpublished data.*

Pierce-Shimomura, J. T., Morse, T. M. and Lockery, S. R. (1999) 'The fundamental role of pirouettes in Caenorhabditis elegans chemotaxis', *Journal of Neuroscience*, 19: 9557-69.

Ponton, F., Chapuis, M. P., Pernice, M., Sword, G. A. and Simpson, S. J. (2011) 'Evaluation of potential reference genes for reverse transcription-qPCR studies of physiological responses in Drosophila melanogaster', *Journal of Insect Physiology*, 57: 840-50.

Portman, D. S. and Dreyfuss, G. (1994) 'RNA annealing activities in HeLa nuclei', *The EMBO Journal*, 13: 213-21.

Potter, C. J., Tasic, B., Russler, E. V., Liang, L. and Luo, L. (2010) 'The Q system: a repressible binary system for transgene expression, lineage tracing, and mosaic analysis', *Cell*, 141: 536-48.

Pulver, S. R., Bayley, T. G., Taylor, A. L., Berni, J., Bate, M. and Hedwig, B. (2015) 'Imaging fictive locomotor patterns in larval Drosophila', *Journal of Neurophysiology*, 114: 2564-2577.

Randel, N., Shahidi, R., Verasztó, C., Bezares-Calderón, L. A., Schmidt, S. and Jékely, G. (2015) 'Inter-individual stereotypy of the Platynereis larval visual connectome', *Elife*, 4: e08069.

Rehmsmeier, M., Steffen, P., Hochsmann, M. and Giegerich, R. (2004) 'Fast and effective prediction of microRNA/target duplexes', *RNA*, 10: 1507-17.

Renn, S. C., Park, J. H., Rosbash, M., Hall, J. C. and Taghert, P. H. (1999) 'A pdf neuropeptide gene mutation and ablation of PDF neurons each cause severe abnormalities of behavioral circadian rhythms in Drosophila', *Cell*, 99: 791-802.

Risse, B., Berh, D., Otto, N., Klämbt, C. and Jiang, X. (2017) 'FIMTrack: An open source tracking and locomotion analysis software for small animals', *PLoS Computational Biology*, 13: e1005530.

Risse, B., Thomas, S., Otto, N., Löpmeier, T., Valkov, D., Jiang, X. and Klämbt, C. (2013) 'FIM, a Novel FTIR-Based Imaging Method for High Throughput Locomotion Analysis', *PLoS One*, 8: e53963-11.

Robertson, J. L., Tsubouchi, A. and Tracey, W. D. (2013) 'Larval defense against attack from parasitoid wasps requires nociceptive neurons', *PLoS One*, 8: e78704.

Robie, A. A., Hirokawa, J., Edwards, A. W., Umayam, L. A., Lee, A., Phillips, M. L., Card, G. M., Korff, W., Rubin, G. M., Simpson, J. H., Reiser, M. B. and Branson, K. M. (2017) 'Mapping the Neural Substrates of Behavior', *Cell*, 170: 393-406.

Roeder, K. D., Tozian, L. and Weiant, E. A. (1960) 'Endogenous nerve activity and behaviour in the mantis and cockroach', *Journal of Insect Physiology*, 4: 45-62.

Ruby, J. G., Jan, C.H. and Bartel, D. P. (2007) ‘Intronic microRNA precursors that bypass Drosha processing', *Nature*, 448: 83-86.

Saalfeld, S., Cardona, A., Hartenstein, V. and Tomancak, P. (2009) 'CATMAID: collaborative annotation toolkit for massive amounts of image data', *Bioinformatics*, 25: 1984-1986.

Santa-Maria, I., Alaniz, M. E., Renwick, N., Cela, C., Fulga, T. A., Van Vactor, D., Tuschl, T., Clark, L. N., Shelanski, M. L., McCabe, B. D. and Crary, J. F. (2015) 'Dysregulation of microRNA-219 promotes neurodegeneration through post-transcriptional regulation of tau', *Journal of Clinical Investigation*, 125: 681-6.

Saudou, F., Amara, D. A., Dierich, A., LeMeur, M., Ramboz, S., Segu, L., Buhot, M. C. and Hen, R. (1994) 'Enhanced aggressive behavior in mice lacking 5-HT1B receptor', *Science,* 265: 1875-8.

Schindelin, J., Arganda-Carreras, I., Frise, E., Kaynig, V., Longair, M., Pietzsch, T., Preibisch, S., Rueden, C., Saalfeld, S., Schmid, B., Tinevez, J. Y., White, D. J., Hartenstein, V., Eliceiri, K., Tomancak, P. and Cardona, A. (2012) 'Fiji: an open-source platform for biological-image analysis', *Nature Methods*, 9: 676-82.

Schleyer, M., Miura, D., Tanimura, T. and Gerber, B. (2015) 'Learning the specific quality of taste reinforcement in larval Drosophila', *Elife*, 4: e04711.

Schneider-Mizell, C. M., Gerhard, S., Longair, M., Zwart, M. F. and Cardona, A. (2016) 'Quantitative neuroanatomy for connectomics in Drosophila', *Elife,* 5: e12059.

Schulze, A., Gomez-Marin, A., Rajendran, V. G., Lott, G., Musy, M., Ahammad, P., Deogade, A., Sharpe, J., Riedl, J., Jarriault, D., Trautman, E. T., Werner, C., Venkadesan, M., Druckmann, S., Jayaraman, V. and Louis, M. (2015) 'Dynamical feature extraction at the sensory periphery guides chemotaxis', *Elife*, 4: e06694.

Schumann, I. and Triphan, T. (2020) 'The PEDtracker: an automatic staging approach for Drosophila melanogaster larvae', *Frontiers in Behavioral Neuroscience*, 14: 612313.

Schützler, N., Girwert, C., Hügli, I., Mohana, G., Roignant, J. Y., Ryglewski, S. and Duch, C. (2019) 'Tyramine action on motoneuron excitability and adaptable tyramine/octopamine ratios adjust', *Proceedings of the National Academy of Sciences of the United States of America*, 116: 3805-3810.

Selbach, M., Schwanhäusser, B., Thierfelder, N., Fang, Z., Khanin, R. and Rajewsky, N. (2008) 'Widespread changes in protein synthesis induced by microRNAs', *Nature,* 455: 58-63.

Simon, A. F., Daniels, R., Romero-Calderón, R., Grygoruk, A., Chang, H. Y., Najibi, R., Shamouelian, D., Salazar, E., Solomon, M., Ackerson, L. C., Maidment, N. T., Diantonio, A. and Krantz, D. E. (2009) 'Drosophila vesicular monoamine transporter mutants can adapt to reduced or eliminated vesicular stores of dopamine and serotonin', *Genetics*, 181: 525-41.

Simpson, J. H. and Looger, L. L. (2018a 'Functional Imaging and Optogenetics in', *Genetics*, 208: 1291-1309.

Sims, D. W., Humphries, N. E., Hu, N., Medan, V. and Berni, J. (2019) 'Optimal searching behaviour generated intrinsically by the central pattern generator for locomotion', *Elife*, 8: e50316.

Sjostrand, F. S. (1958) 'Ultrastructure of retinal rod synapses of the guinea pig eye as revealed by three-dimensional reconstructions from serial sections', *Journal of Ultrastructure Research*, 2: 122-70.

Smibert, P. and Lai, E. C. (2010) 'A view from Drosophila: multiple biological functions for individual microRNAs', Semin Cell *Developmental Biology*, 21: 745-53.

Sokol, N. S. and Ambros, V. (2005) 'Mesodermally expressed Drosophila microRNA-1 is regulated by Twist and is required in muscles during larval growth', *Genes & Development*, 19: 2343-2354.

Sokol, N. S., Xu, P., Jan, Y. N. and Ambros, V. (2008) 'Drosophila let-7 microRNA is required for remodeling of the neuromusculature during metamorphosis', *Genes & Development*, 22: 1591-6.

Stacey, S. M., Muraro, N. I., Peco, E., Labbé, A., Thomas, G. B., Baines, R. A. and van Meyel, D. J. (2010) 'Drosophila glial glutamate transporter Eaat1 is regulated by fringe-mediated notch signaling and is essential for larval locomotion', *Journal of Neuroscience*, 30: 14446-14457.

Stark, A., Brennecke, J., Bushati, N., Russell, R. B. and Cohen, S. M. (2005) 'Animal MicroRNAs confer robustness to gene expression and have a significant impact on 3'UTR evolution', *Cell*, 123: 1133-46.

Stark, A., Brennecke, J., Russell, R. B. and Cohen, S. M. (2003) 'Identification of Drosophila MicroRNA targets', *PLoS Biology*, 1: E60.

Stensmyr, M. C., Dweck, H. K., Farhan, A., Ibba, I., Strutz, A., Mukunda, L., Linz, J., Grabe, V., Steck, K., Lavista-Llanos, S., Wicher, D., Sachse, S., Knaden, M., Becher, P. G., Seki, Y. and Hansson, B. S. (2012) 'A conserved dedicated olfactory circuit for detecting harmful microbes in Drosophila', *Cell*, 151: 1345-57.

Stephens, G. J., Johnson-Kerner, B., Bialek, W. and Ryu, W. S. (2008) 'Dimensionality and Dynamics in the Behavior of C. elegans', *PLoS Computational Biology*, 4: e1000028-10.

Stevens, J. K., Davis, T. L., Friedman, N. and Sterling, P. (1980) 'A systematic approach to reconstructing microcircuitry by electron microscopy of serial sections', *Brain Research*, 2: 265-93.

Struhl, G. and White, R. A. (1985) 'Regulation of the Ultrabithorax gene of Drosophila by other bithorax complex genes', *Cell*, 43: 507-19.

Sun, K. and Lai, E. C. (2013) 'Adult-specific functions of animal microRNAs', *Nature Reviews Genetics*, 14: 535-48.

Sun, K., Westholm, J. O., Tsurudome, K., Hagen, J. W., Lu, Y., Kohwi, M., Betel, D., Gao, F.-B., Haghighi, A. P., Doe, C. and Lai, E. C. (2012) 'Neurophysiological Defects and Neuronal Gene Deregulation in Drosophila mir-124 Mutants', *PLoS Genetics*, 8: e1002515-17.

Sun, L., Li, W., Li, D. and Wang, D. (2020) 'microRNAs involved in the control of toxicity on locomotion behavior induced by simulated microgravity stress in Caenorhabditis elegans', *Scientific Reports,* 10: 17510.

Sun, Y., Zhou, P., Zhao, Q. and Gong, Z. (2019) 'Light Spot-Based Assay for Analysis of Drosophila Larval Phototaxis', *Journal of Visualised Experiments*, 151.

Suster, M. L. and Bate, M. (2002) 'Embryonic assembly of a central pattern generator without sensory input', *Nature,* 416: 174-8.

Suster, M. L., Martin, J. R., Sung, C. and Robinow, S. (2003) 'Targeted expression of tetanus toxin reveals sets of neurons involved in larval locomotion in Drosophila', *Journal of Neurobiology*, 55: 233-46.

Swierczek, N. A., Giles, A. C., Rankin, C. H. and Kerr, R. A. (2011) 'High-throughput behavioral analysis in C. elegans', *Nature Methods*, 8: 592-8.

Szigeti, B., Deogade, A. and Webb, B. (2015) 'Searching for motifs in the behaviour of larval *Drosophila melanogaster* and Caenorhabditis elegans reveals continuity between behavioural states', *Journal of The Royal Society Interface*, 12: 20150899-12.

Takagi, S., Cocanougher, B. T., Niki, S., Miyamoto, D., Kohsaka, H., Kazama, H., Fetter, R. D., Truman, J. W., Zlatic, M., Cardona, A. and Nose, A. (2017) 'Divergent Connectivity of Homologous Command- like Neurons Mediates Segment-Specific Touch Responses in Drosophila', *Neuron*, 96: 1373-1387.

Tal, T. L., Franzosa, J. A., Tilton, S. C., Philbrick, K. A., Iwaniec, U. T., Turner, R. T., Waters, K. M. and Tanguay, R. L. (2012) 'MicroRNAs control neurobehavioral development and function in zebrafish', *The FASEB Journal*, 26: 1452-61.

Tamvacakis, A. N., Senatore, A. and Katz, P. S. (2018) 'Single neuron serotonin receptor subtype gene expression correlates with behaviour within and across three molluscan species', *Proceedings of the Royal Society B: Biological Sciences*, 285: 20180791.

Tastekin, I., Khandelwal, A., Tadres, D., Fessner, N. D., Truman, J. W., Zlatic, M., Cardona, A. and Louis, M. (2018) 'Sensorimotor pathway controlling stopping behavior during chemotaxis in the *Drosophila melanogaster* larva', *Elife*, 7: e38740.

Tastekin, I., Riedl, J., Schilling-Kurz, V., Gomez-Marin, A., Truman, J. W. and Louis, M. (2015) 'Role of the subesophageal zone in sensorimotor control of orientation in Drosophila larva', *Current Biology*, 25: 1448-60.

Tat, T. T., Maroney, P. A., Chamnongpol, S., Coller, J. and Nilsen, T. W. (2016) 'Cotranslational microRNA mediated messenger RNA destabilization', *Elife*, 5: e12880.

Technau, G. M., Rogulja-Ortmann, A., Berger, C., Birkholz, O. and Rickert, C. (2014) 'Composition of a neuromere and its segmental diversification under the control of Hox genes in the embryonic CNS of Drosophila', *Journal of Neurogenetics*, 28: 171-80.

Temin, H. M. and Mizutani, S. (1970) 'RNA-dependent DNA polymerase in virions of Rous sarcoma virus', *Nature,* 226: 1211-3.

Thaler, J. P., Lee, S. K., Jurata, L. W., Gill, G. N. and Pfaff, S. L. (2002) 'LIM factor Lhx3 contributes to the specification of motor neuron and interneuron identity through cell-type-specific protein-protein interactions', *Cell*, 110: 237-49.

Thelen, M. P. and Kye, M. J. (2020) 'The Role of RNA Binding Proteins for Local mRNA Translation: Implications in Neurological Disorders', *Frontiers in Molecular Biosciences*, 6: 161.

Thermann, R. and Hentze, M. W. (2007) 'Drosophila miR2 induces pseudo-polysomes and inhibits translation initiation', *Nature,* 447: 875-8.

Thirumalai, V. and Cline, H. T. (2008) 'Endogenous dopamine suppresses initiation of swimming in prefeeding zebrafish larvae', *Journal of Neurophysiology*, 100: 1635-48.

Thor, S., Andersson, S. G., Tomlinson, A. and Thomas, J. B. (1999) 'A LIM-homeodomain combinatorial code for motor-neuron pathway selection', *Nature,* 397: 76-80.

Thorndike, R. L. (1953) 'Who belongs in the family?', *Psychometrika*, 18: 267-276.

Tian, B. and Manley, J. L. (2017) 'Alternative polyadenylation of mRNA precursors', *Nature Reviews Molecular Cell Biology*, 18: 18-30.

Tian, L., Hires, S. A., Mao, T., Huber, D., Chiappe, M. E., Chalasani, S. H., Petreanu, L., Akerboom, J., McKinney, S. A., Schreiter, E. R., Bargmann, C. I., Jayaraman, V., Svoboda, K. and Looger, L. L. (2009) 'Imaging neural activity in worms, flies and mice with improved GCaMP calcium indicators', *Nature Methods*, 6: 875-81.

Tinbergen, N. (1951) *The Study of Instinct*. Oxford University Press. New York, USA.

Tinbergen, N. (1996) 'The hierarchical organization of nervous mechanisms underlying instinctive behaviour', *Foundations of animal behavior: Classic papers with commentaries*, 406-413.

Truman, J. W. (1990) 'Metamorphosis of the central nervous system of Drosophila', *Journal of Neurobiology*, 21: 1072-84.

Truman, J. W. and Bate, M. (1988) 'Spatial and temporal patterns of neurogenesis in the central nervous system of Drosophila melanogaster', *Developmental Biology*, 125: 145-57.

Tsalik, E. L. and Hobert, O. (2003) 'Functional mapping of neurons that control locomotory behavior in Caenorhabditis elegans', *Journal of Neurobiology*, 56: 178-97.

Tsurudome, K., Tsang, K., Liao, E. H., Ball, R., Penney, J., Yang, J. S., Elazzouzi, F., He, T., Chishti, A., Lnenicka, G., Lai, E. C. and Haghighi, A. P. (2010) 'The Drosophila miR-310 cluster negatively regulates synaptic strength at the neuromuscular junction', *Neuron,* 68: 879-93.

Ugolini, G. (1995) 'Specificity of rabies virus as a transneuronal tracer of motor networks: transfer from hypoglossal motoneurons to connected second-order and higher order central nervous system cell groups', *Journal of Comparative Neurology*, 356: 457-80.

Ugur, B., Chen, K. and Bellen, H. J. (2016) 'Drosophila tools and assays for the study of human diseases', *Disease Models & Mechanisms*, 9: 235-44.

Vallés, A. M. and White, K. (1988) 'Serotonin-containing neurons in Drosophila melanogaster: development and distribution', *Journal of Comparative Neurology*, 268: 414-28.

Verasztó, C., Jasek, S., Gühmann, M., Shahidi, R., Ueda, N., Beard, J. D., Mendes, S., Heinz, K., Bezares-Calderón, L. A. and Williams, E. (2020) 'Whole-animal connectome and cell-type complement of the three-segmented Platynereis dumerilii larva', b*ioRxiv.preprint*, doi: 10.1101/2020.08.21.260984.

Verma, P., Augustine, G. J., Ammar, M. R., Tashiro, A. and Cohen, S. M. (2015) 'A neuroprotective role for microRNA miR-1000 mediated by limiting glutamate excitotoxicity', *Nature Neuroscience*, 18: 379-85.

Viswanathan, G. M., Afanasyev, V., Buldyrev, S. V., Havlin, S., da Luz, M. G. E., Raposo, E. P. and Stanley, H. E. (2001) 'Lévy flights search patterns of biological organisms', *Physica A: Statistical Mechanics and its Applications*, 295: 85-88.

Viswanathan, G. M., Buldyrev, S. V., Havlin, S., da Luz, M. G. E., Raposo, E. P. and Stanley, H. E. (1999) 'Optimizing the success of random searches', *Nature,* 401: 911-914.

Wang, C., Ge, L., Wu, J., Wang, X. and Yuan, L. (2019a) 'MiR-219 represses expression of dFMR1 in Drosophila melanogaster', *Life Sciences*, 218: 31-37.

Wang, P., Cao, T., Chen, J., Jiang, Y., Wang, C., Waddington, J. L. and Zhen, X. (2019b) 'D2 receptor-mediated miRNA-143 expression is associated with the effects of antipsychotic drugs on phencyclidine-induced schizophrenia-related locomotor hyperactivity and with Neuregulin-1 expression in mice', *Neuropharmacology*, 157: 107675.

Wanner, A. A., Genoud, C., Masudi, T., Siksou, L. and Friedrich, R. W. (2016) 'Dense EM-based reconstruction of the interglomerular projectome in the zebrafish olfactory bulb', *Nature Neuroscience*, 19: 816-25.

Ware, R. W. and Lopresti, V. (1975) 'Three-dimensional reconstruction from serial sections', *International Review of Cytology*, 40: 325-440.

Watson, J. D. and Crick, F. H. (1953) 'Molecular structure of nucleic acids: a structure for deoxyribose nucleic acid', *Nature,* 171: 737-738.

Watts, M., Williams, G., Lu, J., Nithianantharajah, J. and Claudianos, C. (2021) 'MicroRNA-210 Regulates Dendritic Morphology and Behavioural Flexibility in Mice', *Molecular Neurobiology*, 58: 1330-1344.

Westholm, J. O. and Lai, E. C. (2011) 'Mirtrons: microRNA biogenesis via splicing', *Biochimie*, 93: 1897-904.

White, J. G., Southgate, E., Thomson, J. N. and Brenner, S. (1986) 'The structure of the nervous system of the nematode Caenorhabditis elegans',

Philosophical Transactions of the Royal Society B: *Biological Sciences*, 314: 1-340.

Wilson, D. M. (1961) 'The central nervous control of flight in a locust', *Journal of Experimental Biology,* 38: 471-490.

Witkos, T. M., Koscianska, E. and Krzyzosiak, W. J. (2011) 'Practical Aspects of microRNA Target Prediction', *Current Molecular Medicine*, 11: 93-109.

Wood, W. E., Roseberry, T. K. and Perkel, D. J. (2013) 'HTR2 Receptors in a Songbird Premotor Cortical-Like Area Modulate Spectral Characteristics of Zebra Finch Song', *Journal of Neuroscience*, 33: 2908-2915.

Wystrach, A., Lagogiannis, K. and Webb, B. (2016) 'Continuous lateral oscillations as a core mechanism for taxis in Drosophila larvae', *Elife*, 5: e15504.

Yin, V. P., Lepilina, A., Smith, A. and Poss, K. D. (2012) 'Regulation of zebrafish heart regeneration by miR-133', *Developmental Biology*, 365: 319-27.

Yoshikawa, S., Long, H. and Thomas, J. B. (2016) 'A subset of interneurons required for Drosophila larval locomotion', *Molecular and Cellular Neuroscience*, 70: 22-29.

Yoshino, J., Morikawa, R. K., Hasegawa, E. and Emoto, K. (2017) 'Neural Circuitry that Evokes Escape Behavior upon Activation of Nociceptive Sensory Neurons in Drosophila Larvae', *Current Biology*, 27: 2499-2504.

Zarin, A. A., Mark, B., Cardona, A., Litwin-Kumar, A. and Doe, C. Q. (2019) 'A multilayer circuit architecture for the generation of distinct locomotor behaviors in Drosophila', *Elife*, 8: e51781.

Zhang, W., Ge, W. and Wang, Z. (2007) 'A toolbox for light control of Drosophila behaviors through Channelrhodopsin 2-mediated photoactivation of targeted neurons', *European Journal of Neuroscience*, 26: 2405-16.

Zhang, Y., Lamba, P., Guo, P. and Emery, P. (2016) 'miR-124 Regulates the Phase of Drosophila Circadian Locomotor Behavior', *Journal of Neuroscience*, 36: 2007-13.

Zhao, C., Sun, G., Li, S. and Shi, Y. (2009) 'A feedback regulatory loop involving microRNA-9 and nuclear receptor TLX in neural stem cell fate determination', *Nature Structural & Molecular Biology*, 16: 365-71.

Zheng, Z., Lauritzen, J. S., Perlman, E., Robinson, C. G., Nichols, M., Milkie, D., Torrens, O., Price, J., Fisher, C. B., Sharifi, N., Calle-Schuler, S. A., Kmecova, L., Ali, I. J., Karsh, B., Trautman, E. T., Bogovic, J. A., Hanslovsky, P., Jefferis, G. S. X. E., Kazhdan, M., Khairy, K., Saalfeld, S., Fetter, R. D. and Bock, D. D. (2018) 'A Complete Electron Microscopy Volume of the Brain of Adult Drosophila melanogaster', *Cell*, 174: 730-743.

Zhou, L., Lim, M. Y. T., Kaur, P., Saj, A., Bortolamiol-Becet, D., Gopal, V., Tolwinski, N., Tucker-Kellogg, G. and Okamura, K. (2018) 'Importance of miRNA stability and alternative primary miRNA isoforms in gene regulation during Drosophila development', *Elife*, 7: e38389.

Zwart, M. F., Pulver, S. R., Truman, J. W., Fushiki, A., Fetter, R. D., Cardona, A. and Landgraf, M. (2016) 'Selective Inhibition Mediates the Sequential Recruitment of Motor Pools', *Neuron,* 91: 615-628.

Zwart, M. F., Randlett, O., Evers, J. F. and Landgraf, M. (2013) 'Dendritic growth gated by a steroid hormone receptor underlies increases in activity in the developing Drosophila locomotor system', *Proceedings of the National Academy of Sciences of the United States of America*, 110: E3878-87.